

**University of Alberta**

**ENGINEERING PEPTIDES FOR ANTICANCER DRUG  
TARGETING AND ANTIMICROBIAL ACTIVITY**

By

**RANIA SOUDY**

A thesis submitted to the Faculty of Graduate Studies and Research  
in partial fulfillment of the requirements for the degree of

**DOCTOR OF PHILOSOPHY**

In

Pharmaceutical Sciences

Faculty of Pharmacy and Pharmaceutical Sciences

© RANIA SOUDY

Spring 2013

Edmonton, Alberta

Permission is hereby granted to the University of Alberta Libraries to reproduce single copies of this thesis and to lend or sell such copies for private, scholarly or scientific research purposes only. Where the thesis is converted to, or otherwise made available in digital form, the University of Alberta will advise potential users of the thesis of these terms.

The author reserves all other publication and other rights in association with the copyright in the thesis and, except as herein before provided, neither the thesis nor any substantial portion thereof may be printed or otherwise reproduced in any material form whatsoever without the author's prior written permission.

## ***Dedication***

*I dedicate this thesis to my small family, my husband Mohamed Elfishawi and my lovely sons, Nour, and Mahmoud who were always there for me providing me with continuous love, support, encouragement and patience. Without their passion I would not have been able to complete my advanced studies.*

*To my beloved parents, Nayel Soudy and Samia Elsharty, for their love, encouragement, and endless support. My parents have supported me in everything I have done throughout my life, and I am so appreciative of the sacrifices that they made to get me where I am today.*

## ABSTRACT

---

Peptides hold great promise for clinical applications such as cancer and antimicrobial therapies. In cancer, conjugation of cancer treatments to tumor specific peptides improves their therapeutic efficiency. On the other side, antimicrobial peptides offer a great alternative for the conventional antibiotics against bacterial resistance and display selective anticancer activities with low toxicity. However, to obtain therapeutically applicable peptides, the chemical structures of lead sequences need to be further manipulated. The two main aims of this thesis were (i) to engineer cancer targeting peptides based on lead sequences NGR and p160 for enhanced proteolytic stability and binding affinity for cancer cells, (ii) engineer synthetic analogues of microcin J25 antimicrobial peptide, and improve its anticancer activity by augmenting its cellular uptake. First, a NGR peptide library was screened using peptide array-whole cell binding assay. This led to the identification several new peptides that targeted aminopeptidase N (CD13) receptor in the CD13<sup>+</sup> cells. Specifically peptide 5 (YNGRT) displayed significant increase in CD13<sup>+</sup> cells uptake compared to the lead peptide and displayed better APN enzyme inhibition. Second, p160 peptide analogues were engineered by replacement of two or three amino acids with D-residues or  $\beta_3$ -amino acids for improved proteolytic stability while maintaining high specificity for breast cancer cells. Three analogues (18-4, 18-9, and 18-10) that exhibited resistance to proteolytic degradation in human serum and in liver homogenate and impart no cell cytotoxicity were identified. Further, two peptide-drug (Doxorubicin) conjugates were examined for their cancer drug targeting

efficiency. Our results demonstrated that the ester conjugate was equally potent to free Dox, with improved specificity to breast cancer cell including Dox resistant cell lines. To accomplish the second goal, six MccJ25 peptide analogues were engineered. Peptides 1 and 6 displayed good activity against *Salmonella newport*. Peptide 1 displayed activity against five other *Salmonella* strains by inhibition of target cell respiration. Circular dichroism and proteases experiments showed that the active peptides adopt a folded structure but not the true lasso structure. Finally, a conjugate of MccJ25 peptide with 18-4 significantly enhanced the anticancer apoptotic activity in breast cancer cells by greater cellular uptake. Peptides identified herein are useful entities that can be translated to pharmacologically valuable structures of clinical value.

## ACKNOWLEDGEMENTS

---

This work would not have been possible without the support of several people.

- ✚ First and foremost, I would like to express my sincere gratitude to my supervisor Dr. Kamaljit Kaur for her guidance and support throughout my research project. Her assistance and insight on a variety of issues has helped me tremendously in my academic endeavors. I always had access to her office to discuss any issue related to research. Most importantly, I had the freedom to make a decision regarding research and discuss with her. This helped me to become more independent as a researcher. She encouraged me to strive for perfection. I will always remember her contribution to help me grow as a person.
- ✚ I would like to extend my special thanks to members of my supervisory committee, Dr. Hasan Uludag, and Dr. Carlos Velazquez for taking time out of their busy schedules to provide feedback and useful discussions on my project. Your timely advice, constructive criticism, and assistance were greatly appreciated and always helpful.
- ✚ I would like to express my appreciation to Dr. Afsaneh Lavasanifar and her laboratory members for providing me with the great opportunity to do cell culture studies in her laboratory and for their help throughout my research. Special thanks to Elaine Moase her lab technician for teaching me cell culture techniques.
- ✚ I would like to thank our collaborators at Canbiocin *Inc.*, in particular, Dr. Liru Wang, for teaching me most of the microbiological techniques done in my studies and Dr. Michael stiles for giving me the chance to work in his company. It was such a valuable experience to meet and collaborate with researchers in the industrial field.
- ✚ I would like to express my appreciation to Dr. John Seubert and his laboratory members, especially, Haitham El-Sikhry for helping me with the fluorescence microscopy studies.

- ✚ I would like to thank Dr. Paul Jurasz and Dr. Aneta Radziwan-Balicka his postdoctoral fellow for helping me with the flow cytometry studies.
- ✚ I would like to thank Dr. Tara Sprules (McGill University, Montreal) who helped me with the NMR experiments and interpretation of the data.
- ✚ I was lucky to work with two great undergraduate students Avneet Gill, and Christopher Chen. Your contribution to my work will not be forgettable.
- ✚ I am so grateful for all my lab members past and present that have been a part of my time here, Dr. Sahar Ahmed, Dr. Wael Soliman, Reem Beleid, Gagandeep Kharaud, Dr. Anu Stella, Krishna Bodapati, and Hashem Etaysh. I would like to thank them all for their unwavering support during my studies. They were always there to cheer me up after a tough day in the Lab.
- ✚ I would like to acknowledge the Department of Pharmaceutical Sciences at University of Alberta for providing a challenging research and learning environment. Mr. Jeff Turchinsky for helping me with ordering supplies and figuring out a lot of stuff that cannot be done without him. Mrs. Joyce Johnson for her help and support for the whole period of my program.
- ✚ I would like to thank my examination committee for contributing immensely towards my thesis.
- ✚ Finally, I would like to thank the following agencies/institutes for the financial support, Egyptian Government for the financial support during my program. NSERC and the Faculty of Pharmacy and Pharmaceutical Sciences, University of Alberta, Canada.

## Table of Contents

---

<b>Chapter 1 : Introduction .....</b>	<b>1</b>
1.1. Peptides Therapeutics.....	2
1.2. Tumor Targeting Peptides .....	3
1.2.1. Limitation of Conventional Cancer Therapy.....	3
1.2.2. Different Tumor Targeting Ligands .....	5
1.2.2.1. Monoclonal Antibodies.....	5
1.2.2.2. Affibodies .....	9
1.2.2.3. Peptides.....	11
1.2.3. Classification of Tumor Targeting Peptides .....	13
1.2.3.1. Tumor Cell Surface Targeting Peptides.....	13
1.2.3.2. Vascular Targeting Peptides .....	17
1.2.4. Methods Used in the Discovery and Optimization of Cancer Targeting Peptides.....	23
1.2.5. Improving the <i>In Vivo</i> Behavior of Peptides .....	27
1.2.5.1. <i>In Vivo</i> Proteolytic Stability.....	27
1.2.5.2. Peptide Affinity Optimization .....	31
1.2.5.3. Improving Tumor Penetration .....	36
1.2.6. Cancer Targeting Peptides in Drug Delivery.....	38
1.2.7. Cancer Targeting Peptides for Diagnostic Application.....	43
1.3. Peptides as Antimicrobial Agents .....	45
1.3.1. Microcins Classification and Mode of Action.....	46
1.3.2. Microcin J25 Biosynthesis and Structure .....	48
1.3.3. Microcin J25 Uptake and Mechanism of Action.....	51

1.3.4. Structural Activity Relationship of Microcin J25.....	52
1.3.5. Potential Applications of Microcins .....	53
1.4. Thesis Proposal .....	56
1.4.1. Thesis Rationale.....	56
1.4.2. Thesis Objective .....	57
1.5. References .....	61

## **Chapter 2 : NGR Peptide Ligands for Targeting CD13/APN Identified through Peptide Array Screening ..... 79**

2.1. Introduction .....	80
2.2. Materials and Methods .....	83
2.2.1. Peptide Array Synthesis.....	83
2.2.2. APN/CD13 Expression Level.....	84
2.2.3. Peptide Array-Cell Binding Assay .....	85
2.2.4. Synthesis of FITC-labeled Peptides .....	86
2.2.5. Peptide Stability and Deamination .....	87
2.2.6. <i>In vitro</i> Cellular Uptake using FACS .....	88
2.2.7. Cellular Uptake using Fluorescence Microscopy .....	89
2.2.8. Aminopeptidase Enzymatic Inhibition. ....	90
2.3. Results and Discussion.....	91
2.3.1. Engineering NGR-based Peptide Library .....	91
2.3.2. Level of Aminopeptidase N (or CD13) Expression .....	94
2.3.3. Peptide Array-Cell Binding Assay .....	96
2.3.4. Evaluation of <i>In vitro</i> Cell Binding .....	100
2.3.5. Inhibition of Aminopeptidase N Activity by Selected Peptides.....	108
2.4. Conclusions .....	112

2.5. References .....	113
-----------------------	-----

### **Chapter 3 : Engineered Proteolytically Stable p160 Cancer Targeting Peptides with High Affinity for Breast Cancer Cells 118**

3.1. Introduction .....	119
3.2. Materials and Methods .....	124
3.2.1. Peptide Synthesis .....	124
3.2.2. Cellular Uptake by Flow Cytometry.....	127
3.2.3. Fluorescence Microscopy .....	129
3.2.4. Serum Stability .....	129
3.2.5. <i>In Vitro</i> Metabolic Stability .....	130
3.2.6. NMR spectroscopy .....	132
3.2.7. CD Spectroscopy .....	133
3.2.8. Cytotoxicity .....	133
3.3. Results .....	134
3.3.1. Design of Peptide 18 Analogues .....	134
3.3.2. <i>In Vitro</i> Cell Binding Assays .....	136
3.3.3. Proteolytic Stability .....	142
3.3.4. Solution conformation .....	145
3.3.5. Cytotoxicity .....	148
3.4. Discussion .....	150
3.5. Concluding Remarks .....	154
3.6. References .....	156

### **Chapter 4 : Novel Peptide-Doxorubicin Conjugates for Targeting Breast Cancer Cells Including the Multidrug Resistant Cells ... 161**

4.1. Introduction .....	162
-------------------------	-----

4.2. Materials and Methods .....	166
4.2.1. Peptide Synthesis .....	168
4.2.2. Synthesis of Peptide-Dox Conjugates .....	169
4.2.3. Dox Release from Conjugates .....	173
4.2.4. <i>In vitro</i> Cell Binding and Uptake Studies.....	174
4.2.5. Confocal Fluorescence Microscopy .....	176
4.2.6. <i>In Vitro</i> Cytotoxicity.....	176
4.2.7. Effect of p-glycoprotein Inhibitors on Cytotoxicity .....	177
4.3. Results .....	178
4.3.1. Design and Synthesis of Peptide-Dox Conjugates. ....	178
4.3.2. Serum Stability and Release of Dox from Conjugates .....	181
4.3.3. <i>In vitro</i> cell uptake studies.....	183
4.3.4. Cell Cytotoxicity.....	190
4.3.5. Effect of Verapamil on Cytotoxicity .....	194
4.4. Discussion .....	195
4.5. Concluding Remarks .....	202
4.6. References .....	203

**Chapter 5 : Synthetic Peptides Derived from the Sequence of a Lasso Peptide Microcin J25 Show Antibacterial Activity ..... 209**

5.1. Introduction .....	210
5.2. Materials and Methods .....	213
5.2.1 Reagents and Equipment .....	213
5.2.2. Peptide Synthesis and Purification .....	215
5.2.3 Microcin J25 Expression and Purification.....	218
5.2.4. Antimicrobial Activity Assay .....	219

5.2.5. Circular Dichroism (CD) Spectroscopy.....	220
5.2.6. Proteolytic Stability .....	221
5.2.7. Oxygen Consumption Determination .....	222
5.2.8. Cell Viability Assay.....	222
5.2.8.1. Cell lines .....	222
5.2.8.2. MTT cytotoxicity assay .....	223
5.3. Results and Discussion.....	224
5.4. Conclusions .....	235
<b>Chapter 6 : A Conjugate of Antimicrobial Peptide Microcin J25 With a Cancer Targeting Peptide Displays Cancer Cell Specific Cytotoxicity.....</b>	<b>240</b>
6.1. Introduction .....	241
6.2. Materials and methods .....	244
6.2.1. Microcin J25 Expression and Purification.....	244
6.2.2. MccJ25-18-4 Conjugate Synthesis .....	245
6.2.3. Cytotoxicity Assay .....	246
6.2.4. Peptide Cellular Uptake.....	247
6.2.5. Detection of Apoptosis Using Annexin V and PI Staining .....	248
6.3. Results and Discussion.....	249
6.3.1. Design and Synthesis of Conjugate .....	249
6.3.2. Cytotoxicity assay.....	252
6.3.3. Peptide Cellular Uptake .....	254
6.3.4. Detection of Apoptosis .....	256
6.4. Conclusions .....	258
6.5. References .....	259

<b>Chapter 7 : Conclusions and Future Directions .....</b>	<b>263</b>
7.1. Conclusions .....	264
7.2. Future directions.....	273
7.3. References .....	278
<b>Appendix .....</b>	<b>280</b>

## LIST OF TABLES

---

<b>Table 1.1.</b> List of some of the FDA approved peptide based therapeutics in the market. ....	2
<b>Table 1.2</b> Targeting peptides either isolated by <i>in vivo</i> biopanning or evaluated <i>in vivo</i> .....	18
<b>Table 1.3.</b> Classification of Microcins .....	48
<b>Table 2.1.</b> Sequence of the NGR peptide library and the relative cell adhesion of the peptides. ....	95
<b>Table 2.2.</b> Amino acid sequence and characterization of the peptides selected from the peptide array-whole cell binding assay. ....	102
<b>Table 3.1.</b> Primary amino acid sequences and characterization (mass spectrometry and HPLC) of cancer targeting peptides studied herein. Substitution of amino acids in analogues 18-1 – 18-10 is shown in blue ( $\alpha$ -amino acids) or red ( $\beta$ -amino acids derived from L-asp). Lower case letters denote D-amino acids, X is Nle, and Z is a $\beta^3$ -residue with a naphthyl side chain. ....	123
<b>Table 4.1.</b> Characterization of peptide doxorubicin conjugates 1 and 2. ....	181
<b>Table 4.2.</b> Effect of Verapamil on IC <sub>50</sub> values of peptide Dox conjugates and Dox in MDA-MB-435 resistant cell line and MDA-MB-435 wild type. ....	195
<b>Table 5.1.</b> The Mass and HPLC purification details for peptide derivatives 1-6 .....	218
<b>Table 5.2.</b> Antibacterial activity of MccJ25 and synthetic peptide derivatives (1 and 6) against Gram-negative bacterial strains .....	227

## List of Figures

---

- Figure 1.1.** Selective tumor targeting using a specific ligand for a receptor that is overexpressed on tumor cells. .... 5
- Figure 1.2.** Schematic representation of different antibody formats, showing intact classic IgG molecules. A variety of antibody variants, including Fab, scFv, and multimeric formats, such as minibodies, diabodies, and Fab' multimers.<sup>16</sup> .... 7
- Figure 1.3.** Antibody-based immunoconjugates are specifically targeted monoclonal antibodies that deliver a cytotoxic payload to their target. The cytotoxic agents can be highly potent drugs, radionuclides or toxins. Such molecules, referred to as antibody-drug conjugates, radioimmunoconjugates and immunotoxins, respectively.<sup>20</sup> ..... 8
- Figure 1.4.** Chemical structure of Cilengitide cyclo(-RGDfV-) peptide. .... 20
- Figure 1.5.** Selection of tumor targeting peptides using *in vivo* phage display. Peptides are displayed on the surface of the phage. Phage recovered from the tumor was amplified and reinjected in mice for another rounds.<sup>87</sup> ..... 25
- Figure 1.6.** Scheme of the split-mix peptide synthesis method. .... 26
- Figure 1.7.** Schematic representation of some commonly used peptide modifications reported to increase proteolytic stability. X and Y represent any chemical group or atom. R1, R2 and R3 correspond to the side chain of any of the 20 natural amino acids ..... 29
- Figure 1.8.** Structures of somatostatin and somatostatin analogs. .... 30
- Figure 1.9.** Chemical structures of various RGD peptides (A) linear RGD, (B) Cyclized RGD, (C) dimers, and (D) tetra-branched peptides. .... 34
- Figure 1.10.** (A) Chemical structures of linear NGR. (B) Chemical structure of cyclic CNGRC peptide (top) and (C) PDB structure (PDB ID: 1FBR) of the human fibronectin type I, 4<sup>th</sup> and 5<sup>th</sup> repeat with GNGRG structure in stick form (bottom). .... 36
- Figure 1.11.** Multistep binding and penetration mechanism of iRGD. The iRGD peptide binds to  $\alpha v$  integrin-expressing cells in tumors. Then peptide is cleaved by a cell surface protease to expose the cryptic CendR element, RXXX/R (red dotted line). The CendR element then mediates binding to neuropilin-1, with resulting penetration of cells and tissues.<sup>113</sup> ..... 38
- Figure 1.12.** (A) Schematic representation of MccJ25 showing the amino acid residues sequence, the lasso structure has two small antiparallel  $\beta$ -sheets between

amino acids 10,11, and 15, 16. (B) Maturation of MccJ25 from the precursor peptide McjA to MccJ25 catalyzed by McjB, and McjC. McJA numbering shown above the sequence, MccJ25 numbering shown below the sequence..... 49

**Figure 1.13.** NMR structures of different lasso peptides.<sup>170</sup> ..... 51

**Figure 2.1.** Expression of aminopeptidase N (APN or CD13) in the cell lines used in this study. Four cell lines, CD13<sup>+</sup> (HUVEC and HT-1080) and CD13<sup>-</sup> (MDA-MB-435 and MDA-231), were incubated with FITC-labeled monoclonal antihuman CD13 antibody (WM15) for 30 min at 4 °C. After washing the cells, the fluorescence of the bound antibody was analyzed by flow cytometry. The mean fluorescence intensity of the cells is shown. .... 96

**Figure 2.2.** Average fluorescence intensity of the peptide bound cells on the cellulose membrane. Cells (75 x 10<sup>3</sup>/mL), CD13<sup>+</sup> (HUVEC or HT-1080) or CD13<sup>-</sup> (MDA-231 or MDA-MB-435), were incubated with the peptide array for 8 hr at 37 °C, followed by labeling of the cells with the CyQUANT dye. The fluorescence intensity of the bound cells was measured using Kodak imager at 465 nm excitation and 535 nm emission. The results are presented as mean fluorescence intensity ± S.D. .... 97

**Figure 2.3.** Solid phase peptide synthesis (SPPS) of FITC-βA-peptide 1 or FITC-1..... 101

**Figure 2.4.** Peptide cell binding and uptake by CD13<sup>+</sup> and CD13<sup>-</sup> cell lines measured using flow cytometry. The peptides (10<sup>-6</sup> mol/L) were incubated with the cells for 30 min at 37 °C. No treatment (NT), and FITC-43 served as negative controls, while FITC-1 served as a positive control. The results are presented as mean fluorescence of cell population (mean ± SD of triplicate wells). .... 103

**Figure 2.5.** Fluorescence microscopy images to evaluate *in vitro* binding of peptide FITC-5 to the cells. (A) HT-1080 (CD13<sup>+</sup>) cells showing uptake of green FITC-5, (B) MDA-MB-435 (CD13<sup>-</sup>) cells after incubation with FITC-5 showing minimal uptake, (C) Zoom-in of a HT-1080 cell using confocal laser microscopy showing intracellular distribution of FITC-5 (scale bar = 12 μm), and (D) HT-1080 cells in the presence of excess unlabelled peptide 5 (10<sup>-4</sup> M) as a competitor. *Green*, signal from FITC labelled peptide; *Blue*, signal from the nuclear staining agent DAPI. .... 104

**Figure 2.6.** (A) Fluorescence microscopy image of a co-culture of HT-1080 (CD13<sup>+</sup>) and MDA-MB-435 (CD13<sup>-</sup>) cells incubated with FITC-5 (green) for 30 min. Peptide (green) was uptaken primarily by HT-1080 cells with very little uptake by MDA-MB-435 cells. The MDA-MB-435 cells were stained blue using cell tracker blue before the experiment. (B) A phase contrast image. Scale bar = 20 μm. .... 105

**Figure 2.7.** (A) Stability of peptide 5 (YNGRT) during storage at 37°C as determined by MALDI-TOF mass spectrometry. MALDI-TOF mass analysis of peptide 5 in DMEM media after incubation at 37 °C for 1 h (B), 4 h (C), and 24 h (D). (B) shows the correct mass for peptide 5 ( $[M+H]^+$  obsd. 610.8; calcd. 610.6), C and D show mass of 593.5, 610.7 and 611.7 corresponding to succinimide derivative, NGR, and *iso*DGR (or DGR), respectively. Inset in (C) shows RP-HPLC of peptide 5 after incubation in DMEM media at 37 °C, at zero time (black) and 4 h (red)..... 107

**Figure 2.8.** Inhibition of aminopeptidase N (APN) activity in the presence of NGR peptides. Intact HT-1080 cells were incubated with peptides or bestatin (a known inhibitor) followed by evaluation of APN activity. The results shown are mean  $\pm$  SD of triplicates..... 109

**Figure 2.9.** Schematic representation of a portion of human fibronectin highlighting NGR motifs present in the type I, II, and III repeats (top). Three dimensional structures of the NGR sequences present in the type I (PDB 1FBR), II (PDB 1QO6), and III (PDB 1FNF) repeats are shown as stick models (bottom). Peptides 21 and 22 most likely form hairpin as found in type I structure (bottom, left to right), peptide 5 folds into type II structure, and peptide 34 which is similar to peptide 5 may form type II structure. An overlay of peptide 5 with type II fold and peptide 34 (red) derived from PDB 3NWJ is shown. LNGRE of type III repeat, which is present in peptide 14, is also shown. .... 111

**Figure 3.1.** Chemical structures of synthesized cancer targeting peptides containing D- or  $\beta$ -amino acids.  $\alpha$ -Amino acids are shown in black (L-amino acids) or blue (D-amino acids) and  $\beta$ -amino acids derived from L-aspartic acid are shown in red..... 125

**Figure 3.2.** Peptide uptake by the cancer cells (top row) MDA-MB-435, MCF-7 and MDA-MB-231, and the control cells (bottom row) HUVEC and MCF-10A measured by flow cytometry. The peptides ( $10^{-5}$  mol/L) FITC-18 (orange), FITC-18-4 (blue), FITC-18-9 (pink), and FITC-18-10 (green) were incubated with the cells for 30 min at 37 °C. Auto-fluorescence of the cells is shown in black. .... 138

**Figure 3.3.** Fluorescence microscopy images of MDA-MB-435 and HUVEC cells after incubation with FITC-18-4 (A) or FITC-18-9 (B) for 30 min at a peptide concentration of  $10^{-5}$  mol/L. Cell nuclei were stained blue with DAPI..... 141

**Figure 3.4.** Optical sectioning using confocal laser microscopy of MDA-MB-435 cells showing intracellular distribution of FITC-labelled peptide 18-9. Cells were incubated with the peptide for 30 min at 37 °C prior to analysis. Scale bars: 20  $\mu$ m. .... 142

**Figure 3.5.** RP-HPLC chromatograms of peptides 18, 18-4, 18-9, and 18-10 after incubation with the human serum (A) and the liver homogenate (B). Peptides

were incubated with the human serum or liver homogenate from mice for different time intervals, namely, 0 h (red), 30 min (black) and 24 h (black) prior to HPLC analysis. Peptides elute around 21-25 minutes. Degradation products from peptide 18 appear around 14-18 minutes, and the remaining peaks are from the media. .... 144

**Figure 3.6.** (A) The NMR solution structures of peptide **p160** in TFE (yellow) and water (red). (B) Comparison of the NMR structures of peptides **p160** (LHS) and 18 (RHS) in TFE. The helical region in 18 extends from Glu3 (E3) to Phe9 (F9). .... 146

**Figure 3.7.** Circular dichroism spectra of peptides (A) 18 and 18-4, and (B) 18-9, and 18-10 in 90% TFE at 25 °C. The peptide concentration was 200 µM. .... 147

**Figure 3.8.** Cytotoxicity of peptides 18-4 (grey), 18-9 (white) and 18-10 (black) compared to doxorubicin (dark grey) monitored in MDA-MB-435 cancer cell line using the MTT assay. Cells were incubated with different concentration of peptides for 48 h. The data represent the mean ± S.D of two independent experiments, and each concentration was done in triplicate. .... 149

**Figure 4.1.** Time-dependent stability of peptide Dox conjugates 1, and 2 in human serum for 48 h. Dox release from the conjugates was determined by C<sub>18</sub> reverse-phase HPLC. The percent of intact conjugate remaining was determined by integrating the area under the curve detected at wavelength of 480 nm. .... 182

**Figure 4.2.** FACS analysis of the uptake of free Dox, peptide Dox conjugates 1 or 2 by different cell lines. Cells (10<sup>6</sup>) were incubated with the different treatments (5 µM) at 37 °C for 2h. Histograms showing peptide uptake by the cancerous cells MCF-7, MDA-MB-435, and MDA-MB-435-MDR, (top row), and the non-cancerous cells MCF-10A and HUVEC (bottom row). Control cells or cell only (black), Dox (red), conjugate 1 (blue), conjugate 2 (green). (B Results of cell uptake presented as change in mean fluorescence intensity relative to untreated cells. Data represent mean SD of triplicate experiments) .... 186

**Figure 4.3.** *In vitro* competition experiment, for cell uptake of free Dox and peptide conjugates 1 and 2 (5 µM) by MCF-7 and MDA-MB-435R cell lines with or without pretreatment with 40 fold excess free 18-4 (200 µM) after 2 h incubation. Results are presented as mean fluorescence intensity. (mean±SD). 187

**Figure 4.4.** Intracellular distribution of free DOX and peptide Dox conjugates 1 and 2 in MDA-MB-345, MCF-10A noncancerous cell line, and MDA-MB-435-MDR cells after 2 h of drug exposure. The cells were treated with equimolar free Dox or Dox conjugates 1, and 2 (5 µM) and visualized under confocal microscope. Merged images display the overlay of nuclear DAPI staining (blue) and Dox autofluorescence (red). Images were obtained at magnification of 400 X. scale bar, 50 µm. .... 190

**Figure 4.5.** (A) In vitro cell cytotoxicity of Dox conjugates 1, and 2 on cancerous cell lines MCF-7, MDA-MB-435, MDA-MB-435-MDR cell lines, and in normal cell lines MCF-10A, and HUVEC. Conjugates cytotoxicity was compared to that of free Dox. Treatments were applied at various concentrations for 48 h in serum free media, and then cell viability was determined using MTT assay. Assay was repeated three times and each conc was in triplicate. Mean±SD, is presented. (B) Cytotoxicity of conjugates 1 and 2 versus free Dox on different cancer cell lines. Mean IC<sub>50</sub> values from three experiments in comparison with doxorubicin. .... 194

**Figure 5.1.** (A) A 58 amino acid McjA precursor peptide is converted into mature antimicrobial form, MccJ25 by McjB and McjC enzymes. The ribbon representation of the lasso structure of MccJ25 (PDB ID code 1Q71)<sup>6</sup> is shown. Antiparallel β-sheets are shown in green and yellow, and the amide bond between residues G1-E8 is shown as stick model. (B) Amino acid sequences of MccJ25 and derived peptides 1-6. Substitutions of amino acids in the peptide derivatives are shown in yellow for cysteine and red for others. .... 213

**Figure 5.2.** Growth curves of microcin J25, peptide 1, and peptide 6 using broth assay against *Salmonella newport*. MICs were defined as the lowest peptide concentration that caused 100% growth inhibition (0.05 AU). .... 228

**Figure 5.3.** Circular dichroism spectra for MccJ25, 1 and 6 in methanol at 25 °C. .... 230

**Figure 5.4.** RP-HPLC chromatograms of peptides 1 (top), 6 (middle) and MccJ25 (bottom) after incubation with pepsin at time 0 and 30 min. On the right side are shown the cleavage sites for the peptides. A linear gradient was run on a C18 Vydac column (4.6 mm x 250 mm) over 35 min from 15 to 50% isopropyl alcohol/water 0.05% (v/v) TFA with a flow rate of 2 mL/min. .... 232

**Figure 5.5.** Effects of treatment with MccJ25, peptide 1 and peptide 6 on the oxygen consumption. Oxygen consumption of bacteria growing in the presence of peptides was expressed as a percentage of the oxygen concentration of the control culture (without peptides). Data correspond to mean values of three independent experiments. Error bars correspond to the standard deviations. .... 234

**Figure 6.1.** (A) Synthesis of MccJ25-18-4 conjugate using on resin fragment condensation. Peptide 18-4 synthesized on a chlorotrityl resin was coupled to MccJ25 peptide using DIC/HOBT for 24 h, and then cleavage from resin and deprotection was done using DCM/TFA mixture. (B) RP-HPLC of purified conjugate compared to native MccJ25. Insert of MALDI-TOF of purified conjugate showing [M+H]<sup>+</sup> 3457.2. .... 251

**Figure 6.2.** (A) *In vitro* MTT cell cytotoxicity of MccJ25-18-4 conjugate, compared to native MccJ25, and free peptide 18-4 in MCF-7, MDA-MB-435, MDA-MB-435-MDR cancer cells, and in normal HUVEC cells. Doxorubicin was

used as positive control. Treatments were applied at various concentrations for 48 h in serum free media. (B) Mean IC<sub>50</sub> values in comparison with doxorubicin. The results shown are the mean values ±SD of three independent experiments, in triplicates. .... 253

**Figure 6.3.** MDA-MB-435 cells was incubated with 10 fold excess of free peptide 18-4 for 10 min at 37 °C, followed by incubation with MccJ25-18-4 conjugate (20 μM) for 48 h, then cell viability was measured using MTT cytotoxicity assay. The results shown are the mean values±SD of three independent experiments, in triplicates. .... 254

**Figure 6.4.** Cell uptake of MccJ25 (A), and MccJ25-18-4 conjugate (B) in MDA-MB-435 cells analyzed by RP-HPLC. Cells were incubated with 20 μM peptide for 48 h and the amount of peptide or peptide conjugate in the cell supernatant and cell lysate was assessed. .... 255

**Figure 6.5.** Flow cytometry analysis of cell death induction in MDA-MB-435. Cells were incubated for 24 h with 20, and 40 μM MccJ25-18-4 conjugate. The left-upper quadrant represents cells stained by PI, while the right bottom quadrant cells stained mainly by Annexin V (early apoptosis). The top right quadrant represents cells stained by both PI and Annexin V (late apoptosis/necrosis). .... 258

**Figure 7.1.** Dual targeting nanocarrier decorated with NGR peptide as well as p18-4 peptide. .... 275

## LIST OF SCHEMES

---

**Scheme 4.1:** Synthesis of peptide-Dox conjugates 1 and 2. Reagents: (a) N-(9-fluorenylmethoxycarbonyloxy) succinimide (Fmoc-OSu), N,N-diisopropylethylamine (DIPEA) in N,N-dimethylformamide (DMF). (b) glutaric anhydride, DMF, DIPEA. (c) Fmoc-NH-W<sub>x</sub>EYAAQkFL-CONH<sub>2</sub>, DMF, NMM, (2-(6-chloro-1H-benzotriazole-1-yl)-1,1,3,3-tetramethylaminium hexafluorophosphate) (HCTU). (d) 20 % piperidine/DMF. .... 180

## LIST OF ABBREVIATIONS

---

aa	Amino acid
ACN	Acetonitrile
ADC	Antibody drug conjugate
ADEPT	Antibody directed enzyme prodrug therapy
AMP	Antimicrobial peptides
APN	Aminopeptidase N
BBB	Blood brain barrier
BCA	Bicinchoninic acid Protein Assay
Boc	t-butoxycarbonyl
BOP	Benzotriazole-1-yl-oxy-tris- (dimethylamino)- phosphoniumhexafluorophosphate
BN	Bombesin
CD	Circular dichroism
CendR	C end rule
DAPI	4',6-diamidino-2-phenylindole
DCB	2,6 dichlorobenzoyl chloride
DCM	Dichloromethane
DIC	<i>N,N'</i> -diisopropylcarbodiimide
DMEM	Dulbecco's modified eagle medium
DMF	<i>N,N</i> -dimethylformamide
DNA	Deoxyribonucleic acid
DOX	Doxorubicin

Et <sub>2</sub> O	Diethylether
FACS	Fluorescence activated cell sorting
Fab	Antigen binding fragment
FAM	5-carboxyfluorescein
FBS	Fetal bovine serum
Fc	Class defining fragment
FDA	Food and Drug Administration
5-FITC	[5 - FITC; fluorescein - 5 - isothiocyanate
Fmoc	9-fluorenylmethyloxycarbonyl
FN	Fibronectin
HCN	Hydrogen, carbon, nitrogen
HCTU	(2-(6-chloro-1H-benzotriazole-1-yl)-1,1,3,3-tetramethylammonium hexafluorophosphate)
HEPES	(4-(2-hydroxyethyl)-1-piperazine ethanesulfonic acid )
hEGFR	Human epidermal growth factor receptor
HOBt	1-hydroxybenzotriazole
Ig	Immunoglobulin
mAb	Monoclonal antibody
LRP-1	Lipoprotein receptor-related protein 1
LHRH	Luteinizing hormone releasing hormone
MALDI-TOF	Matrix-assisted laser desorption ionization time-of-flight

	spectrometry
MBC	Minimum bactericidal concentration
MccJ25	Microcin J25
MDR	Multidrug resistance
MIC	Minimum inhibitory concentration
MRI	Magnetic resonance imaging
MTT	(3-(4,5-Dimethylthiazol-2-yl)-2,5-diphenyl tetrazolium bromide
NMR	Nuclear magnetic resonance
NMM	N-methyl morpholine
NT	Neurotensin
OBOC	One bead one compound
OD	Optical density
OtBu	<i>tert</i> -butoxy
PBS	Phosphate buffer saline
PET	Positron emission tomography
P-gp	P-glycoprotein
PTX	Paclitaxel
RCA	Relative cell adhesion ratio
RNAP	RNA polymerase
RP-HPLC	Reversed-phase HPLC
r.t.	Room temperature
SAR	Structure activity relationship
scFv	Single chain fragment variable

SCID	Severe combined immunodeficiency
SST	Somatostatin
tBu	<i>tert</i> -butyl
TFE	2,2,2-trifluoroethanol
TFA	Trifluoroacetic acid
TIPS	Triisopropylsilane
TNF	Tumor necrosis factor
Trt	Trityl
VEGF	Vascular endothelial growth factor
Vp	Verapamil

## Amino acids Abbreviations

---

Ala (A)	Alanine
Arg (R)	Arginine
Asn (N)	Asparagine
Asp (D)	Aspartic acid
Cys (C)	Cysteine
Gln (Q)	Cysteine
Glu (E)	Glutamic acid
Gly (G)	Glycine
His (H)	Histidine
Leu (L)	Leucine
Lys (K)	Lysine
Phe (F)	Phenylalanine
Pro (P)	Proline
Tyr (Y) Proline	Proline
Val (V)	Valine
Trp (W)	Tryptophan
Nle(X)	Norleucine
$\beta$ -Ala (Z) Norleucine	Norleucine

# **Chapter 1 : Introduction**

## 1.1. Peptides Therapeutics

Peptide based therapeutic market is undergoing a very exciting revival in the last two decades. The pharmaceutical industry becomes highly interested in peptides as potential drug candidates. This interest is at least partially a result of the widespread acceptance of protein therapeutics by patients and physicians, and development of solutions to peptide problems such as short half-life and synthesis on large scale.<sup>1</sup> In addition, therapeutic peptides offered an effective and innovative solution for a wide variety of therapeutic areas with unmet medical needs, in particular, cancer therapy, metabolic disorders (diabetes, obesity, and osteoporosis), treatments for allergy, immunological disorders, and cardiovascular diseases. To date, there are almost 60 marketed peptide drugs worldwide, approximately 270 peptides in clinical-phase trials, and approximately 400 in advanced preclinical phases.<sup>1,2</sup> A list of some of the approved peptide therapies for various applications are depicted in **Table 1.1**<sup>3</sup>

**Table 1.1.** List of some of the FDA approved peptide based therapeutics in the market.

Brand name	Generic name	Indication	Approval year
Sandostatin LAR Depot®	Octreotide acetate	Acromegaly	1988
Lupron Depot®	Leuprolide acetate	Prostate Cancer	1993
Miacalcin®	Calcitonin	Osteoporosis	1995
Fuzeon®	Enfuvirtide	Anti-HIV	2003
Symlin®	Pramlintide	Diabetes	2005
Byetta®	Exenatide	Diabetes	2005

The growth rate in the peptide market is significantly higher than small organic molecules that make up most traditional medications. This is because therapeutic peptides offer several advantages over small entities. First, peptides offer greater efficacy, selectivity and specificity.<sup>4</sup> Second, the degradation products of peptides are amino acids, thus there is low risk of systemic toxicity.<sup>5</sup> Third, peptides have short half-life, so do not accumulate in the tissues, thus there is low risk of complications caused by their metabolites.<sup>5</sup>

In this thesis, we explored the usefulness of peptide therapeutics in two areas which gained high attention from various research groups in the last two decades. The first area is the potential use of tumor-specific peptides for selective delivery of chemotherapeutics in cancer therapy. The second area is the use of antimicrobial peptides either for combating pathogenic strains as an alternative to conventional antibiotics, or their use as anticancer therapy.<sup>6,7</sup>

## **1.2. Tumor Targeting Peptides**

### **1.2.1. Limitation of Conventional Cancer Therapy**

Despite the significant improvement in our understanding of cancer and the different methods used in its treatment, still it remains a leading cause of mortality around the world. An estimated 186,400 new cases of cancer, and 75,700 deaths from cancer will occur in Canada in 2012. Of the newly diagnosed cases, more than one-half will be lung, colorectal, prostate and breast cancers.<sup>8</sup> Difficulty in treating cancer originates from the fact that the standard first line treatments such as surgery, radiation, and chemotherapeutics all have significant limitations.

Surgery and radiation can just destroy primary tumors, and they are unable to eradicate metastatic tumors. In contrast, systemically administered chemotherapeutics can target both primary and metastatic tumors. But they inhibit cell division non-specifically, thereby causing severe toxicities in normal replicating tissues such as hair follicles, bone marrow and digestive system. Side effects that occur as a result of toxicities lead to administration of anticancer chemotherapeutics at suboptimal doses, resulting in the eventual failure of therapy, this is often accompanied by the development of drug resistance and metastatic disease.<sup>9</sup>

A wide array of strategies has been developed to enhance the selective delivery of chemotherapeutic drugs to the tumor site with reduced toxicity, and overcome emergence of multidrug resistance in tumors.<sup>10,11</sup> One avenue to accomplish this feat is targeted delivery of therapeutic molecules to the tumor cells, or tumor microenvironments by means of ligands that are specific for tumor-associated markers or receptors. Researchers have discovered by studying the distinct nature of the tumor tissue and its microenvironment, that tumor cells carry molecular markers that are not expressed or are expressed at much lower levels in normal cells.<sup>12,13</sup> These markers are mostly proteinous in nature, and identification and characterization of ligands with high affinity to these markers can lead to specific accumulation of cytotoxic molecules at the tumor site (**Figure 1.1**).<sup>14</sup> In this regard, different ligands have been identified and studied for tumor selective drug targeting, such as antibodies, peptides, aptamers, affibodies, hormones and some low molecular weight compounds, such as folate and some vitamins. These

ligands allow specific delivery of drugs to the cancer cells either by direct conjugation, or it can be conjugated to the surface of different drug carrier delivery systems, such as liposomes and micelles.

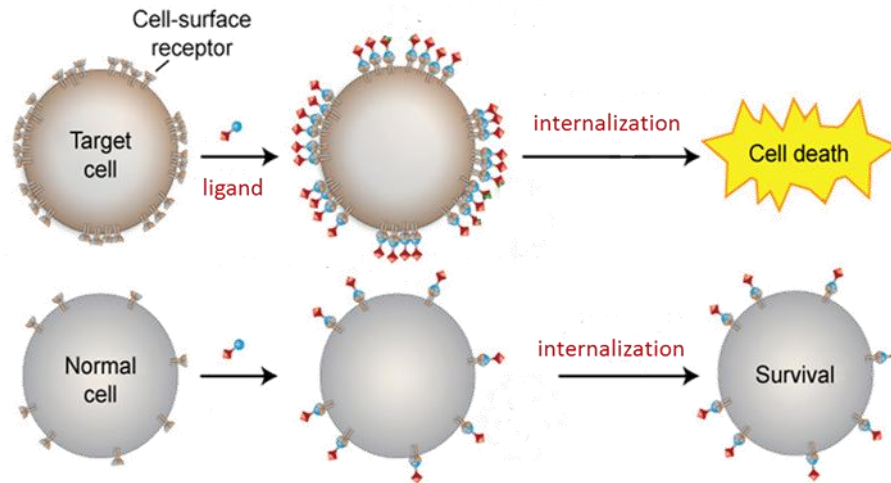


**Figure 1.1.** Selective tumor targeting using a specific ligand for a receptor that is overexpressed on tumor cells.

## 1.2.2. Different Tumor Targeting Ligands

In this section the different ligands of proteinous nature (antibodies, affibodies, and peptides) used in tumor targeting are discussed, and pros and cons of each are presented.

### 1.2.2.1. Monoclonal Antibodies

The identification of tumor specific markers overexpressed by cancer cells has enabled researchers to develop antibodies that can specifically target these

markers. Antibodies are by far the most studied ligands used for tumor targeting. A monoclonal antibody (mAb) or immunoglobulin (Ig) is a Y-shaped protein, and it has five subclasses (IgG, IgA, IgM, IgE, IgD). IgG antibody is the main antibody and almost the exclusively used in therapeutic applications. Structurally, the antigen-binding sites are located on the two Fab tips and immunity functions are mediated by the stem Fc domain (**Fig. 1.2**). Initially, the antibodies used for therapeutic purposes were created by murine hybridoma technology. Consequently, antibodies originated from murine origins elicit an immune response against the antibodies themselves, which in turns reduces the therapeutic efficacy. With the recent development in antibody engineering, small recombinant antibody fragments lacking the Fc site which elicit immune response were developed, including Fab, scFv, and engineered variants (diabodies, triabodies, minibodies and single-domain antibodies). The drawback of using shorter fragments was the reduced antibody binding avidity.<sup>15</sup> Various structures of antibodies and antibody variants are presented in **Figure 1.2**.

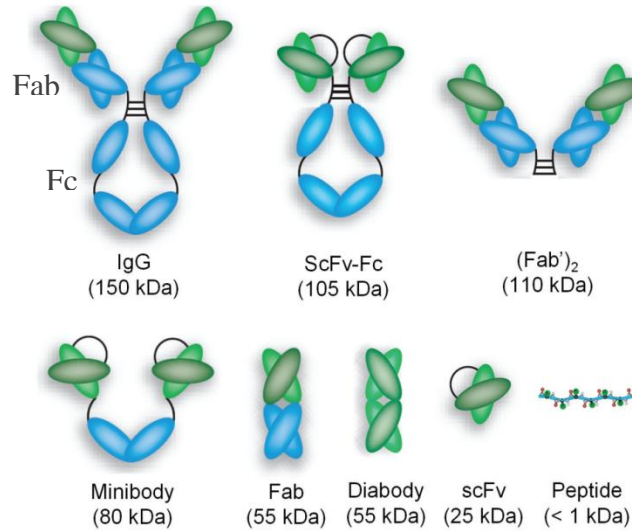


**Figure 1.2.** Schematic representation of different antibody formats, showing intact classic IgG molecules. A variety of antibody variants, including Fab, scFv, and multimeric formats, such as minibodies, diabodies, and Fab' multimers.<sup>16</sup> (Adapted from reference 16, free access)

Targeting antibodies towards markers on the surface of tumor cells has given rise to four strategies (**Figure 1.3**). First, an antibody can be used as a single entity that is therapeutically effective by itself, where it binds to and inhibits tumor growth by inhibiting ancillary functions of these receptors. This approach has been validated through the development of trastuzumab (Herceptin™) and bevacizumab (Avastin™). Second, a drug can be directly attached to a tumor-specific antibody to guide it to tumor cells,<sup>17</sup> an example is gentuzumab ozogamicin (Mylotarg™). A third antibody strategy involves the use of antibodies to guide an attached radioactive element or drug delivery system to the tumor site.<sup>18</sup> This approach was exemplified by pentumomab (Theragyn™), an antibody labeled with yttrium-90. A fourth strategy involves

the use of antibodies to guide a prodrug/drug-releasing enzyme to tumor cells, it is called antibody-directed enzyme prodrug therapy (ADEPT). This technique can be simplified as follows; the monoclonal antibody is given first (with the enzyme attached). A few hours later, a pro-drug is given; the pro-drug is an inactive anti-cancer drug. When the pro-drug comes into contact with the enzyme, a reaction takes place which activates the anti-cancer drug.<sup>19</sup>

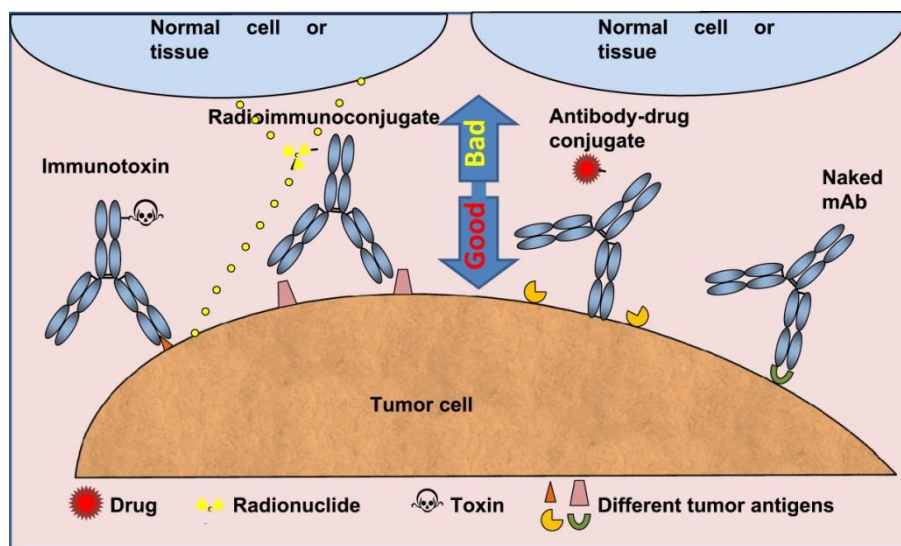


**Figure 1.3.** Antibody-based immunoconjugates are specifically targeted monoclonal antibodies that deliver a cytotoxic payload to their target. The cytotoxic agents can be highly potent drugs, radionuclides or toxins. Such molecules, referred to as antibody-drug conjugates, radioimmunoconjugates and immunotoxins, respectively.<sup>20</sup> (Adapted with permission from reference 20)

Numerous pre-clinical and clinical efficacy studies have shown that antibody drug conjugates enhance the antitumor activity of naked antibodies, plus they reduce the systemic toxicity of the cytotoxic drugs conjugated to the antibody.<sup>17</sup>

To date, there are many FDA approved monoclonal antibodies for cancer treatment (some are listed above) with dozens more in clinical trials.<sup>21</sup>

Although monoclonal antibodies offer many attractive features for tumor targeting, they are also linked with different disadvantages that hamper their clinical application. Antibodies are known to be unstable both in terms of proteolysis and shelf-life. In addition, antibodies are large in size having a molecular weight of approximately 160 kDa, which hinders them from entering the tumor site and increase the manufacturing cost. To overcome this, researchers developed single chain antibodies that are smaller in size, Mw 25 KDa. Furthermore, despite the recent use of humanized antibodies, still their application *in vivo* is limited by their high immunogenicity.<sup>22</sup> Another major problem with mAb therapy is the nonspecific uptake of the antibody molecules into the reticuloendothelial system such as the liver, spleen, and bone marrow causing major toxicities to these organs.<sup>23</sup>

#### **1.2.2.2. Affibodies**

Affibodies are another group of tumor targeting ligands that have been studied. An affibody molecule (Affibody AB) is a small (7 kDa) engineered affinity protein, typically 50-70 amino acids long. It is based on the combinatorial protein engineering of the small and robust  $\alpha$ -helical structure of the domains of protein A.<sup>24</sup> Different studies have shown the excellent targeting capabilities of affibody ligands to the extracellular domain of human epidermal growth factor

receptor 2 (HER2), a marker that is overexpressed in ~ 20-30% of breast cancers. In one study, different affibodies were isolated by *in vitro* phage display from a combinatorial protein library, based on the 58 amino acid residue staphylococcal protein A-derived Z domain.<sup>25</sup> Selected affibody ligands bind to HER2 with nanomolar affinity (KD ~50 nM). In another study, a bivalent affibody ligand was constructed by head-to-tail dimerization and shown to have an improved affinity to HER2 (KD~ 3 nM) compared to the monovalent affibody.<sup>26</sup> Moreover, radiolabeled affibody ligands showed specific binding *in vitro* to native HER2 molecules expressed in human cancer cells. Biodistribution studies in mice carrying SKOV-3 xenografted tumors revealed that significant amounts of radioactivity were specifically targeted to the tumors *in vivo*, and the tumors could easily be visualized with a gamma camera. Furthermore, affibodies showed promising results in targeting HER-2-positive cancer cells by conjugating affibody to nanoparticle encapsulating paclitaxel.<sup>27</sup> These results collectively suggest that affibody ligands would be interesting candidates for specific tumor targeting in clinical applications, such as *in vivo* imaging and radiotherapy.

Despite the smaller size of affibodies with respect to antibodies, still they have some disadvantages which hamper their clinical application. Affibodies are proteins in nature, so any physical or chemical alteration in its secondary structure during preparation or storage can have a significant impact on their biological activity *in vivo*.

### **1.2.2.3. Peptides**

In recent years, investigators have turned their attention to the use of peptides and peptidomimetics in cancer targeting as an alternative to previously mentioned targeting moieties. Peptide-based therapeutics offered multiple advantages in cancer targeting compared to large proteins such as antibodies, and affibodies. Peptides have the potential to penetrate deep into tissues owing to their smaller size, they are generally less immunogenic than recombinant proteins and antibodies. Peptide synthesis is very well developed using automated solid phase methodology, allowing rapid synthesis in good yields and cost effective (synthetic versus recombinant). Peptide conjugation to different cargos is much easier and reproducible than conjugation to big proteins. Moreover, peptides have higher stability (length of storage at room temperature).<sup>28</sup> In addition aforementioned advantages, studies have shown that peptide can mimic carbohydrates to target carbohydrate overexpressed receptors expressed on tumor.<sup>29</sup> It is already known that carbohydrates production by recombinant technology is a tedious process. Peptide mimics solved this dilemma, Fukuda and her colleagues have employed peptide-displaying phage technology and identified peptides that function as carbohydrate ligands,<sup>30</sup> they focused on selectin which normally binds carbohydrates during tumor cell metastasis. Screening a phage display library of small peptides with a selectin probe identified a peptide that binds selectin. When the researchers injected labeled versions of this peptide into mice with tumors, the peptides homed specifically to the tumors and inhibited metastasis.<sup>31</sup>

With the advent of the *in vivo* peptide phage display technology, a variety of peptides were expressed on the surface of phage, and then analyzed for their binding affinity to different tumor markers in different tissue types.<sup>32-34</sup> Using this technique, several peptides that target proteinous antigens preferentially expressed on tumors or tumors microenvironment have been identified, and new ones continue to be discovered.<sup>35</sup> Currently, the peptide tumor-targeted therapies follow two main strategies: i) targeting of tumor cells, via tumor associated antigens, specifically expressed or over expressed by tumor cells and, ii) targeting of tumor vasculature via vascular overexpressed antigens, examples of each groups are presented in section **1.2.3**. The goal of the first strategy is the selective targeted delivery of cytotoxic moieties to cancer cells, with the consequent death of tumor cells and low or no damage to healthy tissues. In the second strategy, the goal is to target tumor vessels and specifically impair them through inhibition of pro-angiogenic growth factors, which produces tumor starvation and reduced tumor cell access to the blood stream with consequent reduced metastasis. The use of peptide-based ligands for selective delivery of a wide variety of therapeutics such as radionuclides, cytotoxic entities, and other agents to malignant tumors is a highly effective targeting approach, and it holds a great promise for clinical applications in cancer diagnosis and therapy.<sup>31</sup> A full database of tumor homing peptides was recently published.<sup>36</sup> The term “cancer targeting peptides” are generally applied for peptides evaluated *in vitro* or *in vivo*, but tumor targeting peptides are for peptides which were assessed *in vivo*.

### 1.2.3. Classification of Tumor Targeting Peptides

Tumor targeting peptides are classified into two general classifications: peptides targeting tumor cell-surface receptors or peptides targeting tumor vasculature. While it is not feasible to discuss all potential cancer targeting peptides discovered so far within the framework of this thesis, one could consider some of the potential peptide sequences which had their *in vivo* targeting capacity evaluated. A list of the *in vivo* evaluated targeting peptides is presented in **Table 1.2**.

#### 1.2.3.1. Tumor Cell Surface Targeting Peptides

Tumor targeting peptides are often selected for their binding to cell surface proteins involved in biological functions such as cell surface receptors, growth factor receptors and cell adhesion molecules. Different peptide sequences targeting various types of cancers have been exploited.

**Breast cancer** In 2001, Zhang *et al.* reported that an *in vitro* phage-displayed peptide library screening against WAC 2 neuroblastoma cell line yielded a linear 12-mer peptide VPWMEPAYQRFL (p160) that also targets the breast cancer cell line MDA-MB-435.<sup>37</sup> Askoxylakis *et al.* in another study showed that p160 is internalized into MDA-MB-435 cells, and clustered at the cellular membrane. Intravenously injected <sup>131</sup>I-labeled p160 was demonstrated to specifically accumulate in xenografts of the breast tumor as compared with heart, spleen, liver and brain and the perfusion of the mice decreased radioactivity in nonspecific tissue.<sup>38</sup> In a way to screen for better analogues of p160, we

developed a high throughput peptide array library screening method in our lab, and we synthesized a library of 70 peptide sequences derived from p160 peptide on a cellulose membrane, and screened it against MDA-MB-435 and MCF-7 human breast cancer cells. Five newly identified peptide analogues of p160 with higher affinity for breast cancer cell lines were discovered, among them, (p11) RGDPAYQGRFL, and (p18) WXEAAYQRFL have displayed 2-3 fold increase in specific affinity for breast cancer cells compared to lead p160.<sup>39</sup>

**Prostate carcinoma** Zitzmann *et al.* used a 12-mer phage-displayed peptide library to screen for ligands of the DU-145 prostate carcinoma cell line.<sup>40</sup> After six rounds of biopanning, all sequenced phage clones were determined to display the same peptide FRPNRAQDYNTN (DUP-1). Synthetic DUP-1 peptide bound and internalized in prostate carcinoma cells DU-145 and PC-3 cells, but not to normal HUVECs or the benign prostate cell line PNT-2. DUP-1 peptide accumulated specifically in DU-145 and PC-3 xenografts *in vivo*, and perfusion decreased non-specific accumulation in the kidney and blood. DUP-1 *in vivo* biodistribution was also evaluated using the AT-1 rat prostate adenocarcinoma model. In rats, DUP-1 accumulated in cancerous prostate tissue threefold compared to normal prostate tissue and muscle. The authors reported that DUP-1 was degraded in human, mouse and rat serum within ~ 10 min and suggested *in vivo* stabilization experiments with this lead structure. Optimization of DUP-1 was carried out to increase stability *in vivo*.<sup>41</sup>

**Hepatocellular carcinoma** Li *et al.* screened a phage-displayed peptide library against recombinant human epidermal growth factor receptor (hEGFR) *in*

*vitro*, and isolated the phage displaying YHWYGYTPQNVI peptide (GE11).<sup>42</sup> Synthetic free GE11 peptide and epidermal growth factor (EGF) inhibited phage binding to human EGF receptor (hEGFR), as well as the EGFR-positive human hepatocarcinoma cell line SMMC-7721. These results demonstrated the binding specificity of GE11 peptide for EGFR and the overlap of EGF and GE11 binding sites. *In vivo* biodistribution studies showed that <sup>125</sup>I-labelled GE11 specifically accumulated in SMMC-7721 tumor in mouse xenografts at 4 h post intravenous injection. Li *et al.* further demonstrated that GE11-coated PEI/DNA polyplexes could target SMMC-7721 xenografts *in vivo*, and cause an 18-fold increase in luciferase expression in the tumor as compared with non-coated PEI/DNA polyplexes.<sup>42</sup>

Du *et al.* screened a pool of disulfide-constrained 7-mer, and linear 12-mer phage displayed peptide libraries *in vitro* against the human hepatocellular carcinoma cell line BEL-7402.<sup>43</sup> Phage, bearing (WP05) TACHQHVRMVRP peptide bound specifically to BEL-7402 cells. Peptide specificity for hepatocellular carcinoma was further demonstrated by showing FAM-labeled WP05 peptide bound to BEL-7402, BEL-7404, SMMC-7721 and HepG2 cells, but not to HL-7702 normal liver cells using fluorescence microscopy and flow cytometry. WP05 phage injected intravenously into mice bearing BEL-7402 tumors accumulated in the tumor as opposed to normal mouse liver tissue.

**Gastric cancer** Akita *et al.* reported the three amino acid motif lysine-leucine-proline (KLP) that targeted peritoneal metastases of gastric cancer derived from the AZ-P7a cell line in BALB /nu mouse xenografts.<sup>44</sup> *In vivo* biopanning with a

phage-displayed peptide library was exploited by peritoneal injection of the library and harvesting metastatic nodules for the binding phages. *In vitro* and *in vivo* competition experiments showed that synthetic SWKLPPS peptide significantly inhibited SWKLPPS-displaying phage from binding to metastases, indicating that targeting was attributed to the peptide moiety. SWKLPPS-coated liposomes accumulated in the peritoneal metastases more efficiently than non-coated liposomes. Furthermore, treatment with SWKLPPS-coated liposomes containing doxorubicin enhanced antiproliferative effects compared with non-targeted control liposomes.

**Pancreatic cancer** Tanaka *et al.* reported that expression of growth factor receptor-bound protein 7 (Grb7) was upregulated in 61% of pancreatic cancer specimens, and this upregulation was correlated with lymph node metastasis.<sup>45</sup> The authors then demonstrated that Grb7 siRNA abrogated Grb7 expression and resulted in reduced pancreatic cancer cell migration into fibronectin. A non-phosphorylated peptide inhibitor of Grb7 SH2 domain G7-18NATE, which was previously identified using filamentous phage display technology was conjugated to a penetratin sequence to facilitate targeting and internalization into human pancreatic cancer cells (Panc-1) for evaluation of metastasis inhibition.<sup>46</sup> Treatment of cells with the peptide conjugate did not alter proliferation, but did reduce migration into fibronectin. To evaluate the peptide inhibitor *in vivo*, BALB/c mice were injected intraperitoneally with Panc-1 cells, followed by peptide inhibitor treatment over 2 weeks. Treatment with the Grb7 inhibitor

peptide successfully targeted Panc-1 cells, and resulted in drastically limited pancreatic tumor cell migration and metastases.

Huang *et al.* screened a 12-mer phage-displayed peptide library *in vitro* against irradiated Capan-2 human pancreatic adenocarcinoma cells, thereafter the isolated binding phage were subjected to subtractive screening on non-irradiated Capan-2 cells.<sup>47</sup> A synthetic peptide SHGFSRHSMTLI (PA1) was shown to target and internalize into irradiated Capan-2 cells, but not to non-irradiated cells using flow cytometry. Furthermore, they showed that intraperitoneally injected PA1 could target subcutaneous xenografts of irradiated Capan-2 tumors in mice, but not non-irradiated xenografts.

### **1.2.3.2. Vascular Targeting Peptides**

#### **a. Peptides Homing to Tumor Blood Vessels**

Molecular, structural, and functional studies have revealed extensive differences between the normal vasculature, and tumor blood vessels which can be used in selective tumor targeting. Tumor blood vessels were shown to be leaky and tortuous.<sup>48</sup> In addition, angiogenic tumor blood vessels express molecular markers that are expressed at low levels or entirely absent in resting quiescent blood vessels, and the ease of accessibility of these surface proteins by the blood stream makes them ideal targets.<sup>49</sup> Furthermore, malignant tumor cells are prone to mutations, in contrast, the tumor vasculature cells are considered to be genetically stable and thus less prone to drug resistance, a common feature of

neoplastic cells due to prolonged treatment with anticancer drugs.<sup>50</sup> Collectively, such favourable characteristics highlighted the significance of vascular targeting approach in cancer therapy.

**Table 1.2.** Targeting peptides either isolated by *in vivo* biopanning or evaluated *in vivo*

Cancer Type	Peptide Sequence (Name)	Selection Method	Receptor
<i>Tumor Specific</i>			
<b>Breast</b>	VPWMEPAYQRFL (p160)	Phage display mouse xenograft	ND
<b>Prostate</b>	FRPNRAQDYNTN (DUP-1)	Phage display mouse xenograft	ND
<b>Hepatocarcinoma</b>	YHWYGYTPQNVVI (GE11)	Phage display mouse xenograft	hEGFR
	TACHQHVRMVRP (WP05)	Phage display mouse xenograft	ND
<b>Pancreatic</b>	Penetratin sequence conjugated G7-18NATE	Phage display mouse xenograft	growth factor receptor-bound protein 7 (Grb7)
	SHGFSRHSM TLI (PA1)	Phage display mouse xenograft	ND
<b>Gastric</b>	SWKLPPS	Phage display mouse xenograft	ND
<i>Tumor Vasculature</i>			
<b>Tumor angiogenic vessels</b>	CDCRGDCFC (RGD-4C)	Phage display mouse xenograft	Integrins ( $\alpha v\beta 3$ and $\alpha v\beta 5$ )
	CNGRCVSGCAGRC (NGR)	Phage display mouse xenograft	Aminopeptidase N
<b>Tumor lymphatic vessels</b>	CGNKRTRGC (LyP-1)	<i>ex vivo/in vivo</i> screen on mouse xenograft	p32/gC1qR

Numerous peptides homing specifically to tumor blood vessels have been identified. (**Table 1.2**) Many of the specific molecular markers in tumor vessels are associated with angiogenesis such as integrins. Angiogenesis, is the formation of new capillaries from pre-existing vessels for tumor nourishment and progression. Anti-angiogenic therapy acts by eliminating new vasculature has

proven to be a promising concept in tumor targeting based on the destruction of tumor microvasculature.<sup>51</sup> RGD (Arg-Gly-Asp)<sup>52</sup>, and NGR (Asn-Gly-Arg)<sup>53</sup> peptide motifs discovered through the *in vivo* phage display represent the first-generation of vascular homing peptides, and they will be discussed in details.

The RGD motif was originally discovered *in vitro* in peptides that bind to different integrins which are overexpressed in vasculature of tumors.<sup>54,55</sup> Thereafter, the RGD peptide was shown to home *in vivo* to malignant melanoma, and breast carcinoma xenografts after intravenous injection into tumor-bearing mice.<sup>52</sup> The RGD peptides have high affinity towards the integrins expressed in the angiogenic vasculature, in particular,  $\alpha\beta3$  and  $\alpha\beta5$ .<sup>54</sup> Along with integrins binding, RGD peptides are also capable of internalizing into the cells, causing cell death, and interrupting angiogenesis process.

A considerable number of synthetic peptides containing RGD have been developed, including ACDCRGDCFCG (RGD-4C), CRGDC (RGD-2C) which have different beneficial abilities.<sup>56</sup> By using knockout mice to show the effects of the RGD-4C peptide, it was shown that RGD-4C has anti-angiogenic effects. Using multiple angiogenesis assays in these knockout strains, RGD-4C repeatedly demonstrated anti-angiogenic capabilities.<sup>57</sup> The use of tumor targeting peptides in general and RGD peptide in particular was validated with Cilengitide (EMD 121974, Merck). It is an anti-angiogenic agent derived from RGD peptide used in the treatment of glioblastoma (**Figure 1.4**). It is the inner salt of a cyclized RGD pentapeptide (cyclo-[Arg-Gly-Asp-DPhe-(NMeVal)]), and it is a selective  $\alpha\beta3$  and  $\alpha\beta5$  integrin antagonist. A number of phase I and II clinical trials for

assessing its anti-angiogenic activity, either as monotherapy or in combinations were conducted, and results showed great targeting efficacy.<sup>58,59</sup> Currently it is undergoing phase III clinical trial. RGD peptides have been widely used for targeting, imaging, and treating tumors in preclinical models.<sup>60,61</sup>

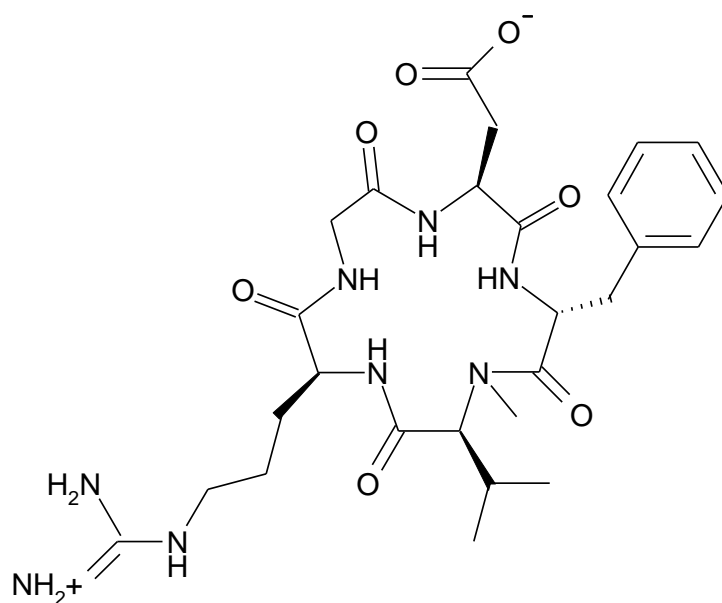


**Figure 1.4.** Chemical structure of Cilengitide cyclo(-RGDfV-) peptide.

The NGR peptide motif was identified in an *in vivo* screen on human breast carcinoma xenografts.<sup>53</sup> Likewise this motif was originally identified as a cell adhesion motif,<sup>55</sup> and it homes selectively to tumor blood vessels and other types of angiogenic vessels. The receptor for the NGR peptide is a peptidase, aminopeptidase N (APN), which is upregulated in the tumor angiogenic blood vessels.<sup>62</sup> APN is not only a biomarker for angiogenic blood vessels, but it plays a functional role in these vessels, antibodies against APN inhibit tumor angiogenesis.<sup>62</sup> Curnis *et al.* reported NGR-conjugated IFN- $\gamma$  stimulated

antitumor activity in lymphoma and fibrosarcoma mouse models as compared with IFN- $\gamma$  alone. Results showed that NGR-TNF treatment decreased tumor growth with smaller doses than free protein.<sup>63</sup> The antitumor activity of NGR-TNF- $\gamma$  was also studied in combination with various chemotherapeutic drugs: doxorubicin, melphalan,<sup>64</sup> cisplatin, paclitaxel, gemcitabine,<sup>65</sup> and compared to the efficacy of the chemotherapeutic drugs alone in various murine tumor models. The results showed that targeted delivery of low doses of NGR-TNF- $\gamma$  to tumor vasculature increased the efficacy of various drugs acting via different mechanisms. Moreover, in transgenic mice, pre-treatment with NGR-TNF- $\gamma$  increased the therapeutic index of doxorubicin and delayed tumor growth significantly without increasing drug-related toxicity.<sup>66</sup> CNGRC-TNF conjugate (NGR-TNF) is being tested in phase I and II clinical studies.<sup>67,68</sup> Studies demonstrated that peptides containing NGR motif can undergo spontaneous deamidation and generate Asp and *iso*Asp degradation products. The transition of NGR to *iso*DGR/DGR is associated with loss of CD13 binding and gain of  $\alpha\beta$ 3-integrin binding.<sup>69</sup>

#### **b. Peptides Homing to Tumor Lymphatics**

Peptides targeting tumor lymphatic vessels have also been identified using phage display (**Table 1.2**).<sup>70,71</sup> The first identified lymphatic homing peptide was the LyP-1 CGNKRTRGC.<sup>72</sup> This peptide was identified using a combination of an *ex vivo/in vivo* screen on MDA-MB-435 xenografts in nude mice. LyP-1 homed to the tumor-associated lymphatic vessels as well as to tumor cells in the hypoxic areas of tumor, but it did not home to the tumor blood vessels. The LyP-

1 receptor is a cell surface form of a mitochondrial protein p32.<sup>73</sup> p32 shows unusual cell surface expression in tumor lymphatics, tumor cells, and a subset of myeloid cells, which adds to the specificity of LyP-1 homing to tumors.<sup>73</sup> Recently, a peptide named RMS-II (CMGNKRSKRPC) was identified to bind to rhabdomyosarcoma cell lines, and it showed some sequence similarity to LyP-1.<sup>74</sup> However, RMS-II homed better to the RMS xenografts *in vivo* than LyP-1. Furthermore, RMS-II recognized tumor blood vessels, and not tumor lymphatic vessels indicating different specificities of these two peptides.<sup>74</sup>

Another study showed that using two lymphatics homing peptides with homologous sequences LyP-1 (CGNKRTRGC) and LyP-2 (CNRRTKAGC), home to lymphatics of different tumor types.<sup>75</sup> LyP-1 recognizes the lymphatics and tumor cells in MDA-MD-435 melanoma, MMTV-PyMT breast carcinoma, and KRIB osteosarcoma xenografts as well as their metastatic lesions but not in the C8161 melanomas, while the LyP-2 peptide homes to the lymphatics of the C8161 melanomas and K14-HPV16 skin and cervical carcinomas but not to the MDA-MB-435 tumors.<sup>75</sup> The specificity of these peptides was further demonstrated by conjugation of the two peptides with different fluorophores followed by simultaneous injection into the same animals.<sup>75</sup> LyP-1 homed only to the lymphatics of MDA-MB-435 tumors and LyP-2 to the lymphatics of K14-HPV16 cervical carcinomas.<sup>75</sup> These studies indicate that tumor lymphatics are similar to tumor blood vessels in that they express tumor type-specific markers that are distinct from the blood vessel markers of the same tumor.

#### **1.2.4. Methods Used in the Discovery and Optimization of Cancer Targeting Peptides**

The discovery of cancer targeting peptides can be accomplished by either a rational design approach or by random combinatorial methods. The rational design approach is initiated by selecting an endogenous peptide sequence known to interact with specific receptor, then using standard synthesis methods to determine region of peptide critical for receptor binding affinity, by carrying out N and C truncation, alanine scan, and D-amino acid scan. Once the minimal sequence is identified and optimized, it can be used in different peptide receptor targeting strategies. Good examples, are octreotide against somatostatin receptor,<sup>76</sup> bombesin against bombesin receptor,<sup>77</sup> and bradykinin analogues against bradykinin receptor.<sup>78</sup>

In contrast, combinatorial peptide libraries enable the random discovery of high affinity peptide ligands to vast number of receptors including ones that have unknown endogenous ligands.<sup>79</sup> The general combinatorial peptide library methods are as follows: phage display combinatorial peptide library, one-bead one compound combinatorial bead library (OBOC), a solution phage display with the affinity chromatography method,<sup>80</sup> and spatially addressable library screening methods, such as the multipin technology, spot synthesis, and light directed synthesis method.<sup>80</sup> The phage display and the OBOC are the most common techniques used for tumor targeting peptides identification.

Phage display peptide library is a biological method first reported by George Smith in 1985.<sup>81</sup> It used a phage mostly filamentous M13 that infect bacterial cells to present peptide or protein sequence on its surface after inserting an expression vector. A phage display library is created by preparing a random mixture of phage clones with each displaying a single peptide on the surface. The library is then exposed to intact cell or a protein target of interest present on solid support (*in vitro*), or directly in mouse (*in vivo*), then cells were removed, washed to elute all non-bound phages, and then amplification of the hit peptide allows for adequate quantity of phage material to be produced, and the encoding region of the phage is then sequenced (**Figure1.5**). The screening of phage-display peptide libraries has been reported in cancer patients as well.<sup>82,83</sup> One limitation of the phage display is the use of only natural amino acids, as it is not possible to generate peptides with D- or unnatural amino acids using phage display, but is possible to have cysteine cyclized libraries with constrained conformation.<sup>84</sup> Different reports have created an entirely D-isomer peptide through a mirror image method using phage display.<sup>85,86</sup> In this context, the phage library expressing the random L isomer peptide will generate L isomer peptide that binds to the D isomer protein target. Thus the natural D isomer peptide will interact with the natural L isomer protein target. In general, phage display method has shown great success in generating multiple lead peptides for the development of tumor targeting therapeutics.<sup>32,53</sup>

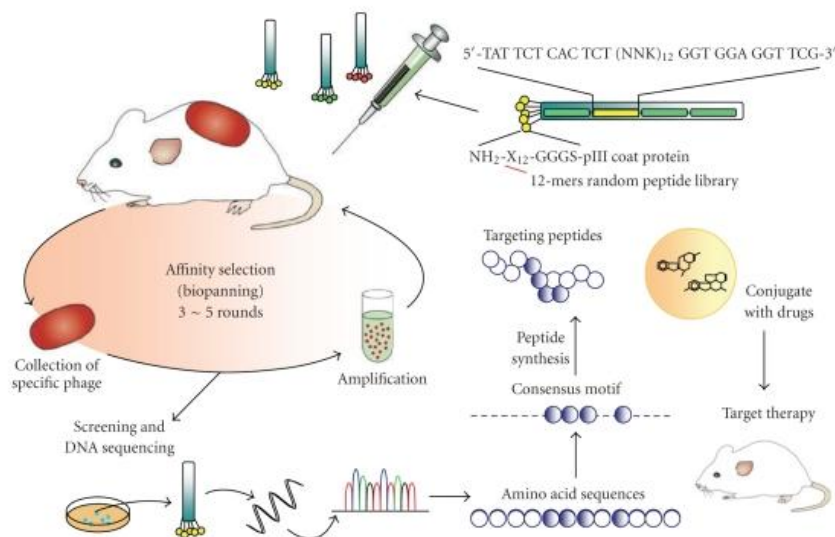


**Figure 1.5.** Selection of tumor targeting peptides using *in vivo* phage display. Peptides are displayed on the surface of the phage. Phage recovered from the tumor was amplified and reinjected in mice for another rounds.<sup>87</sup> (Adapted from reference 87, free access).

One bead one compound library (OBOC) was first discovered by Kit Lam group in 1991.<sup>88</sup> It is a chemical method as previously mentioned. In brief, it involves the creation of an entirely random library on a polymer support using split mix synthesis (**Figure 1.6**). Tentagel polymer is preferred as it supports the screening of a library against the protein of interest or intact cells in aqueous medium. This method start by dividing the resin beads into a number of equal portions, with each portion having single amino acid coupled to it, after reaction completion, all of the resin is combined, thoroughly mixed and once again divided equally following by coupling of the second amino acid. This method has an advantage of the inclusion of non-natural amino acids in sequence. This method has been utilized in the discovery of many cancer targeting peptides.<sup>79,89</sup>



cell lines, and at least five derived sequences that showed 2-3 fold increase in binding affinity to breast cancer cell lines were identified.<sup>39</sup>

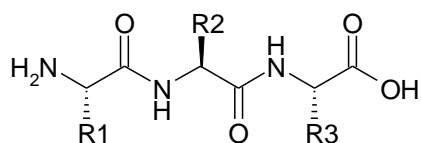
### **1.2.5. Improving the *In Vivo* Behavior of Peptides**

Previously mentioned peptide identification tools have generated a large number of cell-binding peptides with potential therapeutic activities. However, the use of peptides in tumor targeting has its own limitations which restrict its clinical application in cancer therapy. Peptides have low oral bioavailability, short half-life, they can be quickly eliminated from the circulation by the liver and kidneys, they have a low binding affinity to the receptor, and their high conformational flexibility results sometimes in a lack of selectivity leading to side effects. In this respect, I will briefly review in the next section some common approaches that have been undertaken for improving the characteristics of peptides selected from phage-display libraries to allow for their clinical application.

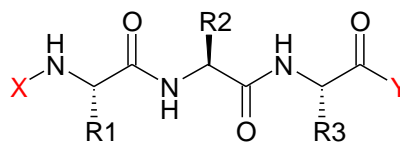
#### **1.2.5.1. *In Vivo* Proteolytic Stability**

Peptide metabolic instability *in vivo* is common for natural L-amino acid peptides as they degrade within minutes. This would in turn affect targeting ability of peptides as reported in different studies.<sup>38,91</sup> Fortunately, this can be overcome by using a variety of peptide backbone structural modifications known

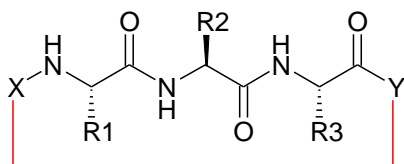
to prevent proteolytic degradation (**Figure 1.7**).<sup>92</sup> For instance, the action of exopeptidases (enzymes hydrolyze from the N- or C-termini) can be avoided by structural modification of the termini, such as amidation of the C-terminus and acetylation of the N-terminus. Moreover, the action of endopeptidases (enzymes hydrolyze within the peptide) may be prevented by modification of the amino acids at the labile sites with various unnatural amino acids such as D-amino acid or beta amino acid. Thus, this renders the site of hydrolysis unrecognizable to the proteolytic enzymes. Peptide cyclization is another established method to increase peptide proteolytic stability, as it diminishes the exposure of the linear peptide sequence to the enzymatic active site.



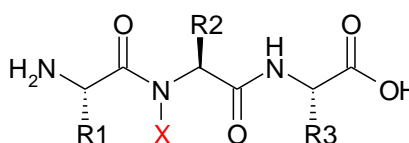
**A. L-amino acid backbone**



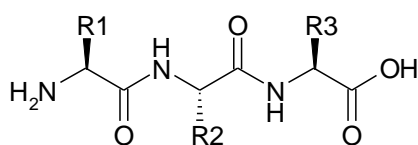
**B. Peptide ends modifications**



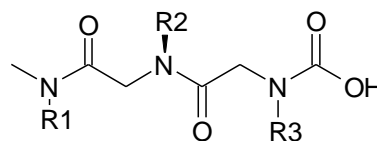
**C. Peptide cyclization**



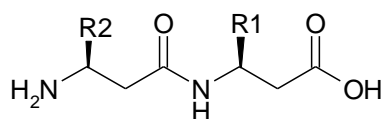
**D. Peptide nitrogen alkylation**



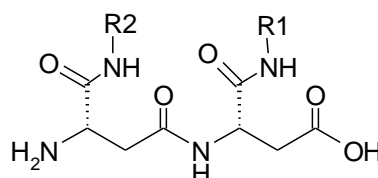
**E. D-amino acid peptide**



**F. Peptoid**



**G. Beta amino acid**



**H. Beta amino acid from L-Asp**

**Figure 1.7.** A schematic representation of some commonly used peptide modifications reported to increase proteolytic stability. X and Y represent any chemical group or atom. R1, R2 and R3 correspond to the side chain of any of the 20 natural amino acids

There are various examples from the literature for peptides modifications to enhance their proteolytic stability; for instance, somatostatin (SST) is a naturally occurring cyclic disulphide-containing peptide with either 14 or 28 amino acids (**Figure 1.8**), that binds to tumors that overexpress SST receptors with high affinity. Both have a short plasma half-life (3 min) which prevent their

*in vivo* use.<sup>93</sup> Several synthetic SST peptide analogs that are more resistant to proteolytic degradation have been prepared by molecular modifications preserving most of the biological activity of the original SST peptide.<sup>94</sup> Introduction of the D-amino acids, and decreasing the ring size to the bioactive core sequence, resulted in an 8-amino acid-containing SST analog, “octreotide” (**Figure 1.8**), that preserves the 4-amino acid motif (Phe-D-Trp-Lys-Thr) of native SST-14 involved in receptor binding and has a significantly longer plasma half-life of 1.5-2 h, making it suitable for clinical application as compared to endogenous SST. Other developed proteolytically stable SST receptor-targeting analogs include lanreotide and vapreotide (RC-160).

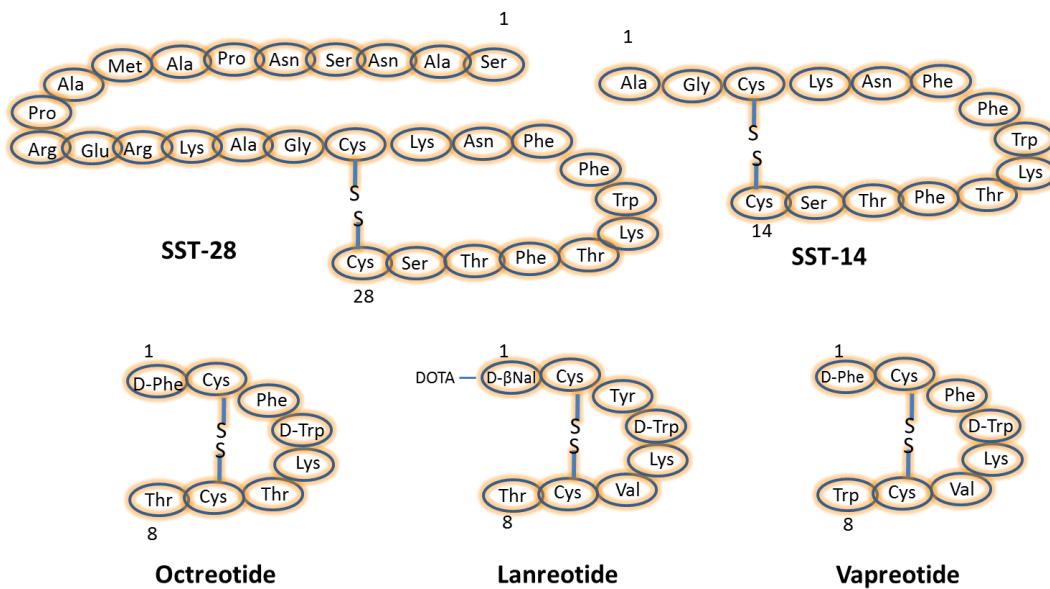


**Figure 1.8.** Structures of somatostatin and somatostatin analogs.

Furthermore, linear RGD-peptides demonstrated high susceptibility to proteolytic degradation.<sup>95</sup> RGD peptide cyclization using disulfide bond linkage in CRGDC confers rigidity to the peptide and it became more stable. Another study showed that D-amino acid modification in RGD flanking residues have yielded RGD-peptide ligands with increased specificity and nanomolar affinity.<sup>96</sup>

### **1.2.5.2. Peptide Affinity Optimization**

Generally, peptides directly isolated from phage display bind to their targets with low affinity (micromolar range). Thus, it would be necessary to increase the affinity of the peptides to their putative receptors to improve their targeting efficiency. As RGD tripeptide motif is well known to bind integrin  $\alpha_v\beta_3$ , there have been many structure activity relationship studies looking at different RGD peptides to identify features that can enhance the binding affinity and the specificity of these molecules.

Cyclization of the RGD moiety besides increasing peptide stability as previously mentioned has produced many compounds with improved affinity, and selectivity for integrin  $\alpha_v\beta_3$ . Structure activity relationship studies showed that RGD peptide cyclization via linkers, such as S-S disulfide, thioether, and rigid aromatic rings or other heterocycles, leads to increased receptor binding affinity and selectivity.<sup>97,98</sup> For instance, ACDCRGDCFCG (RGD-4C) was at least 20-fold more potent than similar peptides with a single disulfide bond, and 200-fold more potent than commonly used linear peptides.<sup>54</sup> Cyclization confers rigidity to

structure, orient conformation at the receptor binding motif similar to that of the natural receptor, which in turn increased binding affinity to integrins. A cyclic RGD pentapeptide framework is found to increase the binding affinity and selectivity regardless of which amino acid is placed at position 5 c(RGDfK), c(RGDfE), and c(RGDfV) (**Figure 1.9**), all three analogues show similar binding affinity.<sup>98</sup> As mentioned previously, the first phase III trial has been launched with cilengitide, a cyclic RGD peptide targeting integrins  $\alpha_v\beta_3$  and  $\alpha_v\beta_5$  in brain cancer glioblastoma.

For a further step towards improving peptide binding affinity, multivalency concept originated.<sup>99</sup> Recently, several laboratories have used bivalent or multivalent cyclic RGD moieties to attain high affinity ( $\sim 10$  nM) for  $\alpha_v\beta_3$ .<sup>100</sup> Since the natural mode of interactions between integrin  $\alpha_v\beta_3$  and RGD-containing proteins, such as vitronectin, and fibronectin, may involve multivalent binding sites, the idea to improve the integrin  $\alpha_v\beta_3$  binding affinity with multivalent cyclic RGD peptides could provide more effective antagonists with better targeting capability, and higher cellular uptake. Multivalent interactions are used in such a way that weak ligand-receptor interactions may become biologically relevant.<sup>101</sup>

As targeting biomolecules for imaging purposes, the first cyclic RGD dimer E[c(RGDfK)]<sub>2</sub> was developed for imaging purposes, and other researchers recently have reported E[c(RGDyK)]<sub>2</sub>.<sup>102</sup> These molecules have about 20 bond distances between the two cyclic RGD motifs and this is not long enough for each

motif to bind to adjacent integrin  $\alpha_v\beta_3$ .<sup>99</sup> However, enhanced binding rate is achieved with dimers as binding of one RGD motif would significantly increase the local concentration of the second RGD motif.<sup>99</sup> (**Figure 1.9 C**)

Besides RGD dimerization, researchers have applied multivalent concept and prepared RGD peptide tetramers and they showed better integrin binding affinity than monomeric and dimeric analogues. Different linkers are used to conjugate monomeric peptides to one another, such as small flexible molecules (e.g., a few ethylene glycol units) or larger carriers (e.g., a leucine zipper variant or the IgG Fc-region).<sup>103</sup> Furthermore, multivalency not only greatly improves the affinity but also facilitates internalization.<sup>104</sup>

Oligo-branched peptides are novel tumor targeting agents that combine the advantages of antibodies and small molecules. They allow multimeric binding with enhanced binding affinity, despite a much smaller size compared to antibodies, it is easily synthesized and chemically modified like small molecules.<sup>105</sup> The solid-phase synthesis of branched peptides was first described by Tam in 1988,<sup>106</sup> and it is based on using trifunctional amino acids to construct branched peptide-based molecules, typically lysine is usually preferred. One lysine will allow synthesis of a two-branched peptide; three lysines will give rise to a tetra-branched peptide and so on (**Figure 1.9D**). It has been suggested that oligo-branched peptides is switching from the strategy of magic bullets to that of magic forks.

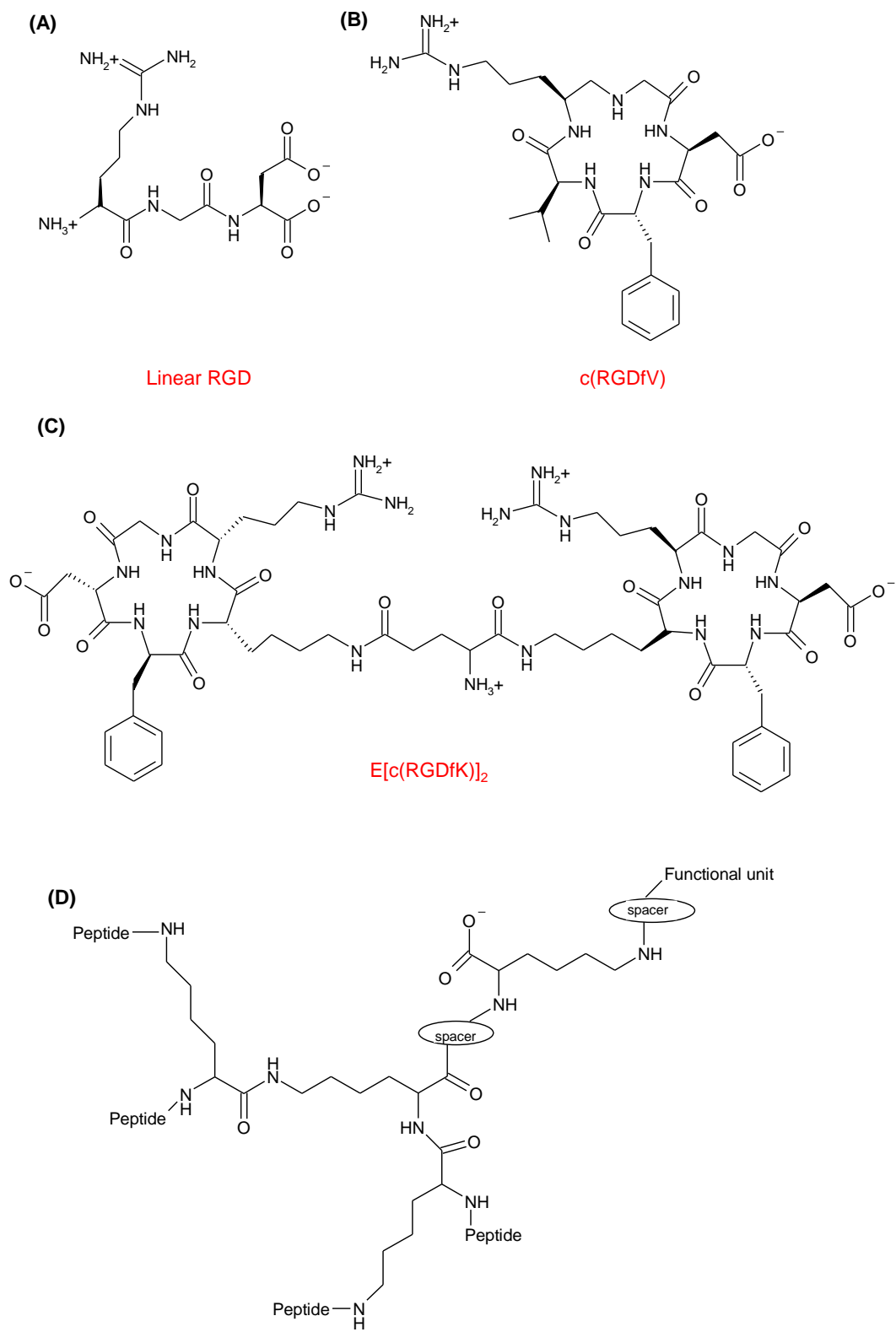


**Figure 1.9.** Chemical structures of various RGD peptides (A) linear RGD, (B) Cyclized RGD, (C) dimers, and (D) tetra-branched peptides.

A proof of concept for the use of oligo-branched peptides as an efficient tool in tumor targeting has been explored with the use of neurotensin peptide (NT) in its tetrameric form (NT4), whose receptor is overexpressed in several human malignancies. NT4 binds to cell membrane receptors more efficiently than the monomeric homologous sequence, and can be coupled to different effector units for either cancer imaging or therapy.<sup>107</sup> Furthermore, conjugation of cytotoxic drugs to NT4 provides an *in vitro* and *in vivo* peptide receptor-mediated cytotoxic effect, increasing drug selectivity toward receptor-positive cells.<sup>107</sup> Another advantage of the use of oligo-branched peptides besides having high binding affinity is the long half-life, as they were found to degrade extremely slow by blood peptidases.<sup>107</sup>

Coming to NGR peptide motif, structure activity relationship studies of CNGRC and GNGRG peptides showed that the presence of Cys residues and disulphide constraint has increased tumor targeting efficiency.<sup>108</sup> Disulphide bond has been shown to constraint bend geometry of CNGRC involving Gly-Arg sequence by stabilizing it.<sup>108</sup> However, molecular dynamic simulation experiments showed that unconstrained GNGRG peptide also tends to form a loop regardless of the fact that it does not have disulphide bridge by populating a  $\beta$ -turn conformation which is stabilized by hydrogen bond between the terminal Gly and Asn. (**Figure 1.10**)

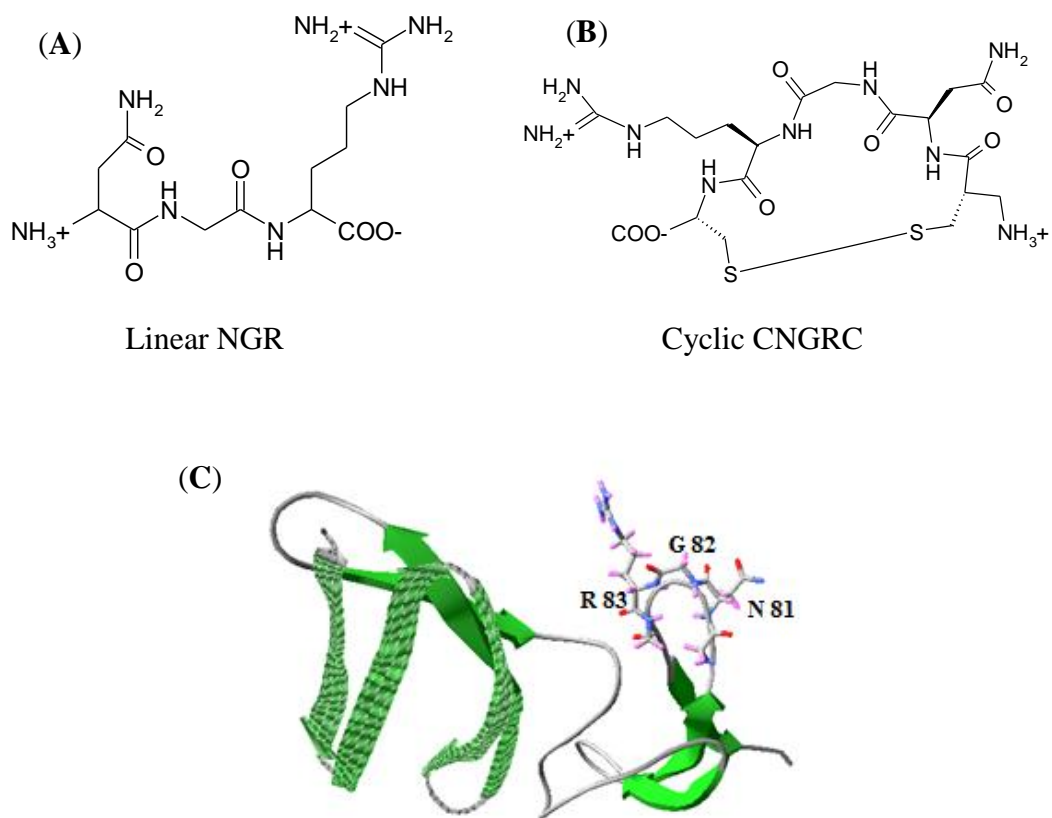


**Figure 1.10.** (A) Chemical structures of linear NGR. (B) Chemical structure of cyclic CNGRC peptide (top) and (C) PDB structure (PDB ID: 1FBR) of the human fibronectin type I, 4<sup>th</sup> and 5<sup>th</sup> repeats with GNGRGR structure in stick form (bottom).

### 1.2.5.3. Improving Tumor Penetration

The success of targeted cancer therapy depends on the ability of the targeted drug molecules to reach primary and/ or metastatic sites, and to penetrate deeply into the tumor.<sup>109</sup> Peptide sequence CRGDKGPDC named the internalizing RGD (iRGD), has been identified by screening cyclic CX<sub>7</sub>C peptide library against tumor vasculature of human prostate cancer.<sup>110</sup> Unlike the conventional RGD peptides discussed above, the iRGD motif has ability to penetrate and become

dispersed throughout the tumor tissue.<sup>110</sup> This motif can also bind to other types of cancer including xenografts of pancreatic ductal, and breast cancer. The mechanism underlying the iRGD tissue penetration occurs through a three-step process: the RGD motif binds to  $\alpha\beta$  integrins on the cell surface, a proteolytic cleavage then exposes a binding motif for neuropilin-1 (CRGDK fragment), and this mediates the penetration into tissue and cells (**Figure 1.11**). The binding motif is following a specific consensus R/KXXR/K named (C-end rule),<sup>109</sup> that is known to bind neuropilin-1 a known mediator of vascular permeability induced by vascular endothelial growth factor (VEGF).<sup>111</sup> Accordingly, the CendR peptides increased vascular leakage and tissue penetration.

In fact, it has been shown that the iRGD peptide can enhance the delivery of chemotherapeutics to solid tumors, added to that it can do so without requiring any chemical conjugation processes with drug molecules. When drugs such as doxorubicin and trastuzumab were co-injected with the iRGD peptide, the drug potency and accumulation in the target site have improved.<sup>110</sup> Also, iRGD conjugated to the surface of loaded nanoparticles used to treat glioblastoma in mice caused eradication of most tumors in one model and delayed tumor development in another model.<sup>112</sup>

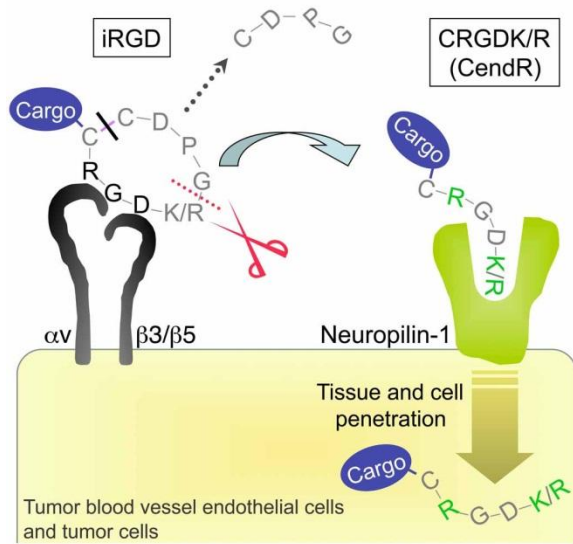


**Figure 1.11.** Multistep binding and penetration mechanism of iRGD. The iRGD peptide binds to  $\alpha_V$  integrin-expressing cells in tumors. Then peptide is cleaved by a cell surface protease to expose the cryptic CendR element, RXXK/R (red dotted line). The CendR element then mediates binding to neuropilin-1, with resulting penetration of cells and tissues.<sup>113</sup> (Adapted with permission from reference 113)

### 1.2.6. Cancer Targeting Peptides in Drug Delivery

Cancer targeting peptides have shown a great promise in both drug delivery to tumors or tumor molecular imaging techniques. Peptide drug targeted delivery to cancer is achieved mainly by either conjugating cancer specific peptides to chemotherapeutic drugs, or use these peptides to decorate the surface of different drug carriers (nanoparticle, micelles, dendrimers, and liposomes ) that encapsulate anticancer drugs and deliver them preferentially to targeted tumor sites.<sup>114,113,115</sup> Each method has its own advantages, peptide drug conjugates have high specificity and they can penetrate the tumor better than a large nanocarrier.<sup>116</sup> Whereas, drug carriers such as liposomes, and polymers can carry more drug molecules per targeting event and have longer circulation

times. Generally speaking, tumor specific delivery of chemotherapeutics by either way increases the therapeutic efficiency of anticancer drugs, and limit toxicity to normal tissue. Accordingly, the phenomena of incomplete tumor response, or the development of drug resistance stemming from suboptimal doses is reduced.<sup>117</sup> Overall, this will maintain the quality of the cancer patient's life while efficiently attacking the cancer.

In drug delivery, peptides offer multiple advantages compared to other methods of delivery such as phages, adenoviruses or antibodies. First, there is a total absence of infectious material. Second, the sequence of the peptide can be reduced just to the binding domain only, thus excluding risks of undesired effects due to side sequences. Peptides can be easily modified with unnatural amino acids or cyclized to improve stability and/or binding affinity. Peptides can be modified with various chemical reactive groups to attach different types of chemical groups from drugs or from drug delivery systems (liposomes, nanoparticles). Peptides can be stored freeze-dried, thus limiting the problems of long term storage, transport and distribution. Overall, peptides are considered as excellent targeting moieties for the selective delivery of chemotherapeutics and diagnostics to tumor sites.

### **Peptide Drug Conjugates**

Initially, research was focusing on generating antibody drug conjugates (ADCs) for tumor selective drug delivery. This approach combined the best features of both small-molecule drugs and antibodies to create a single therapy

that is highly specific and cytotoxic. Apart from ADCs in clinical trials, such as Inotuzumab ozogamicin (CMC-544) for B-cell lymphomas (II), rentuximab vedotin for Lymphomas (phase III), a number of research studies are currently ongoing on many other ADCs.<sup>118</sup> Despite the progress in this field, there are still limitations in using ADC in drug delivery which hamper their widespread application. The main limitation is the synthetic assembly of the antibody drug conjugates. Conjugation of the antibody to the drug mostly occurs at cysteines or lysines on the antibody, the products of such conjugations are heterogeneous, with variations in the number of molecules of drug per antibody and in the sites of attachment.<sup>119</sup> The number of the drug molecules loaded per antibody is also an important variable that has to be controlled. Changing this ratio can affect the properties of the ADC. Increasing the number of drug molecules can potentially lead to higher concentrations of the drug at the target sites. However, greatly modifying the antibody molecule can lead to loss of affinity for the target, aggregation and precipitation of the antibody due to lowered solubility, and faster clearance of the ADC.<sup>120</sup> Peptides drug conjugates offer solutions for most of the mentioned problems, as it is possible to control peptide drug ratio, and the chemistry of conjugation is much easier, owing to the small size of peptide, it can better escape from the vasculature and diffuse through the interstitial space of tumor. Along with that there is a low chance of eliciting an immune response when compared to antibodies.<sup>116</sup> Another advantage is that some peptide drug conjugates were found to escape p-glycoprotein efflux that causes drug resistance,

on the contrary, the activity of many ADCs was poor in cells that express these efflux pumps.<sup>121 122</sup>

Several reported studies have shown a promising future for the use of tumor targeting peptides in drug delivery. Tumor targeting peptides have been extensively studied in the delivery of a wide variety of cargos such as antisense oligonucleotides, toxins, chemotherapeutic drugs and proapoptotic peptides.<sup>123</sup> Remarkable success in targeting the antitumor agent cytokine TNF into tumors has been reported with RGD and NGR peptides, the targeted cytokine was effective in doses as much as 1,000-fold lower than the usual dose and effectively decreasing side effects as a result of the high toxicity of this cytokine.<sup>124</sup> A randomized double-blind phase III study of NGR-TNF (in combination with chemotherapy or supportive care) started in 2010 in patients with malignant pleural mesothelioma (<http://www.clinicaltrialsfeeds.org/clinical-trials/show/NCT01098266>).

Dox (Doxorubicin) and 2-pyrrolino-Dox have also been conjugated to LHRH agonist and antagonist peptides for selectively targeting cancer cells. The ability of LHRH-Dox conjugate to inhibit cancer cell growth (i.e., breast, prostate, mammary, and ovarian cancer cells) was comparable to that of the corresponding individual drugs.<sup>125</sup> *In vivo* studies indicated that the drug-agonist conjugates are less toxic and more potent than the corresponding individual drugs (i.e., Dox and 2-pyrrolino-Dox) this was due to the selectivity of the conjugate to target cancer cells. In another study, a doxorubicin-RGD4C conjugate (doxo-RGD4C) was synthesized for drug targeting to the vasculature of breast tumor model which

express  $\alpha\text{v}\beta\text{3}$  in the angiogenic blood vessels and by the tumor cells themselves. Conjugate proved to be equally effective as free doxorubicin *in vitro* and, more importantly, demonstrated improved inhibition of tumor growth and spreading of metastases in mice.<sup>126</sup> In addition to an improved efficacy, doxo-RGD4C also displayed reduced toxicity to liver and heart.

Peptide drug conjugates found its way to clinical trials. GRN1005 is a novel peptide-drug conjugate composed of three molecules of paclitaxel covalently linked to a 19-amino acid peptide angiopep-2, that targets the low-density lipoprotein receptor-related protein 1(LRP-1), one of the most highly expressed receptors on the surface of the blood brain barrier BBB and it is in phase II clinical trial. GRN1005 was well tolerated and showed activity in heavily pretreated patients with advanced solid tumors, including those who had brain metastases and/or failed prior taxane therapy.<sup>127</sup> GRN1005 is a prodrug, which becomes activated in cells only after it is cleaved by esterases to release active paclitaxel from the peptide. In addition,<sup>128</sup> Emons *et al.* prepared a conjugate of Dox linked to [D-Lys6] LHRH and encouraging results with the conjugate in women with LHRH receptor-positive tumors were obtained, and phase II clinical studies of this conjugate (AN-152, AEZS-108 (Æterna Zentaris Inc)) have started in 2008.<sup>129</sup>

### **Peptide Nanocarrier Conjugates**

The use of peptide decorated drug loaded nanocarriers such as liposomes, micelles, and polymers for tumor targeted delivery has been extensively

studied.<sup>130,131</sup> Reported studies showed that peptide targeted nanocarriers are more effective in reducing tumor growth and in enhancing survival in mice when compared to nontargeted ones. Examples of reported studies are listed below.

Peptide RGD is the first tumor targeting peptide that has been used to decorate nanocarriers to improve the therapeutic efficacy of the loaded chemotherapeutic drug. RGD4C-decorated polymeric micelles effectively improved the therapeutic efficacy of Dox in SCID mice bearing wild or resistant MDA-MB-435 tumor.<sup>132</sup> In another study, NGR liposomal doxorubicin was administered to mice in three cycles of 3 mg/kg/week dosing, it showed rapid tumor regression and metastasis inhibition while mice treated with mismatched peptide targeted liposomal doxorubicin formed large neovasculature.<sup>133</sup> In a third study, peptide p160 decorated micelles showed better binding and internalizing in MDA-MB-435 cells than c(RGDfK)-micelles. It enhanced the selective cytotoxicity of encapsulated paclitaxel (PTX) against MDA-MB-435 cells over normal HUVEC and MCF-10A cells. The extent of this increase in cancer cell encapsulated PTX was more for p160-decorated micelles than c(RGDfK)-decorated ones.<sup>134</sup>

### **1.2.7. Cancer Targeting Peptides for Diagnostic Application**

In recent years, there has been a great interest in the use of cancer targeting peptides for *in vivo* diagnostic applications due to its high tumor selectivity.<sup>135,136</sup> Peptides are considered as an ideal receptor-guided vectors in tumor imaging, this is derived from their favorable pharmacokinetic

characteristics. Peptides can tolerate harsh conditions (pH, temperature, etc.) during chemical modifications and diverse radiolabeling techniques. Because of their compact size, peptides have tumor uptake with concomitant rapid clearance from blood and non-target tissues. Peptides have been attached to a variety of dyes and fluorescently nanoparticles, such as quantum dots, for *in vivo* optical fluorescence imaging.<sup>137</sup>

Different peptide sequences have shown promising results in tumor imaging, the best example is somatostatin analogs that target somatostatin receptor overexpressed in neuroendocrine tumors. <sup>111</sup>In-DTPA-octreotide (<sup>111</sup>In-Octreosan) is the first US Food and Drug administration approved diagnostic radiopeptide for the imaging of patients with neuroendocrine tumors..<sup>138</sup> Other naturally occurring peptides sequences such as, bombesin/gastrin releasing peptides have shown a great promise in the visualization of BN/GPR overexpressing tumors including prostate, breast, and lung cancer.<sup>139</sup> A number of other specific peptides, such as vasoactive intestinal peptide, neurotensin, and cholecystokinin/gastrin are currently under preclinical or clinical investigation to determine their true potential in the diagnosis or treatment of human cancer.<sup>140</sup>

The RGD peptide has been used for targeted delivery of various imaging agents. RGD-conjugated radiolabeled iron oxide nanoparticles were used to image subcutaneous human glioma xenograft tumors using positron emission tomography/magnetic resonance imaging (PET/MRI) dual-modality imaging system.<sup>141</sup> Moreover, the RGD-targeted MRI-detectable, fluorescent liposomes and the RAD-peptide targeted control liposomes accumulated in the tumor by

different mechanisms. The RGD-liposomes were specifically associated with the activated tumor endothelium, while the RAD-liposomes were located in the extravascular compartment.<sup>142</sup> Cyclic NGR peptide (cNGR) was successfully used for targeted imaging of angiogenic vessels in the ischemic heart.<sup>143</sup> These studies show the potential use of peptide-targeted delivery of imaging agents for tumor imaging and visualization.

### **1.3. Peptides as Antimicrobial Agents**

With the widespread of bacterial resistance to current antibiotic drugs, researchers have been interested in the development of antimicrobial peptides (AMPs) as a novel therapeutic approach to treat bacterial infections. In the last three decades, efforts geared towards understanding the structure and function of antimicrobial peptides to gradually replace or reinforce the roles of antibiotics in therapeutic applications.

AMPs are molecules found among all classes of life including animals, plants, bacteria, amphibians, and insects. They are an integral component of the natural defenses of most living organisms against bacteria, viruses, fungi, parasites, and tumor cells. In addition, antimicrobial peptides have also been reported to modulate various processes in the body such as inflammation, chemotaxis, and the release of cytokines.<sup>144</sup> The likelihood of the emergence of resistance for AMPs is thought to be considerably low compared with that of many current antibiotics. This could be due to their non-specific mode of action,

as they disrupt the bacterial cell membrane, and in many cases they may have multiple targets within cells which prevent microorganisms from developing common resistance strategies.<sup>145</sup> To date, several antimicrobial peptides were investigated, and some molecules have reached phase III clinical studies. Among them is a derivative (MSI-78) of magainin, isolated from the skin of the African frog, denoted Pexiganan, for the treatment of impetigo and diabetic foot ulcer.<sup>146</sup> A derivate (IB-367) of pig protegrin, denoted Isegranin, is used for the treatment of oral mucositis.<sup>147</sup> Neuprex (a derivate of the human bactericidal permeability protein, rBPI23) is used for the treatment of sepsis, and Omiganan against catheter associated infections (administered as a 2% gel).<sup>148</sup> Antimicrobial peptides database is a good resource for relevant information on AMPs.<sup>149</sup>

### **1.3.1. Microcins Classification and Mode of Action**

Bacteriocins are ribosomally synthesized, antimicrobial peptides produced from Gram positive or Gram negative bacteria to inhibit the growth of similar or closely related bacterial strain(s).<sup>150</sup> Generally, bacteriocins produced by Gram-negative bacteria can be divided into two groups, namely the colicins and the microcins. Colicins are large (25- to 80-kDa) bactericidal proteins.<sup>151</sup> Microcins are smaller (<10 kDa) in size, and they are non-lethal for the producing strains.<sup>152</sup>

Microcins are antimicrobial peptides produced by and active against *E. coli* and its close relatives. They are actively secreted into the extracellular medium during the late log phase of growth in nutritionally minimal media, except,

MccE492, which is mainly produced during the early log phase.<sup>153</sup> The antimicrobial activity spectrum of the known microcins is directed against genera of *Enterobacteriaceae* such as *Escherichia*, *Salmonella*, *Shigella*, *Citrobacter*, *Klebsiella* and *Enterobacter*. Fifteen microcins have been identified so far. They are classified into two classes. (**Table 1.3**)

**Class I** microcin is a post-translationally modified peptides with a mass of less than 5 kDa with activity against intracellular targets. Members of this group are microcins B17, C7, and J25.<sup>154</sup> **Class II** microcins are unmodified peptides with a molecular mass between 8 and 10 kDa. They exert their function through membrane depolarization. Microcins in this group are further divided to two subclasses **Ia**, that have disulfide bonds, and **Ib** that are linear with C-terminal modifications. Members of this group are microcins E492, H47, 24, L and colicin V.<sup>154</sup>

Microcins are essentially hydrophobic peptides, which most often exhibit a high stability to extreme temperatures and pH(s), and a low sensitivity to proteases, as a result of their posttranslational modifications or/and their compact three-dimensional structures.<sup>155</sup> The microcin group comprises peptides that differ widely with respect to their structure and mode of action. For example, microcin B17, a peptide that contains thiazole and oxazole rings, targets the DNA gyrase, microcin C7, which carries a C-terminal adenosine monophosphate, inhibits protein biosynthesis,<sup>156</sup> and microcin E492 permeabilizes the cytoplasmic membrane in its unmodified as well as in its modified form, and Microcin J25

inhibit RNA polymerase.<sup>157</sup> In the next section, Microcin J25 (MccJ25) antimicrobial peptide structure function relationship will be presented.

**Table 1.3.** Classification of Microcins

Microcin	Class	No of aa	Mechanism of action
MccB17	I	43	DNA gyrase inhibition
MccC7	I	7	Aspartyl-tRNA synthetase inhibition
MccJ25	I	21	RNA polymerase inhibition
MccV	IIa	88	Membrane potential disruption
MccL	IIa	90	nd*
Mcc24	IIa	75	nd
MccS	IIa	103	nd
MccE492	IIb	84	Membrane potential disruption and pore formation
MccM	IIb	77	nd
MccH47	IIb	60	nd
MccI47	IIb	62	nd

### 1.3.2. Microcin J25 Biosynthesis and Structure

Microcin J (MccJ25) is a 21 amino acid peptide.<sup>158</sup> It was originally produced by *E. coli* AY25 cells having the pTUC100 plasmid. It is active against *Enterobacteria*.<sup>159</sup> The 2D-NMR structure MccJ25 reveals that it adopts a characteristic threaded lasso structure. MccJ25 contains a  $\alpha\beta$  bond, which is formed by the amino group of glycine located at the N end of the mature microcin, and the  $\gamma$ -carboxyl group of glutamic acid residue occupying position 8. As a result, the first eight residues of MccJ25 are closed in a ring (**Figure1.12**). And the 13 C-terminal residues (Tyr9–Gly21, a tail) of MccJ25 form a  $\beta$ -hairpin, with the tail being threaded through the ring. This unusual structure is stabilized



Four genes were involved in the production and exportation of MccJ25 outside the producing strain. The *mcjA*, *mcjB*, and *mcjC* plasmid genes are essential for MccJ25 synthesis; the *mcjD* gene is responsible for immunity.<sup>160</sup> The roles of the three producing genes are classified as follows: *mcjA* gene codes for precursor McjA of 58 amino acid residues. The first 37 residues form a leader peptide, which is removed during maturation (**Figure 1.12**). McjB and McjC are responsible for microcin maturation, closing the ring with the lactam bond and cleaving the leader peptide. McjC is similar in sequence and predicted structure of the C-terminal domain of asparagine synthase B (catalyzes the ATP/Mg<sup>2+</sup> dependent conversion of aspartate to asparagine), and  $\beta$ -lactam synthase (catalyzes the formation of the  $\beta$ -lactam ring in clavulanic acid). Thus, McjC forms the lactam ring in MccJ, while McjB is responsible for the proper folding of the precursor and/or the cleavage of the leader peptide.<sup>161</sup> A recent study showed that MccJ25 can be reconstituted *in vitro*, this demonstrated that McjB and McjC are sufficient for converting the precursor into the mature peptide.<sup>162,163</sup>

Owing to the MccJ25 lasso structure, studies showed that it is highly resistant to strong denaturing conditions,<sup>158</sup> temperatures of more than 100 °C, and high concentrations of chaotropic agents (10 M guanidine hydrochloride or 8 M urea). In addition, MccJ25 is resistant to most proteases. Several other examples of lasso peptides have been described so far.<sup>164</sup> (**Figure 1.13**) Although their modes of action are very diverse, the majority of these peptides bind to proteins. For example, the group includes, MS-271, an inhibitor of the calmodulin-activated myosin light chain kinase,<sup>165</sup> anantin, a peptide binding to the atrial natriuretic

factor (ANF),<sup>166</sup> and two closely related peptides, NP-06 and RP 71955, which are active against human immunodeficiency virus 1.<sup>167,168</sup> Capstruin exhibits antimicrobial activity against closely related *Burkholderia* and *Pseudomonas* strains, and the lariatins A and B are active against *Mycobacterium smegmatis*.<sup>169</sup> Capstruin, lariatins, and Microcin J25 are the only lasso peptides with antibacterial activity.

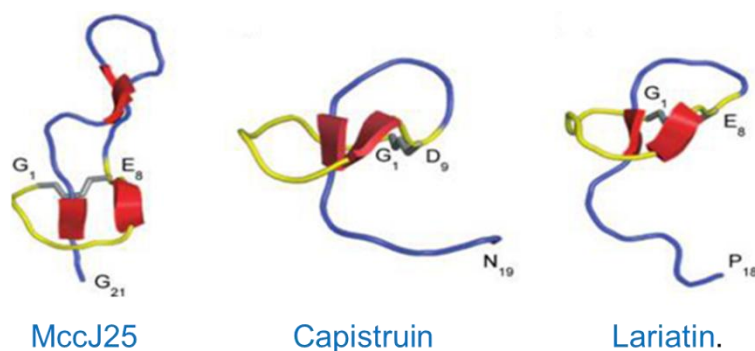


**Figure 1.13.** NMR structures of different lasso peptides.<sup>170</sup> (Adapted with permission from reference<sup>170</sup>)

### 1.3.3. Microcin J25 Uptake and Mechanism of Action

For MccJ25 to exert its action, it needs to be internalized in the bacterial cell. MccJ25 bacterial uptake requires the outer membrane receptor FhuA, and the inner membrane proteins TonB, ExbD, ExbB, and SbmA.<sup>171</sup>

MccJ25 appears to have two intracellular targets: (i) RNA polymerase (RNAP), which has been described in *E. coli* and *Salmonella enterica* serovars,<sup>172,173</sup> and (ii) the respiratory chain, reported first in *S. enterica* serovars

but recently also demonstrated in *E. coli*.<sup>174</sup> It was proved that the observed difference between the actions of microcin on the respiratory chain in *E. coli* and *S. enterica* is due to the relatively low microcin uptake via the chromosomally encoded FhuA. Higher expression of a plasmid encoded FhuA allowed greater uptake of MccJ25 by *E. coli* strains, and the consequent inhibition of oxygen consumption was enhanced. The two mechanisms, inhibition of RNAP and oxygen consumption, are independent of each other.

#### **1.3.4. Structural Activity Relationship of Microcin J25**

The structure activity relationship studies are helpful tool for the design of antimicrobial peptide variants with enhanced antimicrobial activities or altered specificities. Various studies were carried out to elucidate the structure function relationship of MccJ25. Bellomio *et al.* showed that an intact  $\beta$ -hairpin region is crucial for MccJ25 import, but not for inhibition of *E. coli* RNA polymerase or oxygen consumption in *Salmonella* strains.<sup>175</sup> Given that MccJ25-Th19 with deep modifications in  $\beta$ -hairpin region had no effect on *E. coli* growth, but still inhibited RNA polymerase *in vitro* and oxygen consumption in *Salmonella* strains. Another study showed similar results for two MccJ25 derivatives that were obtained by chemical degradation, h16-MccJ25 and h18-MccJ25, lacking  $\beta$ -hairpin region amino acids 13 to 17 and 15 to 17, respectively. Both MccJ25 derivatives efficiently inhibited transcription by wild-type RNAP. These results therefore suggest that it is the unusual ring-tail part of the MccJ25 molecule that

interacts with RNA polymerase. The lack of bactericidal activity of MccJ25-Th19 suggests that the loop region of MccJ25 is important for the peptide uptake.<sup>176</sup>

MccJ25 carries only two charged residues: a positively charged histidine (His5) localized in the lariat ring and a negatively charged glycine (Gly21) at the carboxyl terminus of the molecule. The two charged groups are close in the three-dimensional structure, and were shown to be important for MccJ25 activity.<sup>177</sup> The C-terminal glycine amidation specifically blocked the RNAP inhibition, but not the cell respiration inhibition and peptide uptake.<sup>178</sup> On the other hand, carboxylation of the imidazole ring of MccJ25 His5 decreased the inhibitory effect of the antibiotic on both *E. coli* cell growth and *in vivo* RNA synthesis.<sup>177</sup> Thus, it appeared that the polar histidyl residue is required for MccJ25 transport into the cell, its extrusion outside the cell, or RNAP inhibition.<sup>177</sup>

### **1.3.5. Potential Applications of Microcins**

Based on the knowledge of the biological activities of microcins, several applications may be considered.

*Food preservation.* The extensive use of antibiotics medically and in modern meat production industry has caused antibiotic resistance to evolve in many strains of pathogenic bacteria. In recent years, there has been an increased interest in using bacteria and bacterial products in food preservation rather than chemical or physical preservatives. Inspired by the lantibiotic nisin, a bacteriocin produced by *Lactococcus lactis* approved by the FDA and it is commonly used as a food

preservative inhibits the growth of only Gram-positive bacteria. For Gram negative bacteria, the heterologous production of microcin V in lactic acid bacteria (LAB) was performed.<sup>179</sup> These engineered LABs might be useful in preventing food poisoning caused by Gram-negative pathogenic bacteria in milk and meat products and could extend the shelf-life of these products.<sup>180</sup>

The MccJ25 is active on pathogenic strains of *E. coli*, *Salmonella* and *Shigella*, including strain O157: H7 and non-O157, which are the cause of outbreaks of foodborne diseases. In addition, MccJ25 is the most active microcin against 12 of 15 diarrheagenic *E. coli* tested.<sup>181</sup> MccJ25 was tested for food preservation activity in milk, egg, and meat extracts and was capable of inhibiting the growth of the *E. coli* O157:H7 strains present, suggesting that microcins might be used to control diarrheagenic *E. coli* strains in food products.<sup>181</sup>

*Antibiotic.* Microcins have been shown to be potential alternatives to the currently used antimicrobial agents of quinolones and coumarins, inhibitors of prokaryotic topoisomerase II (DNA gyrase), a central compound in DNA replication. These DNA gyrase antagonists are a rapidly expanding class of agents with promising properties for the treatment of infectious diseases. Microcin B17, produced by *E. coli*, kills in a similar manner as the quinolones and the coumarins, thus defining a third class of DNA gyrase inhibitors.<sup>182</sup> Microcins J25 and L<sup>183</sup> both produced by *E. coli*, exhibit strong antimicrobial activity against *Salmonella enterica* serovars, *typhimurium* and *enteritidis*, which cause diarrheal illness in humans.

*Antitumoral agents.* Besides microcins antimicrobial activity, some microcins can induce apoptosis and this opens a new research area field for potential applications of microcins as antitumoral agents.<sup>184</sup> For example, microcin E294 was shown to induce biochemical and morphological changes typical of apoptosis in human malignant cell lines.<sup>185</sup> Microcin E492 can form amyloid-like fibrils that can be exploited in its formulation as an antitumoral agent, because these fibrils can act as stable depots for the sustained release of a biologically active molecule. Alternatively, live bacteria can be used as a continuous source of microcin E492 production in specific tumors.

Interestingly, Vizan *et al*<sup>186</sup> demonstrated that microcin B17 produced by *E. coli* harboring the plasmid-borne. MccB17 operon inhibits DNA gyrase using a trapping mechanism. The resulting complex leads to accumulation of double-stranded DNA breaks in the bacterial cell. This mode of action is similar to that of quinolones and drugs commonly used for their antineoplastic properties.<sup>186</sup> Microcin B17 harbors structural homology (oxazole and thiazole portions) similar to bleomycin, a peptide used in cancer therapy for more than 30 years and specifically for Hodgkin disease and germinal cancers.<sup>187</sup>

Studies carried out on rat heart mitochondria with microcin J25 have shown that, it disrupt the mitochondrial membrane potential and diminishes the ATP level.<sup>188</sup> MccJ25-Ga is an analogue of microcin J25 which triggers apoptosis in COS-7 cells. This effect was related to the inhibition of mitochondrial RNAP.<sup>189</sup> These results open a new possible avenue of studying microcins in cancer therapy.

## **1.4. Thesis Proposal**

### **1.4.1. Thesis Rationale**

The pharmaceutical industry has gained much interest in peptides therapeutics in the last two decades as a continuous source of drugs in different unmet medical areas. Several investigations highlighted above disclosed the potential use of peptides in tumor targeting/therapy or in antimicrobial therapy. In cancer research, several tumor or tumor vasculature targeting peptides with high tumor specificity and binding affinity have been identified using various biological and chemical screening methods such as p160, and NGR peptides. Peptide p160 is known to specifically bind to breast cancer cells, and NGR is a tripeptide motif that is known to bind aminopeptidase N, an enzyme that is overexpressed on tumor vasculature. A growing number of preclinical and clinical studies revealed that cancer targeting peptides represent an ideal choice for selective tumor drug targeting with respect to the commonly used antibodies, it increased the specificity of diverse cancer therapies for tumor cells and decreased its side effects. However, the number of peptides that has been progressed successfully through the clinics to reach the market is very low compared to the accomplished research. This is because peptides characteristics hamper their application for therapeutic purposes including their liability to proteolytic degradation, low binding affinity, and their unknown toxicology profile when administered systemically.

Along with cancer targeting peptides, the discovery of antimicrobial peptides offers a great alternative for the conventional antibiotics against the emergence of bacterial resistance. Besides, some of antimicrobial peptides showed selective anticancer activities so this also simulated the interest of using them as a new class of anticancer drugs that lack the toxicity of conventional chemotherapeutic agents, and are unaffected by common mechanisms of chemoresistance. As mentioned in the introduction, MccJ25 is a very stable antimicrobial peptide with lasso structure that displayed very promising antibacterial activity against different Gram negative pathogenic strains. In addition, it can induce apoptosis by selectively disrupting the mitochondrial membrane of isolated mitochondria.

Therefore, our hypothesis in the current thesis is that previously identified lead peptide sequences either for tumor targeting or antimicrobial/anticancer activity can be further improved for enhanced specific cancer cell binding, metabolic stability or improved anticancer activity by chemical manipulation of their structures. In other words, from a model peptide of interest (lead peptide) it is often necessary to optimize its chemical structure to obtain valuable entities that could be applied therapeutically.

#### **1.4.2. Thesis Objective**

Our major goal in the current thesis is the optimization of previously discovered lead peptide sequences (peptides **p160**, **NGR**, and **MccJ25**) using rational design strategies or combinatorial screening array methods to enhance

their therapeutic utility in both cancer targeting/ therapy and antimicrobial therapy besides improving their properties as drug candidates. For example, cancer targeting sequences identified in the current thesis would serve as efficient ligands for the selective delivery of various cancer therapeutic agents to breast tumors either for treatment or diagnostic purposes. On the other side, enhancing the cell uptake and cytotoxicity of **MccJ25** by coupling it with our novel internalizing cancer specific peptide will open new avenues of using this proapoptotic peptide in fighting cancer.

The specific objectives are as follows:

In **Chapters 2, 3 and 4**, our objective was to optimize and evaluate the sequences of two previously identified cancer targeting peptide sequences, namely, NGR, and p160 for enhanced proteolytic stability and better binding affinity for putative cancer cells. In **Chapters 5 and 6**, the structure activity relationship studies of antimicrobial peptide microcin J25 was carried out for better understanding of its chemical analogues, moreover, studies were carried out to enhance the therapeutic use of microcin J25 as proapoptotic drug in cancer therapy by conjugating it to cancer targeting peptide to enhance its cell delivery and internalization.

To accomplish these goals the following studies were performed: In **Chapter 2**, a combinatorial screening method was carried out, where, an NGR peptide library based on a lead sequence was synthesised on functionalized cellulose membrane and evaluated using whole cell binding assay that has been established in our lab. The screening was done to identify new NGR targeting

peptides that bind with high affinity and specificity to CD13 receptor widely expressed on tumor vasculature. The novel peptide sequences with enhanced specific affinity for CD13 expressing cells have been identified, and their affinities for CD13 receptor, as well as their enzymatic inhibitory activity were assessed *in vitro*.

In **Chapter 3**, a rational design approach was developed for synthesizing analogues of cancer targeting peptide p160 to improve its proteolytic stability and maintain its specific affinity for breast cancer cells. Two approaches were used to develop the analogues. First, a second generation of p160 analogues was created by introduction of single or double substitutions in the peptide **18** sequence to improve specificity for breast cancer cells. Secondly, proteolytically stable analogues were synthesized based on replacement of a few amino acids with either D-amino acids or in house synthesized novel beta amino acids derived from L-aspartic acid. Peptides that displayed the highest affinity for the cancer cells were manually synthesized and labelled with FITC. The binding ability of these peptides was confirmed using fluorescence imaging and flow cytometry, and the proteolytic stability was evaluated in human serum and liver homogenate.

In **Chapter 4**, our objective was to test the potential use of our novel stable analogue of p160 (peptide **18-4**) for the selective delivery of doxorubicin to cancer cells while preserving normal cells, as well as, its ability to overcome multidrug resistance mechanism in Dox resistant cells. To this end, two peptide drug conjugates **1**, and **2** with different conjugation sites and chemistries were synthesized and characterized. The release of the drug from the conjugates was

studied in human serum. Peptide drug conjugates **1** and **2** and free Dox were evaluated for intracellular delivery, subcellular distribution using flow cytometry, along with confocal microscopy in three cancerous cells (MCF-7, MDA-MB-435, and MDA-MB-435-MDR) and two control cell lines (HUVEC, and MCF-10A). Finally, cell cytotoxicity of the conjugates was measured using MTT assay compared to free Dox.

In **Chapter 5**, our objective was to study the structure activity relationship of **MccJ25** antimicrobial lasso peptide, by designing and synthesizing synthetic analogues based on the **MccJ25** sequence which can acquire conformational folding by a combination of intra-peptide disulfide bond formation and electrostatic or hydrophobic interactions, instead of post-translational modification by McjB and McjC proteins. The synthesis of 6 analogues (**1-6**) derived from the sequence of MccJ25 ranging in length 18-22 residues, antimicrobial activity, solution conformation, stability to proteases and cytotoxicity of this series of synthetic MccJ25 derivatives were reported.

In **Chapter 6**, our objective was to conjugate **MccJ25** to a carrier cancer targeting peptide **18-4** to enhance its cellular uptake and improve its cytotoxicity where it can selectively kill breast cancer cells, including drug-resistant breast cancer cells. The synthesis, characterization, *in vitro* cytotoxicity, cellular uptake, and intracellular anticancer efficacy of **MccJ25-18-4** peptide conjugate was reported.

Finally, the implementation of the outcomes from the work presented in the thesis is discussed in **Chapter 7**.

## 1.5. References

- (1) Glaser, V. Competition mounting in peptide market *Gen. Eng. Biotechnol. News* **2009**, 29.
- (2) Vlieghe, P.; Lisowski, V.; Martinez, J.; Khrestchatsky, M. Synthetic therapeutic peptides: science and market *Drug Discov. Today* **2010**, 15, 40-56.
- (3) Marx, V. Watching peptide drugs grow up. *Chem. Eng. News* **2005**, 83, 17-24.
- (4) Hummel, G.; Reineke, U.; Reimer, U. Translating peptides into small molecules *Mol. BioSyst.* **2006**, 2, 499-508.
- (5) Loffet, A. Peptides as Drugs: Is There a Market? *J. Pept. Sci.* **2002**, 8, 1-7.
- (6) Jenssen, H.; Hamill, P.; Hancock, R. E. W. Peptide Antimicrobial Agents *Clin. Microbiol. Rev.* **2006**, 19, 491-511.
- (7) Rotem, S.; Mor, A. Antimicrobial peptide mimics for improved therapeutic properties *BBA-Biomembranes* **2009**, 1788, 1582-1592.
- (8) Canadian Cancer Statistics **2012**.
- (9) Ferrara, N.; Kerbel, R. S. Angiogenesis as a therapeutic target *Nature* **2005**, 438, 967-974.
- (10) Cho, K.; Wang, X.; Nie, S.; Chen, Z.; Shin, D. M. Therapeutic Nanoparticles for Drug Delivery in Cancer *Clin. Cancer Res.* **2008**, 14, 1310-1316.
- (11) Liang, X.J.; Chen, C.; Zhao, Y.; Wang, P. C. Circumventing Tumor Resistance to Chemotherapy by Nanotechnology *Methods Mol Biol.* **2010**, 596, 467-88.
- (12) Aird, W. C. Phenotypic Heterogeneity of the Endothelium *Circ. Res.* **2007**, 100, 158-173.
- (13) Aird, W. C. Phenotypic Heterogeneity of the Endothelium *Circ. Res.* **2007**, 100, 174-190.
- (14) Wang, B. e. a., eds *Drug Delivery: Principles and Applications*,; Wiley, **2005**.

- (15) Allen, T. M. Ligand-targeted therapeutics in anticancer therapy *Nat. Rev. Cancer* **2002**, *2*, 750-763.
- (16) Hong, H.; Sun, J.; Cai, W. Radionuclide-Based Cancer Imaging Targeting the Carcinoembryonic Antigen *Biomark. Insights* **2008**, *3*, 435-451.
- (17) Gerber, H.-P.; Senter, P. D.; Grewal, I. S. Antibody drug-conjugates targeting the tumor vasculature: Current and future developments *mAbs* **2009**, *1*, 247-253.
- (18) Park, J. W.; Kirpotin, D. B.; Hong, K.; Shalaby, R.; Shao, Y.; Nielsen, U. B.; Marks, J. D.; Papahadjopoulos, D.; Benz, C. C. Tumor targeting using anti-her2 immunoliposomes *J. Control. Release* **2001**, *74*, 95-113.
- (19) Schellmann N, Deckert P., Bachran D, Fuchs H, Bachran C. Targeted enzyme prodrug therapies *Mini. Rev. Med. Chem.* **2010**, *10*, 887-904.
- (20) Litvak-Greenfeld, D.; Benhar, I. Risks and untoward toxicities of antibody-based immunoconjugates *Adv. Drug. Deliv. Rev.* **2012**, *64*, 1782-99.
- (21) Boyiadzis, M.; Foon, K. A. Approved monoclonal antibodies for cancer therapy *Expert Opin. Biol.* **2008**, *8*, 1151-1158.
- (22) Descotes, J. Immunotoxicity of monoclonal antibodies *mAbs* **2009**, *1*, 104-111.
- (23) Neumeister, P.; Eibl, M.; Zinke-Cerwenka, W.; Scarpatetti, M.; Sill, H.; Linkesch, W. Hepatic veno-occlusive disease in two patients with relapsed acute myeloid leukemia treated with anti-CD33 calicheamicin (CMA-676) immunoconjugate *Ann. Hematol.* **2001**, *80*, 119-120.
- (24) Nord, K.; Gunneriusson, E.; Ringdahl, J.; Stahl, S.; Uhlen, M.; Nygren, P.-A. Binding proteins selected from combinatorial libraries of an [alpha]-helical bacterial receptor domain *Nat. Biotech.* **1996**, *15*, 772-777.
- (25) Wikman, M.; Steffen, A.-C.; Gunneriusson, E.; Tolmachev, V.; Adams, G. P.; Carlsson, J.; Ståhl, S. Selection and characterization of HER2/neu-binding affibody ligands *Protein Eng. Des. Sel.* **2004**, *17*, 455-462.
- (26) Steffen AC, W. M., Tolmachev V, Adams GP, Nilsson FY, Ståhl S, Carlsson J. In vitro characterization of a bivalent anti-HER-2 affibody with potential for radionuclide-based diagnostics *Cancer Biother. Radiopharm.* **2005**, *20*, 239-248.
- (27) Alexis, F.; Basto, P.; Levy-Nissenbaum, E.; Radovic-Moreno, A. F.; Zhang, L.; Pridgen, E.; Wang, A. Z.; Marein, S. L.; Westerhof, K.; Molnar, L.

K.; Farokhzad, O. C. HER-2-Targeted Nanoparticle–Affibody Bioconjugates for Cancer Therapy *ChemMedChem* **2008**, *3*, 1839-1843.

(28) Ladner, R. C.; Sato, A. K.; Gorzelany, J.; de Souza, M. Phage display-derived peptides as therapeutic alternatives to antibodies *Drug Discov. Today* **2004**, *9*, 525-529.

(29) Hatakeyama, S.; Sugihara, K.; Shibata, T. K.; Nakayama, J.; Akama, T. O.; Tamura, N.; Wong, S.-M.; Bobkov, A. A.; Takano, Y.; Ohyama, C.; Fukuda, M.; Fukuda, M. N. Targeted drug delivery to tumor vasculature by a carbohydrate mimetic peptide *Proc. Natl. Acad. Sci.* **2011**, *108*, 19587-19592.

(30) Fukuda, M. N. Screening of peptide-displaying phage libraries to identify short peptides mimicking carbohydrates In *Methods Enzymol* **2006**, *416*, 51-60.

(31) Shadidi, M.; Sioud, M. Selective targeting of cancer cells using synthetic peptides *Drug Resist. Update.* **2003**, *6*, 363-371.

(32) Lauren RH Krumpe, T. M. Potential of phage-displayed peptide library technology to identify functional targeting peptides *Expert Opin. Drug Discov.* **2007**, *2*, 525.

(33) Pasqualini, R.; Ruoslahti, E. Organ targeting In vivo using phage display peptide libraries *Nature* **1996**, *380*, 364-366.

(34) Landon, L. A.; Deutscher, S. L. Combinatorial discovery of tumor targeting peptides using phage display *J. Cell. Biochem.* **2003**, *90*, 509-517.

(35) Craig R, L. S. Function and molecular mechanism of tumor-targeted peptides for delivering therapeutic genes and chemical drugs *Mini Rev. Med. Chem.* **2006**, *6*, 757-764.

(36) Kapoor, P.; Singh, H.; Gautam, A.; Chaudhary, K.; Kumar, R.; Raghava, G. P. S. TumorHoPe: A Database of Tumor Homing Peptides *PLoS ONE* **2012**, *7*, e35187.

(37) Zhang, J.; Spring, H.; Schwab, M. Neuroblastoma tumor cell-binding peptides identified through random peptide phage display *Cancer Lett.* **2001**, *171*, 153-164.

(38) Askoxylakis, V.; Zitzmann, S.; Mier, W.; Graham, K.; Krämer, S.; von Wegner, F.; Fink, R. H. A.; Schwab, M.; Eisenhut, M.; Haberkorn, U. Preclinical Evaluation of the Breast Cancer Cell-Binding Peptide, p160 *Clin. Cancer Res.* **2005**, *11*, 6705-6712.

- (39) Ahmed, S.; Mathews, A. S.; Byeon, N.; Lavasanifar, A.; Kaur, K. Peptide Arrays for Screening Cancer Specific Peptides *Anal. Chem.* **2010**, *82*, 7533-7541.
- (40) Zitzmann, S.; Mier, W.; Schad, A.; Kinscherf, R.; Askoxylakis, V.; Krämer, S.; Altmann, A.; Eisenhut, M.; Haberkorn, U. A New Prostate Carcinoma Binding Peptide (DUP-1) for Tumor Imaging and Therapy *Clin. Cancer Res.* **2005**, *11*, 139-146.
- (41) Askoxylakis, V.; Zitzmann-Kolbe, S.; Zoller, F.; Altmann, A.; Markert, A.; Rana, S.; Marr, A.; Mier, W.; Debus, J.; Haberkorn, U. Challenges in Optimizing a Prostate Carcinoma Binding Peptide, Identified through the Phage Display Technology *Molecules* **2011**, *16*, 1559-1578.
- (42) Li Z, Z. R., Wu X, Sun Y, Yao M, Li J, Xu Y, Gu J. Identification and characterization of a novel peptide ligand of epidermal growth factor receptor for targeted delivery of therapeutics *FASEB J.* **2005**, *19*, 1978-1985.
- (43) Du B, Q. M., Zhou Z, Wang P, Wang L, Zhang X, Wu M, Zhang P, Mei B In vitro panning of a targeting peptide to hepatocarcinoma from a phage display peptide library *Biochem. Biophys. Res. Commun.* **2006**, *342*, 956-962.
- (44) Akita, N.; Maruta, F.; Seymour, L. W.; Kerr, D. J.; Parker, A. L.; Asai, T.; Oku, N.; Nakayama, J.; Miyagawa, S. Identification of oligopeptides binding to peritoneal tumors of gastric cancer *Cancer Science* **2006**, *97*, 1075-1081.
- (45) Tanaka, S.; Pero, S. C.; Taguchi, K.; Shimada, M.; Mori, M.; Krag, D. N.; Arii, S. Specific Peptide Ligand for Grb7 Signal Transduction Protein and Pancreatic Cancer Metastasis *J. Natl. Cancer Inst.* **2006**, *98*, 491-498.
- (46) Pero, S. C.; Oligino, L.; Daly, R. J.; Soden, A. L.; Liu, C.; Roller, P. P.; Li, P.; Krag, D. N. Identification of Novel Non-phosphorylated Ligands, Which Bind Selectively to the SH2 Domain of Grb7 *J. Biol. Chem.* **2002**, *277*, 11918-11926.
- (47) Huang, C.; Liu, X. Y.; Rehemtulla, A.; Lawrence, T. S. Identification of peptides that bind to irradiated pancreatic tumor cells *Int. J. Radiat. Oncol. Biol. Phys.* **2005**, *62*, 1497-1503.
- (48) Fukumura, D.; Jain, R. K. Tumor microenvironment abnormalities: Causes, consequences, and strategies to normalize *J. Cell. Biochem.* **2007**, *101*, 937-949.
- (49) Ruoslahti, E. Vascular zip codes in angiogenesis and metastasis. *Biochem. Soc. Trans.* **2004**, *32*, 397-402.

- (50) Boehm, T.; Folkman, J.; Browder, T.; O'Reilly, M. S. Antiangiogenic therapy of experimental cancer does not induce acquired drug resistance *Nature* **1997**, *390*, 404-407.
- (51) Browder, T.; Butterfield, C. E.; Kräling, B. M.; Shi, B.; Marshall, B.; O'Reilly, M. S.; Folkman, J. Antiangiogenic Scheduling of Chemotherapy Improves Efficacy against Experimental Drug-resistant Cancer *Cancer Res.* **2000**, *60*, 1878-1886.
- (52) Pasqualini, R.; Koivunen, E.; Ruoslahti, E.  $\alpha$ v Integrins as receptors for tumor targeting by circulating ligands *Nat. Biotech.* **1997**, *15*, 542-546.
- (53) Arap, W.; Pasqualini, R.; Ruoslahti, E.; Cancer treatment by targeted drug delivery to tumor vasculature in a mouse model *Science* **1998**, *279*, 377-380.
- (54) Koivunen E; Wang B.; Ruoslahti E. Phage libraries displaying cyclic peptides with different ring sizes: ligand specificities of the RGD-directed integrins *Biotechnol. (N. Y.)* **1995**, *13*, 265-270.
- (55) Koivunen, E.; Gay, D. A.; Ruoslahti, E. Selection of peptides binding to the alpha 5 beta 1 integrin from phage display library *J. Biol. Chem.* **1993**, *268*, 20205-20210.
- (56) Maubant, S.; Saint-Dizier, D.; Boutillon, M.; Perron-Sierra, F.; Casara, P. J.; Hickman, J. A.; Tucker, G. C.; Van Obberghen-Schilling, E. Blockade of  $\alpha$ v $\beta$ 3 and  $\alpha$ v $\beta$ 5 integrins by RGD mimetics induces anoikis and not integrin-mediated death in human endothelial cells *Blood* **2006**, *108*, 3035-3044.
- (57) Dickerson, E. B.; Akhtar, N.; Steinberg, H.; Wang, Z.-Y.; Lindstrom, M. J.; Padilla, M. L.; Auerbach, R.; Helfand, S. C. Enhancement of the Antiangiogenic Activity of Interleukin-12 by Peptide Targeted Delivery of the Cytokine to  $\alpha$ v $\beta$ 3 Integrin *Mol. Cancer Res.* **2004**, *2*, 663-673.
- (58) Vermorcken, J. B.; Guigay, J.; Mesia, R.; Trigo, J. M.; Keilholz, U.; Kerber, A.; Bethe, U.; Picard, M.; Brummendorf, T. H. Phase I/II trial of cilengitide with cetuximab, cisplatin and 5-fluorouracil in recurrent and/or metastatic squamous cell cancer of the head and neck: findings of the phase I part *Br. J. Cancer* **2011**, *104*, 1691-1696.
- (59) Stupp, R.; Hegi, M. E.; Neyns, B.; Goldbrunner, R.; Schlegel, U.; Clement, P. M. J.; Grabenbauer, G. G.; Ochsenschein, A. F.; Simon, M.; Dietrich, P.-Y.; Pietsch, T.; Hicking, C.; Tonn, J.-C.; Diserens, A.-C.; Pica, A.; Hermisson, M.; Krueger, S.; Picard, M.; Weller, M. Phase I/IIa Study of Cilengitide and Temozolomide With Concomitant Radiotherapy Followed by Cilengitide and

Temozolomide Maintenance Therapy in Patients With Newly Diagnosed Glioblastoma *J. Clin. Oncol.* **2010**, *28*, 2712-2718.

(60) Duneahoo, A. L.; Anderson, M.; Majumdar, S.; Kobayashi, N.; Berkland, C.; Siahaan, T. J. Cell adhesion molecules for targeted drug delivery *J. Pharm. Sci.* **2006**, *95*, 1856-1872.

(61) Garanger, E.; Boturyn, D.; Dumy, P. Tumor Targeting with RGD Peptide Ligands-Design of New Molecular Conjugates for Imaging and Therapy of Cancers *Anticancer Agents Med. Chem.* **2007**, *7*, 552-558.

(62) Pasqualini, R.; Koivunen, E.; Kain, R.; Lahdenranta, J.; Sakamoto, M.; Stryhn, A.; Ashmun, R. A.; Shapiro, L. H.; Arap, W.; Ruoslahti, E. Aminopeptidase N is a receptor for tumor-homing peptides and a target for inhibiting angiogenesis *Cancer Res.* **2000**, *60*, 722-727.

(63) Curnis, F.; Gasparri, A.; Sacchi, A.; Cattaneo, A.; Magni, F.; Corti, A. Targeted Delivery of IFN $\gamma$  to Tumor Vessels Uncouples Antitumor from Counterregulatory Mechanisms *Cancer Res.* **2005**, *65*, 2906-2913.

(64) Sacchi, A.; Gasparri, A.; Curnis, F.; Bellone, M.; Corti, A. Crucial Role for Interferon  $\gamma$  in the Synergism between Tumor Vasculature-Targeted Tumor Necrosis Factor  $\alpha$  (NGR-TNF) and Doxorubicin *Cancer Res.* **2004**, *64*, 7150-7155.

(65) Sacchi, A.; Gasparri, A.; Gallo-Stampino, C.; Toma, S.; Curnis, F.; Corti, A. Synergistic Antitumor Activity of Cisplatin, Paclitaxel, and Gemcitabine with Tumor Vasculature-Targeted Tumor Necrosis Factor- $\alpha$  *Clin. Cancer Res.* **2006**, *12*, 175-182.

(66) Bertilaccio, M. T. S.; Grioni, M.; Sutherland, B. W.; Degl'Innocenti, E.; Freschi, M.; Jachetti, E.; Greenberg, N. M.; Corti, A.; Bellone, M. Vasculature-targeted tumor necrosis factor-alpha increases the therapeutic index of doxorubicin against prostate cancer *The Prostate* **2008**, *68*, 1105-1115.

(67) Santoro, A.; Rimassa, L.; Sobrero, A. F.; Citterio, G.; Scalfani, F.; Carnaghi, C.; Pessino, A.; Caprioni, F.; Andretta, V.; Tronconi, M. C.; Finocchiaro, G.; Rossoni, G.; Zanoni, A.; Miggiano, C.; Rizzardi, G.-P.; Traversari, C.; Caligaris-Cappio, F.; Lambiase, A.; Bordignon, C. Phase II study of NGR-hTNF, a selective vascular targeting agent, in patients with metastatic colorectal cancer after failure of standard therapy *Eur. J. Cancer* **2010**, *46*, 2746-2752.

(68) Gregorc, V.; De Braud, F. G.; De Pas, T. M.; Scalapogna, R.; Citterio, G.; Milani, A.; Boselli, S.; Catania, C.; Donadoni, G.; Rossoni, G.; Ghio, D.; Spitaleri, G.; Ammannati, C.; Colombi, S.; Caligaris-Cappio, F.; Lambiase, A.; Bordignon, C. Phase I Study of NGR-hTNF, a Selective Vascular Targeting

Agent, in Combination with Cisplatin in Refractory Solid Tumors *Clin. Cancer Res.* **2011**, *17*, 1964-1972.

(69) Curnis, F.; Longhi, R.; Crippa, L.; Cattaneo, A.; Dondossola, E.; Bachi, A.; Corti, A. Spontaneous Formation of L-Isoaspartate and Gain of Function in Fibronectin *J. Biol. Chem.* **2006**, *281*, 36466-36476.

(70) Laakkonen, P.; Åkerman, M. E.; Biliran, H.; Yang, M.; Ferrer, F.; Karpanen, T.; Hoffman, R. M.; Ruoslahti, E. Antitumor activity of a homing peptide that targets tumor lymphatics and tumor cells *Proc. Natl. Acad. Sci. U. S. A.* **2004**, *101*, 9381-9386.

(71) Laakkonen, P.; Zhang, L.; Ruoslahti, E. Peptide Targeting of Tumor Lymph Vessels *Ann. N. Y. Acad. Sci.* **2008**, *1131*, 37-43.

(72) Laakkonen, P.; Porkka, K.; Hoffman, J. A.; Ruoslahti, E. A tumor-homing peptide with a targeting specificity related to lymphatic vessels *Nat. Med.* **2002**, *8*, 751-755.

(73) Fogal, V.; Zhang, L.; Krajewski, S.; Ruoslahti, E. Mitochondrial/Cell-Surface Protein p32/gC1qR as a Molecular Target in Tumor Cells and Tumor Stroma *Cancer Res.* **2008**, *68*, 7210-7218.

(74) Witt, H.; Hajdin, K.; Iljin, K.; Greiner, O.; Niggli, F. K.; Schäfer, B. W.; Bernasconi, M. Identification of a rhabdomyosarcoma targeting peptide by phage display with sequence similarities to the tumour lymphatic-homing peptide LyP-1 *Int. J. Cancer* **2009**, *124*, 2026-2032.

(75) Zhang, L.; Giraudo, E.; Hoffman, J. A.; Hanahan, D.; Ruoslahti, E. Lymphatic Zip Codes in Premalignant Lesions and Tumors *Cancer Res.* **2006**, *66*, 5696-5706.

(76) Capello, A.; Krenning, E. P.; Bernard, B. F.; Breeman, W. A. P.; van Hagen, M. P.; de Jong, M. Increased Cell Death After Therapy with an Arg-Gly-Asp-Linked Somatostatin Analog *J. Nucl. Med.* **2004**, *45*, 1716-1720.

(77) Zhang, X.; Cai, W.; Cao, F.; Schreiber, E.; Wu, Y.; Wu, J. C.; Xing, L.; Chen, X. 18F-Labeled Bombesin Analogs for Targeting GRP Receptor-Expressing Prostate Cancer *J. Nucl. Med.* **2006**, *47*, 492-501.

(78) Stewart, J. M.; Gera, L.; Chan, D. C.; York, E. J.; Simkeviciene, V.; Bunn Jr, P. A.; Taraseviciene-Stewart, L. Combination cancer chemotherapy with one compound: Pluripotent bradykinin antagonists *Peptides* **2005**, *26*, 1288-1291.

- (79) Aina, O. H.; Liu, R.; Sutcliffe, J. L.; Marik, J.; Pan, C.-X.; Lam, K. S. From Combinatorial Chemistry to Cancer-Targeting Peptides *Mol. Pharm.* **2007**, *4*, 631-651.
- (80) Aina, O. H.; Sroka, T. C.; Chen, M.-L.; Lam, K. S. Therapeutic cancer targeting peptides *J. Pept. Sci.* **2002**, *66*, 184-199.
- (81) Smith, G. P. Filamentous Fusion Phage: Novel Expression Vectors that Display Cloned Antigens on the Virion Surface *Science* **1985**, *228*, 1315-1317.
- (82) Krag, D. N.; Shukla, G. S.; Shen, G.-P.; Pero, S.; Ashikaga, T.; Fuller, S.; Weaver, D. L.; Burdette-Radoux, S.; Thomas, C. Selection of Tumor-binding Ligands in Cancer Patients with Phage Display Libraries *Cancer Res.* **2006**, *66*, 7724-7733.
- (83) Samoylova TI, M. N., Globa LP, Cox NR Peptide phage display: opportunities for development of personalized anti-cancer strategies. *Anticancer Agents Med. Chem.* **2006**, *6*, 9-17.
- (84) O'Neil KT, H. R., Jackson SA, Ramachandran NS, Mousa SA, DeGrado WF Identification of novel peptide antagonists for GPIIb/IIIa from a conformationally constrained phage peptide library *Proteins* **1992**, *14*, 509-515.
- (85) Ton, N. M. S.; Mayr, L. M.; Jr, D. L. M.; Milhollen, M. A.; Burgess, M. W.; Kim, P. S. Identification of D-Peptide Ligands Through Mirror-Image Phage Display *Science* **1996**, *271*, 1854-1857.
- (86) Wiesehan, K.; Buder, K.; Linke, R. P.; Patt, S.; Stoldt, M.; Unger, E.; Schmitt, B.; Bucci, E.; Willbold, D. Selection of D-Amino-Acid Peptides That Bind to Alzheimer's Disease Amyloid Peptide A $\beta$ 1-42 by Mirror Image Phage Display *ChemBioChem* **2003**, *4*, 748-753.
- (87) Wu, H.-C.; Chang, D.-K. Peptide-Mediated Liposomal Drug Delivery System Targeting Tumor Blood Vessels in Anticancer Therapy *Journal of Oncology* **2010**, *2010*, 1-8.
- (88) Lam, K. S.; Salmon, S. E.; Hersh, E. M.; Hruby, V. J.; Kazmierski, W. M.; Knapp, R. J. A new type of synthetic peptide library for identifying ligand-binding activity *Nature* **1991**, *354*, 82-84.
- (89) Kappel, J. C.; Fan, Y. C.; Lam, K. S., Application of the "libraries from libraries" concept to "one-bead one-compound" combinatorial chemistry. *Adv Exp Med Biol*, **2009**, *611*, 21-22.
- (90) Winkler DF, A. H., Hilpert K. SPOT synthesis as a tool to study protein-protein interactions. *Methods Mol. Biol.* **2011**, *723*, 105-127.

- (91) Koren, E.; Apte, A.; Sawant, R. R.; Grunwald, J.; Torchilin, V. P. Cell-penetrating TAT peptide in drug delivery systems: Proteolytic stability requirements *Drug Deliv.* **2011**, *18*, 377-384.
- (92) Adessi, C.; Soto, C. Converting a peptide into a drug: strategies to improve stability and bioavailability *Curr. Med. Chem.* **2002**, *9*, 963-978.
- (93) Bauer, W.; Briner, U.; Doepfner, W.; Haller, R.; Huguenin, R.; Marbach, P.; Petcher, T. J.; Pless, J. SMS 201-995: A very potent and selective octapeptide analogue of somatostatin with prolonged action *Life Sci.* **1982**, *31*, 1133-1140.
- (94) Susini, C.; Buscail, L. Rationale for the use of somatostatin analogs as antitumor agents *Ann. Oncol.* **2006**, *17*, 1733-1742.
- (95) Bogdanowich-Knipp, S. J.; Chakrabarti, S.; Siahaan, T. J.; Williams, T. D.; Dillman, R. K. Solution stability of linear vs. cyclic RGD peptides *J. Pept. Res.* **1999**, *53*, 530-541.
- (96) Goodman, S. L.; Hölzemann, G.; Sulyok, G. A. G.; Kessler, H. Nanomolar Small Molecule Inhibitors for  $\alpha\text{v}\beta\text{6}$ ,  $\alpha\text{v}\beta\text{5}$ , and  $\alpha\text{v}\beta\text{3}$  Integrins *J. Med. Chem.* **2002**, *45*, 1045-1051.
- (97) Haubner, R.; Finsinger, D.; Kessler, H. Stereoisomeric Peptide Libraries and Peptidomimetics for Designing Selective Inhibitors of the  $\alpha\text{v}\beta\text{3}$  Integrin for a New Cancer Therapy *Angew. Chem. Int. Ed.* **1997**, *36*, 1374-1389.
- (98) Haubner, R.; Gratias, R.; Diefenbach, B.; Goodman, S. L.; Jonczyk, A.; Kessler, H. Structural and Functional Aspects of RGD-Containing Cyclic Pentapeptides as Highly Potent and Selective Integrin  $\alpha\text{V}\beta\text{3}$  Antagonists *J. Am. Chem. Soc.* **1996**, *118*, 7461-7472.
- (99) Liu, S. Radiolabeled Multimeric Cyclic RGD Peptides as Integrin  $\alpha\text{v}\beta\text{3}$  Targeted Radiotracers for Tumor Imaging *Mol. Pharm.* **2006**, *3*, 472-487.
- (100) Li, Z.-b.; Cai, W.; Cao, Q.; Chen, K.; Wu, Z.; He, L.; Chen, X.  $^{64}\text{Cu}$ -Labeled Tetrameric and Octameric RGD Peptides for Small-Animal PET of Tumor  $\alpha\text{v}\beta\text{3}$  Integrin Expression *J. Nucl. Med.* **2007**, *48*, 1162-1171.
- (101) Mammen M, C. S.-K., Whitesides GM. Polyvalent Interactions in Biological Systems: Implications for Design and Use of Multivalent Ligands and Inhibitors *Angew. Chem.* **1998**, *37*, 2754-2794.
- (102) Zhou, Y., Chakraborty, S., Liu S. Radiolabeled Cyclic RGD Peptides as Radiotracers for Imaging Tumors and Thrombosis by SPECT *Theranostics* **2011**, *1*, 58-82.

- (103) Kubas, H.; Schäfer, M.; Bauder-Wüst, U.; Eder, M.; Oltmanns, D.; Haberkorn, U.; Mier, W.; Eisenhut, M. Multivalent cyclic RGD ligands: influence of linker lengths on receptor binding *Nucl. Med. Biol.* **2010**, *37*, 885-891.
- (104) Boturyn, D.; Coll, J.-L.; Garanger, E.; Favrot, M.-C.; Dumy, P. Template Assembled Cyclopeptides as Multimeric System for Integrin Targeting and Endocytosis *J. Am. Chem. Soc.* **2004**, *126*, 5730-5739.
- (105) Falciani, C.; Pini, A.; Bracci, L. Oligo-branched peptides for tumor targeting: from magic bullets to magic forks *Expert Opin. Biol.* **2009**, *9*, 171-178.
- (106) Tam, J. P. Synthetic peptide vaccine design: synthesis and properties of a high-density multiple antigenic peptide system *Proc. Natl. Acad. Sci.* **1988**, *85*, 5409-5413.
- (107) Falciani, C.; Fabbrini, M.; Pini, A.; Lozzi, L.; Lelli, B.; Pileri, S.; Brunetti, J.; Bindi, S.; Scali, S.; Bracci, L. Synthesis and biological activity of stable branched neurotensin peptides for tumor targeting *Mol. Cancer Ther.* **2007**, *6*, 2441-2448.
- (108) Colombo, G.; Curnis, F.; De Mori, G. M. S.; Gasparri, A.; Longoni, C.; Sacchi, A.; Longhi, R.; Corti, A. Structure-Activity Relationships of Linear and Cyclic Peptides Containing the NGR Tumor-homing Motif *J. Biol. Chem.* **2002**, *277*, 47891-47897.
- (109) Teesalu, T.; Sugahara, K. N.; Kotamraju, V. R.; Ruoslahti, E. C-end rule peptides mediate neuropilin-1-dependent cell, vascular, and tissue penetration *Proc. Natl. Acad. Sci.* **2009**, *106*, 16157-16162.
- (110) Sugahara, K. N.; Teesalu, T.; Karmali, P. P.; Kotamraju, V. R.; Agemy, L.; Greenwald, D. R.; Ruoslahti, E. Coadministration of a Tumor-Penetrating Peptide Enhances the Efficacy of Cancer Drugs *Science* **2010**, *328*, 1031-1035.
- (111) Mamluk, R.; Klagsbrun, M.; Detmar, M.; Bielenberg, D. Soluble neuropilin targeted to the skin inhibits vascular permeability *Angiogenesis* **2005**, *8*, 217-227.
- (112) Agemy, L.; Friedmann-Morvinski, D.; Kotamraju, V. R.; Roth, L.; Sugahara, K. N.; Girard, O. M.; Mattrey, R. F.; Verma, I. M.; Ruoslahti, E. Targeted nanoparticle enhanced proapoptotic peptide as potential therapy for glioblastoma *Proc. Natl. Acad. Sci.* **2011**, *108*, 17450-17455.
- (113) Sugahara, K. N.; Teesalu, T.; Karmali, P. P.; Kotamraju, V. R.; Agemy, L.; Girard, O. M.; Hanahan, D.; Mattrey, R. F.; Ruoslahti, E. Tissue-Penetrating Delivery of Compounds and Nanoparticles into Tumors *Cancer cell* **2009**, *16*, 510-520.

- (114) Wu, H.-C.; Chang, D.-K. Peptide-Mediated Liposomal Drug Delivery System Targeting Tumor Blood Vessels in Anticancer Therapy *Journal of Oncology* **2010**, *2010*.
- (115) Ruoslahti, E.; Bhatia, S. N.; Sailor, M. J. Targeting of drugs and nanoparticles to tumors *J. Cell. Biol.* **2010**, *188*, 759-768.
- (116) Jain, R. K. Delivery of molecular and cellular medicine to solid tumors *J. Control. Release* **1998**, *53*, 49-67.
- (117) Lee, T.-Y.; Wu, H.-C.; Tseng, Y.-L.; Lin, C.-T. A Novel Peptide Specifically Binding to Nasopharyngeal Carcinoma For Targeted Drug Delivery *Cancer Res.* **2004**, *64*, 8002-8008.
- (118) Iyer, U.; Kadambi, V. J. Antibody drug conjugates — Trojan horses in the war on cancer *J. Pharmacol. Toxicol. Methods* **2011**, *64*, 207-212.
- (119) Junutula, J. R.; Raab, H.; Clark, S.; Bhakta, S.; Leipold, D. D.; Weir, S.; Chen, Y.; Simpson, M.; Tsai, S. P.; Dennis, M. S.; Lu, Y.; Meng, Y. G.; Ng, C.; Yang, J.; Lee, C. C.; Duenas, E.; Gorrell, J.; Katta, V.; Kim, A.; McDorman, K.; Flagella, K.; Venook, R.; Ross, S.; Spencer, S. D.; Lee Wong, W.; Lowman, H. B.; Vandlen, R.; Sliwkowski, M. X.; Scheller, R. H.; Polakis, P.; Mallet, W. Site-specific conjugation of a cytotoxic drug to an antibody improves the therapeutic index *Nat. Biotech.* **2008**, *26*, 925-932.
- (120) Firestone, R. A.; Willner, D.; Hofstead, S. J.; King, H. D.; Kaneko, T.; Braslawsky, G. R.; Greenfield, R. S.; Trail, P. A.; Lasch, S. J.; Henderson, A. J.; Casazza, A. M.; Hellström, I.; Hellström, K. E. Synthesis and antitumor activity of the immunoconjugate BR96-Dox *J. Control. Release* **1996**, *39*, 251-259.
- (121) Matsui, H.; Takeshita, A.; Naito, K.; Shinjo, K.; Shigeno, K.; Maekawa, M.; Yamakawa, Y.; Tanimoto, M.; Kobayashi, M.; Ohnishi, K.; Ohno, R. Reduced effect of gemtuzumab ozogamicin (CMA-676) on P-glycoprotein and/or CD34-positive leukemia cells and its restoration by multidrug resistance modifiers *Leukemia* **2002**, *16*, 813-819.
- (122) Takeshita, A.; Shinjo, K.; Yamakage, N.; Ono, T.; Hirano, I.; Matsui, H.; Shigeno, K.; Nakamura, S.; Tobita, T.; Maekawa, M.; Ohnishi, K.; Sugimoto, Y.; Kiyoi, H.; Naoe, T.; Ohno, R. CMC-544 (inotuzumab ozogamicin) shows less effect on multidrug resistant cells: analyses in cell lines and cells from patients with B-cell chronic lymphocytic leukaemia and lymphoma *Br. J. Haematol.* **2009**, *146*, 34-43.
- (123) Laakkonen, P.; Vuorinen, K. Homing peptides as targeted delivery vehicles *Integr. Biol.* **2010**, *2*, 326-337.

(124) Curnis, F.; Gasparri, A.; Sacchi, A.; Longhi, R.; Corti, A. Coupling Tumor Necrosis Factor- $\alpha$  with  $\alpha$ V Integrin Ligands Improves Its Antineoplastic Activity *Cancer Res.* **2004**, *64*, 565-571.

(125) Nagy, A.; Schally, A. V.; Armatis, P.; Szepeshazi, K.; Halmos, G.; Kovacs, M.; Zarandi, M.; Groot, K.; Miyazaki, M.; Jungwirth, A.; Horvath, J. Cytotoxic analogs of luteinizing hormone-releasing hormone containing doxorubicin or 2-pyrrolinodoxorubicin, a derivative 500-1000 times more potent *Proc. Natl. Acad. Sci.* **1996**, *93*, 7269-7273.

(126) Arap, W.; Pasqualini, R.; Ruoslahti, E. Cancer Treatment by Targeted Drug Delivery to Tumor Vasculature in a Mouse Model *Science* **1998**, *279*, 377-380.

(127) Kurzrock, R.; Gabrail, N.; Chandhasin, C.; Moulder, S.; Smith, C.; Brenner, A.; Sankhala, K.; Mita, A.; Elian, K.; Bouchard, D.; Sarantopoulos, J. Safety, Pharmacokinetics, and Activity of GRN1005, a Novel Conjugate of Angiopep-2, a Peptide Facilitating Brain Penetration, and Paclitaxel, in Patients with Advanced Solid Tumors *Mol. Cancer Ther.* **2012**, *11*, 308-316.

(128) Günthert, A. R.; Gründker, C.; Bongertz, T.; Nagy, A.; Schally, A. V.; Emons, G. Induction of apoptosis by AN-152, a cytotoxic analog of luteinizing hormone-releasing hormone (LHRH), in LHRH-R positive human breast cancer cells is independent of multidrug resistance-1 (MDR-1) system *Breast Cancer Res. Treat.* **2004**, *87*, 255-264.

(129) Emons, G.; Kaufmann, M.; Gorchev, G.; Tsekova, V.; Gründker, C.; Günthert, A. R.; Hanker, L. C.; Velikova, M.; Sindermann, H.; Engel, J.; Schally, A. V. Dose escalation and pharmacokinetic study of AEZS-108 (AN-152), an LHRH agonist linked to doxorubicin, in women with LHRH receptor-positive tumors *Gynecol. Oncol.* **2010**, *119*, 457-461.

(130) Pearce, T. R.; Shroff, K.; Kokkoli, E. Peptide Targeted Lipid Nanoparticles for Anticancer Drug Delivery *Adv. Mater.* **2012**, *24*, 3803-3822.

(131) Lee, T.-Y.; Lin, C.-T.; Kuo, S.-Y.; Chang, D.-K.; Wu, H.-C. Peptide-Mediated Targeting to Tumor Blood Vessels of Lung Cancer for Drug Delivery *Cancer Res.* **2007**, *67*, 10958-10965.

(132) Xiong, X.-B.; Ma, Z.; Lai, R.; Lavasanifar, A. The therapeutic response to multifunctional polymeric nano-conjugates in the targeted cellular and subcellular delivery of doxorubicin *Biomaterials* **2010**, *31*, 757-768.

(133) Pastorino, F.; Brignole, C.; Marimpietri, D.; Cilli, M.; Gambini, C.; Ribatti, D.; Longhi, R.; Allen, T. M.; Corti, A.; Ponzoni, M. Vascular Damage and Anti-angiogenic Effects of Tumor Vessel-Targeted Liposomal Chemotherapy *Cancer Res.* **2003**, *63*, 7400-7409.

- (134) Shahin, M.; Ahmed, S.; Kaur, K.; Lavasanifar, A. Decoration of polymeric micelles with cancer-specific peptide ligands for active targeting of paclitaxel *Biomaterials* **2011**, *32*, 5123-5133.
- (135) Heppeler, A.; Froidevaux, S.; Eberle, A. N.; Maecke, H. R. Receptor Targeting for Tumor Localisation and Therapy with Radiopeptides *Curr. Med. Chem.* **2000**, *7*, 971-994.
- (136) Dijkgraaf, I.; Boerman, O. C.; Oyen, W. J. G.; Corstens, F. H. M.; Gotthardt, M. Development and Application of Peptide-Based Radiopharmaceuticals *Anti-Cancer Agents Med. Chem.* **2007**, *7*, 543-551.
- (137) Åkerman, M. E.; Chan, W. C. W.; Laakkonen, P.; Bhatia, S. N.; Ruoslahti, E. Nanocrystal targeting in vivo *Proc. Natl. Acad. Sci.* **2002**, *99*, 12617-12621.
- (138) Rufini, V.; Calcagni, M. L.; Baum, R. P. Imaging of Neuroendocrine Tumors *Semin. Nucl. Med.* **2006**, *36*, 228-247.
- (139) Scopinaro, F.; Vincentis, G.; Varvarigou, A.; Laurenti, C.; Iori, F.; Remediani, S.; Chiarini, S.; Stella, S. 99mTc-bombesin detects prostate cancer and invasion of pelvic lymph nodes *Eur. J. Nucl. Med. Mol.* **2003**, *30*, 1378-1382.
- (140) Okarvi; SM. Peptide-based radiopharmaceuticals and cytotoxic conjugates: potential tools against cancer *Cancer Treat Rev.* **2008**, *34*, 13-26.
- (141) Lee, H.-Y.; Li, Z.; Chen, K.; Hsu, A. R.; Xu, C.; Xie, J.; Sun, S.; Chen, X. PET/MRI Dual-Modality Tumor Imaging Using Arginine-Glycine-Aspartic (RGD)-Conjugated Radiolabeled Iron Oxide Nanoparticles *J. Nucl. Med.* **2008**, *49*, 1371-1379.
- (142) Mulder, W. J. M.; Strijkers, G. J.; Habets, J. W.; Bleeker, E. J. W.; van der Schaft, D. W. J.; Storm, G.; Koning, G. A.; Griffioen, A. W.; Nicolay, K. MR molecular imaging and fluorescence microscopy for identification of activated tumor endothelium using a bimodal lipidic nanoparticle *FASEB J.* **2005**, *19*, 2008-2010.
- (143) Buehler, A.; van Zandvoort, M. A. M. J.; Stelt, B. J.; Hackeng, T. M.; Schrans-Stassen, B. H. G. J.; Bennaghmouch, A.; Hofstra, L.; Cleutjens, J. P. M.; Duijvestijn, A.; Smeets, M. B.; de Kleijn, D. P. V.; Post, M. J.; de Muinck, E. D. cNGR: A Novel Homing Sequence for CD13/APN Targeted Molecular Imaging of Murine Cardiac Angiogenesis In Vivo *Arterioscler. Thromb. Vac. Biol.* **2006**, *26*, 2681-2687.
- (144) Bals, R. Epithelial antimicrobial peptides in host defense against infection *Respir. Res.* **2000**, *1*, 141 - 150.

- (145) Ge, Y.; MacDonald, D. L.; Holroyd, K. J.; Thornsberry, C.; Wexler, H.; Zasloff, M. In Vitro Antibacterial Properties of Pexiganan, an Analog of Magainin *Antimicrob. Agents Chemother.* **1999**, *43*, 782-788.
- (146) Gottler, L. M.; Ramamoorthy, A. Structure, membrane orientation, mechanism, and function of pexiganan — A highly potent antimicrobial peptide designed from magainin *Biochim. Biophys. Acta* **2009**, *1788*, 1680-1686.
- (147) Giles, F. J.; Miller, C. B.; Hurd, D. D.; Wingard, J. R.; Fleming, T. R.; Sonis, S. T.; Bradford, W. Z.; Pulliam, J. G.; Anaissie, E. J.; Beveridge, R. A.; Brunvand, M. M.; Martin, P. J.; Investigators†, P.-C. T. A Phase III, Randomized, Double-blind, Placebo-controlled, Multinational Trial of Iseganan for the Prevention of Oral Mucositis in Patients Receiving Stomatotoxic Chemotherapy (PROMPT-CT Trial) *Leuk. Lymphoma* **2003**, *44*, 1165-1172.
- (148) Melo MN, D. D., Castanho MA Omiganan pentahydrochloride in the front line of clinical applications of antimicrobial peptides *Recent Pat Antiinfect. Drug Discov.* **2006**, *1*, 201-207.
- (149) Seshadri Sundararajan, V.; Gabere, M. N.; Pretorius, A.; Adam, S.; Christoffels, A.; Lehväslaiho, M.; Archer, J. A. C.; Bajic, V. B. DAMPD: a manually curated antimicrobial peptide database *Nucleic Acids Res.* **2011**.
- (150) Cotter, P. D.; Hill, C.; Ross, R. P. Bacteriocins: developing innate immunity for food *Nat. Rev. Micro.* **2005**, *3*, 777-788.
- (151) Pons, A.-M.; Lanneluc, I.; Cottenceau, G.; Sable, S. New developments in non-post translationally modified microcins *Biochimie* **2002**, *84*, 531-537.
- (152) Kolter, R.; Moreno, F. Genetics of Ribosomally Synthesized Peptide Antibiotics *Annu. Rev. Microbiol.* **1992**, *46*, 141-161.
- (153) de Lorenzo; V. Isolation and characterization of microcin E492 from *Klebsiella pneumoniae*. *Arch. Microbiol.* **1984**, *139*, 72-75.
- (154) Duquesne, S.; Destoumieux-Garzon, D.; Peduzzi, J.; Rebuffat, S. Microcins, gene-encoded antibacterial peptides from enterobacteria *Nat. Prod. Rep.* **2007**, *24*, 708-734.
- (155) Pavlova, O.; Severinov, K. Posttranslationally modified microcins *Russ. J. Genet.* **2006**, *42*, 1380-1389.
- (156) Destoumieux-Garzón, D.; Peduzzi, J.; Rebuffat, S. Focus on modified microcins: structural features and mechanisms of action *Biochimie* **2002**, *84*, 511-519.

- (157) Destoumieux-Garzón, D.; Thomas, X.; Santamaria, M.; Goulard, C.; Barthélémy, M.; Boscher, B.; Bessin, Y.; Molle, G.; Pons, A.-M.; Letellier, L.; Peduzzi, J.; Rebuffat, S. Microcin E492 antibacterial activity: evidence for a TonB-dependent inner membrane permeabilization on *Escherichia coli* *Mol. Microbiol.* **2003**, *49*, 1031-1041.
- (158) Blond, A.; Peduzzi, J.; Goulard, C.; Chiuchiolo, M. J.; Barthelemy, M.; Prigent, Y.; Salomon, R. A.; Farias, R. N.; Moreno, F.; Rebuffat, S. The cyclic structure of microcin J25, a 21-residue peptide antibiotic from *Escherichia coli* *Eur. J. Biochem.* **1999**, *259*, 747-755.
- (159) Salomon, R. A.; Farias, R. N. Microcin-25, a novel antimicrobial peptide produced by *Escherichia coli* *J. Bacteriol.* **1992**, *174*, 7428-7435.
- (160) Solbiati, J.; Ciaccio, M.; Farias, R.; Salomon, R. Genetic analysis of plasmid determinants for microcin J25 production and immunity *J. Bacteriol.* **1996**, *178*, 3661-3663.
- (161) Bayro, M. J.; Mukhopadhyay, J.; Swapna, G. V. T.; Huang, J. Y.; Ma, L. C.; Sineva, E.; Dawson, P. E.; Montelione, G. T.; Ebright, R. H. Structure of antibacterial peptide microcin J25: A 21-residue lariat protoknot *J. Am. Chem. Soc.* **2003**, *125*, 12382-12383.
- (162) Duquesne, S.; Destoumieux-Garzon, D.; Zirah, S.; Goulard, C.; Peduzzi, J.; Rebuffat, S. Two enzymes catalyze the maturation of a lasso peptide in *Escherichia coli* *Chem. Biol.* **2007**, *14*, 793-803.
- (163) Yan, K.-P.; Li, Y.; Zirah, S.; Goulard, C.; Knappe, T. A.; Marahiel, M. A.; Rebuffat, S. Dissecting the Maturation Steps of the Lasso Peptide Microcin J25 in vitro *ChemBioChem* **2012**, *13*, 1046-1052.
- (164) Bierbaum, G.; Jansen, A. Tying the Knot: Making of Lasso Peptides *Chem. Biol.* **2007**, *14*, 734-735.
- (165) Katahira, R.; Yamasaki, M.; Matsuda, Y.; Yoshida, M. MS-271, A novel inhibitor of calmodulin-activated myosin light chain kinase from *Streptomyces* sp.—II. Solution structure of MS-271: Characteristic features of the 'lasso' structure *Bioorg. Med. Chem* **1996**, *4*, 121-129.
- (166) Wyss DF, L. H., Manneberg M, Labhardt AM. Anantin--a peptide antagonist of the atrial natriuretic factor (ANF). II. Determination of the primary sequence by NMR on the basis of proton assignments *J. Antibiot. (Tokyo)*. **1991**, *44*, 172-180.
- (167) Frechet, D.; Guitton, J. D.; Herman, F.; Faucher, D.; Helynck, G.; Monegier du Sorbier, B.; Ridoux, J. P.; James-Surcouf, E.; Vuilhorgne, M.

Solution structure of RP 71955, a new 21 amino acid tricyclic peptide active against HIV-1 virus *Biochemistry (Mosc)*. **1994**, *33*, 42-50.

(168) Chokekijchai, S.; Kojima, E.; Anderson, S.; Nomizu, M.; Tanaka, M.; Machida, M.; Date, T.; Toyota, K.; Ishida, S.; Watanabe, K. NP-06: a novel anti-human immunodeficiency virus polypeptide produced by a *Streptomyces* species *Antimicrob. Agents Chemother.* **1995**, *39*, 2345-2347.

(169) Iwatsuki, M.; Tomoda, H.; Uchida, R.; Gouda, H.; Hirono, S.; Ōmura, S. Lariatins, Antimycobacterial Peptides Produced by *Rhodococcus* sp. K01-B0171, Have a Lasso Structure *J. Am. Chem. Soc.* **2006**, *128*, 7486-7491.

(170) Knappe, T.; Linne, U.; Zirah, S.; Rebuffat, S.; Xie, X. L.; Marahiel, M. Isolation and structural characterization of capistruin, a lasso peptide predicted from the genome sequence of *Burkholderia thailandensis* E264 *J. Pept. Sci.* **2008**, *14*, 97-97.

(171) Vincent, P. A.; Morero, R. D. The Structure and Biological Aspects of Peptide Antibiotic Microcin J25 *Curr. Med. Chem.* **2009**, *16*, 538-549.

(172) Vincent, P. A.; Delgado, M. A.; Farias, R. N.; Salomon, R. A. Inhibition of *Salmonella enterica* serovars by microcin J25 *FEMS Microbiol. Lett.* **2004**, *236*, 103-107.

(173) Delgado, M. A.; Rintoul, M. R.; Farias, R. N.; Salomon, R. A. *Escherichia coli* RNA Polymerase Is the Target of the Cyclopeptide Antibiotic Microcin J25 *J. Bacteriol.* **2001**, *183*, 4543-4550.

(174) Bellomio, A.; Vincent, P. A.; de Arcuri, B. F.; Farias, R. N.; Morero, R. D. Microcin J25 Has Dual and Independent Mechanisms of Action in *Escherichia coli*: RNA Polymerase Inhibition and Increased Superoxide Production *J. Bacteriol.* **2007**, *189*, 4180-4186.

(175) Bellomio A, V. P., de Arcuri BF, Salomón RA, Morero RD, Farías RN. The microcin J25 beta-hairpin region is important for antibiotic uptake but not for RNA polymerase and respiration inhibition. *Biochem. Biophys. Res. Commun.* **2004**, *325(4)*, 1454-1458.

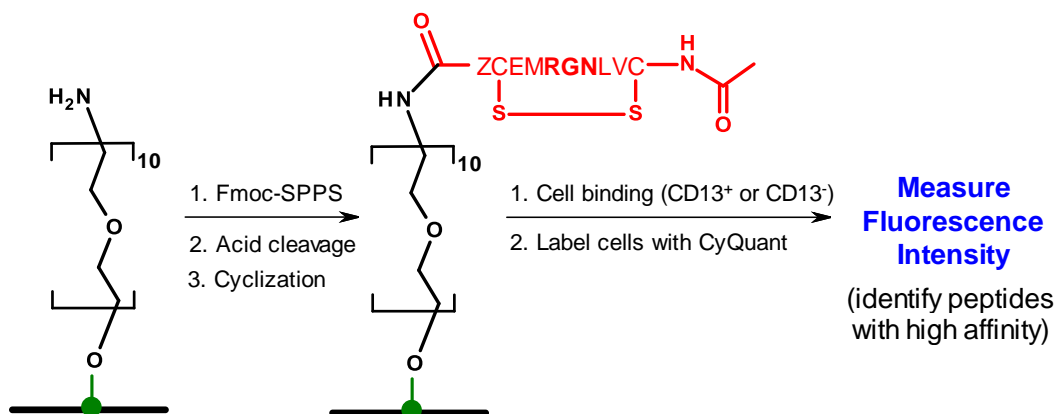
(176) Semenova, E.; Yuzenkova, Y.; Peduzzi, J.; Rebuffat, S.; Severinov, K. Structure-Activity Analysis of Microcin J25: Distinct Parts of the Threaded Lasso Molecule Are Responsible for Interaction with Bacterial RNA Polymerase *J. Bacteriol.* **2005**, *187*, 3859-3863.

(177) Bellomio, A.; Rintoul, M. a. R.; Morero, R. D. Chemical modification of microcin J25 with diethylpyrocarbonate and carbodiimide: evidence for essential histidyl and carboxyl residues *Biochem. Biophys. Res. Commun.* **2003**, *303*, 458-462.

- (178) Vincent, P. A.; Bellomio, A.; de Arcuri, B. F.; Farías, R. N.; Morero, R. D. MccJ25 C-terminal is involved in RNA-polymerase inhibition but not in respiration inhibition *Biochem. Biophys. Res. Commun.* **2005**, *331*, 549-551.
- (179) McCormick, J. K.; Klaenhammer, T. R.; Stiles, M. E. Colicin V can be produced by lactic acid bacteria *Lett. Appl. Microbiol.* **1999**, *29*, 37-41.
- (180) Stiles, M. E., Vederas, J. C., Van Belkum, M. J., Worobo, R. W., Worobo, R. J., McCormick, J. K., Greer, G. G., McMullen, L. M., and Leisner, J. J. USA, 2003; Vol. 20030039632.
- (181) Sable, S.; Pons, A. M.; Gendron-Gaillard, S.; Cottenceau, G. Antibacterial activity evaluation of microcin J25 against diarrheagenic *Escherichia coli* *Appl. Environ. Microbiol.* **2000**, *66*, 4595-4597.
- (182) Yorgey, P.; Lee, J.; Kördel, J.; Vivas, E.; Warner, P.; Jebaratnam, D.; Kolter, R. Posttranslational modifications in microcin B17 define an additional class of DNA gyrase inhibitor *Proceedings of the National Academy of Sciences* **1994**, *91*, 4519-4523.
- (183) Pons, A.-M.; Delalande, F.; Duarte, M.; Benoit, S.; Lanneluc, I.; Sablé, S.; Van Dorsselaer, A.; Cottenceau, G. Genetic Analysis and Complete Primary Structure of Microcin L *Antimicrob. Agents Chemother.* **2004**, *48*, 505-513.
- (184) Cornut, G.; Fortin, C.; Soulieres, D. Antineoplastic properties of bacteriocins: revisiting potential active agents *Am. J. Clin. Oncol.* **2008**, *31*, 399-404.
- (185) Hetz, C.; Bono, M. R.; Barros, L. F.; Lagos, R. Microcin E492, a channel-forming bacteriocin from *Klebsiella pneumoniae*, induces apoptosis in some human cell lines *Proc. Natl. Acad. Sci.* **2002**, *99*, 2696-2701.
- (186) Vizán; J. L., Hernández-Chico; C., del Castillo, I., Moreno, F. The peptide antibiotic microcin B17 induces double-strand cleavage of DNA mediated by *E. coli* DNA gyrase *EMBO J.* **1991**, *10*, 467-476.
- (187) Heddle, J. G.; Blance, S. J.; Zamble, D. B.; Hollfelder, F.; Miller, D. A.; Wentzell, L. M.; Walsh, C. T.; Maxwell, A. The antibiotic microcin B17 is a DNA gyrase poison: characterisation of the mode of inhibition *J. Mol. Biol.* **2001**, *307*, 1223-1234.
- (188) Niklison Chirou, M. a. V.; Minahk, C. J.; Morero, R. D. Antimitochondrial activity displayed by the antimicrobial peptide microcin J25 *Biochem. Biophys. Res. Commun.* **2004**, *317*, 882-886.

(189) Niklison-Chirou, M. V.; Dupuy, F.; Saavedra, L.; Hebert, E.; Banchio, C.; Minahk, C.; Morero, R. D. Microcin J25-Ga induces apoptosis in mammalian cells by inhibiting mitochondrial RNA-polymerase *Peptides* **2011**, *32*, 832-834.

## Chapter 2 : NGR Peptide Ligands for Targeting CD13/APN Identified through Peptide Array Screening



*Rania Soudy, Sahar Ahmed, and Kamaljit Kaur\**, NGR Peptide Ligands for Targeting CD13/APN Identified through Peptide Array Screening Resemble Fibronectin Sequences, *ACS Combinatorial Science*, **2012**, In press.

## 2.1. Introduction

Targeted drug therapy to tumor vasculature has emerged as one of the most promising approaches for the treatment of cancer. In this approach, specific targeting moieties, such as peptides or antibodies, actively guide the drugs to receptors that are uniquely expressed on the tumor vascular tissue.<sup>1,2</sup> Some of these unique molecular markers expressed within tumor associated vessels include  $\alpha\beta3$  and  $\alpha\beta5$  integrins,<sup>3,4</sup> aminopeptidase N (APN or CD13),<sup>5</sup> vascular endothelial growth factor receptors (VEGFRs),<sup>6,7</sup> and matrix metalloproteinases (MMPs).<sup>8</sup> The differential expression of these cancer cell biomarkers make them attractive targets for selective delivery of chemotherapeutic drugs and diagnostic moieties.<sup>9,10</sup>

APN (CD13) is a  $Zn^{2+}$  dependent metalloprotease that has been implicated in various cell functions such as, proliferation, invasion and angiogenesis.<sup>11,12</sup> Specific APN isoforms are highly expressed in various tumors and angiogenic cells, and these are different from the APN forms expressed by the endothelium of normal blood vessels.<sup>13</sup> Yet more recently, it has been shown that APN is selectively expressed in vascular endothelial cells, such as human umbilical vein endothelial cells (HUVEC), and plays multiple roles in angiogenesis.<sup>5,7,14</sup> Thus CD13 has become an attractive molecular tumor marker and potential therapeutic target.<sup>5,15</sup> *In vivo* screening of phage libraries led to the discovery of Asn-Gly-Arg (NGR) peptide motif that binds primarily to the CD13 receptor expressed in the endothelium of angiogenic blood vessels.<sup>16,17</sup> The selective tumor homing

ability of NGR motif led to the use of this peptide for targeted delivery of various antitumor compounds, such as chemotherapeutic drugs,<sup>17</sup> cytokines,<sup>18</sup> viral particles,<sup>19</sup> and liposomes<sup>20</sup> specifically to the tumor vessels. Notably, NGR sequence is also present in fibronectin (FN), an extracellular matrix protein involved in several key cellular processes.<sup>21</sup> Human FN is a large glycoprotein that contains primarily three types of repeating modules, type I, II, and III. NGR with different flanking residues is present in each of the repeating modules of human FN.

Phage display technology has been employed for selecting peptides with high affinity for CD13 associated with the angiogenic blood vessels. Several NGR containing peptide sequences have been identified, such as disulfide bond cyclized CNGRC (cCNGRC) and cCVLNGRMEC, as well as, linear analogues GNGRG and NGRAHA.<sup>17,22</sup> Peptide sequence cCNGRC has been coupled to different anticancer compounds, such as doxorubicin,<sup>17,23</sup> cisplatin<sup>24</sup>, proapoptotic peptides<sup>25</sup>, and tumor necrosis factor- $\alpha$  (TNF).<sup>18</sup> NGR conjugated to TNF (NGR-hTNF) is in phase II clinical trials.<sup>26,27</sup> In addition to disulfide cyclized sequences, N- to C-terminal amide bond cyclized cKNGRE sequence has been studied that displayed enhanced binding affinity for tumor targeting applications.<sup>28</sup> Pentapeptide analogues of NGR synthesized via on-resin click chemistry have also been developed, and show specific binding to purified CD13 receptor, as well as, to the cell lysates from CD13<sup>+</sup> SKOV-3 cancer cells.<sup>29</sup> Structure-function studies with different NGR peptide sequences suggest that the molecular scaffold in which NGR residues are embedded, could affect binding

affinity, specificity, and peptide stability. For instance, studies with cyclic CNGRC and linear GNGRG peptides showed that the presence of disulfide constraint enhances interaction with CD13 improving ten-fold targeting ability.<sup>30</sup> Modification of cCNGRC with proline to produce cCPNGRC improved overall binding affinity to APN, and led to 30-fold lower IC<sub>50</sub> for the inhibition of APN proteolytic activity.<sup>31</sup> In addition, it has been shown that flanking residues play an important role in NGR to isoaspartate-glycine-arginine (isoDGR) conversion with concomitant exchange of receptor affinity from CD13 to  $\alpha v\beta 3$  integrin.<sup>32</sup>

Above studies demonstrate that the specificity and affinity of NGR peptides for the CD13 receptor can be improved by altering the NGR flanking residues. To address this hypothesis, we have designed and screened a library of NGR sequences based on the lead cCVLNGRMEC peptide to identify new peptides with enhanced binding affinity for CD13. A library of 45 peptides was synthesized in an array format on cellulose membrane and the library was screened against CD13<sup>+</sup> and CD13<sup>-</sup> cell lines using a peptide array-whole cell binding assay. We have previously shown that peptide array-whole cell binding assay is a complementary method to phage display for the identification of peptides with higher binding affinity and specificity for cancer cells.<sup>33</sup> Here we show that the library screening led to the identification of five NGR peptides (peptides **5**, **14**, **21**, **22**, and **34**) that display higher binding (up to 5-fold) to CD13<sup>+</sup> cells with negligible binding to CD13<sup>-</sup> cell lines when compared to the lead sequence. These peptides with augmented affinity for the CD13<sup>+</sup> cells also

show improved *in vitro* cellular uptake and specificity using soluble FITC-labeled peptides. Markedly, the peptides identified here are similar to or resemble the NGR sequences present in the human FN protein.

## **2.2. Materials and Methods**

### **2.2.1. Peptide Array Synthesis**

Peptide array consisting of forty five peptide sequences (ranging from 5-mer to 9-mer) in duplicates was synthesized on a cellulose membrane using an AutoSpot as described previously.<sup>33</sup> Briefly, peptide array was synthesized on an amino-PEG500 cellulose membrane derivatized with a polyethylene (PEG) spacer and a free amino terminal group using a semiautomatic robot AutoSpot ASP222 (Intavis AG, Germany). DIGEN software (Jerini Bioteools GmbH, Berlin, Germany) was used for formatting the array. The synthesis was started by anchoring a  $\beta$ -alanine residue (linker) to the cellulose membrane and thereafter peptides were synthesized from the C-terminal end. Fmoc amino acids (0.25 mM/mL) activated with HOBt and DIC were spotted on the membrane in 60 nL aliquots per spot by a robotic syringe, yielding a peptide loading of 0.4  $\mu\text{mol}/\text{cm}^2$ . After coupling of the Fmoc amino acid, the membrane was removed from the synthesizer and was treated with acetic anhydride (2%) to cap any free remaining amino groups. Piperidine (20%) in DMF was used for Fmoc deprotection. After washing, the membrane was air dried and carefully repositioned on the robotic synthesizer to repeat the coupling cycles in order to complete the peptide sequence. At the end, all peptides were N-terminally acetylated. The final

removal of side chain protecting groups was performed by treating the membrane with a cocktail of reagents, comprised of TFA (15 mL), DCM (15 mL), triisopropylsilane (0.9 mL), and water (0.6 mL), for about 3 h. After extensive washing with DCM, DMF, and ethanol, the membrane was dried with cold air. Next, the cyclization of cysteine containing peptides was performed to form the disulfide bond. The membrane was incubated with 20% DMSO in water for 24 h at 4 °C, and finally overnight at r.t. Subsequently, the membrane was washed with ethanol (3 x 3 min), dried, and stored in a sealed bag at -20 °C until use. To ensure cyclization on the membrane, we have previously characterized representative cyclic peptides using a membrane with a cleavable linker.<sup>33</sup> For membrane regeneration, the bound cells were removed after each cell-binding experiment by first washing with ethanol for 5 min, followed by treatment with 0.1 N HCl for 20 min. The peptide array membrane was then washed with DMF (4 x 20 min), ethanol (3 x 3 min), and finally dried in air.

### **2.2.2. APN/CD13 Expression Level**

Fluorescence activated cell sorting (FACS) was performed to quantify the level of expression of APN/CD13 among the selected four cell lines. The human fibrosarcoma HT-1080 (American Type Culture Collection, Manassas, VA) and the human breast cancer cell line MDA-MB-231 were cultured in DMEM with Glutamax containing 10% FCS (Invitrogen). Human umbilical vein endothelial cells (HUVEC) were kind gift from the laboratory of Sandra Davidge, University

of Alberta. These cells were cultivated using Endothelial Cell Growth Medium (EGM, LONZA) containing 20% FCS, 2 mmol/L glutamine, 100 IU/mL penicillin, 100 IU/mL streptomycin, and 2 ng/mL basic fibroblast growth factor (Roche Diagnostics, Mannheim, Germany). The human cancer cell line MDA-MB-435 was cultured in RPMI-1640 with Glutamax containing 10% FCS (Invitrogen, Karlsruhe, Germany), 100 IU/mL penicillin, and 100 IU/mL streptomycin. All cell lines were cultured at 37 °C in a 5% CO<sub>2</sub> incubator. Cells (10<sup>6</sup>) were suspended in FACS buffer (100 µL, PBS with 2% FCS), and incubated with FITC labeled CD13 antihuman antibody (20 µL, WM-15) for 30 min at 4 °C. The cells were washed twice with FACS buffer after centrifugation, the same was done for cells without antibody treatment which served as a negative control, and the APN/CD13 expression level was measured using flow cytometry. FACS experiments were performed on a Beckman Coulter QUANTA™ SC Flow Cytometer. The data was analyzed by CellQuest software and is presented as the average of mean cell fluorescence intensity (± SD) of triplicate wells.

### **2.2.3. Peptide Array-Cell Binding Assay**

Peptide array-whole cell binding was performed following the method developed in our laboratory previously.<sup>33</sup> Briefly, the peptide array membrane was incubated with the cells (20 mL, 75 x 10<sup>3</sup> cells/mL) for 8 h in serum free media. After washing the non-bound cells, the membrane was first frozen at -80 °C for 2 hr followed by thawing at r.t. and incubation with the CyQUANT dye.

The membrane was washed (6x with PBS) and scanned using Kodak imager ( $\lambda_{\text{ex}}$  465 nm, ( $\lambda_{\text{em}}$  535 nm). The net fluorescence intensity of each peptide spot was quantified using Kodak Molecular Imaging Software Version 4.0. An external standard peptide was used to calibrate the fluorescence intensity between scans performed on the same day and on different days. The membrane was regenerated after each cell-binding experiment. Each cell-binding experiment was repeated twice for the four cell lines. The results are presented as average fluorescence intensity ( $\pm$  standard deviation) of two duplicate peptide spots, two scans, and two different experiments. The relative cell adhesion ratio (**Table 2.1**) for each peptide sequence was calculated as the ratio of the average fluorescence of the peptide analogue divided by that of parent peptide **1**.

#### **2.2.4. Synthesis of FITC-labeled Peptides**

Seven FITC-labeled peptides, (FITC-**1**, FITC-**5**, FITC-**14**, FITC-**21**, FITC-**22**, FITC-**34**, FITC-**43**), and two unlabeled peptides (**1** and **22**) were synthesized on an automatic synthesizer (Advanced ChemTech MPS 357, Louisville, KY, USA) following Fmoc solid phase peptide synthesis (SPPS).<sup>34</sup> Peptides were synthesized on 2-chlorotritylchloride resin (0.1 mmol, 1 mmol/g) using DIC/HOBT mixture as coupling agent. After complete peptide synthesis,  $\beta$ -alanine was conjugated to the N-terminal amino group followed by fluorescein isothiocyanate (FITC) coupling. FITC (0.3 mmol) was coupled to peptide using DIPEA (0.6 mmol) in dark for 24 h, followed by extensive washing of the resin.

FITC-labeled peptide was cleaved from the resin, along with the deprotection of the amino acid side chains by TFA/DCM (50:50) mixture. The crude cleaved peptides were precipitated by cold diethyl ether, followed by centrifugation, and lyophilisation. The white powder obtained was solubilized in ACN/H<sub>2</sub>O mixture (20%:80%), then it was further purified using RP-HPLC. Peptide oxidation was carried out by incubating peptide in 20% aqueous DMSO to help in oxidation (r.t., 2 days). Disulfide bond formation was confirmed with Ellman test and MALDI-TOF mass spectrometry. The peptides were purified by RP-HPLC (Varian Prostar HPLC, Walkersville, MD, USA) using a linear gradient of isopropanol/water containing 0.1% TFA and were lyophilized. Purity of the final products was analyzed using analytical RP-HPLC (**Figure A.2**) and MALDI-TOF mass characterization (**Table 2.2** and **Figure A.1**). Stock solution for the peptides was prepared in sterile 10% aqueous acetonitrile and stored at -20 °C. Peptide concentrations were determined by measuring fluorescence at excitation 465 nm and emission 535 nm.

### **2.2.5. Peptide Stability and Deamination**

To evaluate peptide stability, a solution of peptide **5** in DMEM was incubated at 37 °C, mimicking conditions used in the *in vitro* cell binding experiments. At different time intervals, aliquots were removed and peptide stability was monitored using MALDI-TOF mass spectrometry and RP-HPLC. The same experiment was also repeated for peptide in water.

### **2.2.6. *In vitro* Cellular Uptake using FACS**

FACS analysis was used to evaluate the binding of the FITC-labeled peptides to CD13<sup>+</sup> (HUVEC and HT-1080) and CD13<sup>-</sup> (MDA-MB-435 and MDA-MB-231) cell lines. Cells were placed into 6-well plates at a density of 10<sup>6</sup> in culture media (3 mL) at 37 °C for 24 h to adhere to the plate surface. The culture media was replaced with fresh serum-free media (1 mL) containing FITC-labeled peptides at a concentration of 10<sup>-6</sup> mol/L. Cells were incubated with the peptides for 30 min at 37 °C. The media was then removed and the cells were washed to remove the unbound peptides. The cells were scrapped and transferred to centrifuge tubes followed by centrifugation at 1,000 rpm for 7 min. The pellet was resuspended in FACS buffer (2% FCS in PBS), washed once more and then resuspended again in FACS buffer. Untreated cells were subjected to similar steps to detect autofluorescence of the cells. The samples were then subjected to the FACS instrument, Beckman Coulter QUANTA™ SC Flow Cytometer using the FL1 channel (10,000 events/sample). Instrument settings were calibrated so that untreated cells show 1–2% of fluorescence. The mean cell fluorescence was determined ( $\lambda_{\text{ex}}$  485 nm,  $\lambda_{\text{em}}$  525 nm) and the data was analyzed by Quanta SC software.

### 2.2.7. Cellular Uptake using Fluorescence Microscopy

MDA-MB-435 or HUVEC cells (50,000) were cultured on the top of a cover slip at 37 °C for 24 hr. The medium was removed and replaced with fresh serum free medium (1 mL), containing FITC-**5** ( $10^{-6}$  mol/L). The cells were incubated with the peptide for 30 min at 37 °C. After incubation, the medium was removed and the cells were washed with serum free medium (3 x 2 mL). The cells were fixed on ice with 2% formaldehyde for 20 min. The formaldehyde was removed by washing with media (3 times). The cover slips were put on slides containing one drop of DAPI-Antifade (Molecular Probes) to stain the nucleus. The cells were imaged under the fluorescence microscope (Zeiss, Göttingen, Germany) using green and blue filters with 20x magnification. The samples prepared for fluorescence microscopy were also used for visualization by confocal microscopy. Confocal laser scanning microscopy was performed with a Zeiss 510 LSMNLO confocal microscope (Carl Zeiss Microscope Systems, Jena, Germany) with a 40x oil immersion lens. For the competitive binding, the same experiment was carried out in the presence of unlabeled peptide **5** ( $10^{-4}$  mol/L) as a competitor.

A co-culture experiment of HT-1080 and MDA-MB-435 cells was carried out as previously described.<sup>35</sup> Briefly, to visualize the cells and distinguish between HT-1080 and MDA-MB-435 cells in the co-culture, adherent MDA-MB-435 cells were stained using the Blue Cell Tracker fluorescent dye (25 µM) according to the manufacturer's protocol. MDA-MB-435 cells were incubated with dye in serum free media at 37 °C for 35 min, followed by another 30 min in

fresh media. Subsequently, HT-1080 and MDA-MB-435 cells were cultured together in a 24-well plate with cover slip at a density of  $2 \times 10^5$  cells/well for 24 h at 37 °C, and the seeding ratio was 1:1. The following day, cells were incubated with FITC-5 (10  $\mu$ M) in DMEM serum free media for 30 min at 37 °C. After washing with PBS (3 times), cells were fixed using 2% formaldehyde in PBS for 20 min on ice, and the cover slip was placed onto a glass slide over the fluorescence mounting medium. The images were acquired by a fluorescence microscope at 20 $\times$  magnification with FITC and DAPI filters.

#### **2.2.8. Aminopeptidase Enzymatic Inhibition.**

APN activity on the surface of intact HT-1080 cells was measured using Ala-4-nitroanilide (H.Ala-pNA.HCl) as a substrate, and bestatin as a specific inhibitor (positive control). Experiment was carried out as previously described with some modifications.<sup>36</sup> In a typical experiment, cells ( $2 \times 10^5$ ) were seeded in each well of a 24-well culture plate, and after incubation for 24 hr at 37 °C, media was aspirated. The cells were preincubated for 5 min with peptide or bestatin at 0.5 mM concentration in PBS (pH 7.4). Following which Ala-pNA substrate (6 mM) at 37 °C was added directly, and further incubated in the dark for 30 min at 37 °C. The supernatant from each well was collected, centrifuged, and enzyme activity was determined by measuring formation of yellow pNA at 405 nm using a Power Wave X340 microplate reader (Bio-Tek Instrument Inc. USA). To quantify the effect of inhibitors, the remaining activity was expressed as the

percentage of the control activity without inhibitor. All measurements were made in triplicates.

## **2.3. Results and Discussion**

Integrin  $\alpha v\beta 3$  and CD13 (APN) are the most studied receptors for targeting endothelial cells involved in tumor angiogenesis.<sup>3,5,37</sup> Structure of RGD peptides has been optimized and several RGD peptides targeting integrins are undergoing preclinical evaluation for tumor targeting.<sup>38,39</sup> NGR sequence is equally promising for targeting CD13 receptor, however, has been less explored compared to the RGD sequence. In order to optimize the binding affinity and specificity of the NGR sequence, we have designed a peptide array consisting of forty five peptide sequences to screen against CD13 expressing cell lines (CD13<sup>+</sup>), and cells that do not express CD13 (CD13<sup>-</sup>).

### **2.3.1. Engineering NGR-based Peptide Library**

Forty five NGR peptide sequences, cyclic and acyclic, based on the sequence of the CVLNGRMEC peptide<sup>16</sup> (peptide **1**, **Table 2.1**) were designed and synthesized. The key NGR motif was maintained in all the peptides, except the negative controls. Peptide **1**, the lead 9-mer peptide, containing the NGR motif was originally identified by phage display that specifically targets tumor blood vessels.<sup>17</sup> Later it was found that the NGR motif targets the CD13 in the

angiogenic vasculature and in many tumor cell lines.<sup>22</sup> Peptides **2-7** are previously reported sequences or derivatives of reported sequences.<sup>17,21,40,41</sup> Met was replaced with Nle in peptide **2** as well as in the designed sequences to overcome problem associated with Met oxidation. NGR containing peptide **3** was isolated by in vivo phage display to target  $\alpha_5\beta_1$  integrins.<sup>40</sup> Peptides **4** and **5** are conserved NGR sequences present in the natural protein, fibronectin.<sup>22</sup> Peptide **6** is a hybrid of peptides **3** and **4**. Peptide **7** was identified by Lau and coworkers as a peptide ligand for adhesion and proliferation of human lung cancer cells.<sup>41</sup>

The designed peptides in the peptide array were separated into three groups, **8-12**, **13-26**, and **27-37**. Peptides **8-12** (group 1) consisted of Ala scan where all residues in peptide **2**, except the NGR sequence, were substituted with Ala. Next, sequences with N- or C-terminal residues deleted yielded shorter cyclic peptides **13-22** ranging from 5-mer to 8-mer. Peptides **23-26** were linear derivatives of peptide **2**. These were designed to study the effect of disulfide constraint on targeting efficiency. In addition, the linear NGR motif, GNGRG (**26**), is present in the wild type fibronectin sequence.<sup>21,22</sup>

Peptides **27-37** (group 3) involved conservative substitution of the residues in peptide **2**. Peptides **27-37** are peptide **2** analogues with N- (Val2 or Leu3) or C-terminal (Nle7 or Glu8) residues substituted with different amino acids. For instance, Val2 of **2** was substituted with either non-polar Ile or  $\beta$ -Ala to give peptides **27** and **29**, respectively or polar Thr to give peptide **28**. Likewise, Leu3 was substituted with non-polar Val,  $\beta$ -Ala or Nle in analogues **30-32**, respectively.

Peptides **33** and **34** have a hydroxyl containing amino acid (Ser) next to Asn or Arg residues, respectively, of the NGR motif. The C-terminal Glu8 was similarly replaced to give peptides with either negatively charged Asp in analogue **35**, or positively charged Lys in analogue **36**. Peptide **37** has two L-cysteines replaced with D-cysteines. Peptides **38-45** were designed as negative control peptides with scrambled sequences and varying length, and were devoid of the NGR motif. Peptide library consisting of 45 peptides in duplicates (**Table 2.1**) was synthesized on the cellulose membrane in an array format for rapid and facile screening against cancer cell lines. Peptide array was synthesized on non-cleavable cellulose membrane (amino-PEG500) using SPOT synthesis, where the C-terminus of the peptide was attached to the surface of the amino-PEG500 cellulose membrane through  $\beta$ -ala spacer as described previously.<sup>33</sup> Peptides were synthesized by covalent conjugation to the free amino functional group using a stepwise Fmoc-SPPS procedure. Each peptide was synthesized at a concentration of ~50 nmoles which was spread on the membrane in a spot with a diameter of 4 mm. After complete synthesis of the array, the peptides were oxidized (cyclized) on the membrane. To achieve cyclization or disulfide bond formation, the peptide array was incubated in 20% aqueous DMSO at 4 °C for 24 h followed by overnight incubation at room temperature. The stepwise incubations were done to decrease the possibility of degradation and transition of NGR to *iso*DGR/DGR, which is accompanied by the loss of CD13 binding. Recent studies have shown that compounds containing the NGR motif can rapidly deamidate and generate *iso*DGR spontaneously at elevated pH and temperature.<sup>42</sup>

### 2.3.2. Level of Aminopeptidase N (or CD13) Expression

Four cells lines, namely, HUVEC human umbilical cord, HT-1080 fibrosarcoma, MDA-MB-435 melanoma and MDA-MB-231 breast cancer cells were evaluated for APN/CD13 expression using flow cytometry. The CD13 expression level was quantified by the mean fluorescence of the cells after incubation with FITC-labeled antihuman CD13 antibody (CD13mAb or WM15).

The results showed that HUVEC and HT-1080 cells express high level of CD13 with mean cell fluorescence 90 and 46.7, respectively, whereas, MDA-MB-231 and MDA-MB-435 do not express this receptor and show mean cell fluorescence of 7 and 5.2, respectively (**Figure 2.1**). The results match with the reported CD13 expression levels of different cell lines.<sup>43</sup> For subsequent experiments, HUVEC and HT-1080 were selected as CD13<sup>+</sup>, while MDA-MB-435 and MDA-MB-231 served as CD13<sup>-</sup> or negative control cell lines.

**Table 2.1.** Sequence of the NGR peptide library and the relative cell adhesion of the peptides.

Peptide	Peptide Sequence	Relative Cell Adhesion		
		HUVEC	HT-1080	
<b>1</b>	CVLNGRMEC	1.0	1.0	
<b>2</b>	CVLNGR <u>X</u> EC	1.7	1.6	
<b>3</b>	NGRAHA	2.6	1.6	
<b>4</b>	LNGRE	3.2	3.3	
<b>5</b>	<b>YNGRT</b>	<b>5.4</b>	<b>5.5</b>	
<b>6</b>	LNGRAHA	0.4	0.5	
<b>7</b>	cNGRGEQc	1.9	1.3	
<b>Group 1</b>	<b>8</b>	C <u>A</u> LNGRXEC	1.3	2.7
	<b>9</b>	CV <u>A</u> NGRXEC	3.1	1.6
	<b>10</b>	CVLNGR <u>A</u> EC	1.2	2.4
	<b>11</b>	CVLNGR <u>X</u> <u>A</u> C	1.1	0.6
	<b>12</b>	CVLNGRXE <u>A</u>	2.4	2.1
<b>Group 2</b>	<b>13</b>	CVLNGRXC	1.2	2.7
	<b>14</b>	<b>CVLNGREC</b>	<b>3.4</b>	<b>3.9</b>
	<b>15</b>	CVLNGRC	1.9	2.7
	<b>16</b>	CLNGRXEC	0.4	0.8
	<b>17</b>	CVNGRXEC	1.1	2.6
	<b>18</b>	CNGRXEC	0.7	1.1
	<b>19</b>	CLNGRXC	0.5	0.9
	<b>20</b>	CVNGREC	0.8	2.2
	<b>21</b>	<b>CNGRC</b>	<b>3.5</b>	<b>4.2</b>
	<b>22</b>	<b>KCNGRC</b>	<b>4.3</b>	<b>4.8</b>
<b>23</b>	<u>K</u> VLNGRXE	2.0	3.1	
<b>24</b>	<u>G</u> VLNGRME <u>G</u>	1.2	0.8	
<b>25</b>	<u>G</u> VLNGRXE <u>G</u>	1.2	1.6	
<b>26</b>	<u>G</u> NGR <u>G</u>	2.7	2.8	
<b>Group 3</b>	<b>27</b>	C <u>I</u> LNGRXEC	1.2	1.3
	<b>28</b>	C <u>T</u> LNGRXEC	0.5	1.3
	<b>29</b>	C <u>Z</u> LNGRXEC	0.3	1.7
	<b>30</b>	CV <u>V</u> NGRXEC	2.1	2.7
	<b>31</b>	CV <u>Z</u> NGRXEC	1.5	2.1
	<b>32</b>	CV <u>X</u> NGRXEC	3.1	3.9
	<b>33</b>	CV <u>S</u> NGRXEC	2.1	3.9
	<b>34</b>	<b>CVLNGR<u>S</u>EC</b>	<b>3.2</b>	<b>4.5</b>
	<b>35</b>	CVLNGRX <u>D</u> C	3.1	3.7
	<b>36</b>	CVLNGRX <u>K</u> C	1.7	2.0
<b>37</b>	<u>c</u> VLNGRXE <u>c</u>	1.1	3.1	
<b>-ve control</b>	<b>38</b>	CKLARAXEC	0.7	0.9
	<b>39</b>	VLARAXE	1.0	0.6
	<b>40</b>	CVL <u>Q</u> GRXEC	0.4	2.2
	<b>41</b>	CVLARAXEC	0.9	2.1
	<b>42</b>	AVLXGXEA	2.3	5.4
	<b>43</b>	VLGXE	0.4	0.6
	<b>44</b>	CVLGXEC	1.2	2.5
	<b>45</b>	CARAC	0.6	0.8

aa substitution is underlined; X=norleucine; Z=β-alanine, lower case letter=D-aa. RCA is the average ratio of fluorescence of a peptide divided by peptide **1**

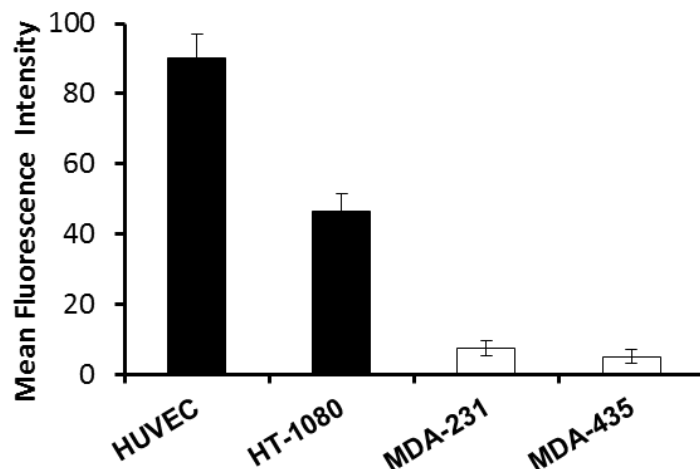


**Figure 2.1.** Expression of aminopeptidase N (APN or CD13) in the cell lines used in this study. Four cell lines, CD13<sup>+</sup> (HUVEC and HT-1080) and CD13<sup>-</sup> (MDA-MB-435 and MDA-231), were incubated with FITC-labeled monoclonal antihuman CD13 antibody (WM15) for 30 min at 4 °C. After washing the cells, the fluorescence of the bound antibody was analyzed by flow cytometry. The mean fluorescence intensity of the cells is shown.

### 2.3.3. Peptide Array-Cell Binding Assay

We have previously shown that peptide array on cellulose membrane provides an excellent platform for whole cell binding and screening of peptides with high relative affinity for the intact cells.<sup>33</sup> Here the NGR peptide array was incubated with the cells to screen for CD13<sup>+</sup> cell binding peptides. Peptide array was incubated with each of the four cell lines, HUVEC, HT-1080, MDA-MB-435, and MDA-MB-231, and the experiment was repeated once. No blocking of the membrane was done before adding the cells, however, after each experiment the cellulose membrane was regenerated to be reused. After incubation, the cells that bound to the cellulose membrane were labeled with CyQuant dye followed by detection with fluorescence. The array was visualized using Kodak imager at

excitation 485 nm and emission at 530 nm. The fluorescence intensity of the spots (shown in **Figure 2.2**) reflecting the amount of bound cells was measured. All the peptides were compared to the wild type peptide **1** and the relative cell adhesion ratio for each peptide binding to cells was determined. The relative cell adhesion ratio for the CD13<sup>+</sup> cells, HUVEC and HT-1080, is listed in **Table 2.1**.

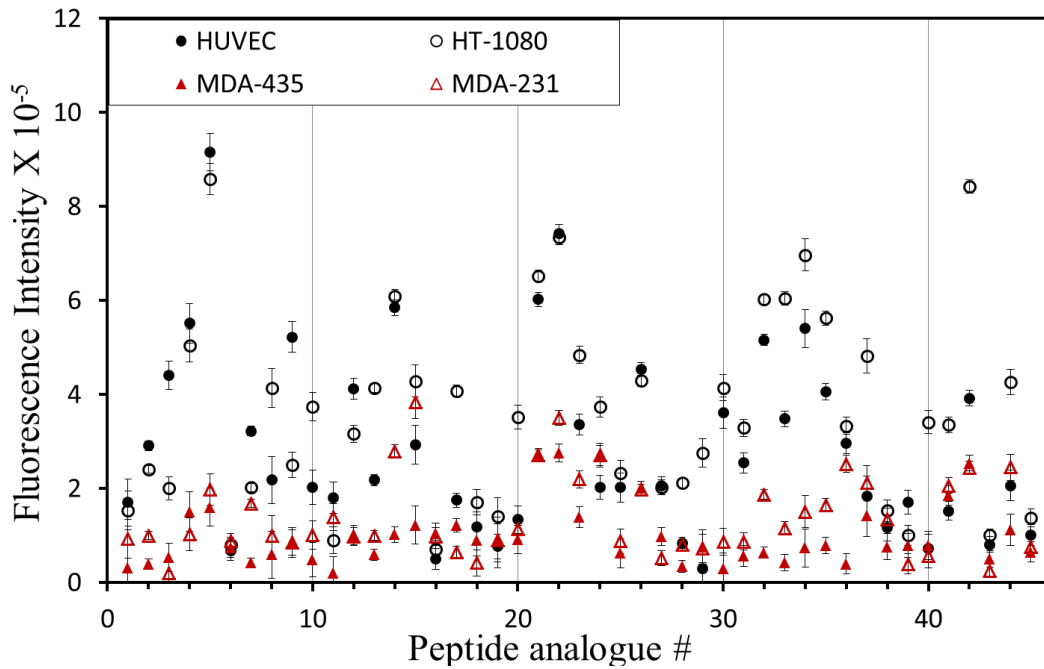


**Figure 2.2.** Average fluorescence intensity of the peptide bound cells on the cellulose membrane. Cells ( $75 \times 10^3/\text{mL}$ ), CD13<sup>+</sup> (HUVEC or HT-1080) or CD13<sup>-</sup> (MDA-231 or MDA-MB-435), were incubated with the peptide array for 8 hr at 37 °C, followed by labeling of the cells with the CyQUANT dye. The fluorescence intensity of the bound cells was measured using Kodak imager at 465 nm excitation and 535 nm emission. The results are presented as mean fluorescence intensity  $\pm$  S.D.

In general, CD13<sup>+</sup> cell lines (HUVEC and HT-1080) showed significant adhesion to the peptides compared to the CD13<sup>-</sup> cells (MDA-MB-435 and MDA-

231). The binding profile of the two CD13<sup>+</sup> cell lines to peptides followed a similar trend, suggesting that the binding was specific to CD13 receptor (**Figure 2.2**). It was noticed that the binding intensities for HT-1080 were slightly higher compared to that for HUVEC, also observed from the relative cell adhesion ratio for the two cell lines (**Table 2.1**). However, based on the expression level of CD13 (**Figure 2.2**) higher binding with the HUVECs was expected. Several factors could account for this. For instance, the sensitivity of the peptide array could decrease after the membrane is regenerated several times. The other reason could be the difference in the levels of *cell-surface* associated receptor and/or the interaction of the peptides with the surface of cancer cell lines versus primary endothelial cells (HUVECs). Peptide array-cell binding assay is mainly a surface interaction and peptides are not internalized by the cells. The two CD13<sup>-</sup> cell lines displayed low binding to the peptide array, with MDA-MB-231 displaying slightly higher binding compared to MDA-MB-435 (**Figure 2.2**). This is most likely due to the experimental conditions as mentioned above.

The relative cell adhesion (RCA) ratio for each peptide was calculated for the two CD13<sup>+</sup> cell lines. This allowed identification of five peptides (**5**, **14**, **21**, **22**, and **34**) that displayed higher binding compared to the other peptides. Among peptide **2-7**, most peptides showed enhanced binding compared to peptide **1**. Peptide **5** showed highest affinity for the cells with more than 5-fold increase in cell binding (RCA 5.4 and 5.5 for HUVEC and HT-1080, respectively) compared to peptide **1**. The peptides from group 1 (ala scan), in general, showed good binding to the cells. Only peptide **11** with Glu8 substituted with Ala showed

relative decrease in binding (RCA 0.6) suggesting that there is a vital electrostatic interaction involved with the receptor. Substitution of Val2 with Ala (peptide **8**) maintained the binding similar to peptide **2** which coincides with the results reported by Honda and coworker.<sup>44</sup> The authors showed that Val2 to Ala replacement gives high cell adhesion effect and induced cell-specific interaction.

Peptides from group 2 with N- or C-terminal deletions showed up to five fold (RCA 4.8) increase in cell binding. Three peptides **14**, **21**, and **22** with RCA of 3 or above were selected from this group. Peptide **14** is an 8-mer with C-terminal Met deleted, whereas, peptides **21** and **22** are short peptides (5-mer and 6-mer, respectively) with mainly NGR and the two terminal cysteines for cyclization. Peptides **14** and **21** also showed low binding to CD13<sup>-</sup> cell lines. Notably peptide **21** has been reported previously and is used widely for tumor targeting.<sup>17</sup> Similarly, peptide **22** resembles reported cKNGRE that showed improved binding to the CD13<sup>+</sup> cells.<sup>28</sup> Linear peptides **24-26** showed less binding compared to the cyclic analogues. Cyclization of the peptide with the two terminal cysteines or the disulfide constraint is critical for the targeting efficiency. Colombo *et al.* found the activity of GNGRG-TNF to be one order of magnitude lower than that of CNGRC-TNF.<sup>30</sup> Our results further confirm that cyclic NGR peptides show enhanced binding to the cells compared to the acyclic NGR counterparts.

Several peptides from group 3 showed augmented binding to the cells compared to peptide **1**. Interestingly, it appears that substitutions of NGR

flanking residues with amino acids containing hydroxyl side chain, such as Ser (peptides **33** and **34**) or Thr (peptide **5**), leads to increase in cell binding. Peptide **34** with highest RCA (3.2 and 4.5) in group 3 peptides was selected for further studies. Negative control peptides (**38-45**) mostly showed low binding to the cells (RCA  $\leq$  2.5) except peptide **42** that displayed RCA of 2.3 and 5.4 for the CD13<sup>+</sup> HUVEC and HT-1080 cell lines, respectively. Peptide **42** is a 8-mer linear peptide devoid of NGR sequence. It may bind to the cells by different mechanism or the interaction could be non-specific. Interestingly, both the CD13<sup>-</sup> cell lines also displayed relatively high binding to peptide **42** compared to other negative control sequences further confirming our conjecture that the binding between peptide **42** and cells could be by non-specific interaction. Peptide **43** with RCA 0.4-0.6 was selected as a negative control peptide for further investigation.

#### **2.3.4. Evaluation of *In vitro* Cell Binding**

Peptides **5**, **14**, **21**, **22**, **34** with enhanced binding to the CD13<sup>+</sup> cells, and peptides **1** and **43** as positive and negative controls, respectively, were chosen for *in vitro* cell uptake studies. Peptides were synthesized using automatic synthesizer on 2-chlorotritylchloride resin using Fmoc-SPSS chemistry, and the N-terminal was labeled with FITC via a  $\beta$ -alanine linker (**Figure 2.3**). Disulfide bond formation or cyclization was carried out by oxidation in 20% aqueous DMSO. Buffer was not used to minimize any potential deamidation and formation of isoaspartate residue which would lead to loss in affinity for the

aminopeptidase N receptor. All peptides were obtained in good yield (40-52%), and were characterized using HPLC and MALDI-TOF showing molecular ion peaks consistent with expected masses (**Table 2.2**). Peptide stock solutions were stored at neutral pH and kept at -20 °C prior to cell studies.

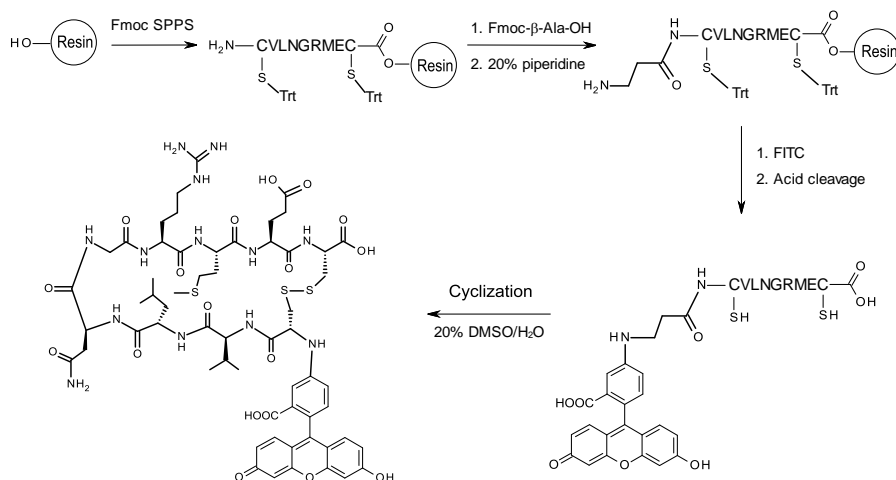


**Figure 2.3.** Solid phase peptide synthesis (SPPS) of FITC-βA-peptide 1 or FITC-1.

The binding or uptake of the soluble FITC-labeled peptides by the cells was studied using fluorescence based experiments, such as, flow cytometry and confocal microscopy. FITC-labeled peptides were incubated with the CD13<sup>+</sup> and CD13<sup>-</sup> cell lines for 30 min at 37 °C followed by removal of the unbound peptides by extensive washing of the cells. Cells were suspended in FACS buffer to evaluate the uptake by flow cytometry. The results (**Figure 2.4**) show that the NGR containing peptides **5**, **14**, **21**, **22**, and **34** display significantly higher uptake

by the CD13<sup>+</sup> cell lines compared to CD13<sup>-</sup> cell lines, as evidenced by the high mean cell fluorescence intensity relative to the untreated cells ( $83 \pm 68.8$  for CD13<sup>+</sup> and  $8.5 \pm 8.5$  for CD13<sup>-</sup>). FITC-labelled peptide **5** (or FITC-**5**) showed the highest uptake followed by the other four peptides, similar to what was observed in the peptide array-cell binding assay.

**Table 2.2.** Amino acid sequence and characterization of the peptides selected from the peptide array-whole cell binding assay.

#	Peptide Sequence	Mass <sup>a</sup> [M+H] <sup>+</sup> Obs. ( Calcd.)	r.t. (min)	Yield <sup>b</sup> (%)
<b>1</b>	CVLNGRMEC	1482.5 (1482.3)	21.7	40
<b>5</b>	YNGRT	1071.3 (1070.4)	13.7	50
<b>14</b>	CVLNGREC	1351.7 (1351.2)	19.5	50
<b>21</b>	CNGRC	1011.1 (1010.4)	12.1	42
<b>22</b>	KCNGRC	1137.9 (1137.1)	11.3	45
<b>34</b>	CVLNGRSEC	1437.4 (1438.1)	22.2	45
<b>43</b>	VLGXE	990.4 (989.1)	9.5	52

<sup>a</sup>MALDI-TOF of FITC-β-Ala-peptide. <sup>b</sup>Purity of the peptides was estimated as the area under the curve of analytical HPLC chromatogram and was found to be 95-98%. r.t. = retention time

When comparing the mean cell fluorescence, the uptake of the peptides by the HUVECs was higher compared to uptake by the HT-1080 cells. This is in agreement with the amount of CD13 receptor expressed by these cell lines (**Figure 2.1**). In addition, HUVECs also express αβ3 integrin receptor and NGR sequence is known to convert into isoDGR under cellular conditions with gain in αβ3 integrin binding activity.<sup>45</sup> Whereas HT-1080 cancer cells do not express αβ3 integrins.<sup>46</sup>

Peptide **5**, a linear 5-mer sequence was further evaluated for cellular uptake by fluorescence microscopy. Fluorescence microscopy image (**Figure 2.5.A**) of CD13<sup>+</sup> HT-1080 cells showed strong intersperse fluorescence, while the CD13<sup>-</sup> MD-435 cells showed much less green fluorescence (**Figure 2.5.B**) demonstrating peptide specificity for the APN/CD13 receptor. **Figure 2.5.C** shows zoomed-in image of the HT-1080 cells, where uniform distribution of FITC-**5** peptide inside the cell and nucleus is visibly observed. The binding of the FITC-**5** peptide was inhibited to a large extent in the presence of 100-fold excess unlabeled peptide **5** (**Figure 2.5D**).

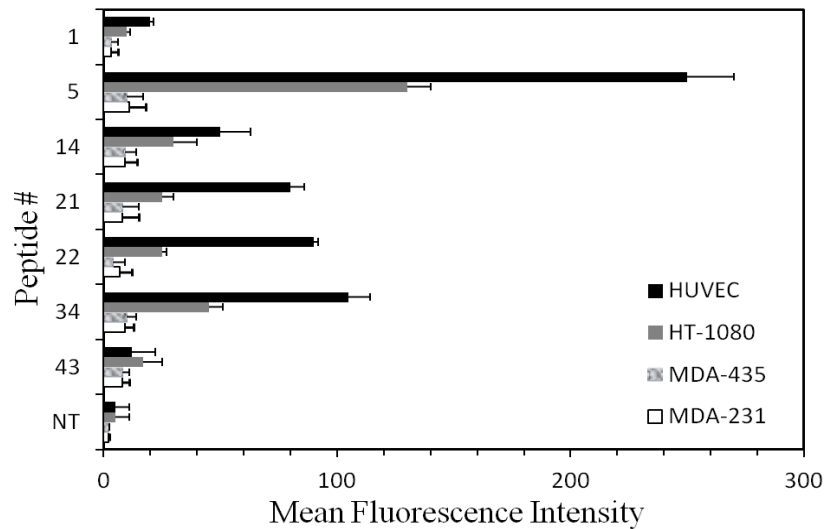


**Figure 2.4.** Peptide cell binding and uptake by CD13<sup>+</sup> and CD13<sup>-</sup> cell lines measured using flow cytometry. The peptides (10<sup>-6</sup> mol/L) were incubated with the cells for 30 min at 37 °C. No treatment (NT), and FITC-43 served as negative controls, while FITC-1 served as a positive control. The results are presented as mean fluorescence of cell population (mean ± SD of triplicate wells).

Finally, a co-culture assay with HT-1080 and MDA-MB-435 cells was performed to study the selectivity of peptide FITC-**5**. CD13<sup>+</sup> HT-1080 cells were

grown together with the CD13<sup>-</sup> MDA-MB-435 cells followed by incubation with FITC-5. As shown in Figure 5, MDA-MB-435 cells, previously stained with blue cell tracker dye, showed much less green fluorescence or peptide uptake compared to the HT-1080 cells. The low uptake of the peptide by the MDA-MB-435 cells (**Figures 2.6**) could be due to the binding of isoDGR peptide of FITC-5 to the  $\alpha\beta 3$  integrin expressed by these cells.<sup>42</sup>

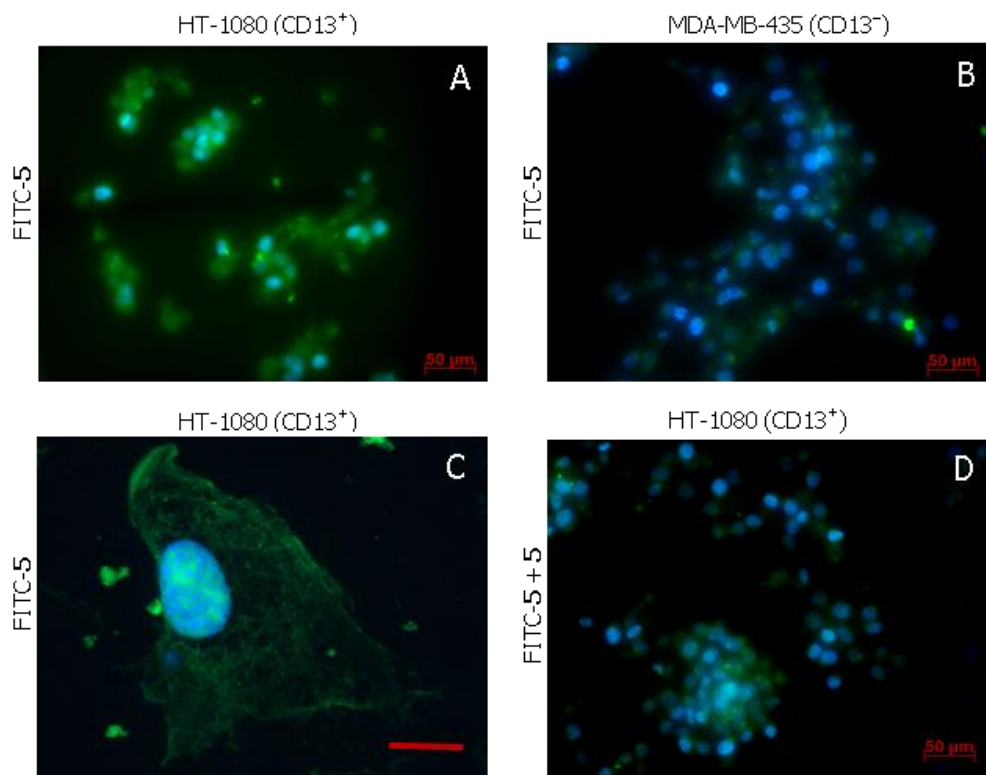


**Figure 2.5.** Fluorescence microscopy images to evaluate *in vitro* binding of peptide FITC-5 to the cells. (A) HT-1080 (CD13<sup>+</sup>) cells showing uptake of green FITC-5, (B) MDA-MB-435 (CD13<sup>-</sup>) cells after incubation with FITC-5 showing minimal uptake, (C) Zoom-in of a HT-1080 cell using confocal laser microscopy showing intracellular distribution of FITC-5 (scale bar = 12  $\mu\text{m}$ ), and (D) HT-1080 cells in the presence of excess unlabelled peptide 5 ( $10^{-4}$  M) as a competitor. *Green*, signal from FITC labelled peptide; *Blue*, signal from the nuclear staining agent DAPI. Images were acquired with identical exposure times and displayed consistently to compare binding between HT-1080 and MDA-MB-435 cells.

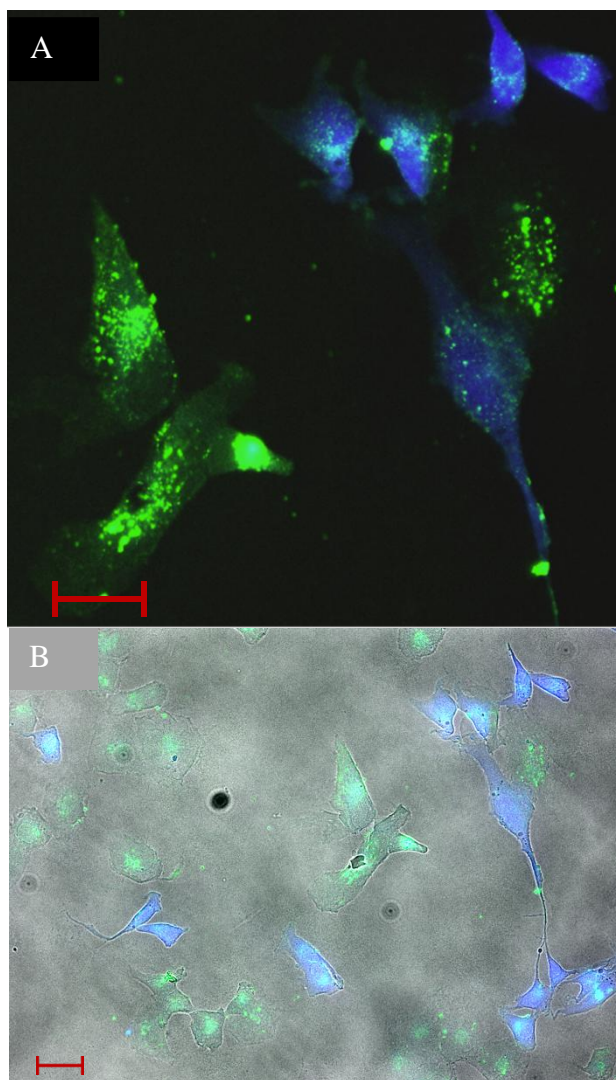


**Figure 2.6.** (A) Fluorescence microscopy image of a co-culture of HT-1080 (CD13+) and MDA-MB-435 (CD13-) cells incubated with FITC-5 (green) for 30 min. Peptide (green) was uptaken primarily by HT-1080 cells with very little uptake by MDA-MB-435 cells. The MDA-MB-435 cells were stained blue using cell tracker blue before the experiment. (B) A phase contrast image. Scale bar = 20  $\mu\text{m}$ .

To investigate the susceptibility of peptides for deamination under condition used in the binding assays, we studied the stability of peptide **5**, a representative NGR sequence, in DMEM media (**Figure 2.7**). Peptide **5** dissolved in DMEM media was incubated at 37 °C, and at different time points (0, 1, 4, 24 h) aliquots

were withdrawn to evaluate the stability of the peptide using MALDI-TOF mass spectrometry and RP-HPLC. Peptide started to disintegrate after 4 hr of incubation as evidenced by the appearance of multiple peaks during HPLC and mass analysis. Mass measurement indicated the presence of NGR peptide along with deaminated *iso*DGR or DGR and succinamide intermediate showing mass of 610.7 ( $[M+H]^+$ ), 611.7 (+1), and 593.5 (-17), respectively (**Figure 2.7**). These results suggest that the NGR sequence in the peptides was maintained during the *in vitro* binding assays which involved half-an-hour incubation of peptide with the cells in DMEM media. Notably, the peptide was completely stable in water under similar conditions.

(A)

Stability of peptide 5 (YNGRT) during storage at 37°C		
Solvent*	Time (h)	Mass $[M+H]^+$ Obs. (Calcd.)
H <sub>2</sub> O	0	610.8 (610.6)
	1	610.7
	4	610.5
	24	610.7
DMEM	0	610.8
	1	610.8
	4	610.7, 611.7, 593.5
	24	610.8, 611.7, 593.5

\* Solvent used to prepare peptide solution for storage. Mass was determined by MALDI-TOF mass spectrometry

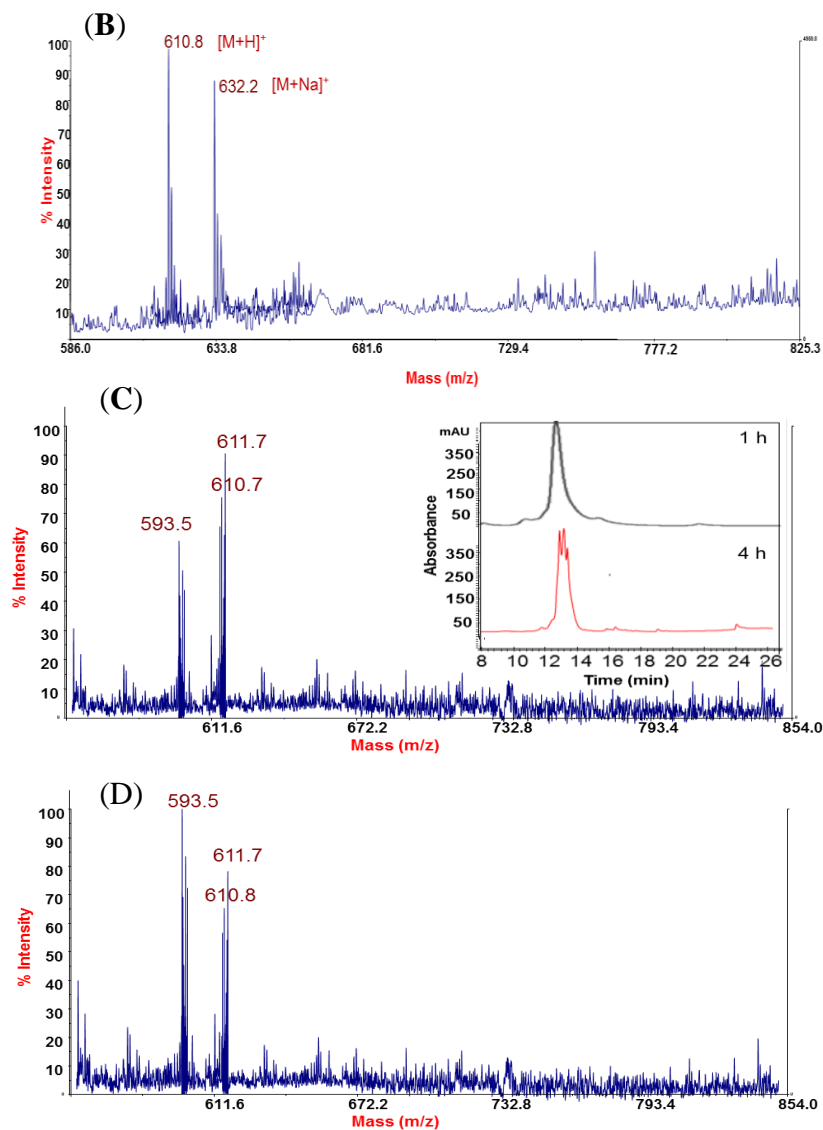


**Figure 2.7.** (A) Stability of peptide 5 (YNGRT) during storage at 37°C as determined by MALDI-TOF mass spectrometry. MALDI-TOF mass analysis of peptide 5 in DMEM media after incubation at 37 °C for 1 h (B), 4 h (C), and 24 h (D). (B) shows the correct mass for peptide 5 ( $[M+H]^+$  obsd. 610.8; calcd. 610.6), C and D show mass of 593.5, 610.7 and 611.7 corresponding to succinimide derivative, NGR, and *iso*DGR (or DGR), respectively. Inset in (C) shows RP-HPLC of peptide 5 after incubation in DMEM media at 37 °C, at zero time (black) and 4 h (red).

Precautions were taken during peptide array synthesis to minimize the chances of NGR peptide deamination. Regardless some deamination may occur during the lengthy cell binding assay and cannot be excluded, which can lead to some loss of CD13<sup>+</sup> cell binding. Several observations suggest that there was minimal deamination during the peptide-array cell binding assay, for instance, the CD13<sup>+</sup> cells showed substantial binding to the peptides and in comparison CD13<sup>-</sup> cells showed much less binding (**Figure 2.2**). If there was significant deamination of the NGR peptides, we would expect a shift in the binding to integrin expressing cell lines MDA-MB-435 and MDA-231. Further, *in vitro* binding studies using FITC labeled soluble peptides confirmed uptake or binding by the CD13<sup>+</sup> cells.

### **2.3.5. Inhibition of Aminopeptidase N Activity by Selected Peptides**

Inhibition of APN enzyme is considered important as it inhibits tumor invasion and angiogenesis causing tumor regression.<sup>47</sup> We examined the ability of five most promising NGR peptides and peptide **1** to inhibit aminopeptidase N activity. Bestatin, a known inhibitor of APN activity, was used as a positive control. Screening of peptides for inhibition of APN activity was carried out at a single substrate concentration of 500  $\mu$ M, as lower concentrations (125  $\mu$ M or lower) did not show noticeable activity. Peptides displayed 10-60% APN inhibition after 30 min incubation, where bestatin showed 92% inhibition (**Figure 2.8**). Peptide **5** was the most efficient in inhibiting APN causing  $60 \pm 4.2\%$  inhibition compared to the cells alone. Peptide **34** showed  $54 \pm 3.9\%$  inhibition, suggesting again the

importance of hydroxyl side chain group in enhancing binding and interaction with CD13<sup>+</sup> cells or the APN enzyme. Peptides **1**, **14**, **21**, and **22** displayed slight inhibition at the tested concentration, ranging from 10 to 20%. Previously it has been reported that CNGRC peptide showed minimal inhibition of APN up to 500  $\mu$ M concentration.<sup>23</sup> A recently identified CPNGRC peptide sequence showed that the addition of a proline residue enhanced binding to the APN enzyme as well as inhibited APN proteolytic activity with an IC<sub>50</sub> of 10  $\mu$ M, a value that is 30-fold lower than that for CNGRC.<sup>31</sup> Noticeably the structural constraints introduced by the NGR flanking residues contribute to the enhanced binding affinity and enzyme inhibition. This study highlights the possible correlation between enhanced binding to APN and APN inhibition.

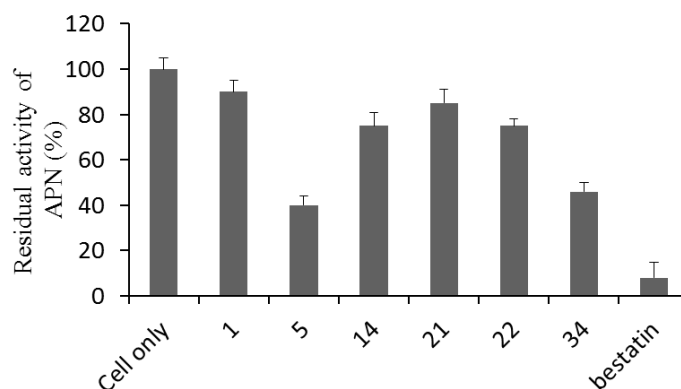


**Figure 2.8.** Inhibition of aminopeptidase N (APN) activity in the presence of NGR peptides. Intact HT-1080 cells were incubated with peptides or bestatin (a known inhibitor) followed by evaluation of APN activity. The results shown are mean  $\pm$  SD of triplicates.

Finally, peptide-array cell binding assay using cellulose bound peptides was able to screen for cyclic and acyclic NGR peptides that bind to CD13<sup>+</sup> cell lines

(**Figure 2.2**). Membrane cell binding results, as well as *in vitro* binding experiments including co-culture fluorescence microscopy suggest that the identified NGR peptides bind selectively to CD13 receptor in CD13<sup>+</sup> cell lines. Previously we established this assay for screening peptides specific for cancer cells with very little binding affinity for the noncancerous HUVECs.<sup>33</sup>

NGR peptides identified from the peptide-array cell binding assay confirmed high uptake in the *in vitro* studies using soluble peptides (**Figure 2.3**). Interestingly, peptide **21** (CNGRC) identified here is a wellknown NGR peptide that has been widely used as a CD13 tumor vasculature targeting peptide, and tumor necrosis factor- $\alpha$  (TNF) conjugate of this peptide is in phase II clinical trials.<sup>18</sup> The newly identified sequences presented in this study, such as peptide **5** and **34**, offer additional advantages to the previously reported NGR sequence. Peptide **5** (YNGRT) was found to be the most promising with a significant increase (up to 13-fold) in uptake by the CD13<sup>+</sup> cells compared to the lead peptide **1**. Peptide **5** is a linear peptide that can be cyclised to further enhance its binding properties toward CD13<sup>+</sup> cells. In addition, the new sequences, such as **5** and **34**, display better APN enzyme inhibition and selectivity toward CD13<sup>+</sup> cells.

Next we observed that YNGRT sequence (peptide **5**), is present in the type II module of fibronectin.<sup>42</sup> Notably, peptide **34** (CVLNGRSEC), the next promising peptide resembles peptide **5**. The NGR flanking residues are similar in the two peptides, namely Tyr versus Leu and Thr versus Ser in **5** and **34**, respectively. The three dimensional (3D) structure of peptide **5** derived from the

fibronectin structure (PDB 1QO6)<sup>48</sup> is shown in Figure 7. An overlay of peptide **5** with LNGRS sequence of peptide **34** (derived from PDB 3NWJ)<sup>49</sup> shows that peptide **34** may also fold into similar conformation. The structures discussed here represent probable solution conformations of the individual peptides as these structures are based on the structure of the peptide in a complete protein. The true 3D structures of peptides, such as **5** and **34** remains to be elucidated

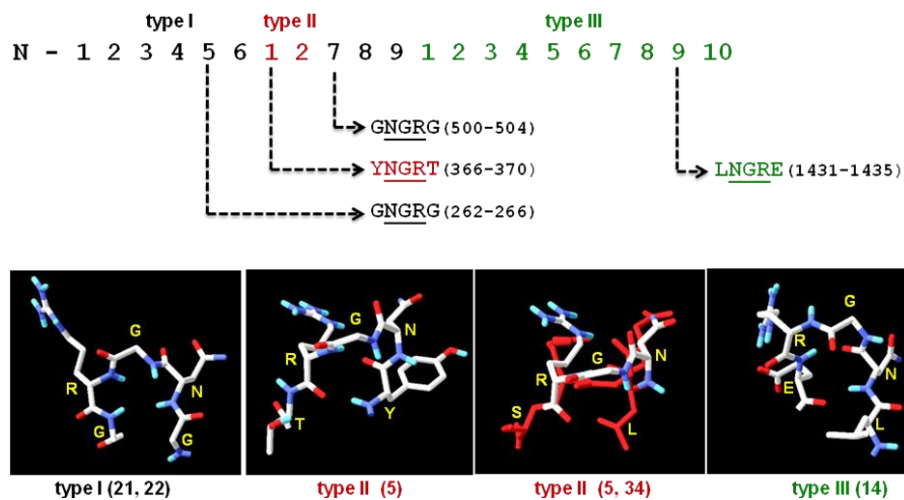


**Figure 2.9.** Schematic representation of a portion of human fibronectin highlighting NGR motifs present in the type I, II, and III repeats (top). Three dimensional structures of the NGR sequences present in the type I (PDB 1FBR), II (PDB 1QO6), and III (PDB 1FNF) repeats are shown as stick models (bottom). Peptides **21** and **22** most likely form hairpin as found in type I structure (bottom, left to right), peptide **5** folds into type II structure, and peptide **34** which is similar to peptide **5** may form type II structure. An overlay of peptide **5** with type II fold and peptide **34** (red) derived from PDB 3NWJ is shown. LNGRE of type III repeat, which is present in peptide **14**, is also shown.

The other high affinity peptides also resemble sequences from fibronectin. Peptides **21** and **22** contain CNGRC which has been shown to be a better analogue of fibronectin sequence GNGRG (**Figure 2.9**).<sup>30</sup> GNGRG belongs to

the type I module (5<sup>th</sup> and 7<sup>th</sup> type I repeats) of fibronectin (PDB 1FBR)<sup>50</sup> and the cyclized CNGRC stabilizes the linear sequence providing higher affinity for CD13.<sup>30</sup> Peptide **14** contains LNGRE sequence which is present in the type III module of fibronectin (PDB 1FNF).<sup>51</sup> Conclusively, all the high affinity peptides identified in the present study are derivatives of the fibronectin NGR sequences. Furthermore, comparison of the uptake results (**Figures 2.2** and **2.4**) as well as the APN activity (**Figure 2.8**) of the high affinity peptides suggests that NGR peptides with type II fibronectin sequence (peptides **5** and **34**) show higher affinity for the CD13 compared to the peptides from type I and type III modules.

#### **2.4. Conclusions**

In conclusion, the NGR peptides identified here are promising sequences for developing tumor vasculature targeted drugs, delivery systems and imaging agents with reduced detrimental off-target effects from the toxic drug or other agents. Our results show that peptide array library screening is a powerful research tool for analyzing peptide-cell interactions with rapid and efficient screening of high binding peptides. Both cyclic and linear peptides containing NGR were identified that closely resemble NGR sequences present in human fibronectin. Consequently, these NGR sequences may have low immunogenicity making them ideal candidates for the development of ligands for targeted delivery to tumor angiogenic vasculature.

## 2.5. References

- (1) Ruoslahti, E.; Bhatia, S. N.; Sailor, M. J. Targeting of drugs and nanoparticles to tumors *J. Cell Biol.* **2010**, *188*, 759-768.
- (2) Liu, Z.; Wu, K. Peptides Homing to Tumor Vasculature: Imaging and Therapeutics for Cancer *Recent Pat. Anti-Cancer Drug Discovery* **2008**, *3*, 202-208.
- (3) Chen, K.; Chen, X. Integrin Targeted Delivery of Chemotherapeutics *Theranostics*. **2011**, *1*, 189–200.
- (4) Brooks, P. C.; Clark, R. A. F.; Chersesh, D. A. Requirement of vascular integrin alpha v beta 3 for angiogenesis. *Science* **1994**, *264*, 569-571.
- (5) Wickström, M.; Larsson, R.; Nygren, P.; Gullbo, J. Aminopeptidase N (CD13) as a target for cancer chemotherapy *Cancer Sci.* **2011**, *102*, 501-508.
- (6) Hicklin, D. J.; Ellis, L. M. Role of the Vascular Endothelial Growth Factor Pathway in Tumor Growth and Angiogenesis *J. Clin. Oncol.* **2005**, *23*, 1011-1027.
- (7) Veikkola, T.; Karkkainen, M.; Claesson-Welsh, L.; Alitalo, K. Regulation of Angiogenesis via Vascular Endothelial Growth Factor Receptors *Cancer Res.* **2000**, *60*, 203-212.
- (8) Silletti, S.; Kessler, T.; Goldberg, J.; Boger, D. L.; Chersesh, D. A. Disruption of matrix metalloproteinase 2 binding to integrin  $\alpha v \beta 3$  by an organic molecule inhibits angiogenesis and tumor growth in vivo *Proc. Natl. Acad. Sci.* **2001**, *98*, 119-124.
- (9) Desgrosellier, J. S.; Chersesh, D. A. Integrins in cancer: biological implications and therapeutic opportunities *Nat. Rev. Cancer* **2010**, *10*, 9-22.
- (10) Allen, T. M. Ligand-targeted therapeutics in anticancer therapy *Nat. Rev. Cancer* **2002**, *2*, 750-763.
- (11) Mina-Osorio, P. The moonlighting enzyme CD13: old and new functions to target *Trends in Mol. Med.* **2008**, *14*, 361-371.
- (12) Fukasawa, K.; Fujii, H.; Saitoh, Y.; Koizumi, K.; Aozuka, Y.; Sekine, K.; Yamada, M.; Saiki, I.; Nishikawa, K. Aminopeptidase N (APN/CD13) is selectively expressed in vascular endothelial cells and plays multiple roles in angiogenesis *Cancer Lett.* **2006**, *243*, 135-143.

(13) Curnis, F.; Arrigoni, G.; Sacchi, A.; Fischetti, L.; Arap, W.; Pasqualini, R.; Corti, A. Differential Binding of Drugs Containing the NGR Motif to CD13 Isoforms in Tumor Vessels, Epithelia, and Myeloid Cells *Cancer Res.* **2002**, *62*, 867-874.

(14) Matteo, P. D.; Arrigoni, G. L.; Alberici, L.; Corti, A.; Gallo-Stampino, C.; Traversari, C.; Doglioni, C.; Rizzardi, G.-P. Enhanced Expression of CD13 in Vessels of Inflammatory and Neoplastic Tissues *J. Histochem. Cytochem.* **2011**, *59*, 47-59.

(15) Pasqualini, R.; Koivunen, E.; Kain, R.; Lahdenranta, J.; Sakamoto, M.; Stryhn, A.; Ashmun, R. A.; Shapiro, L. H.; Arap, W.; Ruoslahti, E. Aminopeptidase N is a receptor for tumor-homing peptides and a target for inhibiting angiogenesis *Cancer Res.* **2000**, *60*, 722-727.

(16) Pasqualini, R.; Koivunen, E.; Ruoslahti, E. A peptide isolated from phage display libraries is a structural and functional mimic of an RGD-binding site on integrins *J. Cell Biol.* **1995**, *130*, 1189-1196.

(17) Arap, W.; Pasqualini, R.; Ruoslahti, E. Cancer Treatment by Targeted Drug Delivery to Tumor Vasculature in a Mouse Model *Science* **1998**, *279*, 377-380.

(18) Curnis, F.; Sacchi, A.; Borgna, L.; Magni, F.; Gasparri, A.; Corti, A. Enhancement of tumor necrosis factor [alpha] antitumor immunotherapeutic properties by targeted delivery to aminopeptidase N (CD13) *Nat. Biotech.* **2000**, *18*, 1185-1190.

(19) Grifman, M.; Trepel, M.; Speece, P.; Gilbert, L. B.; Arap, W.; Pasqualini, R.; Weitzman, M. D. Incorporation of Tumor-Targeting Peptides into Recombinant Adeno-associated Virus Capsids *Mol. Ther.* **2001**, *3*, 964-975.

(20) Pastorino, F.; Brignole, C.; Marimpietri, D.; Cilli, M.; Gambini, C.; Ribatti, D.; Longhi, R.; Allen, T. M.; Corti, A.; Ponzoni, M. Vascular Damage and Anti-angiogenic Effects of Tumor Vessel-Targeted Liposomal Chemotherapy *Cancer Res.* **2003**, *63*, 7400-7409.

(21) Di Matteo, P.; Curnis, F.; Longhi, R.; Colombo, G.; Sacchi, A.; Crippa, L.; Protti, M. P.; Ponzoni, M.; Toma, S.; Corti, A. Immunogenic and structural properties of the Asn-Gly-Arg (NGR) tumor neovasculature-homing motif *Mol. Immunol.* **2006**, *43*, 1509-1518.

(22) Corti, A.; Curnis, F.; Arap, W.; Pasqualini, R. The neovasculature homing motif NGR: more than meets the eye *Blood* **2008**, *112*, 2628-2635.

(23) van Hensbergen, Y.; Broxterman, H. J.; Elderkamp, Y. W.; Lankelma, J.; Beers, J. C. C.; Heijn, M.; Boven, E.; Hoekman, K.; Pinedo, H. M.

A doxorubicin–CNGRC-peptide conjugate with prodrug properties *Biochem. Pharmacol.* **2002**, *63*, 897-908.

(24) Ndinguri, M. W.; Solipuram, R.; Gambrell, R. P.; Aggarwal, S.; Hammer, R. P. Peptide Targeting of Platinum Anti-Cancer Drugs *Bioconjug. Chem.* **2009**, *20*, 1869-1878.

(25) Ellerby, H. M.; Arap, W.; Ellerby, L. M.; Kain, R.; Andrusiak, R.; Rio, G. D.; Krajewski, S.; Lombardo, C. R.; Rao, R.; Ruoslahti, E.; Bredesen, D. E.; Pasqualini, R. Anti-cancer activity of targeted pro-apoptotic peptides *Nat. Med.* **1999**, *5*, 1032-1038.

(26) Santoro, A.; Pressiani, T.; Citterio, G.; Rossoni, G.; Donadoni, G.; Pozzi, F.; Rimassa, L.; Personeni, N.; Bozzarelli, S.; Colombi, S.; De Braud, F. G.; Caligaris-Cappio, F.; Lambiase, A.; Bordignon, C. Activity and safety of NGR-hTNF, a selective vascular-targeting agent, in previously treated patients with advanced hepatocellular carcinoma *Br. J. Cancer* **2010**, *103*, 837-844.

(27) Santoro, A.; Rimassa, L.; Sobrero, A. F.; Citterio, G.; Sclafani, F.; Carnaghi, C.; Pessino, A.; Caprioni, F.; Andretta, V.; Tronconi, M. C.; Finocchiaro, G.; Rossoni, G.; Zanoni, A.; Miggiano, C.; Rizzardi, G.-P.; Traversari, C.; Caligaris-Cappio, F.; Lambiase, A.; Bordignon, C. Phase II study of NGR-hTNF, a selective vascular targeting agent, in patients with metastatic colorectal cancer after failure of standard therapy *Eur. J. Cancer* **2010**, *46*, 2746-2752.

(28) Negussie, A. H.; Miller, J. L.; Reddy, G.; Drake, S. K.; Wood, B. J.; Dreher, M. R. Synthesis and in vitro evaluation of cyclic NGR peptide targeted thermally sensitive liposome *J. Controlled Release* **2010**, *143*, 265-273.

(29) Metaferia, B. B.; Rittler, M.; Gheeya, J. S.; Lee, A.; Hempel, H.; Plaza, A.; Stetler-Stevenson, W. G.; Bewley, C. A.; Khan, J. Synthesis of novel cyclic NGR/RGD peptide analogs via on resin click chemistry *Bioorg. Med. Chem. Lett.* **2010**, *20*, 7337-7340.

(30) Colombo, G.; Curnis, F.; De Mori, G. M. S.; Gasparri, A.; Longoni, C.; Sacchi, A.; Longhi, R.; Corti, A. Structure-Activity Relationships of Linear and Cyclic Peptides Containing the NGR Tumor-homing Motif *J. Biol. Chem.* **2002**, *277*, 47891-47897.

(31) Plesniak, L. A.; Salzameda, B.; Hinderberger, H.; Regan, E.; Kahn, J.; Mills, S. A.; Teriete, P.; Yao, Y.; Jennings, P.; Marassi, F.; Adams, J. A. Structure and Activity of CPNGRC: A Modified CD13/APN Peptidic Homing Motif *Chem. Biol. Drug Des.* **2010**, *75*, 551-562.

(32) Curnis, F.; Cattaneo, A.; Longhi, R.; Sacchi, A.; Gasparri, A. M.; Pastorino, F.; Di Matteo, P.; Traversari, C.; Bachi, A.; Ponzoni, M.; Rizzardi, G.-

P.; Corti, A. Critical Role of Flanking Residues in NGR-to-isoDGR Transition and CD13/Integrin Receptor Switching *J. Biol. Chem.* **2010**, *285*, 9114-9123.

(33) Ahmed, S.; Mathews, A. S.; Byeon, N.; Lavasanifar, A.; Kaur, K. Peptide Arrays for Screening Cancer Specific Peptides *Anal. Chem.* **2010**, *82*, 7533-7541.

(34) Soliman, W.; Wang, L.; Bhattacharjee, S.; Kaur, K. Structure–Activity Relationships of an Antimicrobial Peptide Plantaricin S from Two-Peptide Class IIb Bacteriocins *J. Med. Chem.* **2011**, *54*, 2399-2408.

(35) Kocbek, P.; Obermajer, N.; Cegnar, M.; Kos, J.; Kristl, J. Targeting cancer cells using PLGA nanoparticles surface modified with monoclonal antibody *J. Controlled Release* **2007**, *120*, 18-26.

(36) Bauvois, B.; Puiffe, M.-L.; Bongui, J.-B.; Paillat, S.; Monneret, C.; Dauzonne, D. Synthesis and Biological Evaluation of Novel Flavone-8-acetic Acid Derivatives as Reversible Inhibitors of Aminopeptidase N/CD13 *J. Med. Chem.* **2003**, *46*, 3900-3913.

(37) Hwang, R.; Varner, J. The role of integrins in tumor angiogenesis *Hematol. Oncol. Clin. North Am.* **2004**, *18*, 991-1006.

(38) Haubner, R.; Weber, W. A.; Beer, A. J.; Vabuliene, E.; Reim, D.; Sarbia, M.; Becker, K.-F.; Goebel, M.; Hein, R.; Wester, H.-J.; Kessler, H.; Schwaiger, M. Noninvasive Visualization of the Activated  $\alpha\beta 3$  Integrin in Cancer Patients by Positron Emission Tomography and [18F]Galacto-RGD *PLoS Med* **2005**, *2*, e70.

(39) Sugahara, K. N.; Teesalu, T.; Karmali, P. P.; Kotamraju, V. R.; Agemy, L.; Greenwald, D. R.; Ruoslahti, E. Coadministration of a Tumor-Penetrating Peptide Enhances the Efficacy of Cancer Drugs *Science* **2010**, *328*, 1031-1035.

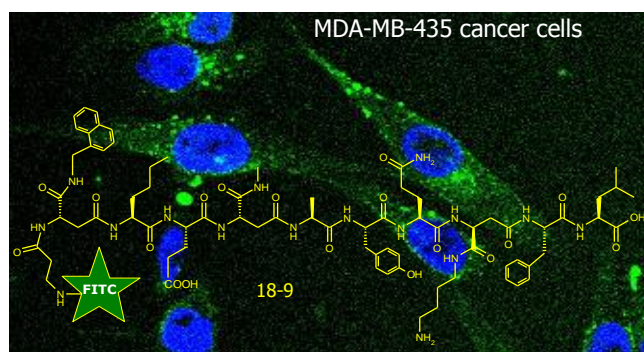
(40) Koivunen, E.; Gay, D. A.; Ruoslahti, E. Selection of peptides binding to the alpha 5 beta 1 integrin from phage display library *J. Biol. Chem.* **1993**, *268*, 20205-20210.

(41) Lau, D. H.; Guo, L.; Liu, R.; Song, A.; Shao, C.; Lam, K. S. Identifying peptide ligands for cell surface receptors using cell-growth-on-bead assay and one-bead one-compound combinatorial library *Biotechnol. Lett.* **2002**, *24*, 497-500.

(42) Curnis, F.; Longhi, R.; Crippa, L.; Cattaneo, A.; Dondossola, E.; Bachi, A.; Corti, A. Spontaneous Formation of L-Isoaspartate and Gain of Function in Fibronectin *J. Biol. Chem.* **2006**, *281*, 36466-36476.

- (43) Shim, J. S.; Kim, J. H.; Cho, H. Y.; Yum, Y. N.; Kim, S. H.; Park, H.-J.; Shim, B. S.; Choi, S. H.; Kwon, H. J. Irreversible Inhibition of CD13/Aminopeptidase N by the Antiangiogenic Agent Curcumin *Chem. Biol.* **2003**, *10*, 695-704.
- (44) Okochi, M.; Nomura, S.; Kaga, C.; Honda, H. Peptide array-based screening of human mesenchymal stem cell-adhesive peptides derived from fibronectin type III domain *Biochem. Biophys. Res. Commun.* **2008**, *371*, 85-89.
- (45) Spitaleri, A.; Mari, S.; Curnis, F.; Traversari, C.; Longhi, R.; Bordignon, C.; Corti, A.; Rizzardi, G.-P.; Musco, G. Structural Basis for the Interaction of isoDGR with the RGD-binding Site of  $\alpha\text{v}\beta\text{3}$  Integrin *J. Biol. Chem.* **2008**, *283*, 19757-19768.
- (46) Berditchevski, F.; Zutter, M. M.; Hemler, M. E. Characterization of novel complexes on the cell surface between integrins and proteins with 4 transmembrane domains (TM4 proteins) *Mol. Biol. Cell* **1996**, *7*, 193-207.
- (47) Aozuka, Y.; Koizumi, K.; Saitoh, Y.; Ueda, Y.; Sakurai, H.; Saiki, I. Anti-tumor angiogenesis effect of aminopeptidase inhibitor bestatin against B16-BL6 melanoma cells orthotopically implanted into syngeneic mice *Cancer Lett.* **2004**, *216*, 35-42.
- (48) Bocquier, A. A.; Potts, J. R.; Pickford, A. R.; Campbell, I. D. Solution structure of a pair of modules from the gelatin-binding domain of fibronectin *Structure* **1999**, *7*, 1451-S1453.
- (49) Fucile, G.; Garcia, C.; Carlsson, J.; Sunnerhagen, M.; Christendat, D. Structural and biochemical investigation of two Arabidopsis shikimate kinases: The heat-inducible isoform is thermostable *Protein Sci.* **2011**, *20*, 1125-1136.
- (50) Williams, M. J.; Phan, I.; Harvey, T. S.; Rostagno, A.; Gold, L. I.; Campbell, I. D. Solution Structure of a Pair of Fibronectin Type 1 Modules with Fibrin Binding Activity *J. Mol. Biol.* **1994**, *235*, 1302-1311.
- (51) Leahy, D. J.; Aukhil, I.; Erickson, H. P. 2.0 Å Crystal Structure of a Four-Domain Segment of Human Fibronectin Encompassing the RGD Loop and Synergy Region *Cell* **1996**, *84*, 155-164.

## Chapter 3 : Engineered Proteolytically Stable p160 Cancer Targeting Peptides with High Affinity for Breast Cancer Cells



*Rania Soudy, Avneet Gill, Tara Sprules, Afsaneh Lavasanifar, and Kamaljit Kaur\**, Proteolytically stable cancer targeting peptides with high affinity for breast cancer cells. *J. Med. Chem.*, **2011**, 54 (21), 7523–7534.

### 3.1. Introduction

Chemotherapeutic agents are used in conjunction with other treatment options such as surgery, radiation, and hormonal therapy to combat cancer.<sup>1,2</sup> A major hurdle associated with current chemotherapeutic agents is that they enter healthy tissues in the body with indiscriminate cytotoxicity and do not preferentially accumulate at tumor sites.<sup>3,4</sup> To improve the specific uptake of therapeutic agents to cancerous cells in tumors, different strategies have been developed. One of the most effective strategies is to target anticancer drugs preferentially to the tumor site using targeting ligands such as engineered antibodies<sup>5,6</sup> tumor homing peptides<sup>7,8</sup> affibodies<sup>9,10</sup> and aptamers<sup>11</sup> that target specific receptors on particular types of cancer cells. Recently, a number of tumor homing peptides have been reported that specifically target cancer cells and show promising results for tumor targeted drug delivery. Peptides being smaller than other targeting ligands, have excellent tissue penetration properties and can be easily conjugated to drugs and oligonucleotides by chemical synthesis. Peptides are nearly invisible to the immune system and are not taken up in the reticuloendothelial system like antibodies, so are expected to cause minimal or no side effects to bone marrow, liver and spleen.<sup>12</sup>

A number of peptides have been identified by peptide phage display for targeting breast cancer cell types.<sup>13-15</sup> One of those is a dodecapeptide identified through phage display by Zhang et al, referred to as peptide p160.<sup>16</sup> Peptide p160 displays high affinity for the human breast cancer cell lines MDA-MB-435 and

MCF-7 *in vitro* with very little affinity for primary endothelial HUVEC cells<sup>16-18</sup>. Furthermore, *in vivo* biodistribution experiments in tumor-bearing mice, p160 showed a higher uptake in tumors than in organs such as heart, liver, lung, and kidney. Relative to the RGD-4C peptide, p160 showed high accumulation in tumor versus normal organs.<sup>18</sup>

Experiments with p160 peptide suggest that a cancer specific receptor is involved in the cellular binding of the peptide.<sup>18</sup> A competitive binding experiment in the presence of increasing concentration of the unlabeled p160 peptide showed reduced uptake of labeled p160 in the MDA-MB-435 cancer cells. In contrast, unspecific competitors such as octreotide and D-p160 (D-isomer) showed no effect on the uptake of the labeled p160. Further, the internalization of the radiolabeled and the FITC-labeled p160 was inhibited in the presence of the unlabeled peptide and was suppressed at 4 °C. Using p160 as a lead peptide, we designed and synthesized a library of 70 peptides on a cellulose membrane. Screening of the library for cancer specific peptides led to the identification of decapeptide **18** which displayed up to 3-fold higher binding affinity for MDA-MB-435 and MCF-7 cancer cell lines compared to the p160 peptide, with negligible affinity for HUVEC cells.<sup>19</sup> The apparent dissociation constant of peptide **18** for recognizing MDA-MB-435 cells was found to be in the low micromolar range ( $K_d$  42  $\mu$ M).

Despite the potential of peptide **18** as a potent tumor homing peptide, its applicability would be largely hampered by its instability toward proteases. A fast degradation of p160 peptide by the serum proteases has been observed.<sup>17,18</sup> The

susceptibility of  $\alpha$ -peptides, such as p160 and peptide **18**, to *in vivo* proteolysis severely diminishes their bioavailability in tissues and organs. This presents a significant hurdle and a major impediment in the development of  $\alpha$ -peptides into clinically useful products.<sup>20</sup> To overcome this, peptides have to be chemically modified so that their blood clearance is minimized in comparison with their rate of uptake at the target sites. The most common strategies used to increase peptide proteolytic stability include introduction of D- or unnatural amino acids and peptide cyclization.<sup>21,22</sup> Introduction of peptidomimetic  $\beta$ -amino acids in an  $\alpha$ -peptide imparts stability against degradation. For instance, mixed  $\alpha/\beta$ -peptides synthesized by replacement of  $\alpha$ - with  $\beta$ -amino acids display proteolytic stability against different proteases compared to the corresponding  $\alpha$ -peptides.<sup>23-28</sup>

The objective of the current study was to develop analogues of cancer targeting peptide **18** to improve proteolytic stability and maintain specific affinity for breast cancer cells. The hypothesis was that peptide **18** can be converted into a proteolytically stable peptide by replacement of a few amino acids while maintaining the secondary structure of the peptide and specific affinity for breast cancer cells. Two approaches were used to develop the analogues. First, a second generation of p160 analogues was created by introduction of single or double substitutions in the peptide **18** sequence to improve specificity for breast cancer cells. Secondly, proteolytically stable analogues of peptide **18** were explored.

Accordingly, we have designed and synthesized ten FITC-labeled peptide **18** analogues (**Table 3.1**). All the analogues display high affinity for cancer cells compared to non-cancerous cells. Three analogues (**18-4**, **18-9**, and **18-10**)

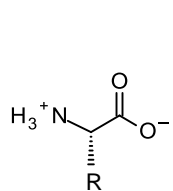
display exceptional resistance to proteolytic degradation in human serum and show higher uptake (up to 3.5-fold) by the breast cancer cell lines MDA-MB-435, MDA-231, MCF-7 compared to peptide **18**. These analogues show low affinity for control (non-cancerous) MCF-10A and HUVEC cells. One of the analogues, **18-4**, consists of two L- to D-amino acid replacements in **18**, whereas the other two (**18-9** and **18-10**) contain three  $\alpha$ - to  $\beta^3$ -amino acid (derived from L-Asp)<sup>29</sup> substitutions. Here we show for the first time that L-Asp can be used as an effective and inexpensive  $\beta$ -amino acid replacement onto which side-chain mimics can be placed by making amide analogues on the  $\alpha$ -carboxylate. The analogues maintain a stable secondary structure like the parent peptide **18**, and impart no cytotoxicity. This study demonstrates discovery of three novel proteolytically stable breast cancer targeting peptides with potential applicability in anti-cancer drug delivery and cancer diagnostics.

**Table 3.1.** Primary amino acid sequences and characterization (mass spectrometry and HPLC) of cancer targeting peptides studied herein. Substitution of amino acids in analogues 18-1 – 18-10 is shown in blue ( $\alpha$ -amino acids) or red ( $\beta$ -amino acids derived from L-asp). Lower case letters denote D-amino acids, X is Nle, and Z is a  $\beta^3$ -residue with a naphthyl side chain.

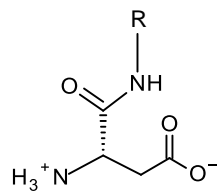
Peptide	Amino acid Sequence	[M+H] <sup>+</sup> <sup>a</sup>		Yield (%)	Rt <sup>b</sup> (min)	
		Calcd.	Obsd.		Sol 1	Sol 2
<i><math>\alpha</math>-Peptides</i>						
<b>18</b> ( <i>control</i> )	WXEAA <sup>Y</sup> QRFL	1367.7	1367.9	70	23.2	29.4
<b>18-1</b>	<b>Y</b> XEAA <sup>Y</sup> QRFL	1343.5	1343.1	60	24.5	29.2
<b>18-2</b>	W <b>E</b> EAA <sup>Y</sup> QRFL	1383.6	1384.8	70	24.3	29.1
<b>18-3</b>	W <b>L</b> EAA <sup>Y</sup> Q <b>R</b> <b>Y</b> L	1383.6	1383.5	75	24	29.0
<b>18-4</b>	W <b>x</b> EAA <sup>Y</sup> Q <b>r</b> FL	1367.7	1367.9	63	23.1	29.3
<i>Mixed <math>\alpha/\beta</math>-Peptides</i>						
<b>18-5</b>	W <b>X</b> EAA <sup>Y</sup> Q <b>K</b> FL	1454.5	1454.4	45	24.1	29.3
<b>18-6</b>	W <b>X</b> EAA <sup>Y</sup> Q <b>R</b> FL	1482.1	1483.1	50	24.6	29.4
<b>18-7</b>	W <b>X</b> EAA <sup>Y</sup> Q <b>R</b> FL	1537.2	1538.2	48	24.9	29.7
<b>18-8</b>	W <b>X</b> EAA <sup>Y</sup> Q <b>R</b> FL	1538.4	1538.2	51	24.7	29.5
<b>18-9</b>	<b>Z</b> XEAA <sup>Y</sup> Q <b>K</b> FL	1522.1	1522.6	40	24.9	33.2
<b>18-10</b>	<b>Z</b> XEAA <sup>Y</sup> Q <b>K</b> FL	1522.1	1522.1	35	24.9	33.1

<sup>a</sup>MALDI-TOF of  $\beta$ -Ala-peptide.

<sup>b</sup>RP-HPLC retention time of FITC-labeled peptides. Gradient used on a Vydac C18 analytical column was Sol 1: 15-50% IPA/water (0.1% TFA) in 35 min with a flow rate of 1 mL/min, and Sol 2: 15-55% ACN/water (0.1% TFA) in 35 min with a flow rate of 1 mL/min.



$\alpha$ -amino acid



$\beta^3$ -amino acid

## 3.2. Materials and Methods

### 3.2.1. Peptide Synthesis

Eleven 10-mer peptides (**Table 3.1, 18-1 – 18-10**) were synthesized manually using solid phase peptide synthesis on 2-chlorotrityl-chloride resin (0.2 mmol, 1 mmol/g) as described previously.<sup>19,25</sup> The chemical structures of the peptides containing D- or  $\beta$ -amino acids are shown in **Figure 3.1**. The first Fmoc-amino acid was coupled using DIPEA for 6 hours. Further amino acids were coupled at two-fold excess using HCTU/HOBt/NMM as activating mixture in DMF. After coupling for 2 hours at room temperature, the ninhydrin test<sup>30</sup> was performed to estimate the completeness of the reaction. For mixed  $\alpha/\beta$ -peptide analogues (**18-5 - 18-10**),  $\beta$ -amino acids were added to the backbone of the peptide following Fmoc/allyl combined solid-phase synthesis as previously described.<sup>25,29</sup> Briefly, N- $\alpha$ -Fmoc-L-aspartic acid  $\alpha$ -allyl ester was coupled to the growing peptide in DMF using HCTU/HOBT (2 equiv each), and NMM (4.5 equiv) for 2 h at room temp. After coupling, palladium catalyzed deprotection of the side chain allyl from carboxyl group was done under nitrogen using mixture of Pd (PPh<sub>3</sub>)<sub>4</sub> (0.08 equiv) and PhSiH<sub>3</sub> (8 equiv) in DCM/DMF (45 min x 3). Following deallylation, the corresponding amine (RNH<sub>2</sub>, 4 equiv) was coupled using the same coupling reagents as mentioned above for 4 hr. Amine side chains used for  $\beta^3$  amino acid syntheses were as follows: methylamine (Sigma) for alanine, n-butylamine (Sigma) for norleucine, t-butyl-N-(4-aminobutyl) carbamate (TCI-EP) for arginine, benzylamine (Sigma) for phenylalanine, 1-

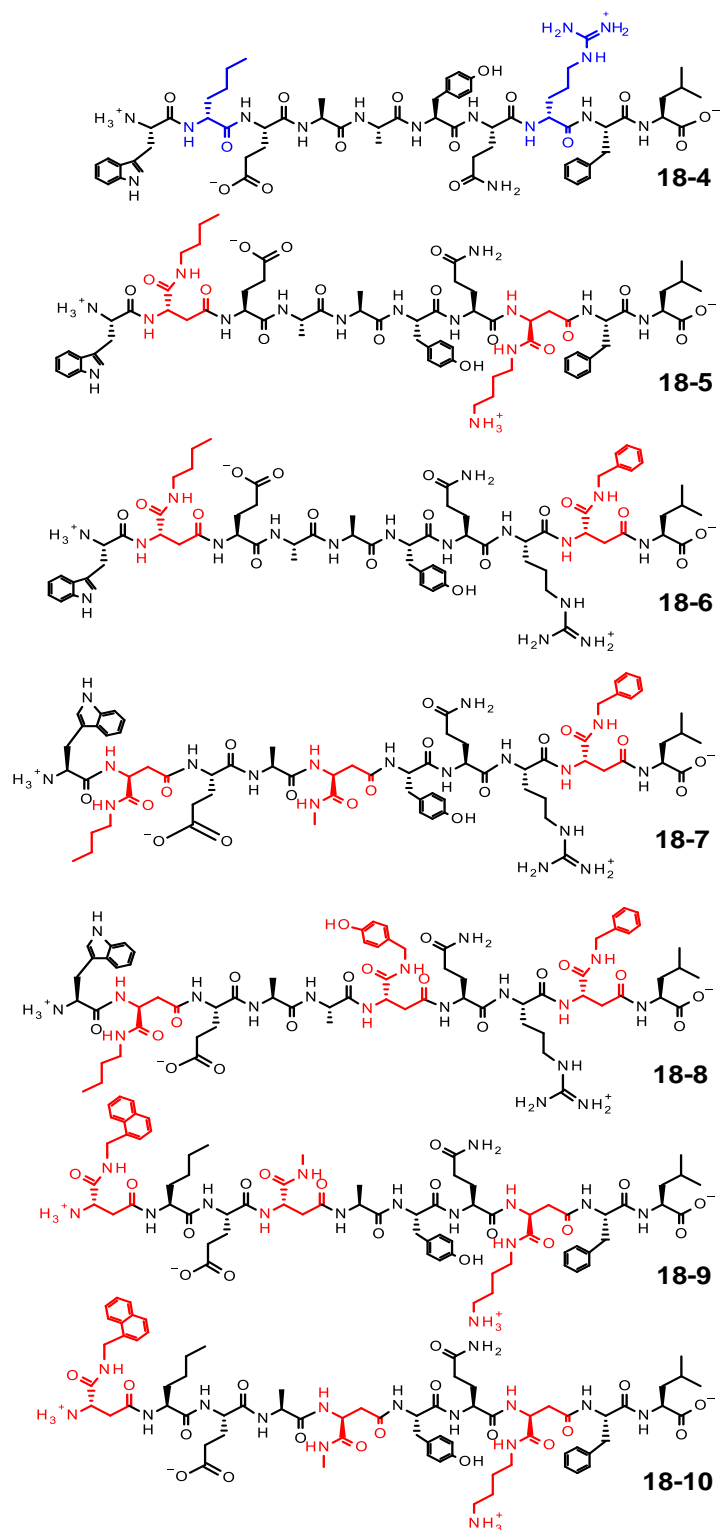


**Figure 3.1.** Chemical structures of synthesized cancer targeting peptides containing D- or  $\beta$ -amino acids.  $\alpha$ -Amino acids are shown in black (L-amino acids) or blue (D-amino acids) and  $\beta$ -amino acids derived from L-aspartic acid are shown in red.

naphthalenemethylamine (Alfa Aesar) for tryptophan, 4-*tert*-butoxybenzylamine (Otava) for tyrosine. and double coupling. In this case, the concentration of amines should not exceed 2 equivalents to prevent cleavage of Fmoc protecting group before complete coupling. Fmoc groups were removed by treatment with 20% piperidine in DMF, two times each for 7 minutes. After completion of the synthesis, peptides were cleaved from resin and all protecting groups were removed using cleavage mixture (50:50% TFA/DCM, 5% TIPS) at room temperature for 1 hr, followed by washing the resin with the cleavage reagent twice. The cleaved peptide combined with TFA washes was concentrated by rotary evaporation. Cold Et<sub>2</sub>O (40 mL) was added to precipitate the peptide, and then centrifuged. Crude peptides were dissolved in water and purified using reversed-phase HPLC (Varian Prostar 210, USA) to obtain pure peptides in 45% to 70% yield. The purity of the peptides was confirmed by HPLC and MALDI-TOF mass spectrometry (**Figures A.4, A.5**). The purity of the peptides was verified to be greater than 95% by RP-HPLC. The HPLC analysis and mass spectrometric data of the peptides are summarized in **Table 3.1**. All the peptides were labeled with fluorescein 5-isothiocyanate (5-FITC) through their N-terminus via a β-alanine spacer. The stepwise procedure for FITC conjugation to peptide **18** is shown in **Figure A.3**. FITC-β-ala-peptides (or FITC-peptides) were verified to be greater than 95% pure by RP-HPLC (Figure A.4).

## **Cell Culture**

All cancer cell lines and human mammary epithelial cell line MCF-10A were purchased from the American Type culture collection (ATCC) and additives were from Invitrogen. Human breast cancer cell line MDA-MB-435 was cultured in RPMI-1640 media supplemented with 10% FBS, 100 IU/ml penicillin, and 100 IU/ml streptomycin, whereas, MCF-7 and MDA-231 were cultured in DMEM media containing 10% FBS, 100 IU/ml penicillin, and 100 IU/ml streptomycin. Human mammary epithelial cell line (MCF-10A) was cultured in minimal essential growth media MEGM (Lonza, Cedarlane) supplemented with same additives as before. Human umbilical vein endothelial cells (HUVEC), a kind gift from the laboratory of Sandra Davidge, University of Alberta, were cultivated using Endothelial Cell Growth Medium EGM, (Lonza, Cedarlane) containing 20% FBS, 2 mmol/L glutamine, 100 IU/ml penicillin, 100 IU/ml streptomycin, and 2 ng/mL basic fibroblast growth factor (Roche Diagnostics, Mannheim, Germany). All cell lines were cultivated at 37 °C in a 5% CO<sub>2</sub>-95% O<sub>2</sub> incubator and growth media were replaced every 48 h.

### **3.2.2. Cellular Uptake by Flow Cytometry**

The cellular uptake of the synthesized analogues (**18-1–18-10**) was evaluated against three human breast cancer cell lines (MDA-MB-435, MCF-7, and MDA-MB-231) and two non-cancerous cell lines (MCF-10A and HUVEC) using flow cytometer (Becton-Dickinson Facsort). Cells were grown in T-75 culture flasks

containing media supplemented with FBS and antibiotics until 80% confluence. After washing twice with PBS, cells were detached from the surface by incubation with trypsin solution at 37 °C. Cells were centrifuged at 500 g for 5 min, re-suspended in media, counted by hemocytometer, and diluted to  $10^3$  cells/mL with media. Next, they were seeded in 6 well tissue culture plate at a density of  $10^6$  in 3 mL of culture medium at 37 °C for 24 h. The following day, cells were washed by PBS and incubated in serum free media containing FITC-labelled peptides at a concentration of  $10^{-5}$  mol/L for 30 min at 37 °C. Then the cells were washed 3 times with PBS, trypsinized to remove any surface bound peptides, and centrifuged at 5000 g for 5 min. The pellets were resuspended in FACS solution (10% FBS in PBS), and flow cytometry was performed. A total of 10,000 events were collected monitoring fluorescein - 5 - isothiocyanate (5-FITC). The autofluorescence of the cells only without treatment was measured to differentiate between the peptide-bound labelled cells and autofluorescence of unlabeled cells. Fluorescence up to the measured intersect was called autofluorescence and represented cut-off point value. Cells in which fluorescence was higher than that value were considered labelled with 5-FITC. Competitive binding assays were performed using MDA-MB-435 cancer cell line with FITC-**18-4** and FITC-**18-9** in the presence of 50-fold excess of unlabelled **18-4** and **18-9** respectively. After incubation for 30 min at 37 °C, the cells were washed with ice cold PBS. Thereafter, FACS analysis was performed as described above. All experiments for binding were repeated 2-3 times.

### 3.2.3. Fluorescence Microscopy

MDA-MB-435 or HUVEC cells (50,000) were cultured on the top of a cover slip at 37 °C for 24 hr. The medium was removed and replaced with fresh serum free medium (1 mL), containing FITC-labeled peptides (**18-4**, **18-9**) at a concentration of  $10^{-5}$  mol/L. The cells were incubated with the peptides for 30 min at 37 °C. After incubation, the medium was removed and the cells were washed with serum free medium (3 x 2 mL). The cells were fixed on ice with 2% formaldehyde for 20 min. The formaldehyde was removed by washing with media (3 times). The cover slips were put on slides containing one drop of DAPI-Antifade (Molecular Probes) to stain the nucleus. The cells were imaged under the fluorescence microscope (Zeiss) using green and blue filters with 20x magnification. The samples prepared for fluorescence microscopy were also used for visualization by confocal microscopy to confirm internalization. Confocal laser scanning microscopy was performed with a Carl Zeiss inverted confocal microscope (Zeiss 510 LSMNLO, Jena, Germany) with a 40x oil immersion lens. Confocal stacks were processed using the Carl Zeiss LSM 5 Image software, which also operates the confocal microscope.

### 3.2.4. Serum Stability

The proteolytic stability of selected peptides (**18**, **18-4**, **18-9**, and **18-10**) in the presence of human serum was evaluated using HPLC analysis. Human serum (250 µL) was added to RPMI media (650 µL) in 1.5 mL eppendorf tube to mimic

biological system. The temperature was equilibrated at  $37 \pm 1$  °C for 15 min before adding 100  $\mu$ L of peptide stock solution (1 mM solution in 100% sterile water). The initial time was recorded and at known time intervals (0, 0.5, 1, 5 and 24 hr) an aliquot of reaction solution (100  $\mu$ L) was removed and added to methanol (200  $\mu$ L) for precipitation of serum proteins present in the human serum. The cloudy solution produced was cooled to 4 °C for 15 min and then spun at 500 *g* for 15 min to pellet the serum proteins. The supernatant (50  $\mu$ L) was injected on to RP-HPLC (Vydac C18 column) using an auto-injector to eliminate manual injection error. A linear gradient from 12-100% IPA/water in 35 min with a flow rate of 1.5 mL/min was used and the absorbance of the eluting peaks was detected at 214 nm. The concentration of peptides and degradable products was measured by integrating the area under the curve and their identity was confirmed using MALDI-TOF mass spectrometry.

### **3.2.5. *In Vitro* Metabolic Stability**

The *in vitro* metabolic stability was determined by incubating the peptides with the liver homogenate. The liver homogenate was prepared as described previously.<sup>31</sup> Briefly, liver was collected from male CD-1 mice. After cleaning and washing in ice-cold HEPES buffer (pH 7.4), approximately 0.98 g was transferred to a 50 mL centrifugation tube. Ice-cold HEPES buffer (5 mL) was added, and the organ was homogenized with an Ultra-Turrax (IKA, Staufen, Germany) for 1 min on ice. The homogenate was shaken, and subsequently

centrifuged at 14,000 rpm for 20 min at 4 °C. Aliquots of the supernatant was transferred into microtubes, and stored at -80 °C until use. Before use, the protein content of each homogenate was determined using Bicinchoninic acid Protein Assay (BCA) to generate a stock solution with a protein concentration of 14.7 mg/mL by dilution with HEPES buffer.

For the metabolic stability of the peptides, an aliquot (100 µL) from the peptide stock solutions (**18-4**, **18-9**, and **18-10**) prepared in 5% ACN/water mixture (1 mM) was added to 900 µL of liver extract (200 µL of homogenate, 700 µL of RPMI media, pH 7.4, 2.94 mg of protein in total). The mixture was incubated at 37 °C while shaking, and an aliquot (100 µL) was taken out at regular time intervals. The enzymatic reaction was stopped by mixing the sample with methanol (300 µL). This also allowed proteins precipitation, after which the samples were cooled at 0 °C for 30 min. Thereafter, centrifugation at 14,000 rpm for 10 min yielded a clear supernatant, which was analyzed by reversed-phase HPLC on Vydac C18 column with UV detection at 220 nm wavelength. Cleavage products were separated by analytical reversed phase HPLC using 15-55% IPA/water over 35 min and analyzed by MALDI-TOF mass spectrometry. Blank solutions as well as the control  $\alpha$ -peptide (peptide **18**) were similarly treated for comparison. The percent of hydrolysis was determined from the integration of “area under the curve” of the peaks.

### 3.2.6. NMR spectroscopy

All NMR experiments and structure elucidation was done by Dr. Tara Sprules at McGill University. NMR samples of synthetic peptide p160 (VPWXEPAYQRFL) were prepared in water (90% H<sub>2</sub>O:10% D<sub>2</sub>O, or 100% D<sub>2</sub>O) or TFE (100% CF<sub>3</sub>CD<sub>2</sub>OH or 100% CF<sub>3</sub>CD<sub>2</sub>OD) (Cambridge Isotope Laboratories, Inc). Samples of **18** were prepared in a mixture of TFE and water (80% CF<sub>3</sub>CD<sub>2</sub>OH:20% H<sub>2</sub>O or 80% CF<sub>3</sub>CD<sub>2</sub>OD:20% D<sub>2</sub>O). Spectra were recorded at 15°C. The complete chemical shift assignments for p160 and **18** are listed in **Table A.1**. 2D TOCSY (60 ms mixing time), COSY, ROESY (mixing time 200 ms) and NOESY (mixing time 100, 200 and 300 ms) spectra were recorded on Varian INOVA 500 MHz spectrometer equipped with an HCN (hydrogen, carbon, nitrogen) cold probe and pulsed-field gradients. Upper distance restraints for p160 structure calculations in TFE were obtained from 200 ms mixing time 2D-[1H,1H]-NOESYs recorded at 500 MHz (amide region) and 800 MHz (aliphatic and aromatic regions). Upper distance restraints for p160 structure calculations in H<sub>2</sub>O were obtained from 200 ms mixing time 2D[1H-1H] ROESY spectra recorded at 500 MHz. Upper distance restraints for **18** structure calculations were obtained from 200 ms mixing time 2D-[1H,1H]-NOESYs recorded at 500 MHz. Calculations of the complete three-dimensional structures were performed with the program CYANA v 2.1.<sup>32</sup> Input data and structure calculation statistics are summarized in **Tables A.2** and **A.3**. The final calculation was started with 100 randomized conformers to converge to the final

conformation. A bundle of the 20 lowest energy CYANA conformers were used to represent the NMR structure of the peptides.

### **3.2.7. CD Spectroscopy**

The circular dichroism (CD) measurements were made on Olis CD spectrometer (Georgia, USA) at 25 °C in a thermally controlled quartz cell with a 0.02 cm path length over 190-260 nm. The samples were prepared by dissolving the peptides in 90% TFE/water mixture containing 0.05% TFA. The final peptide concentration for the CD measurements was 200 µM. Data were collected every 0.05 nm and were average of 8 scans. The bandwidth was set at 1.0 nm and the sensitivity at 50 mdeg. The response time was 0.25 s. In all cases, baseline scans of aqueous buffer were subtracted from the experimental readings. The CD data was normalized and expressed in terms of mean residue ellipticity (deg cm<sup>2</sup> dmol<sup>-1</sup>).

### **3.2.8. Cytotoxicity**

The cytotoxicity of peptide analogues **18-4**, **18-9** and **18-10** was tested by measuring the cell growth inhibition using MTT assay.<sup>33</sup> Breast cancer human cells MDA-MB-435 were seeded in 96-well plates (Corning Inc., MA, USA) at a concentration of  $1 \times 10^4$  cells/well per 200 µL RPMI serum free media supplemented with antibiotics (100 IU/mL penicillin, 100 IU/mL streptomycin), and incubated at 37 °C in 5% CO<sub>2</sub> atmosphere. After 24 hours, the cells were treated with different concentrations of the peptides (1-100 µM) prepared in sterile water and incubated for 48 h. Doxorubicin was used as a positive control

and the untreated cells were used as a negative control. The culture media was discarded and replaced with 20  $\mu\text{L}$  MTT solution (5 mg/mL in cell media) and 100  $\mu\text{L}$  cell medium, Then the cells were incubated for another 3.5 hr. All experiments were done in triplicate, and the data in the form of the mean is presented. Following incubation, the media was sucked out, and the purple formozan product precipitated in each well was solubilized in DMSO (150  $\mu\text{L}$ ). After gentle shaking for 10 min at room temperature, absorbance was measured at 570 nm using a VERSA max microtitre reader (Molecular Devices, Sunnyvale, CA, USA) with a reference wavelength of 650 nm. The percentage cell viability was expressed as the absorbance ratio of cells treated with peptides to untreated cells dissolved in complete media.

### 3.3. Results

#### 3.3.1. Design of Peptide 18 Analogues

Peptide **18** is a linear 10-mer peptide with a net charge of zero that shows high binding affinity to breast cancer cells compared to non-cancerous cells *in vitro*.<sup>19</sup> In our earlier experiments, **18** was identified through screening a cellulose membrane-bound peptide array library against cancer cells. The peptide array library was based on a cancer targeting dodecapeptide, p160.<sup>16,19</sup> Deletion of the two N-terminal residues (Val-Pro) of p160 and one Pro $\rightarrow$ Ala substitution yields decapeptide **18** (**Figure 3.1**). Using peptide **18** as a starting point, here we have designed ten analogues of **18** for selective binding to breast cancer cells. The

synthesis of the peptides was done on solid phase as described in the methods section. The mass spectrometry data and the HPLC elution time of the peptides are listed in **Table 3.1**.

First, three  $\alpha$ -peptide sequences (**18-1** - **18-3**) were designed to introduce one or more substitution(s) in **18**, such as Trp1→Tyr1, Nle2→Glu2 or Leu2, and Phe9→Tyr9, based on the results of our initial peptide array (based on p160) screening.<sup>19</sup> Next, in peptide analogue **18-4**, two residues, Nle2 and Arg8, were substituted with D-amino acids to enhance proteolytic stability as well as increase binding affinity to cancer cells. These residues have been identified as the labile sites in the peptide by Askoxylakis and coworkers.<sup>17</sup>

Finally, a number of mixed  $\alpha/\beta$ -peptides (**18-5** - **18-10**, **Figure 3.1**) were designed to improve the proteolytic stability of the lead peptide **18**. Analogues **18-5** and **18-6** contain substitution of two labile residues with  $\beta^3$ -amino acids.  $\alpha/\beta$ -Peptides **18-7** - **18-10** each contain three  $\alpha$  to  $\beta^3$  replacements to maximize resistance to proteolysis. These analogues were fabricated following a sequence based design strategy reported by Horne *et al.*<sup>23,24,34</sup> Here  $\alpha$  and  $\beta$  amino acid residues were distributed in a repeating heptad pattern ( $\alpha\alpha\beta\alpha\alpha\beta$ ) that yields  $\beta$ -residues along one side of the helix.<sup>34</sup> The replacement sites in these four analogues were selected to sample different positions in the heptad repeat. The  $\beta^3$ -amino acids used in this study were derived from L-aspartic acid.<sup>29</sup>

### 3.3.2. *In Vitro* Cell Binding Assays

The binding of the peptide analogues to different mammalian cell lines was compared to the lead peptide **18** using flow cytometry. FITC-labelled peptides (**18**, **18-1** – **18-10**) were screened for specific binding to three breast cancer cell lines, namely, MDA-MB-435, MDA-MB-231 and MCF-7, and two non-cancerous cell lines, MCF-10A and HUVEC. The results show that all 10 analogues display significant binding to the three breast cancer cell lines, as evidenced by the increase in the percentage of fluorescently labelled positive cells, relative to the untreated cells (40-100%  $\pm$ 10 for the treated, and 1% for untreated groups). The uptake pattern of all the peptides was similar for the three cancer cell lines with slightly higher uptake for MCF-7 at the concentrations tested. This is in agreement with previous studies that showed that p160 has 7-fold higher binding to MCF-7 compared to MDA-MB-435.<sup>18</sup> Among all the peptides evaluated, peptides **18-4**, **18-9**, and **18-10** showed the highest binding to the cancer cells (**Figure 3.2**).

When comparing the binding affinity of  $\alpha$ -peptide analogues (**18-1** - **18-4**) and peptide **18** to cancer cells, it was found that the hydrophobic and/or aromatic substitutions (Trp1 $\rightarrow$ Tyr1, Nle2 $\rightarrow$  Leu2 and Phe9 $\rightarrow$ Tyr9) were more tolerated than the charged amino acid substitution (Nle2 $\rightarrow$ Glu2). For instance, peptides **18-1** and **18-3** with aromatic or hydrophobic substitutions displayed equal or slightly higher binding affinity ( $\geq$ 1.5-fold), whereas **18-2** with Nle2Glu substitution showed a three-orders of magnitude decrease in binding. The percentage increase in fluorescence (of **18-2** incubated with cells) compared to

cells only was  $14\pm 3\%$ ,  $60\pm 5\%$ , and  $33\pm 8\%$  for MDA-MB-435, MCF-7, and MDA-MB-231 cells, respectively. Peptide **18** has an average of  $74\pm 10\%$  increase in fluorescence for the three cell lines. This correlates with our previous observation where a p160 analogue with Phe9Lys charged substitution showed a marked decrease in binding with respect to the parent peptide.<sup>25</sup> In addition, the overall charge for **18-2** is -1 which may also hinder its interaction with negatively charged surface of the cancer cells.<sup>35</sup> Peptide **18-4**, with D-amino acid substitutions at N1e2 and Arg8, was well tolerated and showed up to 3.5 fold increase in peptide affinity to cancer cell lines. As shown in **Figure 3.2**, the mean fluorescence intensities of **18** and **18-4**, respectively, were  $10\pm 2$  and  $35\pm 2$  when incubated with MDA-MB-435,  $22\pm 2$  and  $68\pm 2$  with MCF-7, and  $16\pm 2$  and  $45\pm 2$  when incubated with MDA-MB-231 cells. In earlier studies D-p160 with all amino acids replaced with the D-isoforms showed no uptake by the cancer cells and was used as a negative control peptide.<sup>18</sup> The results presented here, however, suggest that the configuration of the two amino acids most likely did not alter the interaction with the receptor. In general, these results reflect that hydrophobic substitutions are beneficial and such interactions increase specific binding of the peptide to the cancer cell.

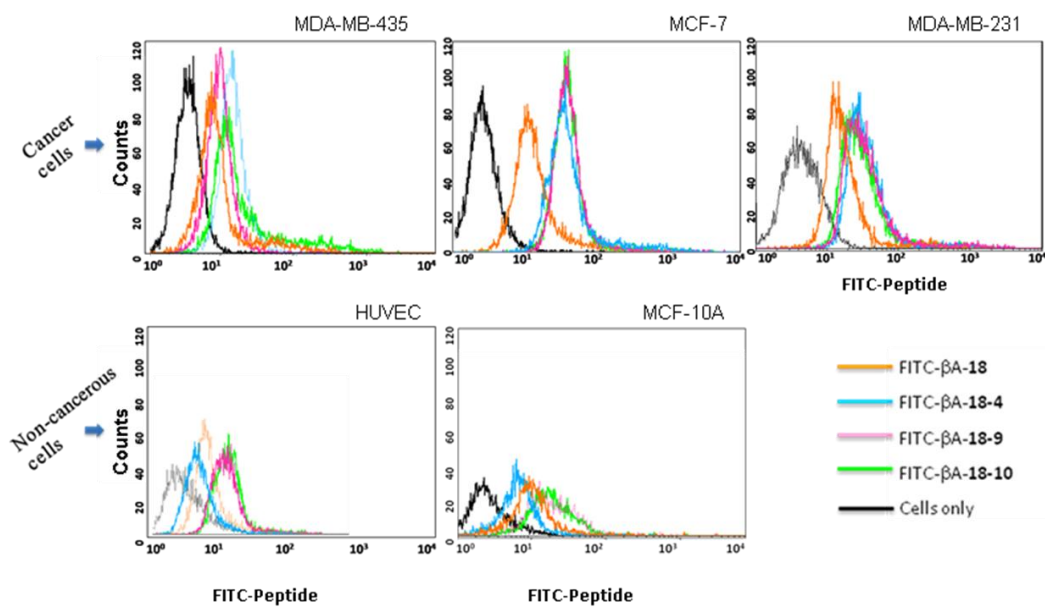


**Figure 3.2.** Peptide uptake by the cancer cells (top row) MDA-MB-435, MCF-7 and MDA-MB-231, and the control cells (bottom row) HUVEC and MCF-10A measured by flow cytometry. The peptides ( $10^{-5}$  mol/L) FITC-18 (orange), FITC-18-4 (blue), FITC-18-9 (pink), and FITC-18-10 (green) were incubated with the cells for 30 min at 37 °C. Auto-fluorescence of the cells is shown in black.

Mixed  $\alpha/\beta$ -peptide analogues (**18-5 - 18-10**) with two or three  $\beta$ -amino acid substitutions and variation in the position of the  $\beta$ -residues were also well tolerated. Peptides **18-5**, **18-6**, **18-7**, and **18-8** displayed similar affinity to cancer cells, whereas, **18-9** and **18-10** showed a marked increase ( $\sim 3$  fold) in binding to cancer cells, compared to the parent peptide **18** (**Figures A.6** and **3.2**). Peptides **18-9** and **18-10** each have three  $\alpha \rightarrow \beta^3$ -amino acid substitutions. The polarity of the side chains was maintained, namely, Trp1 was replaced with a  $\beta^3$ -amino acid with naphthyl side chain, Ala4 or Ala5 was replaced with methyl, and Arg9 was substituted with a  $\beta^3$ -amino acid with a butylamine side chain. These substitutions led to a slight increase in hydrophobicity of the peptide as observed

from the increase in the HPLC retention time of the peptide (**Table 3.1**). Previously, Askoxylakis *et al.* also reported a similar observation where replacement of Ala7 with  $\beta$ -alanine in p160 resulted in a more than 2-fold increase in binding to WAC 2 cells when compared to the native p160.<sup>17</sup>

Based on the initial screening results for peptide uptake by cancer cells, three peptides **18-4**, **18-9**, and **18-10** were selected for further study. The binding affinity and specificity of the selected peptides were evaluated against non cancerous cell lines MCF-10A and HUVEC. MCF-10A cells are derived from human fibrocystic mammary tissue, whereas, HUVEC endothelial cells were isolated from normal human umbilical vein. The three peptides displayed significantly lower binding to the control cells versus strong preferential binding to breast cancer cells after 30 min incubation (**Figures 3.2**). The percent increase in fluorescence (relative to the untreated cells) was  $36\pm 2\%$ ,  $50\pm 3\%$ , and  $55\pm 3\%$  for MCF-10A cells, and  $12\pm 1\%$ ,  $30\pm 5\%$ , and  $35\pm 4\%$  for HUVEC when incubated with peptides **18-4**, **18-9**, and **18-10**, respectively. These peptides showed 85-100% increase in fluorescence when incubated with cancer cells showing that peptides bind preferentially to cancer cells. It is also observed that the peptides have relatively higher binding to MCF-10A compared to HUVEC, and this is most likely due to the presence of low levels of the putative receptor in normal mammary cells. Peptides **18-9** and **18-10** displayed similar affinity profiles for the cancer and control cells with **18-9** showing slightly better selectivity. Therefore, **18-9** was selected for subsequent experiments.

In a parallel experiment the binding specificity and cellular uptake of **18-4** and **18-9** peptides were studied using fluorescence microscopy in MDA-MB-435 and HUVEC cells. The fluorescently (FITC) labeled peptides were incubated with cells for 30 min at 37 °C and the peptide distribution was examined. Both the FITC-labeled peptides were found to be strongly bound to the cell membrane of MDA-MB-435 cancer cells, and were also uniformly distributed inside the cells (**Figure 3.3, LHS**). In contrast, the uptake of the peptides by control HUVEC cells was minimal under the same experimental conditions (**Figure 3.3, RHS**). To further prove that most peptide molecules were not only surface bound but also internalized, we performed optical sectioning of MDA-MB-435 cells treated with **18-9** (**Figure 3.4**). The focal plane was changed from bottom to top in the vertical axis range of 32.8  $\mu\text{m}$  at an interval of 1.64  $\mu\text{m}$  and, as shown in **Figure 3.4** it was found that most of the peptide bound to MDA-MB-435 cells was internalized by the cells.

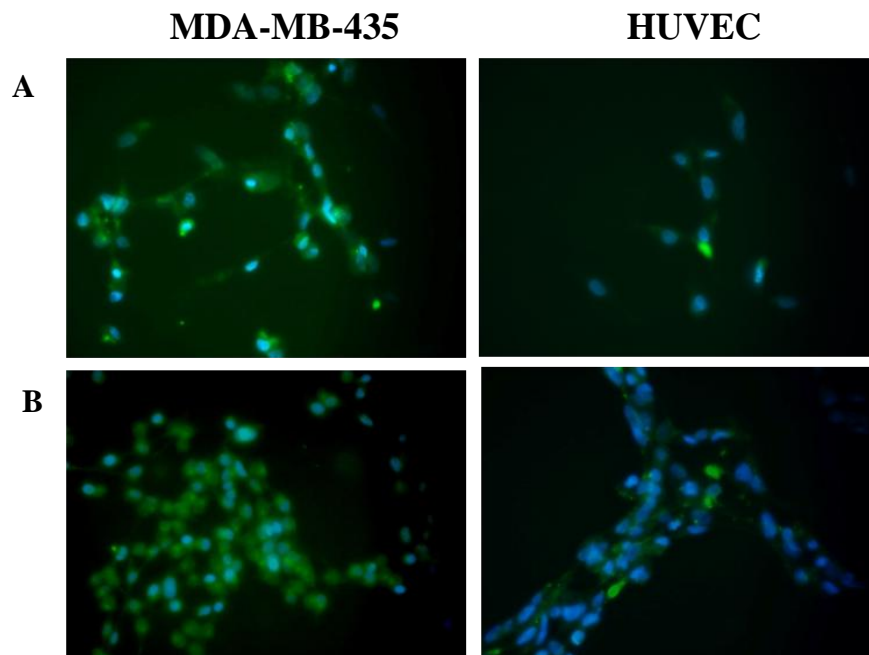


**Figure 3.3.** Fluorescence microscopy images of MDA-MB-435 and HUVEC cells after incubation with FITC-18-4 (A) or FITC-18-9 (B) for 30 min at a peptide concentration of  $10^{-5}$  mol/L. Cell nuclei were stained blue with DAPI.

The specificity of the peptides was evaluated by a competitive binding experiment. MDA-MB-435 cells were incubated with FITC-labeled peptides ( $10^{-5}$  mol/L) in the presence of a 50-fold excess of unlabeled **18-4** or **18-9** for 30 min and fluorescence was measured using flow cytometry. Both the peptides led to a substantial decrease in fluorescence when incubated with excess of unlabelled peptide. Peptide **18-4** caused an up to 50% decrease in binding of the FITC-peptide, and **18-9** led to about a 40% decrease in binding, suggesting specific binding of the peptides to the cancer cells. **Figure A.7**

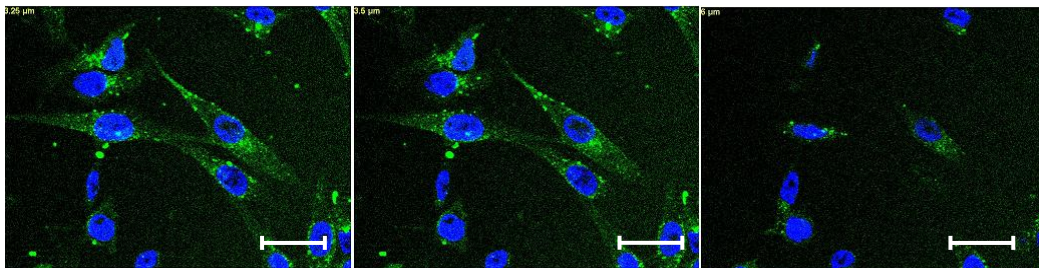


**Figure 3.4.** Optical sectioning using confocal laser microscopy of MDA-MB-435 cells showing intracellular distribution of FITC-labelled peptide 18-9. Cells were incubated with the peptide for 30 min at 37 °C prior to analysis. Scale bars: 20  $\mu\text{m}$ .

### 3.3.3. Proteolytic Stability

Next, the ability of these peptides (**18-4**, **18-9**, and **18-10**) to be recognized and processed by proteolytic enzymes was explored. Susceptibility to proteolytic digestion by human serum was compared to  $\alpha$ -peptide **18**. Peptides were incubated with human serum at 37 °C and aliquots were removed for analysis at different time points up to 24 h. Serum was used in high specific concentration (25% serum) to be rate limiting so that a control  $\alpha$ -peptide is degraded within 10 min. Degradation products were separated by reversed-phase HPLC in order to facilitate characterization by mass spectrometry.

**Figure 3.5A** shows the HPLC chromatograms of serum incubated with peptides for 0 and 24 hours. Peptide **18** was completely degraded within 30 min, giving two main degradation products which appear after 10 min of incubation with serum. The degradation products of peptide **18** show masses of 997.1 g/mol and 878.1 g/mol, which correspond to EAAYQRFL and WXEAAAYQ sequences,

respectively. This was in accordance with previous serum stability studies done for the p160 peptide.<sup>18</sup> In contrast, peptides **18-4**, **18-9**, and **18-10** were stable for more than 24 h after incubation with human serum. Serum aliquots were taken at 0.5, 1, 5 and 24 hours after incubation with the peptides and the peptides were found to be 100% intact.

Peptides were also exposed to the liver homogenate to evaluate proteolytic stability. Incubation of peptides **18-4**, **18-9**, and **18-10** with the homogenate up to 48 h did not result in any detectable degradation (**Figure 3.5B**). In contrast, under similar conditions the  $\alpha$ -peptide **18** was completely fragmented in 15 min. It was observed that proteolysis predominantly arises from the cleavage of the N-terminal amino acids, probably due to aminopeptidase activity. The degradation products for peptide **18** detected by HPLC were isolated, and characterized by mass spectrometry. The main degradation products with masses 868.2 g/mol, 797.2 g/mol and 727.4 g/mol corresponded to the sequences AAYQRFL, AYQRFL, and YQRFL, respectively. These results reveal that introduction of D-amino acids or  $\beta^3$ -residues in the peptide sequences confers substantial resistance to proteolytic degradation relative to their  $\alpha$ - peptide counterpart **18**. Such insertion of D- or  $\beta$ -amino acids in the peptide backbone tends to protect neighboring amide bonds from proteolytic cleavage.<sup>27,36</sup>

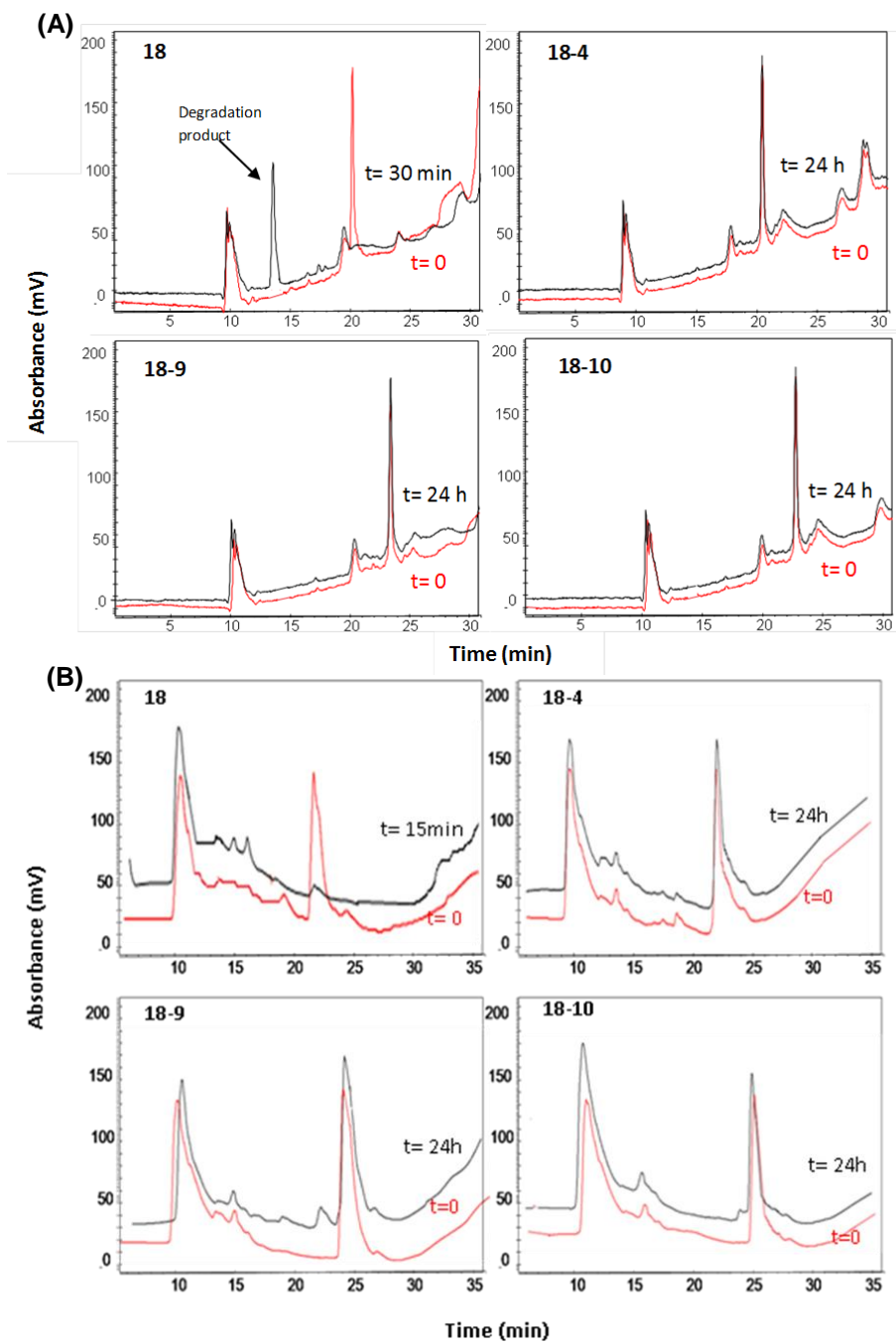


**Figure 3.5.** RP-HPLC chromatograms of peptides 18, 18-4, 18-9, and 18-10 after incubation with the human serum (A) and the liver homogenate (B). Peptides were incubated with the human serum or liver homogenate from mice for different time intervals, namely, 0 h (red), 30 min (black) and 24 h (black) prior to HPLC analysis. Peptides elute around 21-25 minutes. Degradation products from peptide 18 appear around 14-18 minutes, and the remaining peaks are from the media.

### 3.3.4. Solution conformation

Peptide **18** was discovered by screening a library of peptides based on the sequence of lead peptide p160. In order to understand the structural basis for the increased binding to the cancer cells of **18** compared to p160, we evaluated the NMR solution structures of these two peptides. First the NMR structure of p160 was obtained in water and TFE. Peptide p160 was found to be helical in TFE, however displayed no regular secondary structure in water. An overlay of multiple structures of p160 in the two solvents showed that the peptide was more stabilized in TFE as compared to water, demonstrated by the floppy N- and C-termini in the latter solvent (**Figure 3.6 A**). As these peptides are expected to bind the cell surface during interaction with the cancer cells, TFE may be the more relevant solvent to study their solution conformation. Accordingly, we looked at the NMR structure of peptide **18** in 80% TFE and found that peptide **18** is more helical than p160 (**Figure 3.6 B**). In addition, peptide **18** presents three distinct faces, with aromatic residues W1, Y6, and F9 on one side, hydrophobic residues N1e2, A4, and A5 on another side, and polar residues Q7 and R8 present on the third face. The helical structure and the distinct binding faces could explain the stability of peptide **18** and increased affinity for the putative cancer cell surface receptor.

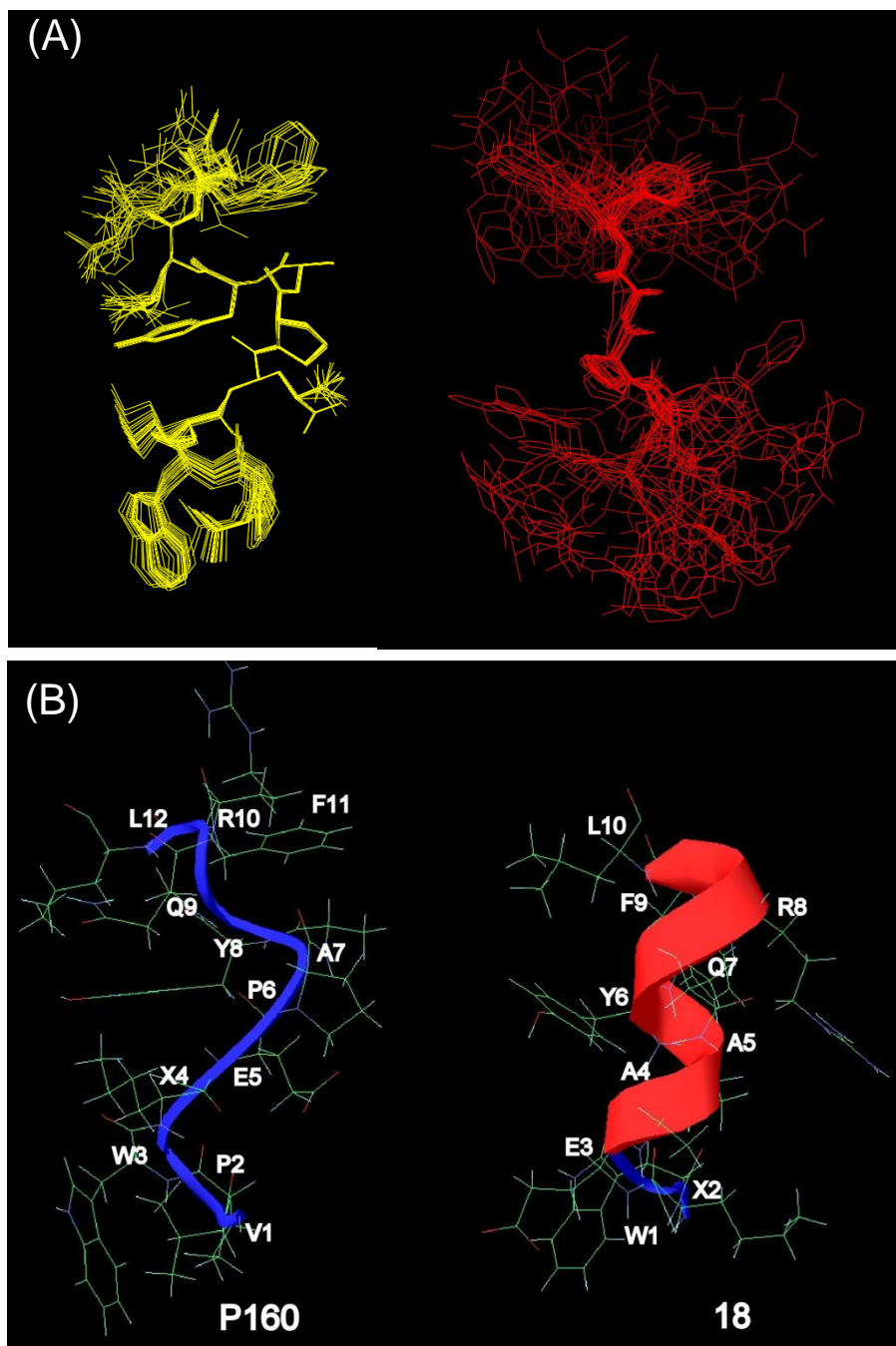


**Figure 3.6.** (A) The NMR solution structures of peptide p160 in TFE (yellow) and water (red). (B) Comparison of the NMR structures of peptides p160 (LHS) and 18 (RHS) in TFE. The helical region in 18 extends from Glu3 (E3) to Phe9 (F9).

The solution conformation of peptide **18** and peptide analogues **18-4**, **18-9**, and **18-10** were compared using circular dichroism (CD) spectroscopy (**Figure 3.7**). The CD measurements were performed in 90% TFE/water, at 200  $\mu$ M

concentration. Peptide **18** showed a strong minimum at 205 nm ( $\Theta = -7.0 \times 10^3$ ) with a shoulder at 231 nm. The minimum observed typically for helical peptides at 222 nm was not present. This is presumably due to diminished ellipticity at 222 nm in short helical peptides which consist of less than 5 turns.<sup>37,38</sup> Peptide analogue **18-4**, with Nle2 and Arg8 replaced with D-amino acids in the sequence of **18**, showed a similar CD

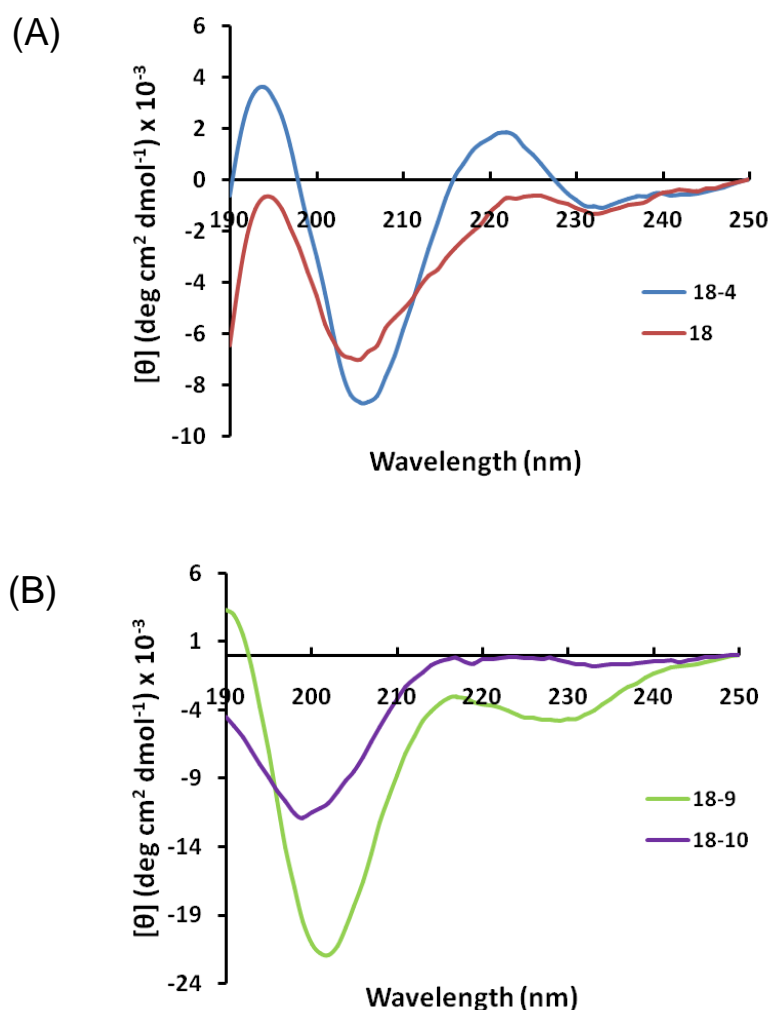


**Figure 3.7.** Circular dichroism spectra of peptides (A) 18 and 18-4, and (B) 18-9, and 18-10 in 90% TFE at 25 °C. The peptide concentration was 200  $\mu$ M.

spectrum to **18**, suggesting that the helical secondary structure is maintained. Interestingly, peptide **18-4** showed a slight increase in the molar ellipticity at 205 nm ( $\Theta = -8.7 \times 10^3$ ) and 195 nm ( $\Theta = 3.9 \times 10^3$ ) compared to peptide **18**. In this context, previous studies have shown that D-residues can indeed be comfortably accommodated in right-handed-helix structures, as demonstrated by recent crystal structures of synthetic peptides containing multiple D-residues placed in host L-amino acid sequences.<sup>39,40</sup>

The CD spectra of mixed  $\alpha/\beta$ -peptides **18-9** and **18-10** showed marked difference from the  $\alpha$ -peptides. With three  $\beta$ -amino acids replacing three  $\beta$ -residues in a 10-mer peptide, the CD of **18-9** and **18-10** showed a minima around 200-202 nm ( $-22 \times 10^3$  and  $-12 \times 10^3$ , respectively), and a small shoulder at 230 nm (**Figure 3.7 B**). CD spectra of several types of mixed  $\alpha/\beta$ -peptides have been reported and suggest formation of a helix-like conformation is signalled by the strong minimum at 203-207 nm.  $\alpha/\beta$ -Peptides that do not fold display little CD signal in this region.<sup>24,41</sup> This confirms our conjecture regarding the helical nature of **18-9** and **18-10**.

### 3.3.5. Cytotoxicity

Peptides **18-4**, **18-9**, and **18-10** were evaluated for their cytotoxic effects on MDA-MB-435 breast cancer cell line using the MTT assay. Doxorubicin (Dox) was used as a positive control. Different concentrations of the peptides and

Dox were incubated with the cells and after 48 h of incubation the percent cell viability was plotted as a function of the peptide concentration (**Figure 3.8**). The results showed that Dox displayed significant cytotoxicity with almost complete cell inhibition at 15  $\mu\text{M}$  concentration. In contrast, all the tested peptides exhibited negligible toxicity on the cells with cell viability  $>98\pm 5\%$  at concentrations up to 100  $\mu\text{M}$ . This is consistent with our previous results which showed very low cytotoxicity of peptides synthesized from  $\beta^3$ -amino acids derived from L-Asp.<sup>25</sup> Dox displays toxicity in the nanomolar range against most cell lines; however, it shows relatively low toxicity against MDA-MB-435 cells as observed here and elsewhere.<sup>42,43</sup>

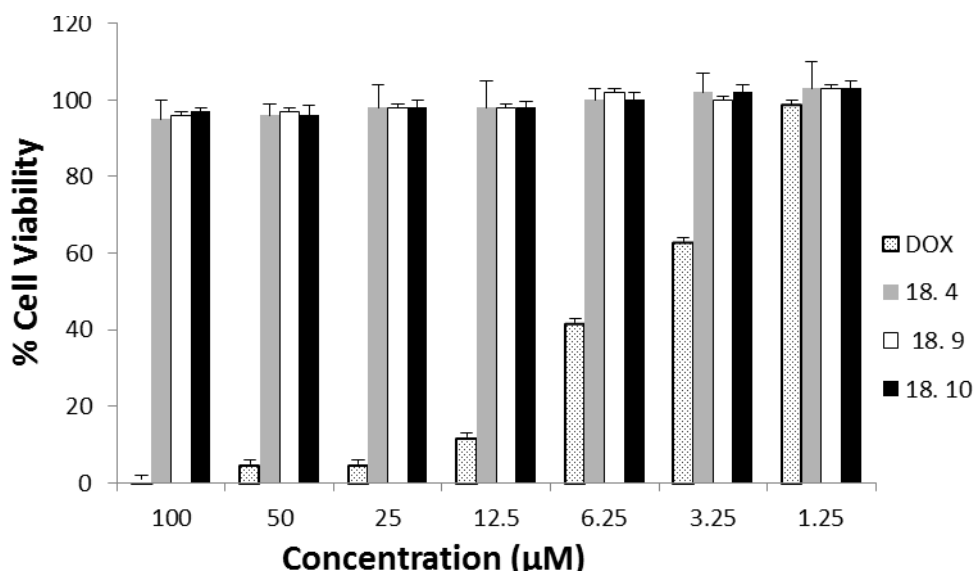


**Figure 3.8.** Cytotoxicity of peptides 18-4 (grey), 18-9 (white) and 18-10 (black) compared to doxorubicin (dark grey) monitored in MDA-MB-435 cancer cell line using the MTT assay. Cells were incubated with different concentration of peptides for 48 h. The data represent the mean  $\pm$  S.D of two independent experiments, and each concentration was done in triplicate.

### 3.4. Discussion

Chemotherapy and hormonal therapy play important roles in breast cancer treatment. Nevertheless, emergence of drug resistance, and negative side effects of these therapeutic regimens necessitates the search for specific tumor targeting agents. The clinical success of monoclonal antibodies such as Herceptin, Zevalin, Rituxan in the treatment of human cancer has validated the cell surface targeting approach in cancer therapy.<sup>44-46</sup> Peptides can be better cell surface targeting agents than antibodies, in particular when used as carriers for cytotoxic payloads such as chemotherapeutic agents or radionuclides. Peptides are smaller, safer, and more stable at room temperature with increased shelf life.<sup>47</sup> However, peptide applicability is limited due to fast proteolytic degradation. For instance, peptides p160 (shown previously)<sup>18</sup> and **18** display minimal stability in human serum as they are completely degraded within 1 hour after incubation with human serum (**Figure 3.5**). In addition, previous *in vivo* investigation of p160 stability in mice revealed a fast degradation of p160 in serum with appearance of degradation products after 2 minutes in circulation.<sup>18</sup> After i.v. administration, <sup>131</sup>I-labeled p160 showed higher uptake in tumors than in most normal organs, but also showed elevated levels in the blood. This could be due to the interaction of p160 with serum proteins or the presence of degraded fragments that are unable to bind tumor and circulate in the bloodstream.<sup>18</sup>

Our objective in this study was to design proteolytically stable peptides with high specificity for cancer cells. The results show that we have designed and synthesized at least three peptide analogues derived from peptide **18** that are

proteolytically stable and display increased affinity for breast cancer cells compared to peptide **18**. Peptide **18-4**, where two labile residues were replaced with D-amino acids, was completely stable in the presence of human serum and liver homogenate from mice (**Figure 3.5**), and showed up to 3.5-fold enhanced binding to cancer cells (**Figure 3.2**). Replacement of  $\alpha$ -residues with  $\beta$ -amino acids derived from L-Asp yielded two proteolytically stable peptides (**18-9** and **18-10**) with better binding profiles (2.8-3.1 fold) than peptide **18**. Interestingly, both these peptides include replacement of one residue each from the three distinct binding faces (aromatic, hydrophobic, and polar) identified in the NMR solution structure of peptide **18**. Replacement of W1, A4/A5, and R8 in peptide **18** with  $\beta$ -amino acids to yield **18-9** or **18-10** seems to align the side chains better for binding to cancer cells compared to substitutions in peptides **18-7** and **18-8**, where more than one residue has been replaced from a single binding face. Peptides **18-7-18-10** were designed to yield a stripe of beta residues running along one side of the helix to stabilize secondary structure and increase receptor interaction. Such substitutions based on sequence based design strategy have generated different promising ligands.<sup>23,24,34</sup> The CD spectra suggest that peptides **18-9** and **18-10** are folded in solution (**Figure 3.7**), however, the exact nature of the fold will require elucidation of the three dimensional structure. Like peptide **18**, which binds MDA-MB-435 cells with an apparent dissociation constant ( $K_d$ ) of 41.9  $\mu\text{M}$ ,<sup>19</sup> analogues **18-4** and **18-9** also recognize cancer cells with low micromolar affinity (data not shown).

It has now become clear that replacement of a few isolated  $\alpha$ -residues in an  $\alpha$ -peptide confers proteolytic stability.<sup>24,28</sup> In this study, replacement of 2 (**18-4**) or 3 residues (**18-9** and **18-10**) in a 10-mer peptide with D- or  $\beta^3$ -amino acids led to complete proteolytic stability (**Figure 3.5**). It is important to note that the  $\beta$ -amino acids used in this study are derived from L-Asp (**Table 3.1**) and are different from the  $\beta^3$ -amino acids synthesized from homologation of  $\alpha$ -residues.<sup>48,49</sup> The advantage of using  $\beta^3$ -amino acids derived from L-Asp is that they are readily synthesized during peptide assembly and are cheaper than the commercially available ones.<sup>29</sup> Further, the addition of  $\beta$ -amino acid side chain on the  $\alpha$ -carboxylate of L-Asp during peptide assembly allows introduction of a variety of unnatural side chains. This provides flexibility to control physicochemical properties of peptides and modulate binding affinity and selectivity.

Peptide sequences containing the amino acid sequences RGD or NGR have been widely used for tumor targeting and have made important contributions in the field of targeted drug delivery and medical imaging. These peptides have been shown to deliver a variety of cargo to cancer sites including cytotoxic drugs, cytokines, antiangiogenic compounds, viral particles, fluorescent compounds, contrast agents, DNA complexes, and other biologic response modifiers.<sup>50,51</sup> The RGD peptides target integrins such as  $\alpha v \beta 3$  and  $\alpha v \beta 5$ , whereas NGR binds CD13 (aminopeptidase N). Both integrins and CD13 are highly expressed on tumour vasculature. Recently Sugahara *et al* showed that coadministration of a new generation RGD analogue, iRGD, improved the therapeutic index of various anti-

cancer agents such as doxorubicin, nanoparticles carrying drug, and a monoclonal antibody trastuzumab. Chemical conjugation of iRGD to these entities was not required.<sup>52</sup>

Askoxylakis et al. showed that radiolabelled p160 achieved better tumor targeting *in vivo* compared to RGD-4C. P160 and p160 derived peptides such as **18**, **18-4**, and **18-9** show high specificity for cancer cells (**Figure 3.2**), although the receptor for these peptides is not yet known. The plausibility of receptor mediated binding to the cancer cells is shown here by competition experiments (**Figure A.7**) and also by Askoxylakis *et al*.<sup>18</sup> These peptides are also internalized by the cells (**Figures 3.3 and 3.4**) and therefore can deliver drugs inside the cancer cells. Recently, we showed that p160-coated polymeric micelles display better binding and internalizing in MDA-MB-435 cells than c(RGDfK)-micelles.<sup>53</sup> In addition, p160-decorated micelles showed better results over c(RGDfK)-micelles with respect to selective cytotoxicity of encapsulated paclitaxel (PTX) against MDA-MB-435 cells over normal HUVEC and MCF-10A cells. The better interaction of PTX-nanocarriers with cancer cells over normal cells achieved through p160 targeted ligand is expected to improve the biodistribution of the drug. Better homing of the drug into malignant cells and away from normal tissues can lead to better *in vivo* therapeutic index for the encapsulated PTX. This may also lead to a better penetration of the targeted drug carrier into the tumor mass. Consequently, peptides **18-4**, **18-9**, and **18-10** identified here could serve as better cancer targeting peptides, responding to the

continuous demand for short peptide ligands for cancer specific diagnostic and therapeutic probes.

### 3.5. Concluding Remarks

Three analogues of peptide **18**: **18-4**, **18-9**, and **18-10**, with high specific binding to breast cancer cell lines were discovered in the current investigation. These analogues exhibit resistance to proteolytic degradation and impart no cytotoxicity. These peptides have a high degree of secondary structure which correlates with their binding affinity and internalization. We envision our peptide analogues as useful, proteolytically stable lead peptides that can either directly couple to an anticancer drug, decorate a drug carrier that encapsulates the drug (e.g., liposomes, micelles, and polymeric nanoparticles), or conjugate with a diagnostic moiety such as a fluorophore or nonmetallic isotope. Targeted therapy using cancer targeting peptides restricts the toxic effect of a drug to the malignant tissues, thereby increasing the efficacy and decreasing the undesired side effects of the drug. Hence, the peptides reported here would serve as favorable candidates for use in cancer drug targeting or diagnosis. The strategy used to develop these breast cancer specific peptide analogues involved two steps. First, a synthetic library based on peptide p160, identified from phage display by Zhang et al,<sup>16</sup> was screened for specific binding to breast cancer cells (done previously).<sup>19</sup> Second, analogues of peptide **18** identified from the above screening were engineered for proteolytic stability while maintaining high

specificity for breast cancer cells. The step wise procedure delineated here may be adapted for developing peptide analogues for targeting other cancer cell types.

### 3.6. References

- (1) Takimoto, C. H.; Calvo, E. Principles of Oncologic Pharmacotherapy In Cancer Management: A Multidisciplinary Approach, 11th ed.; Pazdur, R., Wagman, L. D., Camphausen, K. A., Hoskins, W. J., Eds.; CMP: Manhasset, NY, **2008**.
- (2) Abrous-Anane, S.; Savignoni, A.; Daveau, C.; Pierga, J.-Y.; Gautier, C.; Reyal, F.; Dendale, R.; Campana, F.; Kirova, Y. M.; Fourquet, A.; Bollet, M. A. Management of Inflammatory Breast Cancer After Neoadjuvant Chemotherapy *Int. J. Radiat. Oncol. Biol. Phys.* **2011**, *79*, 1055-1063.
- (3) Raschi, E.; Vasina, V.; Ursino, M. G.; Boriani, G.; Martoni, A.; De Ponti, F. Anticancer drugs and cardiotoxicity: Insights and perspectives in the era of targeted therapy *Pharmacol. Ther.* **2010**, *125*, 196-218.
- (4) Bosslet, K.; Straub, R.; Blumrich, M.; Czech, J.; Gerken, M.; Sperker, B.; Kroemer, H. K.; Gesson, J.-P.; Koch, M.; Monneret, C. Elucidation of the Mechanism Enabling Tumor Selective Prodrug Monotherapy *Cancer Res.* **1998**, *58*, 1195-1201.
- (5) Junutula, J. R.; Raab, H.; Clark, S.; Bhakta, S.; Leipold, D. D.; Weir, S.; Chen, Y.; Simpson, M.; Tsai, S. P.; Dennis, M. S.; Lu, Y.; Meng, Y. G.; Ng, C.; Yang, J.; Lee, C. C.; Duenas, E.; Gorrell, J.; Katta, V.; Kim, A.; McDorman, K.; Flagella, K.; Venook, R.; Ross, S.; Spencer, S. D.; Lee Wong, W.; Lowman, H. B.; Vandlen, R.; Sliwkowski, M. X.; Scheller, R. H.; Polakis, P.; Mallet, W. Site-specific conjugation of a cytotoxic drug to an antibody improves the therapeutic index *Nat. Biotech.* **2008**, *26*, 925-932.
- (6) Govindan, S. V.; Goldenberg, D. M. New Antibody Conjugates in Cancer Therapy *TheScientificWorldJOURNAL* **2010**, *10*, 2070-2089.
- (7) Aina, O. H.; Sroka, T. C.; Chen, M.-L.; Lam, K. S. Therapeutic cancer targeting peptides *Pept. Sci.* **2002**, *66*, 184-199.
- (8) Laakkonen, P.; Zhang, L.; Ruoslahti, E. Peptide Targeting of Tumor Lymph Vessels *Ann. N. Y. Acad. Sci.* **2008**, *1131*, 37-43.
- (9) Lyakhov, I.; Zielinski, R.; Kuban, M.; Kramer-Marek, G.; Fisher, R.; Chertov, O.; Bindu, L.; Capala, J. HER2- and EGFR-Specific Affiprobe: Novel Recombinant Optical Probes for Cell Imaging *Chembiochem* **2010**, *11*, 345-350.
- (10) Eigenbrot, C.; Ultsch, M.; Dubnovitsky, A.; Abrahmsén, L.; Härd, T. Structural basis for high-affinity HER2 receptor binding by an engineered protein *Proc. Natl. Acad. Sci. U.S.A.* **2010**, *107*, 15039-15044.

- (11) Shangguan, D.; Meng, L.; Cao, Z. C.; Xiao, Z.; Fang, X.; Li, Y.; Cardona, D.; Witek, R. P.; Liu, C.; Tan, W. Identification of Liver Cancer-Specific Aptamers Using Whole Live Cells *Anal. Chem.* **2008**, *80*, 721-728.
- (12) Aina, O. H.; Liu, R.; Sutcliffe, J. L.; Marik, J.; Pan, C.-X.; Lam, K. S. From Combinatorial Chemistry to Cancer-Targeting Peptides *Mol. Pharm.* **2007**, *4*, 631-651.
- (13) Shukla, G. S.; Krag, D. N. Selection of tumor-targeting agents on freshly excised human breast tumors using a phage display library. *Oncol. Rep.* **2005**, *13(4)* 757-764.
- (14) Shadidi, M.; Sioud, M. Selection of peptides for specific delivery of oligonucleotides into cancer cells *Methods Mol. Biol.* **2004**, *252*, 569-580.
- (15) Shukla, G. S.; Krag, D. N. Novel  $\beta$ -lactamase-random peptide fusion libraries for phage display selection of cancer cell-targeting agents suitable for enzyme prodrug therapy *J. Drug Target.* **2010**, *18*, 115-124.
- (16) Zhang, J.; Spring, H.; Schwab, M. Neuroblastoma tumor cell-binding peptides identified through random peptide phage display *Cancer Lett.* **2001**, *171*, 153-164.
- (17) Askoxylakis, V.; Mier, W.; Zitzmann, S.; Ehemann, V.; Zhang, J.; Kramer, S.; Beck, C.; Schwab, M.; Eisenhut, M.; Haberkorn, U. Characterization and Development of a Peptide (p160) with Affinity for Neuroblastoma Cells *J. Nucl. Med.* **2006**, *47*, 981-988.
- (18) Askoxylakis, V.; Zitzmann, S.; Mier, W.; Graham, K.; Krämer, S.; von Wegner, F.; Fink, R. H. A.; Schwab, M.; Eisenhut, M.; Haberkorn, U. Preclinical Evaluation of the Breast Cancer Cell-Binding Peptide, p160 *Clin. Cancer Res.* **2005**, *11*, 6705-6712.
- (19) Ahmed, S.; Mathews, A. S.; Byeon, N.; Lavasanifar, A.; Kaur, K. Peptide Arrays for Screening Cancer Specific Peptides *Anal. Chem.* **2010**, *82*, 7533-7541.
- (20) Gorris, H. H.; Bade, S.; Röckendorf, N.; Albers, E.; Schmidt, M. A.; Fránek, M.; Frey, A. Rapid Profiling of Peptide Stability in Proteolytic Environments *Anal. Chem.* **2009**, *81*, 1580-1586.
- (21) Adessi, C.; Soto, C. Converting a peptide into a drug: strategies to improve stability and bioavailability *Curr. Med. Chem.* **2002**, *9 (9)*, 963-978.
- (22) Gentilucci, L.; De Marco, R.; Cerisoli, L. Chemical Modifications Designed to Improve Peptide Stability: Incorporation of Non-Natural Amino

Acids, Pseudo-Peptide Bonds, and Cyclization *Curr. Pharm. Des.* **2010**, *16*, 3185-3203.

(23) Horne, W. S.; Price, J. L.; Keck, J. L.; Gellman, S. H. Helix Bundle Quaternary Structure from  $\alpha/\beta$ -Peptide Foldamers *J. Am. Chem. Soc.* **2007**, *129*, 4178-4180.

(24) Horne, W. S.; Johnson, L. M.; Ketas, T. J.; Klasse, P. J.; Lu, M.; Moore, J. P.; Gellman, S. H. Structural and biological mimicry of protein surface recognition by  $\alpha/\beta$ -peptide foldamers *Proc. Natl. Acad. Sci.* **2009**, *106*, 14751-14756.

(25) Ahmed, S.; Kaur, K. The Proteolytic Stability and Cytotoxicity Studies of L-Aspartic Acid and L-Diaminopropionic Acid derived  $\beta$ -Peptides and a Mixed  $\alpha/\beta$ -Peptide *Chem. Biol. Drug Des.* **2009**, *73*, 545-552.

(26) Frackenpohl, J.; Arvidsson, P. I.; Schreiber, J. V.; Seebach, D. The Outstanding Biological Stability of  $\beta$ - and  $\gamma$ -Peptides toward Proteolytic Enzymes: An In Vitro Investigation with Fifteen Peptidases *Chembiochem* **2001**, *2*, 445-455.

(27) Hook, D. F.; Bindschädler, P.; Mahajan, Y. R.; Šebesta, R.; Kast, P.; Seebach, D. The Proteolytic Stability of 'Designed'  $\beta$ -Peptides Containing  $\alpha$ -Peptide-Bond Mimics and of Mixed  $\alpha,\beta$ -Peptides: Application to the Construction of MHC-Binding Peptides *Chem. Biodiversity* **2005**, *2*, 591-632.

(28) Aguilar, M.-I.; Purcell, A. W.; Devi, R.; Lew, R.; Rossjohn, J.; Smith, A. I.; Perlmutter, P. [small beta]-Amino acid-containing hybrid peptides- new opportunities in peptidomimetics *Org. Biomol. Chem.* **2007**, *5*, 2884-2890.

(29) Ahmed, S.; Beleid, R.; Sprules, T.; Kaur, K. Solid-Phase Synthesis and CD Spectroscopic Investigations of Novel  $\beta$ -Peptides from L-Aspartic Acid and  $\beta$ -Amino-L-alanine *Org. Lett* **2006**, *9*, 25-28.

(30) Kaiser E, C. R., Bossinger CD, Cook PI. Color test for detection of free terminal amino groups in the solid-phase synthesis of peptides *Anal. Biochem.* **1970**, *34* 595-598.

(31) Svenson, J.; Vergote, V.; Karstad, R.; Burvenich, C.; Svendsen, J. S.; De Spiegeleer, B. Metabolic Fate of Lactoferricin-Based Antimicrobial Peptides: Effect of Truncation and Incorporation of Amino Acid Analogs on the In Vitro Metabolic Stability *J. Pharmacol. Exp. Ther.* **2010**, *332*, 1032-1039.

(32) Güntert, P. Automated NMR protein structure calculation with CYANA *Meth. Mol. Biol.* **2004**, *278*, 353-378.

(33) van de Loosdrecht AA, B. R., Ossenkoppele GJ, Broekhoven MG, Langenhuijsen MM. A tetrazolium-based colorimetric MTT assay to quantitate

human monocyte mediated cytotoxicity against leukemic cells from cell lines and patients with acute myeloid leukemia *J. Immunol. Methods* **1994**, *174*, 311-320

(34) Horne, W. S.; Boersma, M. D.; Windsor, M. A.; Gellman, S. H. Sequence-Based Design of  $\alpha/\beta$ -Peptide Foldamers That Mimic BH3 Domains *Angew. Chem., Int. Ed.* **2008**, *47*, 2853-2856.

(35) Schröder-Borm, H.; Bakalova, R.; Andrä, J. The NK-lysin derived peptide NK-2 preferentially kills cancer cells with increased surface levels of negatively charged phosphatidylserine *FEBS Lett.* **2005**, *579*, 6128-6134.

(36) Horne, W. S.; Gellman, S. H. Foldamers with Heterogeneous Backbones *Acc. Chem. Res.* **2008**, *41*, 1399-1408.

(37) Aravinda, S.; Datta, S.; Shamala, N.; Balaram, P. Hydrogen-Bond Lengths in Polypeptide Helices: No Evidence for Short Hydrogen Bonds *Angew. Chem.* **2004**, *116*, 6896-6899.

(38) Mahalakshmi, R.; Shanmugam, G.; Polavarapu, P. L.; Balaram, P. Circular Dichroism of Designed Peptide Helices and  $\beta$ -Hairpins: Analysis of Trp- and Tyr-Rich Peptides *Chembiochem* **2005**, *6*, 2152-2158.

(39) Aravinda, S.; Shamala, N.; Desiraju, S.; Balaram, P. A right handed peptide helix containing a central double D-amino acid segment. *Chem. Commun.* **2002**, *20*, 2454-2455.

(40) Karle, I. L.; Gopi, H. N.; Balaram, P. Crystal structure of a hydrophobic 19-residue peptide helix containing three centrally located d amino acids *Proc. Natl. Acad. Sci. U. S. A.* **2003**, *100*, 13946-13951.

(41) Sadowsky, J. D.; Fairlie, W. D.; Hadley, E. B.; Lee, H.-S.; Umezawa, N.; Nikolovska-Coleska, Z.; Wang, S.; Huang, D. C. S.; Tomita, Y.; Gellman, S. H. ( $\alpha/\beta+\alpha$ )-Peptide Antagonists of BH3 Domain/Bcl-xL Recognition: Toward General Strategies for Foldamer-Based Inhibition of Protein-Protein Interactions *J. Am. Chem. Soc.* **2006**, *129*, 139-154.

(42) Serova, M.; Galmarini, C. M.; Ghoul, A.; Benhadji, K.; Green, S. R.; Chiao, J.; Faivre, S.; Cvitkovic, E.; Le Tourneau, C.; Calvo, F.; Raymond, E. Antiproliferative effects of sapacitabine (CYC682), a novel 2[prime]-deoxycytidine-derivative, in human cancer cells *Br. J. Cancer* **2007**, *97*, 628-636.

(43) Teixeira, R.; Barbosa, L.; Maltha, C.; Rocha, M.; Bezerra, D.; Costa-Lotuf, L.; Pessoa, C.; Moraes, M. Synthesis and Cytotoxic Activity of Some 3-Benzyl-5-Arylidenefuran-2(5H)-ones *Molecules* **2007**, *12*, 1101-1116.

(44) Govindan, R. Cetuximab in Advanced Non-Small Cell Lung Cancer *Clin. Cancer Res.* **2004**, *10*, 4241s-4244s.

- (45) Sandler, A. B.; Johnson, D. H.; Herbst, R. S. Anti-Vascular Endothelial Growth Factor Monoclonals in Non-Small Cell Lung Cancer *Clin. Cancer Res.* **2004**, *10*, 4258s-4262s.
- (46) Albanell J, A. J., Baselga J, Codony-Servat J, Molina MA, Rojo F Trastuzumab (Herceptin), a humanized anti-HER2 receptor monoclonal antibody, inhibits basal and activated HER2 ectodomain cleavage in breast cancer cells *Cancer Res.* **2001**, *61*, 4744-4749.
- (47) Shadidi, M.; Sioud, M. Selective targeting of cancer cells using synthetic peptides *Drug Resist. Updates* **2003**, *6*, 363-371.
- (48) Cheng, R. P.; Gellman, S. H.; DeGrado, W. F.  $\beta$ -Peptides: From Structure to Function *Chem. Rev.* **2001**, *101*, 3219-3232.
- (49) Seebach, D.; Gardiner, J.  $\beta$ -Peptidic Peptidomimetics *Acc.Chem. Res.* **2008**, *41*, 1366-1375.
- (50) Auzzas, L.; Zanardi, F.; Battistini, L.; Burreddu, P.; Carta, P.; Rassa, G.; Curti, C.; Casiraghi, G. Targeting v3 Integrin: Design and Applications of Mono- and Multifunctional RGD-Based Peptides and Semipeptides *Curr. Med. Chem.* **2010**, *17*, 1255-1299.
- (51) Wickström, M.; Larsson, R.; Nygren, P.; Gullbo, J. Aminopeptidase N (CD13) as a target for cancer chemotherapy *Cancer Sci.* **2011**, *102*, 501-508.
- (52) Sugahara, K. N.; Teesalu, T.; Karmali, P. P.; Kotamraju, V. R.; Agemy, L.; Greenwald, D. R.; Ruoslahti, E. Coadministration of a Tumor-Penetrating Peptide Enhances the Efficacy of Cancer Drugs *Science* **2010**, *328*, 1031-1035.
- (53) Shahin, M.; Ahmed, S.; Kaur, K.; Lavasanifar, A. Decoration of polymeric micelles with cancer-specific peptide ligands for active targeting of paclitaxel *Biomaterials* **2011**, *32*, 5123-5133.

# **Chapter 4 : Novel Peptide-Doxorubicin Conjugates for Targeting Breast Cancer Cells Including the Multidrug Resistant Cells**

#### 4.1. Introduction

Breast cancer is the most common malignancy affecting women in North America and Europe, it is the second leading cause of death in American women behind lung cancer.<sup>1</sup> Anthracyclines (e.g., daunomycin, doxorubicin, epirubicin, idarubicin) are antineoplastic agents widely used in the treatment of various types of cancer, including breast tumors.<sup>2</sup> Doxorubicin (Dox) is one of the anthracycline-type antitumor agents that acts by inhibition of topoisomerase II and stabilization of a ternary drug-topoisomerase II (TOPO II)-DNA complex, causing DNA damage and induction of apoptosis.<sup>3</sup> Clinical application of Dox is limited by side effects such as nausea, vomiting, diarrhea, myelosuppression and a dose-limiting cardiotoxicity. In addition, the intrinsic or acquired resistance of tumor cells to doxorubicin reduces the response to the medication.<sup>4</sup> Several approaches aimed at improving the selectivity of Dox, and decreasing the chances for tumor resistance have been pursued. Among such approaches, conjugation of Dox to tumor-specific ligands that preferentially recognize cell surface receptors highly expressed in tumor tissues and minimally expressed on normal tissue has been deeply investigated over the past 20 years.<sup>5-7</sup> Conjugation of Dox with targeting ligand would offer two main functional roles. First, it directs the anticancer drug specifically to tumor cells, enhancing drug accumulation in tumor and thereby reduces adverse side effects. Second, it works as a penetration enhancer increasing the drug influx by tumor cells. Different targeting ligands have been employed as tumor targeting ligands for Dox delivery with great success *in vitro* and *in vivo* models such as peptides,<sup>8-11</sup> proteins,<sup>12</sup> and

antibodies.<sup>13</sup> Researchers have shown great interest in using peptides as drug carriers compared to other targeting ligands. The interest in peptides is derived from their flexibility in chemical modifications. Peptides are relatively easy to prepare and can tolerate harsh conditions (pH, temperature, etc.) during chemical modifications. Owing to their compact size, peptides have high tumor uptake. Added to their low toxicity and low immunogenicity, peptides are ideal candidates as receptor guided carrier in tumor targeting.<sup>14</sup>

A number of peptide doxorubicin conjugates have been reported in the literature for targeted delivery of Dox to tumors,<sup>15,16</sup> or tumor vasculature.<sup>17,18</sup> These conjugates increase the ability of the drug to recognize tumor cells as well as mediate its internalization which result in increase in drug activity and reduction in drug toxicity. Generally, *in vitro* and *in vivo* results of different peptide Dox conjugates displayed improved selectivity and decreased side effects, as well as it can circumvent multidrug resistance pathways.<sup>10,11,16,19-21,22,23</sup> For example, the cyclic pentapeptide (CNGRC) Dox conjugate was synthesized to target CD13 on the surface of the SK-UT-1 cells, the Dox-CNGRC conjugate showed similar antitumor activity to that of free Dox in human ovarian cancer xenograft model.<sup>8</sup> AN-152, a luteinizing hormone-releasing hormone (LHRH) conjugate of Dox was reported to bind specifically to LHRH receptors overexpressed on human breast cancer cells and in various human carcinoma cell lines, and expressed in low levels in healthy cells. *In vitro* results showed that AN-152 is more effective than Dox in inducing apoptosis in LHRH- positive human breast cancers. And it was also more potent against LHRH receptor

bearing cancers *in vivo* with less peripheral toxicity than Dox.<sup>24</sup> Emons *et al.* prepared a conjugate of Dox linked to [D-Lys6] LHRH and encouraging results with the conjugate in women with LHRH receptor-positive tumors were obtained, and a couple of phase II clinical studies of this conjugate (AN-152, AEZS-108 (Æterna Zentaris Inc)) were carried out, and they showed interesting results, and other phase II trials are ongoing.<sup>15,25,26</sup> In another study, matrix metalloproteinase (MMP)-activated prodrugs were synthesized by coupling MMP-cleavable peptides to Dox and they were evaluated in mouse model with HT-1080 xenografts. These studies showed that MMP selective conjugates were preferentially metabolized in HT1080 xenografts, relative to heart and plasma, leading to 10-fold increase in the tumor/heart ratio of doxorubicin. The conjugate was more effective than doxorubicin in reducing tumor growth, besides it did not show any bone marrow cytotoxicity.<sup>27</sup> Arap *et al.* reported a number of doxorubicin conjugates with a divalent RGD-4C peptide (ACDCRGDCFCG). These conjugates showed improved activity and toxicity profile over doxorubicin in a MDA-MB-435 mammary carcinoma model in which integrin  $\alpha v \beta_3$  is expressed in the tumor vessels as well as on the tumor cells themselves.<sup>28</sup>

Despite the encouraging results of using peptides to generate peptide Dox conjugates for selective tumor delivery and enhanced drug therapeutic index, still the use of alpha peptides in drug delivery is limited because of its fast proteolytic degradation which would affect its targeting ability causing the adjournment for these conjugates to reach clinics.<sup>29-31</sup> One study showed that intracellular delivery of therapeutic molecules with TATp-modified carriers was limited by cleavage

with proteolytic enzymes present in the circulation or in the cell cytoplasm which hindered by the rapid metabolic degradation of the peptide by cells or body fluids.<sup>32</sup>

Recently, we reported the synthesis of a 10-mer peptide **18-4** (WxEYAAQrFL) that preferentially bind and internalize into breast cancer cells, and minimally bind to normal mammary epithelial cells.<sup>33</sup> Peptide **18-4** was derived from peptide p160 (VPWMEYPAQRFL) that has specific binding to breast cancer cells,<sup>34</sup> it has two D-amino acid substitutions at the enzymatic labile sites which added complete proteolytic stability in human serum and liver homogenate, in addition, it is potentially safe with minimal cellular toxicity.<sup>33</sup> We hypothesize that conjugation of peptide **18-4** to Dox through a hydrolysable linker will create a breast cancer specific prodrug, which can selectively target and deliver Dox to breast cancerous cells, with reduced delivery to normal cells. In addition, conjugation can overcome the p-glycoprotein efflux, the mechanism involved in multidrug resistance (MDR). For the ease of conjugation to Dox a variant of peptide **18-4** was used in the current study, peptide **18-4** [r8k] having the 8<sup>th</sup> amino acid arginine substituted with lysine.

The main objective of the current study was to study the selective breast cancer-targeting potential of peptide **18-4** [r8k] Dox conjugates, and their ability to overcome p-glycoprotein multidrug resistance pathway in both drug-sensitive and drug-resistant cancer cells. To this end, two peptide Dox conjugates **1** and **2** with different conjugation sites and chemistries were synthesized and characterized. In conjugate **1**, Dox was conjugated to peptide **18-4** [r8k] through

ester linkage at C14-OH, and in conjugate **2** Dox was attached to peptide through amide linkage at NH<sub>2</sub> of the sugar moiety. Dox release from the conjugates was studied in human serum. Peptide Dox conjugates **1** and **2** were evaluated for intracellular delivery, subcellular distribution compared to free Dox using flow cytometry along with confocal microscopy in three cancerous cell (MCF-7, MDA-MB-435, and MDA-MB-435-MDR) and two control cell lines (HUVEC, and MCF-10A). Finally, cell cytotoxicity of the conjugates was measured using MTT assay compared to free Dox. Results showed that the two peptide Dox conjugates **1** and **2** can enter both sensitive and resistant cell lines, with minimal uptake in normal cells compared to free Dox. Cellular uptake is partially mediated by a cell specific receptor, as the amount of internalized conjugates significantly decreased in presence of excess of the free peptide. Importantly, conjugate **1** is equally cytotoxic to Dox in drug sensitive breast cancer cells, and 4 times more potent than free Dox in Dox resistant cell line. Overall, peptide 18-4 [r8k] Dox conjugate **1** showed better breast targeting efficacy than conjugate **2**, most likely due to the slow release of Dox from the stable amide linkage.

## **4.2. Materials and Methods**

### **Materials**

Doxorubicin hydrochloride (Dox.HCl) salt was purchased from Ontario Chemicals Inc. (Ontario, CA). Because of Dox toxicity, all precautions for handling Dox were taken according to the Material safety data sheet delivered by the manufacturer. Rink amide resin (0.4 mmol/g), (2-(6-chloro-1H-benzotriazole-

1-yl)-1,1,3,3-tetramethylammonium hexafluorophosphate) (HCTU), 1-hydroxybenzotriazole (HOBt), N-(9-Fluorenylmethoxycarbonyloxy) succinimide (Fmoc-OSu), and the Fmoc-amino acids were purchased from NovaBiochem (San Diego, CA). The side chains of amino acids used in peptide synthesis were protected as follows: *tert*-butyl (tBu) for tyrosine, *tert*-butoxy (OtBu) for glutamic acid, trityl (Trt) for glutamine and, *t*-butoxycarbonyl (Boc) for lysine and tryptophan. *N,N'*-diisopropylcarbodiimide (DIC), *N,N*-dimethylformamide (DMF), *N*-methyl morpholine (NMM), trifluoroacetic acid (TFA), glutaric anhydride, *N,N*-diisopropylethylamine (DIPEA), piperidine and all other reagents were purchased from Sigma-Aldrich. All commercial reagents and HPLC solvents were used with no further purification.

## Equipment

Solid phase synthesis of peptide on rink amide resin was done using automatic peptide synthesizer (Advanced ChemTech MPS 357, Louisville, KY, USA) using DIC and HOBt as coupling agents. <sup>1</sup>H NMR spectra were recorded using Bruker 600 MHz spectrometers operating at 600 MHz for <sup>1</sup>H with tetramethylsilane as an internal standard. Chemical shifts ( $\delta$ ) are reported in parts per million (ppm), and *J* values are quoted in hertz (Hz). HPLC purification and analysis were carried out on a Varian Prostar HPLC system (Walkersville, MD, USA) using Vydac C18 semi-preparative (10 x 25 cm, 5  $\mu$ m), and analytical (4.6 x 25 cm, 5  $\mu$ m) columns. Purity of the generated compounds was assessed as the percentage surface area of the peaks at 220 nm. Mass spectra were recorded on a matrix-assisted laser desorption ionization time-of-flight (MALDI-TOF) Voyager

spectrometer (Applied Biosystems). FACS experiments were performed on a Beckman Coulter QUANTA™ SC Flow Cytometer and analyzed by CellQuest software. Imaging experiments were done using confocal laser scanning microscopy a Quorum WaveFX spinning disk confocal system (Quorum Technologies Inc., Guelph, Canada). Cytotoxicity plate readings were performed using VersaMax microtiter reader (Molecular Devices, Sunnyvale, CA, U.S.).

#### 4.2.1. Peptide Synthesis

Peptide **18-4** [r8k] used in the current study has two modifications relative to previously reported peptide **18-4**,<sup>33</sup> it has 8 D-Arg substituted with D-Lys to facilitate side chain attachment to Dox, and the C-terminal is amidated to prevent side reactions during Dox coupling in solution. The Fmoc protected peptide (Fmoc-NH-W<sub>x</sub>EAAYQkFL-CONH<sub>2</sub>) with C-terminal amide was synthesized via solid phase methodology using rink amide methylbenzhydrylamine (MBHA) resin (0.4 mmol). The synthesis was carried out using an automatic peptide synthesizer, double coupling procedures were performed with DIC/HOBT activation, 3 fold excess of amino acid and 2 h coupling time.<sup>35</sup> Cleavage of the N-terminal Fmoc protected peptide from the resin and removal of all the protecting groups was performed by agitating the peptide-resin with a mixture of trifluoroacetic acid (TFA)/triisopropylsilane/water (90:5:5) for 2 h. The acid wash was concentrated and Et<sub>2</sub>O was added until a white precipitate separated. The precipitate was centrifuged from the solvent,

dissolved in ACN/water, purified by C18 semi-preparative reverse phase HPLC using a gradient of ACN-H<sub>2</sub>O (30–70% containing 0.05% TFA, 2 ml/min, 45 min run time), and lyophilized to give peptide as a white powder (193 mg, 38% based on estimated loading of peptide-resin). Theoretical calculated [M+H]<sup>+</sup> for Fmoc protected peptide was 1492.7; found MALDI-TOF-[M+H]<sup>+</sup> 1492.3. Analytical HPLC revealed a purity of 97% at 220 nm, t<sub>R</sub>=38 min.

#### **4.2.2. Synthesis of Peptide-Dox Conjugates**

Two peptide-Dox conjugates were synthesized using glutaric anhydride as a linker. In conjugate **1**, the peptide was attached to Dox through the 14-OH group, and in conjugate **2** the peptide was attached to the primary amine group of the sugar moiety of Dox.

##### **Synthesis of Peptide-Dox Conjugate 1 (ester)**

**Synthesis of N-Fmoc Doxorubicin (2).** To a solution of Dox HCl (**1**) (50 mg, 86 μmol) in DMF (1ml), Fmoc-OSu (30 mg, 90 μmol), and DIPEA (30 μl, 172 μmol) were added, and the reaction mixture was stirred at room temperature for 3 h. The solution was evaporated and resulting N-Fmoc-Dox crystals were precipitated by trituration using 0.1% TFA in water (3 X 10), and washed with cold diethyl ether to remove excess of Fmoc-OSu (3 X 15). The resulting red solid was collected and purified using HPLC (15% - 50% IPA /H<sub>2</sub>O in 35 min, then till 100 in 15 min t<sub>R</sub> =31 min) to give **2** as a red powder 39 mg, yield 60%. HPLC purity was 95 %. <sup>1</sup>H NMR (600 MHz, DMSO-d<sub>6</sub>) δ (ppm) 7.96 (m, 1H), 7.72 (m,

2H), 7.56 (m, 1H), 7.36 (m, 2H), 7.29 (m, 2H), 7.06 (m, 2H), 5.45 (m, 1H), 5.24 (m, 2H), 4.76 (m, 2H), 4.35 (m, 1H), 4.16 (m, 2H), 4.06 (s, 3H), 3.8 (m, 2H), 3.62 (m, 1H), 3.23 (d, 1H, J = 17.7 Hz), 2.35 (m, 1H), 2.16 (m, 1H), 1.8 (m, 1H), 1.31 (d, J = 6.2 Hz, 3H). MALDI-TOF, calcd [M+H]<sup>+</sup> 766.2, found [M+H]<sup>+</sup> 767.7, 790.7 (M + Na)<sup>+</sup>.

**Synthesis of N-Fmoc Doxorubicin-14-O-Hemiglutarate (3).** DIPEA (36  $\mu$ l, 200  $\mu$ mol) was added dropwise to a solution of N-Fmoc doxorubicin **2** (78 mg, 100  $\mu$ mol) and glutaric anhydride (11.4 g, 100  $\mu$ mol) in DMF (1 mL) under stirring. The mixture was stirred at room temperature overnight. Again the solvent was evaporated and precipitated by trituration using 0.1% TFA in water (3 X 10). The solvent was removed after centrifugation. The resulting residue mixture was purified using RP-HPLC (15% - 50% IPA /H<sub>2</sub>O in 35 min, then till 100 in 15 min t<sub>R</sub> = 38 min) to give **3** as a red powder 66 mg, yield 75%. HPLC purity was 95%. <sup>1</sup>H NMR (600 MHz, DMSO-d<sub>6</sub>)  $\delta$  (ppm) 7.96 (m, 1H), 7.74 (m, 2H), 7.56 (m, 2H), 7.36 (m, 2H), 7.29 (m, 2H), 7.06 (m, 2H), 5.45 (m, 1H), 5.35 (m, 2H), 5.2 (m, 2H), 4.35 (m, 1H), 4.18 (m, 2H), 4.05 (s, 3H), 3.8 (m, 2H), 3.6 (m, 1H), 3.23 (m, 1H), 2.95 (m, 1H), 2.79 (t, 2H, J = 7.0 Hz), 2.71 (t, 2H, J = 7.0 Hz), 1.98-2.2 (m, 4H), 1.23 (d, J = 6.3 Hz, 3H). MALDI-TOF, calcd [M+H]<sup>+</sup> 880.2, found 902.5 [M + Na]<sup>+</sup>.

**Peptide-Dox Conjugate 1.** A solution of N-Fmoc-Dox-14-O- hemiglutarate (**3**) (32 mg; 37  $\mu$ mol) in DMF (1ml) was added to peptide N-Fmoc-18-4 [r8k] (55

mg, 37  $\mu\text{mol}$ ). Then HCTU (41.3 mg, 100  $\mu\text{mol}$ ), 1-hydroxybenzotriazole HOBT (13.5 mg, 100  $\mu\text{mol}$ ) and DIPEA (52  $\mu\text{l}$ , 300  $\mu\text{mol}$ ) were added. The resulting solution was stirred at room temperature for 4 h. The solvent was removed, and the residual oil was treated with ethyl acetate. The resulting solid was dissolved in DMF, and 300  $\mu\text{l}$  piperidine was added to remove the Fmoc protecting group. After 5 min, the reaction mixture was placed on ice and acidified by the addition of a mixture containing 300  $\mu\text{l}$  of TFA, and 2 ml DMF. The solvent was evaporated in vacuum, and the crude solid was obtained by trituration with ethyl acetate. The solid was then dissolved in 70% ACN/water mixture containing 0.1% TFA. The resulting residue mixture was purified using RP-HPLC (15% - 50% ACN /H<sub>2</sub>O in 35 min, then till 100 in 15 min  $t_{\text{R}}=38.2$  min). The relevant fractions for each injection were combined and the resulting solution was lyophilized to give peptide-doxorubicin conjugate TFA salt as a red solid of 31 mg, 45% yield. HPLC purity 95%. MALDI-TOF,  $m/z$  calcd 1908.7, found 1908.1  $[\text{M}+\text{H}]^{+1}$ .

### **Synthesis of Peptide-Dox Conjugate 2 (amide)**

***N*-Glutryl-doxorubicin (4).** Dox HCl (23 mg, 40  $\mu\text{mol}$ ) was reacted with glutaric anhydride (4.5 mg, 40  $\mu\text{mol}$ ) in presence of 2 eq. DIPEA (13.8  $\mu\text{L}$ , 80  $\mu\text{mol}$ ) in 1 ml DMF at room temperature for 2 h. The reaction mixture was diluted by 2 ml of ACN/water mixture and was purified by RP-HPLC (15% to 35% ACN/ H<sub>2</sub>O in 35 min,  $t_{\text{R}}= 20$  min) to give **4** as a red powder 17 mg, yield 70%. HPLC, purity 97%. <sup>1</sup>H-NMR  $\delta\text{H}$ ( CD<sub>3</sub>OH): 7.88 (1H, d), 7.88 (1H, t), 7.62 (1H, t), 3.97 (3H, s), 4.91 (1H, t), 2.11 and 2.18 (1+1 H, dd), 5.53 (1H,s), 2.27 (3H, s),

2.93 (2H, s), 5.22 (1H, d), 1.42 and 1.84 (1+1 H, dd and t), 3.96 (1H), 7.6 (1H, d), 3.40 (1H), 4.75 (1H, d), 4.19(1H, q), 1.13 (3H, d), 2.31 (4H, t). MALDI-TOF: m/z calcd 657.2, found 679.2 [M+Na]<sup>+</sup>, 696.2 [M+K]<sup>+</sup>.

**Peptide-Dox Conjugate 2.** The purified N-Fmoc **18-4** [r8k] peptide (55 mg, 37  $\mu$ mol), was reacted with *N*-Glutryl-doxorubicin (**4**) (25 mg, 37  $\mu$ mol) in 1ml DMF using HCTU (15 mg, 37  $\mu$ mol), HOBT (4.9 mg, 37  $\mu$ mol) in presence of DIPEA (12.1  $\mu$ l, 70  $\mu$ mol). The reaction mixture was stirred for 4 hr. The solvent was removed, and the residual oil was treated with ethyl acetate. The resulting solid was dissolved in DMF, and 300  $\mu$ l piperidine was added to remove the Fmoc protecting group. After 5 min, the reaction mixture was placed on ice and acidified by the addition of a mixture containing 300  $\mu$ l of TFA, and 2 ml DMF. The solvent was evaporated in vacuum, and the crude solid was obtained by trituration with ethyl acetate. The produced solid was diluted by an eluent and purified on RP-HPLC (gradient, ACN /H<sub>2</sub>O in 35 min, then till 100 in 15 min, 2 mL/min, t<sub>R</sub> = 36.5 min). The relevant fractions for each injection were combined and the resulting solution was lyophilized to give doxorubicin-peptide conjugate TFA salt as a red solid of 16 mg (23% yield). HPLC purity 94%. MALDI-TOF, m/z calcd for 1908.9, found 1908.7 (M + H)<sup>+</sup>. All the tested compounds are produced as TFA salts. Previous experiments performed with DPV-maleimide conjugates, which were synthesized as TFA salts, *in vitro* and *in vivo* showed that the use of TFA for synthesis is not associated with toxicity up to 1 mM concentration.<sup>21</sup>

**Conjugates Stock Solutions.** Conjugates were dissolved in 100% DMSO to obtain a concentrated (7 mM) stock solution. Before measurements, appropriate aliquots of this solution were diluted with cell media to the desired concentration. The concentration of Dox was estimated using fluorescence spectrophotometer with excitation 470 nm and emission at 585 nm wavelength. The inherent fluorescence intensity of Dox was measured, and the calibration curve was prepared. The amount of Dox in the conjugates was estimated using a calibration curve.

#### **4.2.3. Dox Release from Conjugates**

The release of Dox from conjugates **1**, and **2** was evaluated in human serum and RPMI cell media. 200  $\mu$ l of 1 mM stock solution of peptide drug conjugates **1** and **2** was incubated in 1.8 ml of human serum in PBS (human serum conc is 25%), or in 1.8 ml serum free DMEM media at 37 °C with shaking. About 100  $\mu$ l of the reaction solution was removed at different time intervals (starting from 30 min to 48 h), diluted with 300  $\mu$ l methanol to quench the reaction, and the filtrate was analyzed by Vydac C18 analytical HPLC with detection at 220 nm. The mobile phase was ACN/water 0.05% trifluoroacetic acid with gradient from 15-35 % in 35 min, and the flow rate was set at 1.0 mL/min. The peak area was used to calculate the percentage of released Dox and remaining conjugate at a given time. The relative percentage of intact conjugates was plotted

at specific time points of incubation, and degradation products were confirmed using HPLC and MALDI-TOF analysis. The reported  $t_{1/2}$  is the time required for serum to hydrolyze 50% of the initial substrate.

#### **4.2.4. *In vitro* Cell Binding and Uptake Studies**

##### **Cell Lines**

All cancer cell lines, and human mammary epithelial cell line MCF-10A were purchased from the American type culture collection (ATCC), and additives were from Invitrogen, and they were all maintained at 37 °C in a 5% CO<sub>2</sub> incubator. The cells media and the growth conditions are mentioned in Chapter 3.

Innate fluorescence of Dox allowed the use of flow cytometry and confocal microscopy to study cell binding and internalization of free Dox or its peptide conjugates **1**, and **2**. A flow cytometry method for measuring uptake of free doxorubicin, or conjugates **1** and **2** in different cancer and non-cancerous cells was carried out as previously described.<sup>33</sup> MCF-7, MDA-MB-435, MDA-MB-435-MDR, HUVEC and MCF-10A were grown in 75 cm<sup>2</sup> culture flasks with full medium to ~80% confluence, then they were dissociated with trypsin-EDTA, counted and resuspended in medium at  $1 \times 10^3$  cells/mL. Cells were plated into 24-well plates ( $10^6$  cells per well) and allowed to adhere overnight. Before treatment with drug, cell medium was removed, and cells were washed with PBS (0.5 ml). Cells were then treated with either free or Dox conjugates (5 μM) for 2 h in serum free media to ensure that the conjugates will not hydrolyze to free Dox.

Following that, the cell medium was removed, washed with PBS and trypsinized, and trypsinization was quenched with 5 mL of cell medium at 4 °C. Cells were pelleted by centrifugation at 500 g for 5 minutes at 25 °C. The supernatant was decanted, and the cells were resuspended in 750 µl of FACS solution (2% FBS in PBS). Drug treatments were done in such a manner that all cell treatment times would end at approximately the same time to ensure comparable measurements with the FACScan instrument. FACS experiments were performed on a Beckman Coulter QUANTA™ SC Flow Cytometer and data obtained were analyzed using the CellQuest software. Cells were analyzed with excitation at 470 nm, with emission monitored at 590 nm. Instrument settings were optimized for the cell line, and held constant for all experiments; 10,000 cells were analyzed for each sample. Fluorescence histogram was generated using Cell Quest software. Each experiment was performed three times, and the results are expressed as the mean change in fluorescence intensity ± standard deviation. In order to evaluate that the uptake of Dox conjugates **1** and **2** was merely due to the peptide, a competition experiment was performed. We preincubated  $1 \times 10^5$  either MCF-7 cells or MDA-MB-435-MDR with 200 µM free peptide **18-4** [r8k] for 10 min, and then the conjugates were added as previously mentioned and incubated for 2 h. At the end of this incubation, the cells were finally washed and cellular uptake was measured as previously mentioned

#### 4.2.5. Confocal Fluorescence Microscopy

Dox and Dox conjugates **1**, **2** binding to MDA-MB-435 (positive), MDA-MB-435-R (Dox resistant) and MCF-10A (negative) cells, as well as internalization and cellular distribution assays were performed using confocal fluorescence microscope. Cells were seeded on glass coverslips in 24-well plates ( $5 \times 10^4$  cells per well). After 2 h, the cells were washed with serum-free medium treated with 5  $\mu$ M free Dox or peptide Dox conjugates **1** and **2** (prepared in serum-free medium prior to use) and incubated at 37 °C for 2 h equivalent to the incubation time of cellular uptake. At the end of the treatment, the cells were examined under laser confocal fluorescence microscope with a 40 $\times$  oil immersion objective. To detect nuclei, the cells were stained with 1  $\mu$ g/mL of 40, 6-diamidino-2-phenylindole (DAPI) (Sigma-Aldrich) at room temperature for 10 min and visualized by fluorescence microscopy at  $\lambda_{\text{ex}} = 350$  nm, and  $\lambda_{\text{em}} = 460$  nm. Dox fluorescence was detected at  $\lambda_{\text{ex}} = 470$  nm and  $\lambda_{\text{em}} = 580$  nm

#### 4.2.6. *In Vitro* Cytotoxicity

The cytotoxicity of free Dox and peptide Dox conjugates **1** and **2** against different cell lines was investigated using the 3-(4,5-dimethylthiazol-2-yl)-2,5-diphenyltetrazolium bromide (MTT) assay as previously described in Chapter 3. The compounds were used in the 0.025-100  $\mu$ M concentration range, and the cells were further incubated in serum free media at 37 °C to prevent premature release of Dox from conjugates either for 2 h then washed and allowed to grow for 48 h,

or directly incubated for 48 h; each sample was tested in triplicate. Short term exposure to the conjugates (2 h) was to measure the difference in rate of uptake of the conjugates with respect to free Dox. Untreated cells were used as negative control and Dox treated cells treated as positive control. After 48 h of incubation, media was removed and cells were further incubated with 20  $\mu$ L MTT solution (5 mg/mL in cell media) and 100  $\mu$ L cell medium, the plates were further incubated for 4 h. The purple formazan pellets were then solubilized in 200  $\mu$ L DMSO. After gentle shaking for 10 min at room temperature, absorbance was measured at 570 nm using a VersaMax microtiter reader with a reference wavelength of 650 nm. The percentage cell viability was expressed as expressed as a percentage of the absorbance of untreated cells.

#### **4.2.7. Effect of p-glycoprotein Inhibitor Verapamil on Cytotoxicity**

For the *in vitro* studies with Verapamil (Vp), cells were preincubated with verapamil Vp (10  $\mu$ M) for 30 min before adding different concentrations (0.025-100  $\mu$ M) of either free Dox or conjugates **1** and **2**. The viability MTT assay was performed in triplicate. The mean and the standard deviation of cell viability for each treatment was determined, converted to the percentage of viable cells relative to the control and plotted versus log drug concentration, and fitted to a sigmoidal curve. The IC<sub>50</sub> were estimated from sigmoidal regressions with Graph Pad Prism 3.02 software.

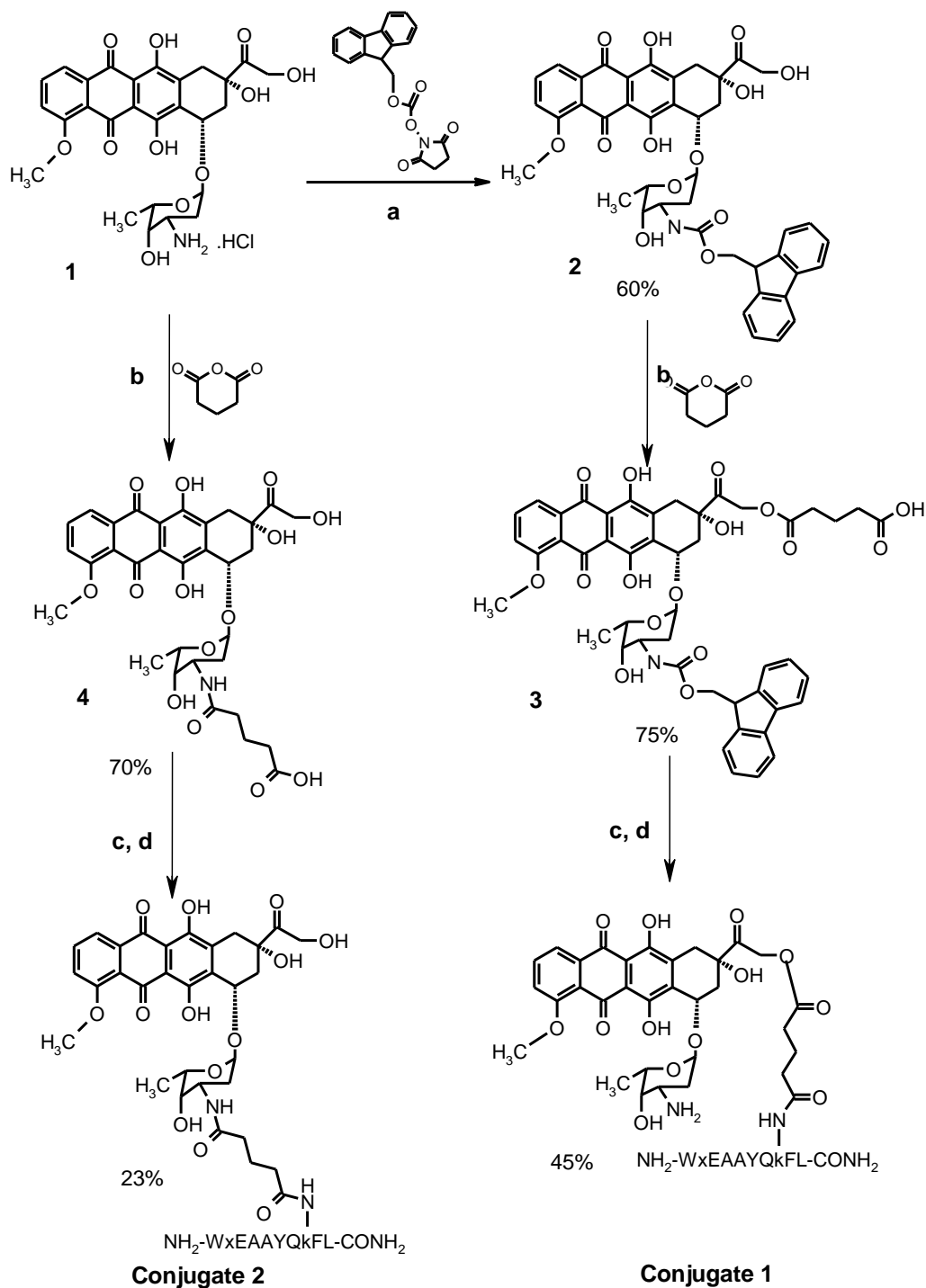
## 4.3. Results

### 4.3.1. Design and Synthesis of Peptide-Dox Conjugates.

Two peptide **18-4** [r8k] doxorubicin conjugates **1** and **2** were synthesized with different conjugation chemistries. Peptide **18-4** has 8 D-Arg substituted with D-Lys to facilitate side chain attachment to Dox, the peptide preserved the binding affinity to breast cancer cells as confirmed using flow cytometry cell uptake study. (data not shown) In conjugate **1**, the peptide was conjugated to Dox via an ester bond at position C14 following the procedure described previously <sup>6</sup> (**Scheme 4.1**). Fmoc protected Dox (N-Fmoc-Dox) was prepared by linking Fmoc-OSu with Dox at the amino group. N-Fmoc-doxorubicin was reacted with glutaric anhydride in the presence of DIPEA to yield the intermediate N-Fmoc doxorubicin-14-hemiglutarate. The N-Fmoc-Dox-14-O-hemiglutarate was then conjugated with Fmoc-NH-Wx<sub>x</sub>EYAAQkFL-CONH<sub>2</sub> through D-Lys, and the Fmoc groups were removed with piperidine.

On the other hand, in conjugate **2** the peptide was conjugated to Dox through an amide bond at the amine group of the sugar moiety via glutarate spacer. It was prepared as shown in **scheme 4.1**.<sup>36</sup> The amino group in the sugar moiety of Dox was reacted directly with glutaric anhydride in the presence of diisopropylethylamine (DIPEA) to give Dox-hemiglutarate, then it was further reacted with peptide lysine side chain in DMF in the presence of HCTU/HOBt and the Fmoc amine protecting group was removed with piperidine. The intermediates were identified using RP-HPLC, MALDI-TOF, (**Figure A.8., and**

**A.9)** and 1D-NMR. The Dox-peptide conjugates identity was confirmed using RP-HPLC and MALDI-TOF:  $[M+H]^+$  1908.1 and 1908.7 for conjugates **1** and **2**, respectively (**Table 4.1, Figure A.8**). The purity of the final products was confirmed using analytical HPLC and the percentage of the peak surface area was used to assess the purity (94-95%). Conjugate **1** was obtained in a higher yield and it was easier in purification than conjugate **2**, which had a complex mixture of byproducts, the masses of byproducts showed masses equivalent to Dox conjugated to 2, and 3 peptides molecules. The yields from Dox.HCl starting compound to the final product were 45% and 23% for conjugates **1** and **2** respectively.



**Scheme 4.1:** Synthesis of peptide-Dox conjugates 1 and 2. Reagents: (a) N-(9-fluorenylmethoxycarbonyloxy) succinimide (Fmoc-OSu), N,N-diisopropylethylamine (DIPEA) in N,N-dimethylformamide (DMF). (b) glutaric anhydride, DMF, DIPEA. (c) Fmoc-NH-WxEYAAQkFL-CONH<sub>2</sub>, DMF, NMM, (2-(6-chloro-1H-benzotriazole-1-yl)-1,1,3,3-tetramethylaminium hexafluorophosphate) (HCTU). (d) 20 % piperidine/DMF.

**Table 4.1.** Characterization of peptide doxorubicin conjugates 1 and 2.

Peptide-Dox conjugate	Mass <sup>a</sup> [M+H] <sup>+</sup> Obs. (Calcd.)	Retention time (min) <sup>b</sup>	Purity (%) <sup>c</sup>	Yield (%)	t <sub>1/2</sub> <sup>d</sup>
Conjugate 1	1908.1 (1908.7)	38.2	95	45	2 h
Conjugate 2	1908.7 (1908.9)	36.5	94	23	48 h

<sup>a</sup>MALDI-TOF of the conjugates. <sup>b</sup>Gradient system 15-35% acetonitrile/water each 0.05% trifluoroacetic acid in 35 min, then up to 100% acetonitrile in 15 min. <sup>c</sup>Purity of peptide was estimated as the area under the curve of analytical HPLC chromatogram. <sup>d</sup>Time required for the peptide to reach 50% of its initial concentration in human serum.

#### 4.3.2. Serum Stability and Release of Dox from Conjugates

The proteolytic stability of the conjugates in human serum was evaluated. Peptide-Dox conjugates **1**, and **2**, with a final concentration of 100  $\mu$ M were incubated with human serum at 37 °C. Aliquots were removed at different time points (0.5, 1, 2, 3, 4, 8, 12, 24, 48 h) for analysis using RP-HPLC. Degradation products were separated and identified using MALDI-TOF. **Figure 4.1** displays the typical time-profile of Dox release from conjugates in the presence of human serum. As expected, conjugate **2** (amide) was more stable to proteolytic degradation in human serum compared to conjugate **1** (ester). Conjugate **1** degraded with estimated half-life of 2 h, and for conjugate **2** the half-life was 48 h (**Table 4.1**). The serum degraded products identified in HPLC were doxorubicin and peptide **18-4** [r8k] hemiglutarate with no degradation of the proteolytically stable peptide.<sup>33</sup> These data reveal that both conjugates **1** and **2** are stable enough to allow sufficient time for cancer cell targeting.

In addition, the stability of conjugates **1** and **2** was evaluated in DMEM serum free media that have been used in cell uptake and cytotoxicity studies. This was done to ensure that the cell uptake was due to intact conjugate rather than any of its degradation products (e.g. free Dox). Results revealed that in conjugate **1** only a traceable amount of Dox (3%) was released from the conjugates after 24 h incubation, and conjugate **2** was completely stable (data is not shown).

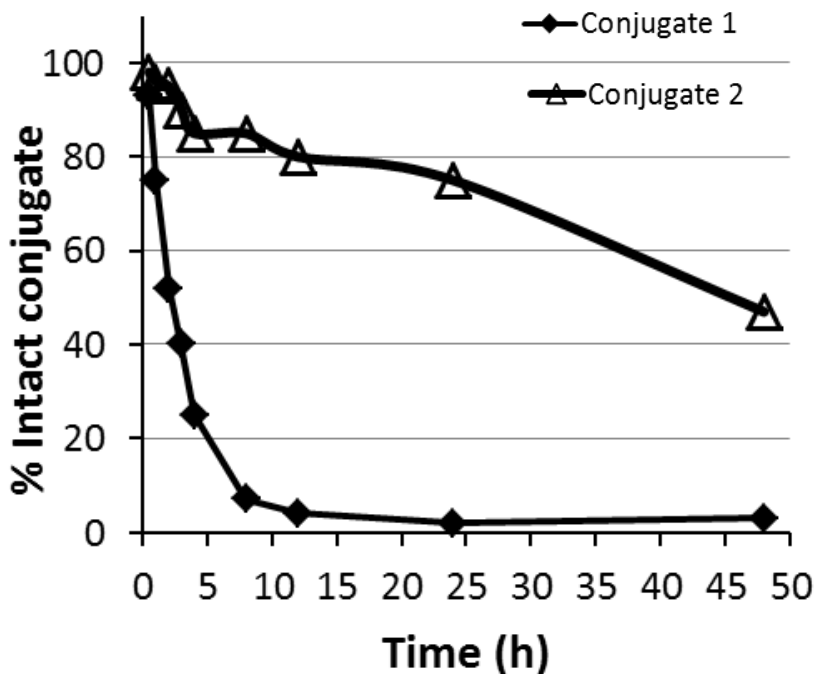


**Figure 4.1.** Time-dependent stability of peptide Dox conjugates 1, and 2 in human serum for 48 h. Dox release from the conjugates was determined by C<sub>18</sub> reverse-phase HPLC. The percent of intact conjugate remaining was determined by integrating the area under the curve detected at wavelength of 480 nm.

### 4.3.3. *In vitro* cell uptake studies

To test whether the conjugates can be selectively delivered to breast cancer cells and preserve normal ones, the cellular Dox level in different cells treated with the conjugates were compared with cells treated with free Dox. The binding and internalization studies were done using fluorescence based techniques based on Dox inherent fluorescence at ( $\lambda_{\text{ex/em}}$  470/580 nm). For flow cytometry experiments, the free Dox or peptide-Dox conjugates **1** and **2** (5  $\mu\text{M}$ ) were incubated with the cells ( $1 \times 10^5$ ) for 2 h at 37 °C in serum free media to keep conjugates intact. Then the inherent fluorescence of the Dox in the free form and the two conjugates were compared and measured based on changes in the mean fluorescence intensity of Dox labeled cells compared to untreated cells (**Figure 4.2**). FACS measurements were carried out after 2 h incubation since the cell viability at this time point was greater than 98%. At later times, the viability of the cells started to go down to determine cellular drug accumulation. The experiment was carried out in three breast cancer cell lines, MCF-7, MDA-MB-435, and MDA-MB-435-MDR, and two noncancerous cell lines, MCF-10A and HUVEC.

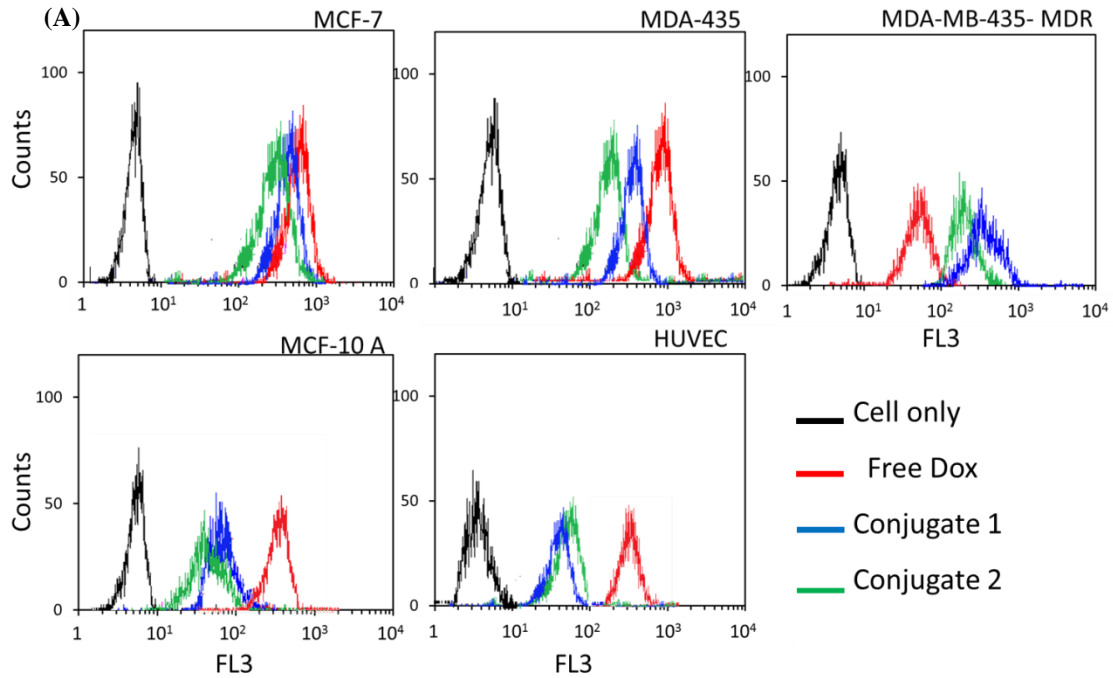
**Uptake using Flow Cytometry** Flow cytometry results showed that the two conjugates **1** and **2** displayed significant cellular uptake in breast cancer cells MCF-7 and MDA-MB-435 after 2 h incubation, as evidenced by the increase in mean fluorescence intensity of treated cells relative to the untreated cells. Interestingly, the level of conjugates **1** and **2** uptake in MCF-7 was higher than in MDA-MB-435, which is consistent with previous studies that proved that our

peptide **18-4** has higher cellular uptake in MCF-7 cells.<sup>33</sup> Based on mean fluorescence intensity, conjugate **1** showed 1.2 fold increase in breast cancer cell uptake compared to conjugate **2**. (**Figure 4.2**) While free Dox showed 1.2-1.5 fold, and 2.2-2.6 fold increase in MCF-7, and MDA-MB-435 cell uptake respectively compared to both conjugates. This increase in uptake for free Dox could be due to the different mechanisms for cell internalization, Dox is known to enter cell by direct diffusion due to its small molecular weight, while the peptide Dox conjugates are believed to enter the cell through a specific receptor by endocytosis.

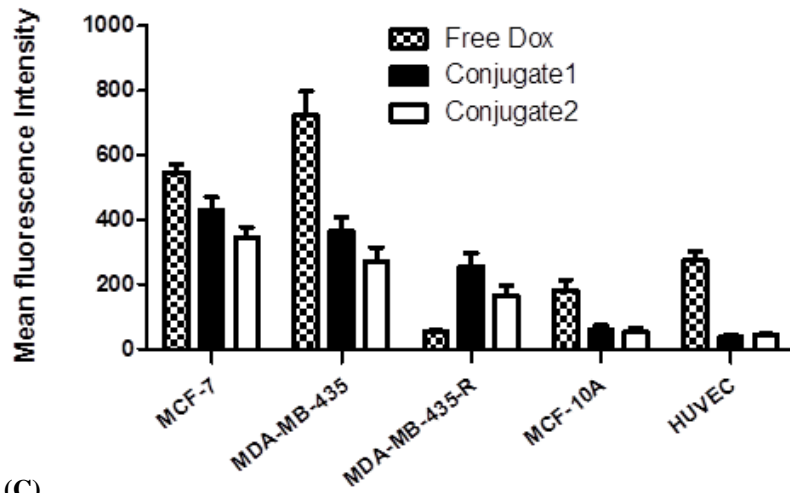
Compared to free Dox peptide-Dox conjugates **1** and **2** are expected to have higher specificity to breast cancer cells with respect to normal cells. We compared the selectivity of the two conjugates to free Dox by detecting the conjugates cell uptake in two non-cancerous cell lines MCF-10A and HUVEC, and we determined the ratio of the mean fluorescence intensity in cancer cells compared to mean fluorescence intensity in HUVEC cells (selectivity index). The two conjugates **1** and **2** displayed significant decrease in cellular uptake to control cells versus strong preferential binding to breast cancer cells after 2 h of incubation (**Figure 4.2C**). Conjugate **1** was 10.5-11 more selective for breast cancerous cells (MCF-7, MDA-MB-435) over HUVEC cells, and conjugate **2** was 6-8 times more selective to breast cancer cells compared to normal HUVEC. On the other hand, free Dox was 2.6 times more selective for breast cancer cells over HUVEC cells. These data reflects that the two peptide-Dox conjugates have 5-6 fold increase in breast cancer selectivity compared to free Dox.

The cell uptake of the conjugates was further assessed in a doxorubicin-resistant cell that expresses pgp (MDA-MB-435-MDR) compared to free Dox. Conjugates **1** and **2** showed 4.7 and 3 fold increase in cell uptake compared to free Dox with mean fluorescence intensity of  $256.6 \pm 2$  and  $166.6 \pm 2$ , respectively. These results showed that our peptide-Dox conjugates can escape the pgp doxorubicin-resistance pathway. In general, cell uptake results suggest that conjugate **1** has better uptake and breast cancer specificity for both doxorubicin-sensitive and resistant cells.

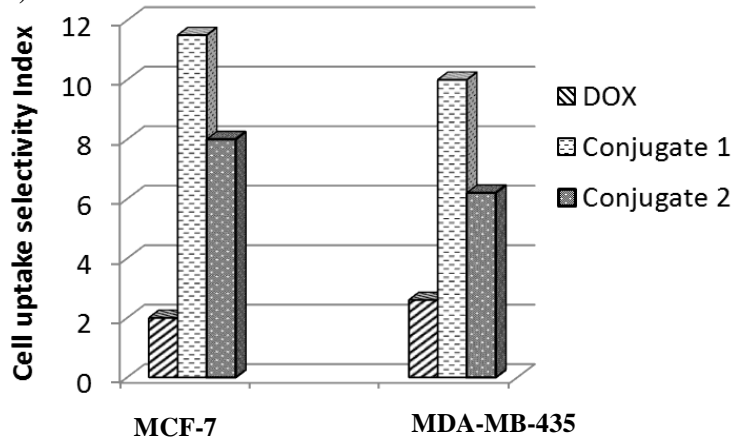
To prove that the uptake of the conjugates was merely due to the peptide and investigate the possible role of receptor mediated cell binding, a competition experiment was carried out using MCF-7 and MDA-MB-435-MDR cell lines in the presences of 40x excess of free peptide **18-4** [r8k]. The cells were preincubated with free peptide **18-4** [r8k] for 10 min, and then treated with free Dox or peptide-Dox conjugates **1** and **2** for 2 h in serum free media. No significant change in the amount of free Dox was observed in cells with or without peptide preincubation (**Figure 4.3**). However, for conjugates **1** and **2** the intracellular accumulation was significantly reduced; the mean fluorescence intensity in the presences of 40x free peptide 18-4 decreased to 50% of its value when its incubated with cells without peptide pretreatment. The conjugates uptake was not completely inhibited by the free peptide, this could be due to the incomplete blockage of the putative receptor with the concentration of the tested peptide, but these results still prove that the conjugates uptake was induced by the peptide.



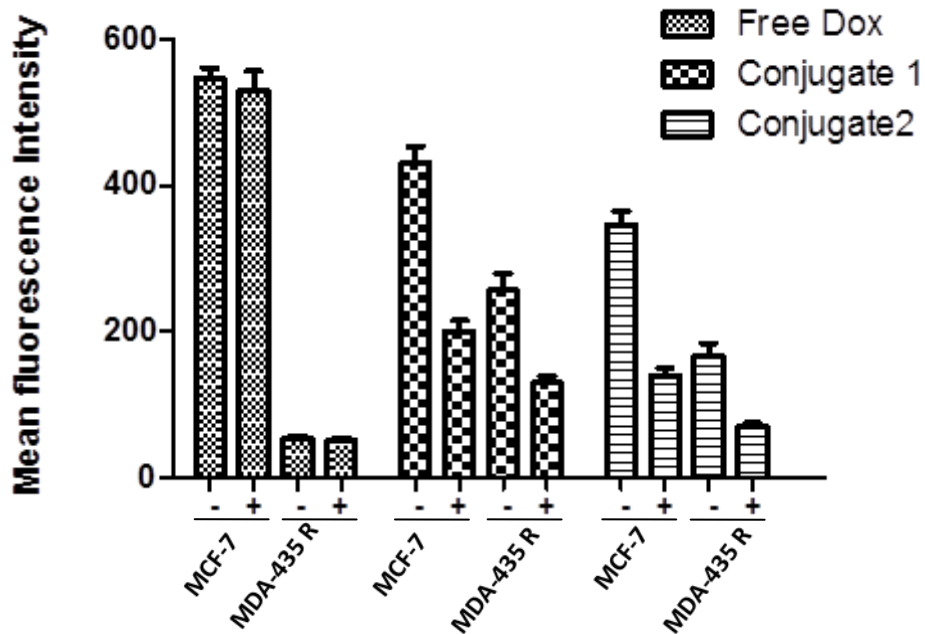
(B)



(C)

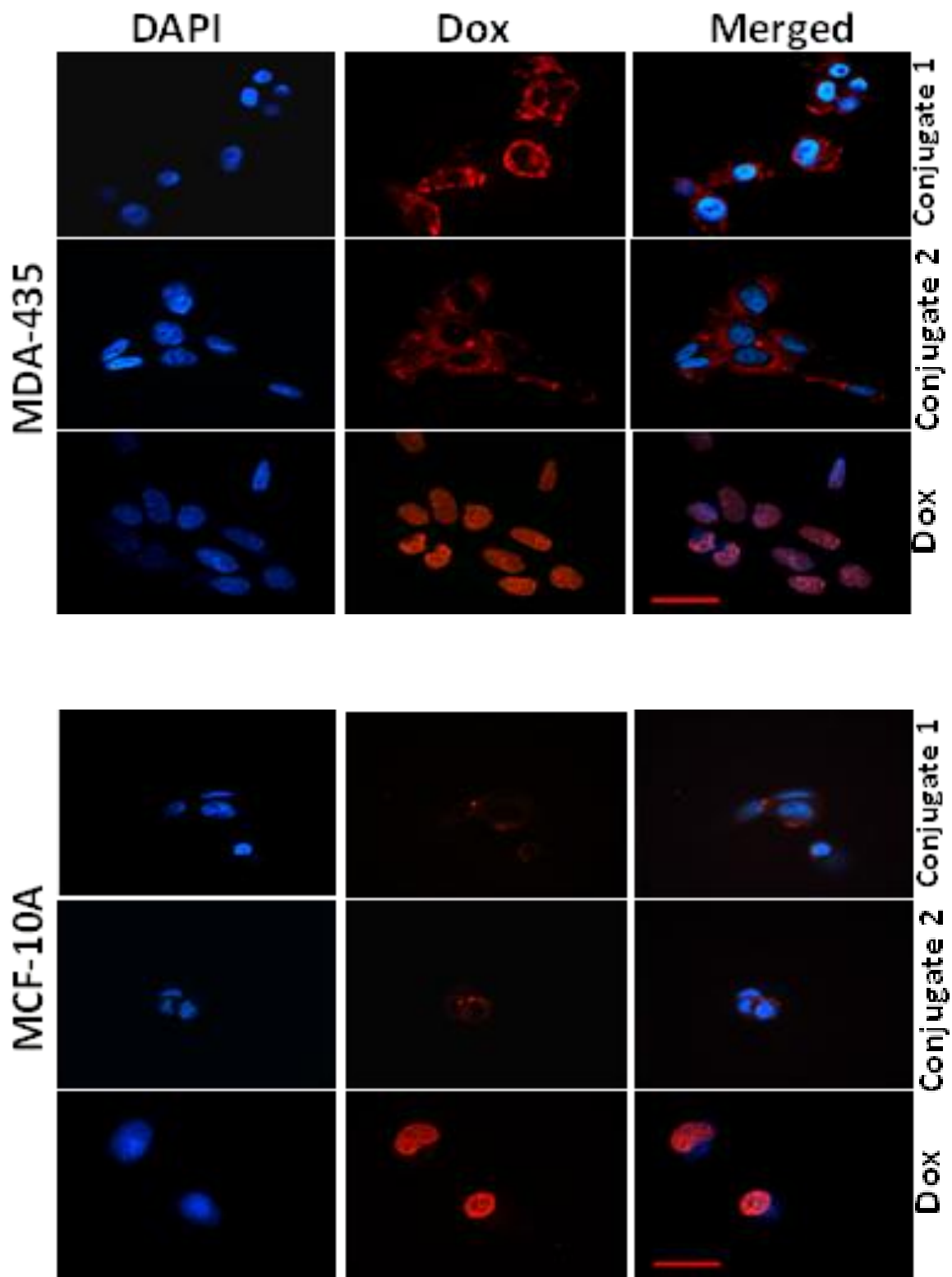


**Figure 4.2.** FACS analysis of the uptake of free Dox, peptide Dox conjugates 1 or 2 by different cell lines. Cells ( $10^6$ ) were incubated with the different treatments ( $5 \mu\text{M}$ ) at  $37^\circ\text{C}$  for 2h. (A) Histograms showing peptide uptake by the cancerous cells MCF-7, MDA-MB-435, and MDA-MB-435-MDR, (top row), and the non-cancerous cells MCF-10A and HUVEC (bottom row). Control cells or cell only (black), Dox (red), conjugate 1 (blue), conjugate 2 (green). (B) Results of cell uptake presented as change in mean fluorescence intensity relative to untreated cells. Data represent mean SD of triplicate experiments. (C) Cell uptake selectivity index is the ratio of the mean fluorescence intensity in breast cancer cells divided by the mean fluorescence in HUVEC cells.



**Figure 4.3.** *In vitro* competition experiment, for cell uptake of free Dox and peptide conjugates 1 and 2 ( $5 \mu\text{M}$ ) by MCF-7 and MDA-MB-435R cell lines with (+) or without (-) pretreatment with 40 fold excess free 18-4 peptide ( $200 \mu\text{M}$ ) after 2 h incubation. Results are presented as mean fluorescence intensity. (mean $\pm$ SD).

**Uptake using Confocal Microscopy.** Confocal cell images were used to determine intracellular conjugate localization and accumulation in cells with respect to free Dox. Three cell lines, MDA-MB-435, Dox resistant MDA-MB-435R, and non-cancerous MCF-10A cells were incubated with free Dox or drug conjugates **1** or **2** for 2 h at 37 °C and Dox distribution was examined using confocal microscopy. Images showed that both conjugates **1** and **2** have high internalization by the MDA-MB-435 and MDA\_MB-435-R cancer cells, whereas the uptake by control MCF-10A cells was minimal under the same experimental conditions. Interestingly, Dox resistant cell lines also showed higher binding and internalization of the conjugates compared to free Dox. Results clearly show that there are marked differences between the intracellular distribution of the peptide Dox conjugates and free Dox in the examined cell lines. It is important to note that peptide Dox conjugates were found diffused mainly into the cytoplasm of all cell lines, and Dox was concentrated in nucleus. **Figure 4.4** This again proves the selectivity of our conjugates for breast cancer cells and their ability for cell internalization.



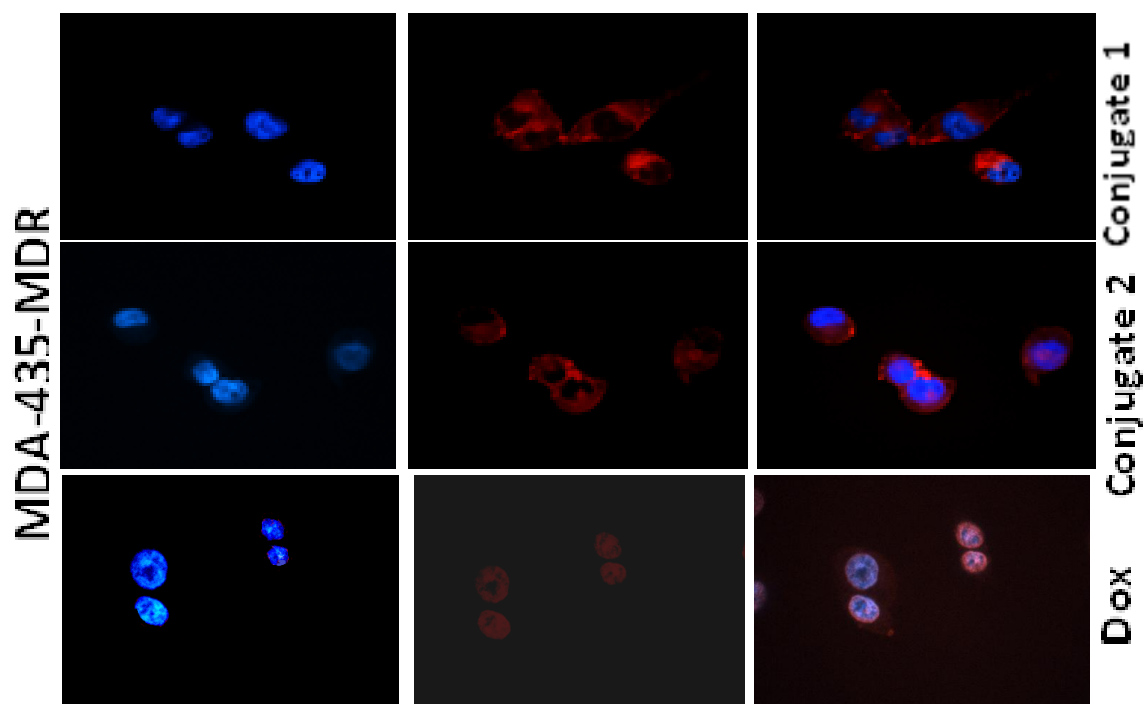


**Figure 4.4.** Intracellular distribution of free DOX and peptide Dox conjugates 1 and 2 in MDA-MB-345, MCF-10A noncancerous cell line, and MDA-MB-435-MDR cells after 2 h of drug exposure. The cells were treated with equimolar free Dox or Dox conjugates 1, and 2 (5  $\mu$ M) and visualized under confocal microscope. Merged images display the overlay of nuclear DAPI staining (blue) and Dox autofluorescence (red). Images were obtained at magnification of 400 X. scale bar, 50  $\mu$ m.

#### 4.3.4. Cell Cytotoxicity

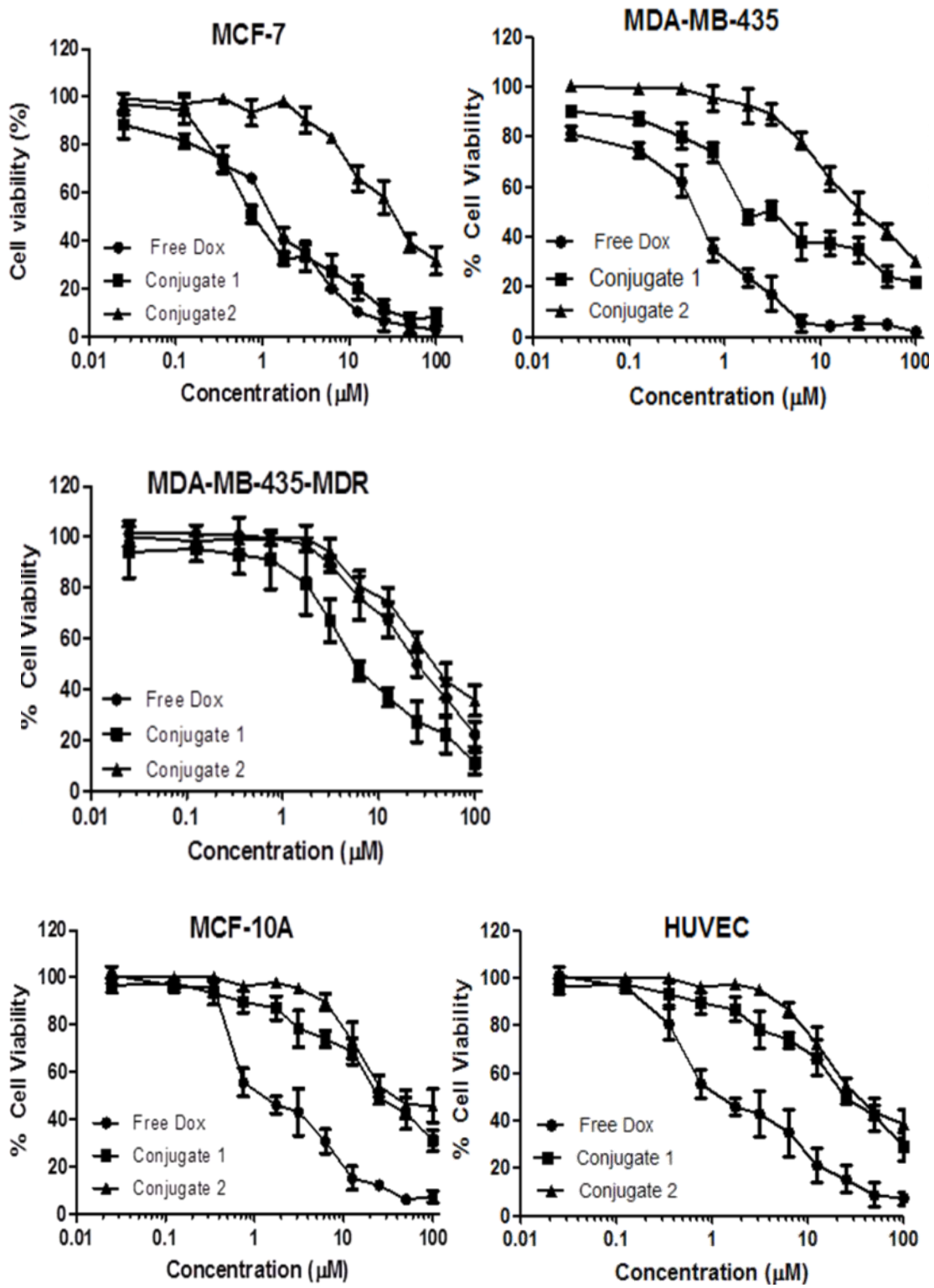
In order to compare the cytotoxic effects of Dox conjugates **1** and **2** with free Dox, a cytotoxicity assay was conducted for three cancerous cells (MCF-7, MDA-MB-435, and MDA-MB-435-MDR) and two non-cancerous cells MCF-10A, and HUVEC. The cells were incubated with a series of concentrations of free Dox or Dox conjugates **1** and **2** in the range of 0.025–100  $\mu$ M. and the cell viability was evaluated using the MTT method and characterized by the IC<sub>50</sub> values. The experiments were carried out in serum free media to prevent

premature release of Dox from the conjugates. The cytotoxicity experiment was done initially by treating the different cells with different treatments for 2 h, and then further incubation for 48 h to simulate short duration *in vivo* exposure, and to assess the degree of selectivity of our conjugates to cancerous cells versus normal cells. (**Table A.4.**) Results showed that at shorter treatment time conjugate **1** was 2 times less cytotoxic to MDA-435 and MCF-7 cells compared to free Dox, and this results correlates with the cell uptake studies which showed that the amount of cell uptake of conjugate **1** by both cells was half that of free Dox. Although conjugate **2** showed 2-2.7 fold decrease in the amount uptaken by cells, we observed that conjugate **2** is 9-15 times less cytotoxic to breast cancer cells relative to free Dox, and this could be due to the high stability of the amide conjugate, and the low level of amidases inside the cells that could release the free active Dox from its conjugate. To detect the degree of selectivity of our conjugates for breast cancerous cells versus normal cells, we found that conjugate **1** was 8 times less cytotoxic to MCF-10A than cancerous cells and it has even lower cytotoxicity to normal HUVEC cells and this proves the selectivity of conjugate **1** to breast cancer cells. For MDA-MB-435-R cells, we found that conjugate **1** was 5 times more cytotoxic than free Dox and this correlates with the cell uptake studies.

On 48 h incubation with the different treatments, we observed that conjugate **1** was equally toxic to free Dox (equal  $IC_{50}$ ) in MCF-7, and 2 fold less cytotoxic in MDA-MB-435 breast cancerous cells. On the other side, conjugate **2**

was almost 20x less cytotoxic to breast cancerous cells compared to free Dox and again this could be attributed to the stability of the amide conjugate inside the cells. Furthermore, the cytotoxicity ( $IC_{50}$ ) of conjugate **1** in a doxorubicin-resistant cell model MDA-MB-435-MDR is 4x more than free Dox. (**Figure 4.5 B**). In normal HUVEC and MCF-10A cells the two conjugates showed unexpected results, although both conjugates have different Dox release profiles they showed equal  $IC_{50}$ , both were 35-40 times less toxic to normal cells compared to breast cancer cells, this can be attributed to the different amount of enzymes (esterases, amidases) in normal cells compared to breast cancer cells. On the other side, free Dox was equally cytotoxic (equal  $IC_{50}$ ) for breast cancer cells, as well as, normal cells. Taken altogether, these results provide clear evidence that conjugate **1** has optimal characteristics for selective Dox targeting to breast cancer cells compared to conjugate **2**.

(A)



(B)

Treatment	IC <sub>50</sub> ± SD (μM)				
	MCF-7	MDA-MB-435	MDA-MB-435-MDR	MCF-10A	HUVEC
Free Dox	1.2±0.27	0.6±0.07	21.9±4.2	1.2±0.15	1.1±0.5
Conjugate 1	0.9±0.07	1.5±0.09	5.4±0.62	35.1±2.2	42.3±2.4
Conjugate 2	19.1±2.8	18.6±2.5	19.7±3.1	40.5±4.3	50.9±3.2

**Figure 4.5.** (A) In vitro cell cytotoxicity of Dox conjugates 1, and 2 on cancerous cell lines MCF-7, MDA-MB-435, MDA-MB-435-MDR cell lines, and in normal cell lines MCF-10A, and HUVEC. Conjugates cytotoxicity was compared to that of free Dox. Treatments were applied at various concentrations for 48 h in serum free media, and then cell viability was determined using MTT assay. Assay was repeated three times and each conc was in triplicate. Mean±SD, is presented. (B) Cytotoxicity of conjugates 1 and 2 versus free Dox on different cancer cell lines. Mean IC<sub>50</sub> values from three experiments in comparison with doxorubicin.

#### 4.3.5. Effect of Verapamil on Cytotoxicity

To verify that conjugate **1** and **2** are able to circumvent the action of Pgp drug pumps, experiments were performed with an inhibitor of Pgp function, verapamil (Vp). Verapamil is known to block the export of molecules from the cell by the Pgp.<sup>37</sup> Therefore; we determined the effect of verapamil on the accumulation and cytotoxicity of the free and conjugated doxorubicin in MDA-MB-435 and MDA-MB-435-MDR cells. Vp 10 μM was added to cultured cells prior to the cytotoxic compound and was able to increase the sensitivity of the

resistant cells to doxorubicin 14-fold, Verapamil lowered the IC<sub>50</sub> values of doxorubicin in MDA-MB-435-MDR from 21.9 to 1.5 μM (Table 4.2). In case of Vp followed by conjugate 1 treatment, only a moderate increase in sensitivity was observed (1.7-fold), and the same was observed in conjugate 2. The difference between doxorubicin and conjugate 1 cytotoxicity following Vp treatment suggests that conjugate 1 is a poor substrate for Pgp mediated cell extrusion, which could result in an increase in the intracellular concentration of the therapeutic molecule.

**Table 4.2.** Effect of Verapamil on IC<sub>50</sub> values of peptide Dox conjugates and Dox in MDA-MB-435 resistant cell line and MDA-MB-435 wild type.

Treatment	IC <sub>50</sub> ± SD, μM	
	MDA-MB-435	MDA-MB-435-MDR
Dox	0.65 ± 0.07	21.9 ± 4.0
Dox and Vp	0.15 ± 0.03	1.56 ± 0.09
Conjugate 1	1.50 ± 0.09	5.40 ± 0.62
Conjugate 1 and Vp	0.83 ± 0.05	3.10 ± 0.06
Conjugate 2	18.6 ± 2.50	19.7 ± 1.1
Conjugate 2 and Vp	15.5 ± 1.70	14.4 ± 3.2

#### 4.4. Discussion

In order to increase the therapeutic efficacy of doxorubicin (DOX) while decreasing its systemic toxicity various strategies have been exploited for its

tumor-targeted delivery. Targeting Dox selectively to tumor can be direct or indirect. Indirect conjugation, such as entrapping it in submicron carriers like liposomes,<sup>38</sup> polymeric micelles,<sup>39</sup> and nanoparticles<sup>40,41</sup> or coupled it to lactosaminated human albumin.<sup>42,43</sup> and there are clinically approved liposomal preparation of Dox such as Doxil®, and Caelyx® which showed reduced cardiotoxicity. On the other hand, direct conjugation of Dox could be done by conjugating Dox to targeting ligand such as monoclonal antibodies (mAbs),<sup>44</sup> or peptide ligands that would target specific tumor overexpressed cell surface markers. Peptides as targeting ligands can overcome the shortcomings of antibodies. Peptides have excellent cell permeability, small molecular weight, they are easily synthesized, they have flexibility in chemical conjugation, and they are more stable at room temperature with increased shelf life. Furthermore, one antibody molecule can only be conjugated with 1-3 drug molecules, which leads to a low drug loading (<1%). As a result, only highly potent drugs ( $IC_{50} = 10^{-9}$ - $10^{-11}$  M) can be used for this antibody drug approach.<sup>45</sup> But the size of the peptide-drug conjugate is small enough to efficiently penetrate tissues, and drug loading can be as high as 20-30%.

Application of peptide ligands in tumor targeting is hindered by their fast proteolytic degradation. In the current study, a 10-mer peptide (**18-4** [r8k] or WxEYAAkFL) with high selectivity for breast cancer cells over normal cells and improved stability in biological fluids was conjugated to Dox to enhance its breast cancer targeting specificity. Previous studies have shown that peptide chemical linkages of different types and stability (enzymatic labile, acid labile) may

critically influence Dox activity. For example, conjugation of Dox to LHRH at position 14-OH through an ester linkage fully preserved the binding affinity of the peptide carrier and the cytotoxic activity of Dox.<sup>46</sup> In another study Dox has been conjugated to Vectocell peptides through ester and amide chemical linkers at positions C-14-OH and amino group of Dox sugar, respectively. Results showed that conjugation via chemically stable bonds (amide) of Dox resulted in significant decrease in activity, while conjugation via an ester bond at C14-OH position increased the antitumor efficacy compared to free Dox.<sup>16</sup> Other contradictory results for amide conjugates were reported, which showed that peptide Dox amide conjugates at the amino group of the sugar moiety preserved the Dox activity.<sup>36,47</sup> Therefore, in the current study we used the two previously mentioned enzymatically cleavable chemistries for conjugation of Dox to peptide **18-4** [r8k] to study the effect of peptide conjugation chemistry on the cytotoxicity, cellular uptake of Dox, and their ability to overcome multidrug resistance. Two peptide-Dox conjugates were synthesized, an ester conjugate (esterase sensitive) and an amide conjugate (amidase sensitive).

Although peptide **18-4** cell entry mechanism is not fully elucidated, previous results showed that it interacts with a specific receptor and it can enter cell through endocytosis.<sup>33</sup> Therefore, to efficiently target breast cancer cells peptide-Dox conjugates must preserve the binding ability to its putative receptor. Our *in vitro* flow cytometry cell binding and uptake results demonstrated that both conjugates **1** and **2** can effectively enter breast cancer cells (MDA-MB-435 and MCF-7) with high specificity and they had minimal uptake in normal cells (MCF-

10A, HUVEC). Peptide-Dox conjugates **1** and **2** displayed 5-6 fold improvement in breast cancer selectivity relative to free Dox. (**Figure 4.5**) This enhancement in the cell uptake selectivity is the result of specific interaction between the **18-4** [r8k] peptide with its target receptors on the breast cancer cells that are not expressed on normal cells. This was confirmed by competition studies where free peptide (40x) competed with peptide-Dox conjugates for cell interaction, (**Figure 4.3**) which points to the involvement of receptor mediated endocytosis in the uptake of peptide-Dox conjugates. This observation is also in line with what was reported for the parent peptide p160.<sup>34</sup> These data suggest that peptide **18-4** [r8k] binding and internalization into breast cancer cells was preserved in the drug conjugates as proved by the high breast cancer cellular internalization and minimal uptake by control cells.

In agreement with flow cytometry results, confocal microscopy images showed much higher fluorescence intensity in MDA-MB-435 breast cancerous cells than in normal MCF-10A after incubation with peptide-Dox conjugates **1** and **2**. While the fluorescence was equally intense in both MDA-MB-435 and MCF-10A cells when treated with free Dox. (**Figure 4.4**) Microscopy images also showed that peptide-Dox conjugates and free Dox have different localization inside the cells. Peptide conjugates was mainly detected in the nucleus, while the conjugates were clearly distributed in the cytoplasm and perinuclear zone. This could be explained by different mechanisms of Dox and conjugates uptake. Free Dox is a small molecule that could pass rapidly through the cell membrane by diffusion, whereas the peptide-Dox conjugates deliver their content by interaction

with a target receptor expressed on the cell surface and subsequently uptaken through receptor mediated endocytosis. Similar phenomena were also observed with other peptide carriers conjugated with Dox. For example, Dox conjugates with a cyclic pentapeptide (CNGRC)<sup>8</sup> and an epidermal growth factor receptor (EGFR) binding peptide (NH<sub>2</sub>- CMYIEALDKYAC-COOH) exhibited the same cytoplasmic distribution as observed in our studies.<sup>16</sup> They suggested that the small hydrophobic Dox entered the cytoplasm in a passive manner and rapidly diffused into the nucleus, whereas the Dox conjugates were only visible in cytoplasmic and perinuclear areas but not in the nucleus, indicating a distinct entry pathway of the conjugate from the free Dox.

*In vitro* cytotoxicity studies demonstrated that chemical bond and conjugation position greatly affect drug activity. The results of cytotoxicity studies for conjugate **1** were in line with that of cell uptake. **Figure 4.5** showed that conjugate **1** had very similar IC<sub>50</sub> as free Dox in breast cancerous cells MDA-MB-435 and MCF-7. Thus, exposure of cells to ester conjugate is cytotoxic in the same concentration range as the parent compound. Conjugate **2**; however, showed lower cytotoxicity (20 fold decrease in IC<sub>50</sub>) compared to free Dox. As both peptide conjugates showed efficient breast cancer cell uptake, so this difference in activity between the two conjugates can be credited to the lower rate and extent of Dox release from the amide conjugate compared to ester conjugate as evidenced by the Dox release studies. The cytotoxicity seems to be more dependent on the cleavability of the Dox rather than the degree of cell uptake. (**Figure 4.1**) Our serum stability studies showed that conjugate **1** (ester) degrades faster than

conjugate **2** (amide) with a half-life of 2 h compared to 48 h for the latter one. MALDI-analysis of the degradation products revealed that the only hydrolysis product appearing during this incubation was the free Dox, and peptide remain intact up to 48 h consistent with our previous results.<sup>33</sup> Similar decreases in potency have been observed for other amide peptide Dox conjugates.<sup>10,21,48</sup> Other reported results highlighted the significance of such conjugates in the slow release of drug on longer exposure times, where the amide conjugates of Dox showed high cytotoxicity comparable to free Dox on longer incubation times which reaches 120 h.<sup>49</sup> Along with conjugate **1** efficient toxicity to breast cancer cells, cytotoxicity results showed that it is 35-40 ( $IC_{50}$  1.2  $\mu$ M) times more selective to breast cancerous cells than free Dox ( $IC_{50}$  35-43  $\mu$ M) against the non-tumorigenic MCF-10A and HUVEC cells.

In the present study, we have also demonstrated that coupling doxorubicin with peptide **18-4** [r8k] through an ester conjugate efficiently increased its cellular uptake (evidenced by flow cytometry and fluorescence microscopy), besides it increases its cytotoxicity in doxorubicin resistant MDA-MB-435 cells. Conjugation to the peptide led to an  $IC_{50}$  that was ~ 5-fold less than free doxorubicin (21.9 versus 5.4  $\mu$ M). (**Figure 4.4, Figure 4.5**) This increase in cytotoxicity in Dox resistant cells might be explained by the different cell internalization pathway and by the fact that peptide-Dox conjugates are not recognized by the pgp. Free Dox enter cell by passive diffusion, whereas the conjugates are internalized by endocytosis in membrane limited organelles, which protect the drug from degradation in the cytoplasm of cancer cells and therefore

increase its cell inducing activity. Different studies have shown that coupling peptides to free Dox can overcome pgp resistance pathway through bypassing the pgp pump<sup>10,11,16</sup> To further prove that the conjugates can bypass the pgp pump, the effect of verapamil on the accumulation and cytotoxicity of the conjugated drug was determined in MDA-MB-435-MDR cells. Verapamil is a calcium channel blocker that has been known for a long time to inhibit anthracycline efflux by direct interference with pgp, thus increasing the intracellular accumulation of the drugs.<sup>50</sup> Co-treatment of MDA-MB-435-MDR resistant cells with free doxorubicin and verapamil caused a marked increase in intracellular drug level, leading to potent cytotoxicity against the cells. Consequently, verapamil lowered the IC<sub>50</sub> 14 fold from 21.9 to 1.56  $\mu$ M. By contrast, the co-treatment of cells with peptide Dox conjugates and verapamil caused no marked decrease in the cytotoxicity of Dox conjugate **1** and **2**.

Overall, conjugation of Dox to peptide **18-4** [r8k] through an ester linkage was superior to amide conjugate in terms of Dox cell uptake, cytotoxicity and overcome multidrug resistance pgp pathway in breast tumor cells. It enhanced the Dox selectivity for breast cancerous cells; ester conjugate was 40 times more selective to the tumorigenic cell line (MDA-MB-435) vs. the non-tumorigenic MCF-10A cells breast cancerous cells compared to free drug. For further confirmation of the targeting ability of peptide **18-4**, another study was done by our research group, where peptide **18-4** decorated liposomes showed 5 fold decrease in relative tumor volume compared to non-decorated liposomes in nude mice breast tumor model.<sup>51</sup>

#### 4.5. Concluding Remarks

In conclusion, the data indicate that peptide **18-4** [r8k] Dox conjugation through an ester linkage targets breast cancer cells more effectively than Dox alone. Breast cancer targeted delivery would increase the therapeutic index of the targeted drug. Moreover, our ester drug conjugate is capable of bypassing the multidrug resistance due to altered drug uptake and intracellular fate, consequently enhancing drug activity. The peptide **18-4** [r8k] mentioned has advantages compared to other peptide-carrier like poly(lysine), poly(arginine) or HIV-TAT derived peptides which contain a large number of positively charged amino acids and have shown to be cytotoxic,<sup>52-54</sup> and compared to other hormone peptides that was used in delivery which might cause hormonal side effects. The results presented here might be useful to construct other chemotherapeutic peptide drug conjugates to be targeted specifically to breast cancer tumor, which would serve as a valuable candidate for further preclinical and eventually clinical evaluation in humans.

#### 4.6. References

- (1) Jemal, A.; Siegel, R.; Xu, J.; Ward, E. Cancer Statistics, 2010 *CA. Cancer J. Clin.* **2010**, *60*, 277-300.
- (2) Sweatman, T. W.; Israel, M. *In Cancer Therapeutics. Experimental and Clinical Agents*; Teicher, B. A., Eds.; Humana Press: Totowa, NJ. 1997.
- (3) Momparler, R. L.; Karon, M.; Siegel, S. E.; Avila, F. Effect of Adriamycin on DNA, RNA, and Protein Synthesis in Cell-free Systems and Intact Cells *Cancer Res.* **1976**, *36*, 2891-2895.
- (4) Ozben, T. Mechanisms and strategies to overcome multiple drug resistance in cancer *FEBS Lett.* **2006**, *580*, 2903-2909.
- (5) Nagy, A.; Armatis, P.; Cai, R.-Z.; Szepeshazi, K.; Halmos, G.; Schally, A. V. Design, synthesis, and in vitro evaluation of cytotoxic analogs of bombesin-like peptides containing doxorubicin or its intensely potent derivative, 2-pyrrolinodoxorubicin *Proc. Natl. Acad. Sci.* **1997**, *94*, 652-656.
- (6) Nagy, A.; Schally, A. V.; Armatis, P.; Szepeshazi, K.; Halmos, G.; Kovacs, M.; Zarandi, M.; Groot, K.; Miyazaki, M.; Jungwirth, A.; Horvath, J. Cytotoxic analogs of luteinizing hormone-releasing hormone containing doxorubicin or 2-pyrrolinodoxorubicin, a derivative 500-1000 times more potent *Proc. Natl. Acad. Sci.* **1996**, *93*, 7269-7273.
- (7) Nagy, A.; Schally, A. V.; Halmos, G.; Armatis, P.; Cai, R.-Z.; Csernus, V.; Kovács, M.; Koppán, M.; Szepesházi, K.; Kahán, Z. Synthesis and biological evaluation of cytotoxic analogs of somatostatin containing doxorubicin or its intensely potent derivative, 2-pyrrolinodoxorubicin *Proc. Natl. Acad. Sci.* **1998**, *95*, 1794-1799.
- (8) van Hensbergen, Y.; Broxterman, H. J.; Elderkamp, Y. W.; Lankelma, J.; Beers, J. C. C.; Heijn, M.; Boven, E.; Hoekman, K.; Pinedo, H. M. A doxorubicin-CNGRC-peptide conjugate with prodrug properties *Biochem. Pharmacol.* **2002**, *63*, 897-908.
- (9) Aroui, S.; Brahim, S.; De Waard, M.; Bréard, J.; Kenani, A. Efficient induction of apoptosis by doxorubicin coupled to cell-penetrating peptides compared to unconjugated doxorubicin in the human breast cancer cell line MDA-MB 231 *Cancer Lett.* **2009**, *285*, 28-38.

- (10) Mazel, M.; Clair, P.; Rousselle, C.; Vidal, P.; Scherrmann, J.-M.; Mathieu, D.; Temsamani, J. Doxorubicin-peptide conjugates overcome multidrug resistance *Anticancer. Drugs* **2001**, *12*, 107-116.
- (11) Lee, G. Y.; Song, J.-h.; Kim, S. Y.; Park, K.; Byun, Y. Peptide-doxorubicin conjugates specifically degraded by matrix metalloproteinases expressed from tumor *Drug Develop. Res.* **2006**, *67*, 438-447.
- (12) Kratz, F.; Beyer, U.; Roth, T.; Tarasova, N.; Collery, P.; Lechenault, F.; Cazabat, A.; Schumacher, P.; Unger, C.; Falken, U. Transferrin conjugates of doxorubicin: Synthesis, characterization, cellular uptake, and in vitro efficacy *J. Pharm. Sci.* **1998**, *87*, 338-346.
- (13) Inoh, K.; Muramatsu, H.; Torii, S.; Ikematsu, S.; Oda, M.; Kumai, H.; Sakuma, S.; Inui, T.; Kimura, T.; Muramatsu, T. Doxorubicin-Conjugated Anti-Midkine Monoclonal Antibody as a Potential Anti-Tumor Drug *Jpn. J. Clin. Oncol.* **2006**, *36*, 207-211.
- (14) Aina, O. H.; Liu, R.; Sutcliffe, J. L.; Marik, J.; Pan, C.-X.; Lam, K. S. From Combinatorial Chemistry to Cancer-Targeting Peptides *Mol. Pharm.* **2007**, *4*, 631-651.
- (15) Nagy, A.; Schally, A. V. Targeting of Cytotoxic Luteinizing Hormone-Releasing Hormone Analogs to Breast, Ovarian, Endometrial, and Prostate Cancers *Biol. Reprod.* **2005**, *73*, 851-859.
- (16) Ai, S.; Duan, J.; Liu, X.; Bock, S.; Tian, Y.; Huang, Z. Biological Evaluation of a Novel Doxorubicin-Peptide Conjugate for Targeted Delivery to EGF Receptor-Overexpressing Tumor Cells *Mol. Pharm.* **2011**, *8*, 375-386.
- (17) Arap, W.; Pasqualini, R.; Ruoslahti, E. Cancer Treatment by Targeted Drug Delivery to Tumor Vasculature in a Mouse Model *Science* **1998**, *279*, 377-380.
- (18) Burkhart, D. J.; Kalet, B. T.; Coleman, M. P.; Post, G. C.; Koch, T. H. Doxorubicin-formaldehyde conjugates targeting  $\alpha\beta3$  integrin *Mol. Cancer Ther.* **2004**, *3*, 1593-1604.
- (19) de Groot, F. M. H.; Broxterman, H. J.; Adams, H. P. H. M.; van Vliet, A.; Tesser, G. I.; Elderkamp, Y. W.; Schraa, A. J.; Jan Kok, R.; Molema, G.; Pinedo, H. M.; Scheeren, H. W. Design, Synthesis, and Biological Evaluation of a Dual Tumor-specific Motive Containing Integrin-targeted Plasmin-cleavable Doxorubicin Prodrug *Mol. Cancer Ther.* **2002**, *1*, 901-911.
- (20) Liang, J. F.; Yang, V. C. Synthesis of doxorubicin-peptide conjugate with multidrug resistant tumor cell killing activity *Bioorg. Med. Chem. Lett.* **2005**, *15*, 5071-5075.

- (21) Meyer-Losic, F.; Quinonero, J.; Dubois, V.; Alluis, B.; Dechambre, M.; Michel, M.; Cailler, F.; Fernandez, A.-M.; Trouet, A.; Kearsey, J. Improved Therapeutic Efficacy of Doxorubicin through Conjugation with a Novel Peptide Drug Delivery Technology (Vectocell) *J. Med. Chem.* **2006**, *49*, 6908-6916.
- (22) Hanušová, V.; Boušová, I.; Skálová, L. Possibilities to increase the effectiveness of doxorubicin in cancer cells killing *Drug Metab. Rev.* **2011**, *43*, 540-557.
- (23) Buchholz, S.; Keller, G.; Schally, A. V.; Halmos, G.; Hohla, F.; Heinrich, E.; Koester, F.; Baker, B.; Engel, J. B. Therapy of ovarian cancers with targeted cytotoxic analogs of bombesin, somatostatin, and luteinizing hormone-releasing hormone and their combinations *Proc. Natl. Acad. Sci.* **2006**, *103*, 10403-10407.
- (24) Günthert, A. R.; Gründker, C.; Bongertz, T.; Nagy, A.; Schally, A. V.; Emons, G. Induction of apoptosis by AN-152, a cytotoxic analog of luteinizing hormone-releasing hormone (LHRH), in LHRH-R positive human breast cancer cells is independent of multidrug resistance-1 (MDR-1) system *Breast Cancer Res. Treat.* **2004**, *87*, 255-264.
- (25) Emons, G.; Kaufmann, M.; Gorchev, G.; Tsekova, V.; Gründker, C.; Günthert, A. R.; Hanker, L. C.; Velikova, M.; Sindermann, H.; Engel, J.; Schally, A. V. Dose escalation and pharmacokinetic study of AEZS-108 (AN-152), an LHRH agonist linked to doxorubicin, in women with LHRH receptor-positive tumors *Gynecol. Oncol.* **2010**, *119*, 457-461.
- (26) Emons, G.; Sindermann, H.; Engel, J.; Schally, A. V.; Gründker, C. Luteinizing Hormone-Releasing Hormone Receptor-Targeted Chemotherapy Using AN-152 *Neuroendocrinology* **2009**, *90*, 15-18.
- (27) Albright, C. F.; Graciani, N.; Han, W.; Yue, E.; Stein, R.; Lai, Z.; Diamond, M.; Dowling, R.; Grimminger, L.; Zhang, S.-Y.; Behrens, D.; Musselman, A.; Bruckner, R.; Zhang, M.; Jiang, X.; Hu, D.; Higley, A.; DiMeo, S.; Rafalski, M.; Mandlekar, S.; Car, B.; Yeleswaram, S.; Stern, A.; Copeland, R. A.; Combs, A.; Seitz, S. P.; Trainor, G. L.; Taub, R.; Huang, P.; Oliff, A. Matrix metalloproteinase-activated doxorubicin prodrugs inhibit HT1080 xenograft growth better than doxorubicin with less toxicity *Mol. Cancer Ther.* **2005**, *4*, 751-760.
- (28) Arap; W., Pasqualini; R., Ruoslahti; E. Cancer treatment by targeted drug delivery to tumor vasculature in a mouse model *Science* **1998**, *279*, 377.

- (29) Garner, P.; Sherry, B.; Moilanen, S.; Huang, Y. In vitro stability of  $\alpha$ -Helical peptide nucleic acids ( $\alpha$ PNAs) *Bioorg. Med. Chem. Lett.* **2001**, *11*, 2315-2317.
- (30) Tréhin, R.; Nielsen, H. M.; Jahnke, H.-G.; Krauss, U.; Beck-Sickinger, A. G.; Merkle, H. P. Metabolic cleavage of cell-penetrating peptides in contact with epithelial models: human calcitonin (hCT)-derived peptides, Tat(47-57) and penetratin(43-58) *Biochem. J.* **2004**, *382*, 945-956.
- (31) Foerg, C.; Weller, K.; Rechsteiner, H.; Nielsen, H.; Fernández-Carneado, J.; Brunisholz, R.; Giralt, E.; Merkle, H. Metabolic Cleavage and Translocation Efficiency of Selected Cell Penetrating Peptides: A Comparative Study with Epithelial Cell Cultures *The AAPS Journal* **2008**, *10*, 349-359.
- (32) Koren, E.; Apte, A.; Sawant, R. R.; Grunwald, J.; Torchilin, V. P. Cell-penetrating TAT peptide in drug delivery systems: Proteolytic stability requirements *Drug Deliv.* **2011**, *18*, 377-384.
- (33) Soudy, R.; Gill, A.; Sprules, T.; Lavasanifar, A.; Kaur, K. Proteolytically Stable Cancer Targeting Peptides with High Affinity for Breast Cancer Cells *J. Med. Chem.* **2011**, *54*, 7523-7534.
- (34) Askoxylakis, V.; Zitzmann, S.; Mier, W.; Graham, K.; Krämer, S.; von Wegner, F.; Fink, R. H. A.; Schwab, M.; Eisenhut, M.; Haberkorn, U. Preclinical Evaluation of the Breast Cancer Cell-Binding Peptide, p160 *Clin. Cancer Res.* **2005**, *11*, 6705-6712.
- (35) Soliman, W.; Wang, L.; Bhattacharjee, S.; Kaur, K. Structure–Activity Relationships of an Antimicrobial Peptide Plantaricin S from Two-Peptide Class IIb Bacteriocins *J. Med. Chem.* **2011**, *54*, 2399-2408.
- (36) Majumdar, S.; Kobayashi, N.; Krise, J. P.; Siahaan, T. J. Mechanism of Internalization of an ICAM-1-Derived Peptide by Human Leukemic Cell Line HL-60: Influence of Physicochemical Properties on Targeted Drug Delivery *Mol. Pharm.* **2007**, *4*, 749-758.
- (37) Wigler, P. Cellular drug efflux and reversal therapy of cancer *J. Bioenerg. Biomembr.* **1996**, *28*, 279-284.
- (38) Du, H.; Cui, C.; Wang, L.; Liu, H.; Cui, G. Novel Tetrapeptide, RGDF, Mediated Tumor Specific Liposomal Doxorubicin (DOX) Preparations *Mol. Pharm.* **2011**, *8*, 1224-1232.
- (39) Lee, G. Y.; Park, K.; Kim, S. Y.; Byun, Y. MMPs-specific PEGylated peptide–DOX conjugate micelles that can contain free doxorubicin *Eur. J. Pharm. Biopharm.* **2007**, *67*, 646-654.

- (40) Pan, L.; He, Q.; Liu, J.; Chen, Y.; Ma, M.; Zhang, L.; Shi, J. Nuclear-Targeted Drug Delivery of TAT Peptide-Conjugated Monodisperse Mesoporous Silica Nanoparticles *J. Am. Chem. Soc.* **2012**, *134*, 5722-5725.
- (41) Xiong, X.-B.; Lavasanifar, A. Traceable Multifunctional Micellar Nanocarriers for Cancer-Targeted Co-delivery of MDR-1 siRNA and Doxorubicin *ACS Nano* **2011**, *5*, 5202-5213.
- (42) Stefano, G. D.; Lanza, M.; Kratz, F.; Merina, L.; Fiume, L. A novel method for coupling doxorubicin to lactosaminated human albumin by an acid sensitive hydrazone bond: synthesis, characterization and preliminary biological properties of the conjugate *Eur. J. Pharm. Sci.* **2004**, *23*, 393-397.
- (43) Di Stefano, G.; Fiume, L.; Baglioni, M.; Bolondi, L.; Chieco, P.; Kratz, F.; Pariali, M.; Rubini, G. Efficacy of doxorubicin coupled to lactosaminated albumin on rat hepatocellular carcinomas evaluated by ultrasound imaging *Digest. Liver Dis.* **2008**, *40*, 278-284.
- (44) Hebert, C.; Norris, K.; Sauk, J. J. Targeting of Human Squamous Carcinomas by SPA470-doxorubicin Immunoconjugates *J. Drug Target.* **2003**, *11*, 101-107.
- (45) Hughes, B. Antibody–drug conjugates for cancer: poised to deliver? *Nat. Rev. Drug Discov.* **2010**, *9*, 665-667.
- (46) Halmos, G.; Nagy, A.; Lamharzi, N.; Schally, A. V. Cytotoxic analogs of luteinizing hormone-releasing hormone bind with high affinity to human breast cancers. *Cancer Lett.* **1999**, *136*, 129–136.
- (47) Liang, J. F.; Yang, V. C. Synthesis of doxorubicin–peptide conjugate with multidrug resistant tumor cell killing activity *Bioorg. Med. Chem. Lett.* **2005**, *15*, 5071-5075.
- (48) Miklán, Z.; Orbán, E.; Csík, G.; Schlosser, G.; Magyar, A.; Hudecz, F. New daunomycin–oligoarginine conjugates: Synthesis, characterization, and effect on human leukemia and human hepatoma cells *Pept. Sci.* **2009**, *92*, 489-501.
- (49) Chhikara, B. S.; Mandal, D.; Parang, K. Synthesis, Anticancer Activities, and Cellular Uptake Studies of Lipophilic Derivatives of Doxorubicin Succinate *J. Med. Chem.* **2012**, *55*, 1500-1510.
- (50) Ford, J. M.; Hait, W. N. Pharmacology of drugs that alter multidrug resistance in cancer *Pharmacol. Rev.* **1990**, *42*, 155-199.
- (51) Shahin, M.; Soudy, R.; El-Sikhry, H.; Seubert, J. M.; Kaur, K.; Lavasanifar, A. *Cancer Letters* **2012**, In press.

(52) Benjouad, A.; Mabrouk, K.; Moulard, M.; Gluckman, J.-C.; Rocht, H.; Van Rietschoten, J.; Sabatier, J.-M. Cytotoxic effect on lymphocytes of Tat from human immunodeficiency virus (HIV-1) *FEBS Lett.* **1993**, *319*, 119-124.

(53) Gurwell, J. A.; Nath, A.; Sun, Q.; Zhang, J.; Martin, K. M.; Chen, Y.; Hauser, K. F. Synergistic neurotoxicity of opioids and human immunodeficiency virus-1 Tat protein in striatal neurons in vitro *Neuroscience* **2001**, *102*, 555-563.

(54) Saar, K.; Lindgren, M.; Hansen, M.; Eiríksdóttir, E.; Jiang, Y.; Rosenthal-Aizman, K.; Sassian, M.; Langel, Ü. Cell-penetrating peptides: A comparative membrane toxicity study *Anal. Biochem.* **2005**, *345*, 55-65.

## Chapter 5 : Synthetic Peptides Derived from the Sequence of a Lasso Peptide Microcin J25 Show Antibacterial Activity

Peptide		MIC ( $\mu\text{M}$ ) against <i>S. newport</i>
 $\overbrace{\text{GGAGHVPEYFVGIGTPISFYG}}^{\text{1-8}}$	MccJ25	0.5
 $\overbrace{\text{GGACHVPEYFVGIGTPISFC}}^{\text{1-8}}$	1	25
 $\overbrace{\text{CGAGFHVPCYFVGRGTPISFYG}}^{\text{1-9}}$	6	30

Rania Soudy, Liru Wang and Kamaljit Kaur\*, Synthetic peptides derived from the sequence of a lasso peptide microcin J25 show antibacterial activity, *J. Bioorg. Medicinal Chem.*, **2012**, 20(5), 1794-1800.

## 5.1. Introduction

Microcin J25 (MccJ25) is a 21-residue ribosomally synthesized antimicrobial peptide that adopts a remarkable threaded-lasso structure.<sup>1-3</sup> MccJ25 displays bactericidal activity against a range of food-borne disease-causing Gram-negative pathogens including diarrheagenic *E. coli* strains.<sup>4</sup> The lasso-structure of the peptide consists of a lactam ring (known as lariat ring) formed between the N-terminus Gly1 and the side chain of Glu8 (**Figure 5.1**).<sup>5-7</sup> The C-terminal tail (Tyr9-Gly21) passes through the ring forming a  $\beta$ -hairpin structure made of a type I  $\beta$ -turn (Val11-Gly14) and two short double stranded antiparallel  $\beta$ -sheets, residues 6-7/19-20 and 10-11/15-16.

The active mature MccJ25 is produced and exported by four plasmid-encoded genes *mcjABCD*.<sup>8</sup> McjA encodes a linear 58-residue precursor peptide which is converted into mature peptide by two enzymes, McjB and McjC.<sup>9,10</sup> McjB, a putative peptidase, cleaves the 37-residue leader peptide from the precursor peptide, whereas, McjC is believed to catalyze the lactam bond formation. McjD helps in the transport of the active antibiotic peptide out of the producing cell.<sup>11</sup> The lasso-structure confers several properties to MccJ25, such as, resistance to proteolytic degradation,<sup>12,13</sup> stability towards chaotropes, organic solvents, and extreme temperatures.<sup>14</sup> Such properties make MccJ25 a potential candidate for a number of applications including food preservation and treatment of food-borne diseases.

Different variants of MccJ25, prepared by site directed mutagenesis, have been reported for studying structure activity relationship (SAR).<sup>15,16</sup> Pavlova *et*

*al.* performed a complete mutational scanning analysis of MccJ25 by making more than 380 MccJ25 variants with a single amino acid substitution.<sup>16</sup> Each single amino acid variant was tested for production and export from *E.coli*. In addition, the variants that were produced were analyzed for the ability to inhibit RNA polymerase (RNAP) and bacterial growth. Several residues in the lactam ring and the tail region were found to be important for the production of MccJ25 and inhibition of bacterial growth. Another study reported MccJ25 variants containing two or three amino acid substitutions where the peptides retain the lasso structure and the antimicrobial function.<sup>15</sup> These studies demonstrate that peptide lasso scaffold of MccJ25 is quite tolerant to amino acid substitutions. Additional SAR studies of MccJ25 have suggested that the lactam ring region and the tail  $\beta$ -hairpin loop play distinct roles in the peptide's antimicrobial activity.<sup>17,18</sup> In particular, using a thermolysin-digested MccJ25 cleaved between residues 10 and 11 it was demonstrated that the  $\beta$ -hairpin (residues 10-16) is crucial in the import of MccJ25 through FhuA, but not for RNAP and respiration inhibition.<sup>18</sup> The roles played by specific residues in the peptide have also been reported.<sup>19,20</sup> The C-terminal glycine was found to be important for RNAP inhibition,<sup>19</sup> while site specific mutation of His-5 demonstrated that this residue was important for recognition by the inner membrane receptor SbmA.<sup>20</sup>

Attempts have also been made to chemically synthesize MccJ25 variants, such as, macrocyclic head-to-tail 21-residue MccJ25, a 21-residue variant with side chain-to-backbone lactam ring between  $\alpha$ -amino of Gly<sup>1</sup> and  $\gamma$ -carboxyl of Glu<sup>8</sup>, and a recently reported MccJ25 model peptide (cMccJ25) where Gly<sup>1</sup> and

Glu<sup>8</sup> are replaced with nearly isosteric azidoacetic acid and propargyl glycine, respectively.<sup>5,6,21</sup> In the later variant (cMccJ25), the copper-catalyzed click reaction between the azide and the terminal alkyne permits cyclization of cMccJ25 without the influence of the maturation enzymes.<sup>21</sup> None of these synthetic peptides showed any antibacterial activity.

We hypothesized that peptides with antibacterial activity can be designed based on the MccJ25 sequence where a folded conformation is acquired by a combination of intra-peptide disulfide bond formation and electrostatic or hydrophobic interactions, instead of post-translational modification by McjB and McjC proteins. To test our hypothesis, six peptides (**1-6**) derived from the sequence of MccJ25 ranging in length 18-22 residues were designed and synthesized (**Figure 5.1**). We report herein the results of antimicrobial activity, solution conformation, stability to proteases and cytotoxicity of this series of synthetic MccJ25 derivatives.



CA). The side chains of amino acids were protected as follows: tert-butyl (tBu) for serine, threonine, tyrosine, tert-butyl ester (OtBu) or allyl ester (OAll) for glutamic acid, tert-butoxycarbonyl (Boc) for lysine, trityl (trt) for cysteine and histidine, 2-(1H-7-Azabenzotriazol-1-yl)-1,1,3,3-tetramethyluronium hexafluorophosphate methanaminium (HATU), 5, 5'-dithiobis-2-nitrobenzoic acid (Ellman's reagent), N-methyl morpholine (NMM), triisopropylsilane (TIS), diisopropylethylamine (DIPEA) and trifluoroacetic acid (TFA) were purchased from Aldrich, while piperidine was purchased from Caledon (Canada). All other reagents were purchased from Sigma-Aldrich. All commercial reagents and solvents were analytical grade and were used as received.

RP-HPLC purification and analysis were carried out on a Varian Prostar (210 USA) HPLC system using Vydac semi-preparative C18 (1 x 25 cm, 5  $\mu$ m), analytical C8 (0.46 x 25 cm, 5  $\mu$ m) and Agilent preparative C18 (21.2 x 25 cm, 7  $\mu$ m) columns. Compounds were detected by UV absorption at 220 nm. Mass spectra were recorded on a MALDI Voyager time-of-flight (TOF) spectrometer (Voyager<sup>TM</sup> Elite) or on a Waters micromass ZQ. Absorbance of the purple formazan product observed during MTT assay was measured using VERSA max microplate reader (Molecular Devices, Sunnyvale, CA, USA). All the procedures regarding the cell culture maintenance and treatment of cells were carried out in a level II biosafety cabinet.

## 5.2.2. Peptide Synthesis and Purification

### General procedure

Stepwise synthesis of peptides **1-6** was done manually on a 0.2-mmol scale of Wang resin (1.0% DVB cross-linked), following the standard Fmoc solid-phase peptide chemistry as described previously.<sup>22</sup> Attachment of the first amino acid (5 equivalent) was carried out using 2, 6 dichlorobenzoylchloride (DCB) in DMF/pyridine mixture. Successive couplings were performed by dissolving an excess (2 equiv) of Fmoc-protected amino acid and Castro reagent (BOP) in presence of (HOBt) to prevent racemization in DMF. Coupling efficiency was monitored using the ninhydrin (Kaiser) test.<sup>23</sup> The coupling step was repeated (double coupling) if Kaiser test was found positive. In addition, a test cleavage was performed after each five residues were coupled, and the desired product was confirmed by MALDI-TOF mass spectrometry. Each peptide was cleaved from the resin using a mixture of 95% TFA, 5% triisopropylsilane, 5% water, for 120 minutes at room temperature with mechanical shaking. The filtrate from the cleavage reactions was collected, combined with TFA washes (3 x 2 min, 1 mL), and concentrated in vacuum. Cold diethyl ether (~ 15 mL) was added to precipitate the crude cleaved peptide. After triturating for 2 min, the peptide was collected upon centrifugation and decantation of the ether. The peptides were then purified using RP-HPLC.

### **On resin amide cyclization (Peptides 1 and 2)**

For peptides **1** and **2**, side chain of Glu was protected as allyl ester (OAll). After complete assembly of the protected peptide on the resin, the side chain protecting group (allyl) of Glu8 (peptide **1**) or Glu18 (peptide **2**) was first removed. Deprotection of the allyl from carboxyl group was carried out with Pd(PPh<sub>3</sub>)<sub>4</sub> (0.08 equiv) and PhSiH<sub>3</sub> (8 equiv) in DCM/DMF (45 mins x 3) under nitrogen. The N-terminus Fmoc group was removed using 20% piperidine/DMF. The desired lactam linkage was then formed using HATU/DIPEA (2 equivalent) as the activating agents for 3 hours in DMF, after which complete cyclization was achieved. It was confirmed using ninhydrin test and MALDI-TOF.

### **Oxidative folding and disulfide formation**

The purified linear (analogues **3-6**) or lactam cyclized peptides (**1-2**) were dissolved in 50 mM Tris buffer (pH 8.3) to a final concentration of 0.1 mM. The peptide solution was then treated with 20% DMSO to assist in oxidation and enhance peptide solubility. The reaction mixture was left stirring overnight at room temperature in an open flask. The oxidation was monitored using Ellman test,<sup>24</sup> and MALDI-TOF mass analysis. The oxidation was complete in 48 h. A mass spectrum with M-2 indicated loss of two protons and formation of the oxidized peptide.

## Peptide Purification

Purification of the peptides was done in two stages. First, the crude linear or lactam cyclized peptides were reconstituted in 30-50% aqueous acetonitrile and purified on a semi-preparative Vydac C18 reversed-phase (RP) HPLC column (10 x 250 mm, 5  $\mu$ m, flow rate = 2 mL/min, monitored at 220 nm) using different linear gradients of acetonitrile/water or isopropyl alcohol/water (0.05% TFA, v/v) mixtures. The peptides were oxidized to form the disulfide bond, and were subjected to another RP-HPLC purification using preparative C18 HPLC column (21.2 x 250 mm, 7  $\mu$ m). This purification was essentially done to remove the salts from the reaction mixture. The collected fractions were evaporated on the rotary evaporator followed by lyophilization to obtain the pure peptide. The identity and purity of the peptides were assessed by analytical HPLC (**Figure A.10**) and MALDI-TOF mass spectrometry (**Figure A.11**). The details of the purification methods and the elution time of each peptide are listed in **Table 5.1**. In general, pure peptides were obtained with an overall yield of 7-32% and purity greater than 95%.

**Table 5.1.** The Mass and HPLC purification details for peptide derivatives 1-6

Peptide	Linear [M+H] <sup>+</sup> Obs. (Calcd.)	Oxidized [M+H] <sup>+</sup> Obs. (Calcd.)	HPLC method <sup>1</sup>	Elutio n Time (min)	Yield (%)
<b>Analogues with disulfide and amide bond formation</b>					
<b>1</b>	2036.5 (2036.7)	2033.6 (2034.5)	25-50% 45 min <sup>2</sup>	35	10
<b>2</b>	1801.7 (1801.5)	1798.6 (1799.1)	10-30% 40 min	26	7
<b>Analogues with disulfide bond and electrostatic interaction</b>					
<b>3</b>	2102.4 (2102.8)	2100.5 (2100.4)	20-50% 35 min <sup>2</sup>	18	15
<b>4</b>	2125.4 (2125.1)	2123.7 (2123.4)	10-45% 35 min	26	29
<b>Analogues with disulfide bond and hydrophobic interaction</b>					
<b>5</b>	2014.5 (2014.8)	2012.8 (2012.5)	20-50% 50 min <sup>2</sup>	28	30
<b>6</b>	2335.6 (2335.7)	2332.9 (2333.6)	17-43% 35 min	19	32

<sup>1</sup>The HPLC methods listed is for unoxidized linear peptides.

<sup>2</sup>The solvent used was acetonitrile/H<sub>2</sub>O with 0.05% TFA; for all other peptides the solvent used was isopropyl alcohol/H<sub>2</sub>O system (0.05% TFA).

### 5.2.3 Microcin J25 Expression and Purification

The expression and purification of native MccJ25 were performed as described previously with some modifications.<sup>12</sup> Briefly, the high copy number plasmid pTUC202 (a gift from Rutgers University, USA) which carries the MccJ25 biosynthetic gene cluster was transformed to competent *E. coli* MC4100 cells. The cells were grown in M9 minimal media (2 L) for 24 h at 37 °C. The culture supernatant was obtained by centrifugation at 4000 g for 15 min, and then

subjected to three successive purification steps. First, the supernatant was applied to flex column filled with XAD16 resin (Aldrich, CA). Followed by elution in two successive steps with 30:70 (v/v) and 80:20 (v/v) methanol/water mixtures. Antibacterial assay was used to follow the peptide. MccJ25 found in 80:20 (v/v) methanol/water fraction was next applied to C18 Megabond column (Varian, USA). Three successive elution steps were carried out with 40:60 (v/v), 60:40 (v/v) and 80:20 (v/v) methanol/water mixtures. The 80:20 (v/v) fraction was further purified using C18 RP-HPLC (2 mL/min flow rate and absorbance monitored at 220 nm) under linear gradient from 55-80% methanol/water (0.05% TFA) in 45 min. The concentration of the peptide was determined spectrophotometrically at 278 nm (molar absorptivity 3340 M/L),<sup>18</sup> and the yield was 2 mg.

#### **5.2.4. Antimicrobial Activity Assay**

The minimum inhibitory concentrations (MICs) of peptides **1**, **6** and MccJ25 were determined by liquid growth inhibition assays in sterile 96-well plate using LB as growth media.<sup>25</sup> Peptide stock solutions were prepared in 20% methanol/water (1 mM for MccJ55 and 2.5 mM for **1** and **6**), and were serially double diluted in sterile water to give concentrations ranging from 0.01 to 100  $\mu$ M for MccJ25, and 0.5 to 250  $\mu$ M for **1** and **6**. Similar concentration of methanol/water alone without the peptide did not change the growth of bacteria. Bacterial culture (180  $\mu$ L) diluted in LB media were added to the microplate wells

to obtain optical density (OD<sub>620</sub>) of 0.02-0.05, followed by addition of peptide solutions (20 μL). Each peptide concentration was tested in triplicate. Control wells contained the peptide in LB media as well as untreated bacterial cells. After incubation of the microplates for 24 h at 37 °C, the turbidity (OD) was read at 620 nm on a plate reader. MICs were defined from a growth curve as the lowest peptide concentrations that caused 100% growth inhibition (0.05 AU). Three representative growth curves of microcin J25, peptide **1**, and peptide **6** obtained using broth assay against *Salmonella newport* are shown in Figure S4. Standard deviations derived from MIC outcome of three graphs for three repeated experiments were calculated. Concentrations of peptides stocks solutions were determined by absorbance at 280 nm described previously.<sup>26</sup> The minimum bactericidal concentration (MBC) was determined from wells showing complete inhibition. An LB agar plate was seeded on the surface with 10 μL from each clear well and incubated (24 h, 37°C). The MBC was defined as the lowest concentration giving no growth on an LB plate afterwards.

#### **5.2.5. Circular Dichroism (CD) Spectroscopy**

The CD measurements for the peptides (MccJ25, **1** and **6**) were made on an Olis CD spectrometer (Georgia, USA) at 25 °C in a thermally controlled quartz cell over 190-260 nm. All samples were dissolved in 100% methanol with a final concentration of 200 μM. The length of the cuvette was 0.02 cm and number of scans was set to 10. Smoothing and correction of the background spectra was

performed afterwards. The CD data was normalized and expressed in terms of mean residue ellipticity ( $\text{deg cm}^2 \text{ dmol}^{-1}$ ). CD spectra were analyzed using quantitative curve fitting using the CDPro software analysis program as described previously.<sup>27</sup>

### 5.2.6. Proteolytic Stability

The proteolytic stability of peptides **1** and **6** compared to native MccJ25 was evaluated against two digestive enzymes (pepsin and chymotrypsin). The susceptibility of **1** and **6** for chymotrypsin cleavage was assessed using spot on lawn method as reported previously.<sup>13</sup> Peptide analogues **1** and **6** (10  $\mu\text{L}$  of 200  $\mu\text{M}$ ) were spotted onto LB plates and chymotrypsin solution (10  $\mu\text{L}$  of 0.5  $\text{mg/mL}$ ) was placed 1 cm away from the peptide spots. After the drops had dried, the plates were overlaid with 4 mL of soft agar inoculated with  $10^7$  cells of a clinical isolate of *Salmonella enterica* serovar Newport. After overnight incubation at 37 °C, the growth inhibition zones around the drops were recorded. MccJ25 was used as control at 5  $\mu\text{M}$  concentration.

Pepsin was dissolved in 0.1 N HCl (4% w/w) and then peptide **1** or **6** was added (150  $\mu\text{M}$ ).<sup>28</sup> The solution was incubated at 37 °C and the degradation was stopped at specific time points 0 min, 30 min, 1 hr, by taking 100  $\mu\text{L}$  aliquots into 10  $\mu\text{L}$  0.1 N NaOH containing 70% methanol to precipitate the enzyme. Sample was centrifuged at 16000 g for 10 min, and the supernatant containing the

cleavage mixture was injected in RP-HPLC. Fractions were collected for mass detection using MALDI-TOF to determine the labile sites. Also fragments were analyzed for antibacterial activity using spot on Lawn as described earlier. For sake of comparison the same experiment was repeated for native MccJ25.

### **5.2.7. Oxygen Consumption Determination**

Oxygen consumption was determined as previously described.<sup>29</sup> *Salmonella newport* strain were grown to exponential phase (OD<sub>600</sub> 0.4-0.5) in LB media. Samples were diluted in LB media to an OD<sub>600</sub> of 0.2. Cells were then incubated at 37 °C with either MccJ25 (0.25 μM), **1** (25 μM), or **6** (30 μM) for 35 min. Thereafter, the average rate of respiration for subsequent 5 min was polographically measured with a 2 mL Gilson Clarke electrode oxygraph at 37 °C. A control experiment in the absence of peptide was carried out similarly.

### **5.2.8. Cell Viability Assay**

#### **5.2.8.1. Cell lines**

Tumor cell lines used in this study included MDA-MB-435 and MCF7 breast cancer cell lines. MDA-MB-435 cells were cultured in RPMI 1640 medium (Sigma) supplemented with FBS (10%), penicillin (50 μg/mL), and streptomycin (0.05 g/mL) in a humidified atmosphere (5% CO<sub>2</sub>) at 37 °C. MCF7

cells were grown in DMEM media supplemented with same additives as stated above.

#### **5.2.8.2. MTT cytotoxicity assay**

The cellular toxicity of MccJ25 and the peptide derivatives was determined by measuring the cell growth inhibition using MTT assay.<sup>30</sup> Two cancer cell lines were used, MDA-MB-435 and MCF7 cells. Cells were seeded in 96 well plates (Corning Inc., MA, USA) at a concentration of  $1 \times 10^4$  cells/well (100  $\mu$ L) in complete media and were incubated at 37 °C in 5% CO<sub>2</sub> atmosphere. After 24 hours, the cells were treated with aseptic samples. Samples (1 mM, MccJ25 and peptides) were prepared in sterile 10% DMSO/water followed by filtration through 0.2  $\mu$ M filter. The cell culture media were added to the 96 well plate (180  $\mu$ L/well) followed by addition of peptide sample solution (20  $\mu$ L/well), serially double diluted to give concentrations ranging from 0.3125 to 100  $\mu$ M. Doxorubicin was used as a positive control and untreated cells were used as a negative control. The plates were incubated for another 24 hours following which the culture media was aspirated and replaced with 20  $\mu$ L MTT solution (5 mg/mL in cell media) and 100  $\mu$ L cell medium. The cells were incubated for 3.5 hours to allow interaction with MTT solution. Following incubation, the media was removed by vacuum, and the purple formazan product precipitated in each well was solubilized in DMSO (100  $\mu$ L), and the absorbance was measured at 570 nm using microtitre reader. The percentage cell viability was expressed as the absorbance ratio of cells treated with peptides to untreated cells dissolved in

complete media. All experiments were done in triplicate, and the data is presented in the form of mean.

### **5.3. Results and Discussion**

Six peptides were designed on the basis of the MccJ25 sequence following the strategy that intra-peptide interactions will lead to active peptide derivatives. Peptides were designed to form folded conformation by intra-peptide (i) disulfide and amide bond formation (analogues **1** and **2**), (ii) disulfide and electrostatic interactions (**3** and **4**), or (iii) disulfide and hydrophobic interactions (**5** and **6**). In peptide **1**, the lactam ring of MccJ25 between G1 and E8 was maintained, and a disulfide bond between C4 and C20 (C-terminal) was introduced to hold the C-terminal of the peptide in place. In all other peptides (**2-6**), the isopeptide bond between G1 and E8 was replaced with a disulfide bond. Peptide **2**, an 18-residue peptide, utilized an amide bond to tie the N-terminal C1 with the C-terminal E18. Peptides **3** and **4** contain substitution of a ring residue and one residue from the tail region with positively and negatively charged amino acids, respectively, for electrostatic interactions (H5K, Y20E in **3** and G4K, Y20E in **4**). Similarly, peptides **5** and **6** contain substitution or insertion with hydrophobic amino acids, such as G4F in **5**. Peptide **6** consists of a larger 9-residue N-terminal ring, as expansion of the ring was thought to facilitate the insertion of the C-terminal into the N-terminal lariat ring by interaction between F5 and F19 and/or Y20. An aromatic hydrophobic Phe (F) residue was inserted between G4 and H5 for

enhanced van der Waals and stacking interactions with the C-terminal F19 and Y20. In addition, I13R and/or T15G substitutions (replacement of hydrophobic Ile with basic guanidine containing Arg and Thr with a methyl side chain with Gly with no side chain) were introduced in peptides **2**, **5**, and **6** to increase solubility. These mutations have been reported to yield higher inhibitory activity compared to the wild-type MccJ25.<sup>16</sup>

Peptides **1-6** were synthesized as linear peptides using Fmoc solid-phase peptide synthesis. For peptides **1** and **2**, the lactam bond formation was achieved on the solid-phase, followed by cleavage from the resin. The second ring (disulfide bond) was then formed in solution. Peptides **3-6** were cleaved from the resin as linear peptides followed by oxidation to form disulfide bond. The electrostatic or hydrophobic interactions in the peptides were initiated when the peptides were cleaved from the solid phase and the side chain protections were removed. Native MccJ25 was expressed using pTUC202 plasmid in *E. coli* MC4100 in M9 minimal media.<sup>12</sup> Crude peptides were purified using semi-preparative reversed-phase HPLC prior to characterization by electrospray and/or MALDI-TOF mass spectrometry (**Table 5.1**). All peptides were purified up to >95% purity as shown by analytical RP-HPLC and mass spectrometry (Figures A.10 and A.11), and were obtained with an overall yield of 7-32%.

The antibacterial activity of MccJ25 and peptides **1-6** was evaluated against a number of Gram-negative pathogens. Twelve *Salmonella* strains and two *E. coli* strains were used to obtain the activity profile of the peptides using liquid growth inhibition assay (**Table 5.2**).<sup>25</sup> Peptides **1** and **6** displayed good

activity (low micromolar range) against *S. newport* with MIC values of 25 and 30  $\mu\text{M}$ , respectively (**Figure 5.2**). Compared to the native MccJ25 (MIC 0.5  $\mu\text{M}$ ), these peptides were 50-60 fold less potent. Interestingly, **1** also displayed activity against several (five) other *Salmonella* strains including two MccJ25 resistant strains. For all of these strains, MIC of **1** was in the range of 75-90  $\mu\text{M}$ . The MIC of MccJ25 was also higher (compared to *S. newport*) for the three MccJ25 sensitive strains. Peptides **1-6** were also tested for inhibition of Gram-positive bacteria, such as *S. aureus* ATCC 6538 and *E. faecalis* ATCC 19433. These peptides showed no activity against Gram-positive strains.

A number of different MIC values of MccJ25, ranging from 5 nM to 0.22  $\mu\text{M}$ , against *S. newport* have been reported previously.<sup>3,12,31,32</sup> In this study, we found the MIC value of MccJ25 to be 0.5  $\mu\text{M}$  against a clinical isolate of *S. newport*. This variation in MIC values could be due to the difference in the experimental conditions used, such as spot-on-lawn assay, liquid growth assay, media with or without supplements, or the difference in the strains used.

**Table 5.2.** Antibacterial activity of MccJ25 and synthetic peptide derivatives (1 and 6) against Gram-negative bacterial strains

Strains <sup>a</sup>	MIC <sup>b</sup> (μM) of Peptides		
	MccJ25	1	6
<i>S. newport</i>	0.5 ± 0.05	25 ± 3.0	30 ± 4.0
<i>S. enteritidis</i> PT8	1.5 ± 0.8	80 ± 3.0	-
<i>S. enteritidis</i> ATCC13076	1.8 ± 0.7	-	-
<i>S. enteritidis</i> AFLB 11	2.0 ± 0.6	-	-
<i>S. enteritidis</i> AFLB 41	1.6 ± 1.0	-	-
<i>S. enteritidis</i> AFLB 81	1.7 ± 1.2	-	-
<i>S. typhimurium</i> AFLB 25	2.8 ± 0.8	85 ± 5.2	-
<i>S. typhimurium</i> ATCC 13311	-	75 ± 6.5	-
<i>S. heidelberg</i> ATCC 8326	-	83 ± 6.1	-
<i>S. montevideo</i> 20	-	-	-
<i>S. paratyphi</i>	1.5 ± 1.0	-	-
<i>S. choleresius</i> ATCC 10708	1.5 ± 0.6	90 ± 5.7	-
<i>E. coli</i> DH5a	5.0 ± 1.0	-	-
<i>E. coli</i> MC4100	5.0 ± 2.0	-	-

<sup>a</sup>Details for the bacterial strains are provided in Table S2 (supplementary data).

<sup>b</sup>MIC value is the last concentration of the peptide (μM) giving 100% inhibition of the strain. -, no activity detected up to 250 μM. Data are represented as means ± standard errors of the means. The values are results of at least three independent measurements.

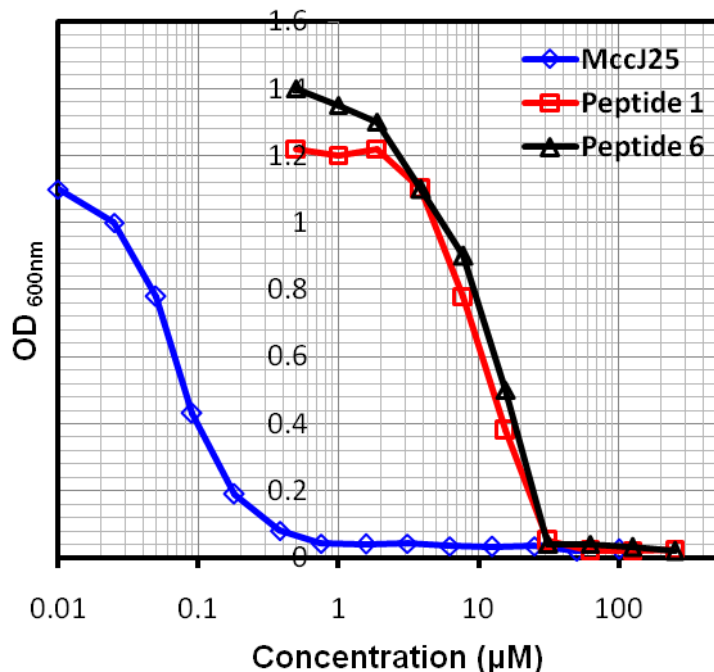


**Figure 5.2.** Growth curves of microcin J25, peptide 1, and peptide 6 using broth assay against *Salmonella Newport*. MICs were defined as the lowest peptide concentration that caused 100% growth inhibition (0.05 AU).

Furthermore, peptides **1** and **6** were found to be bactericidal similar to MccJ25.<sup>4</sup> The minimum bactericidal concentrations (MBCs) of peptides **1** and **6** against *S. Newport* were 31.25 and 62.5 µM, respectively. The MBCs of peptide **1** against *S. enteritidis* ATCC P76, *S. typhimurium* ATCC 13311, and *S. choleraesuis* ATCC 10708 were 125 µM each. A number of synthetic analogues of MccJ25 have been reported, however, none of them display activity against Gram-negative pathogens.<sup>6,7,13,21</sup> To our knowledge, peptides **1** and **6** are the first synthetic derivatives of MccJ25 that display antibacterial activity. Peptides **2-5** lacked antimicrobial activity against all of the tested strains up to 250 µM concentration. One striking feature of peptides **2-5** was the replacement of lactam

bond with a disulfide linkage. Although the same is true for peptide **6**, but the replacement was better tolerated due to the expanded 9-residue lariat ring. A variant of peptide **6** with 8-residue lactam ring (CGAFHVPCYFVGRGTPISFYG) was synthesized (not shown here) and was found to be inactive suggesting larger lactam ring facilitates interaction between the C-terminal tail and the N-terminal ring. The reduced activity of **1** and **6** compared to the native MccJ25 could be due to the loss of characteristic lasso conformation.

Circular dichroism (CD) spectroscopy was used to study the folding behavior of peptides **1** and **6** in solution. Methanol was used as a solvent for CD studies due to the limited solubility of the peptides in water. Moreover, methanol has been used previously to elucidate the solution structure (NMR structure) of MccJ25.<sup>6</sup> The CD spectra of peptides **1** and **6** in methanol were very different from MccJ25 suggesting different folded structures in solution (**Figure 5.3**). The CD spectrum of MccJ25 in methanol displayed a minimum at 200 nm ( $\Theta = -3.2 \times 10^3$ ) and a maximum at 225 nm ( $\Theta = 1.1 \times 10^3$ ) with a positive shoulder at 215 nm (**Figure 5.3**) consistent with the previously reported spectrum.<sup>33</sup> A negative peak at 200 nm is characteristic of unstructured peptides; however, this peak has also been attributed to small  $\beta$ -sheets or  $\beta$ -turn secondary structures such as in  $\beta$ -defensins.<sup>34</sup> The positive band at ca. 225 and 210 nm have been attributed to the Phe  $L_a$  and Tyr  $L_a$  transitions.<sup>35</sup> CD of peptide **1** showed a broad minimum at 208 nm with low intensity ( $\Theta = -1.5 \times 10^3$ ), whereas, peptide **6** displayed a minimum at 210 nm ( $\Theta = -5.0 \times 10^3$ ) with a shoulder at 226 nm ( $\Theta = -1.8 \times 10^3$ ). Quantitative analysis of the secondary structure of peptide **6** with CDPro<sup>36</sup>

suggested that there is little  $\beta$ -sheet conformation ( $\sim 15\%$  residues form  $\beta$ -sheet) compared to MccJ25 (39%). Peptide **6** showed the presence of increased helical folding. These results suggest that both the active peptides (**1** and **6**) may adopt a constrained and compact folded structure, however, do not adopt the true lasso structure as observed in MccJ25.

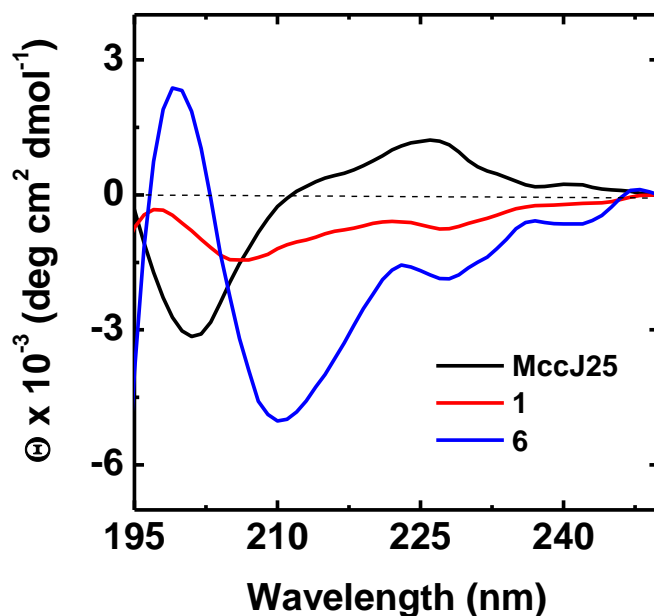
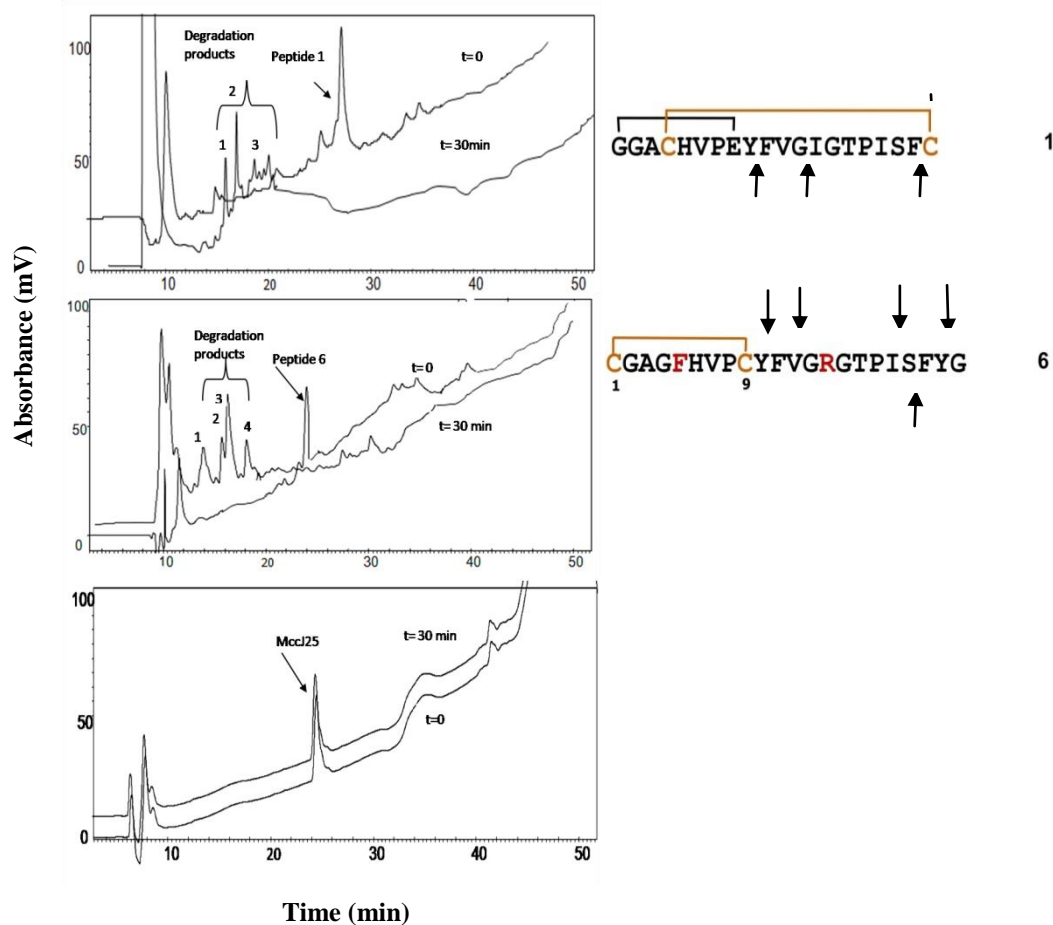


**Figure 5.3.** Circular dichroism spectra for MccJ25, **1** and **6** in methanol at 25 °C.

Furthermore, the absence of lasso conformation in peptides **1** and **6** was confirmed by enzyme stability studies. MccJ25 is known to be highly stable to degradation in the presence of proteolytic enzymes, such as chymotrypsin, trypsin, carboxypeptidase and pepsin.<sup>12</sup> In contrast, both **1** and **6** were not stable in the presence of chymotrypsin and pepsin. During the antimicrobial assay, the

circular growth inhibition zones of **1** and **6** were distorted to a crescent-shape in the presence of a drop of chymotrypsin. Likewise, reversed-phase HPLC analysis of peptides **1** and **6** incubated with pepsin for 30 minutes showed complete degradation of the peptides (**Figure 5.4**). For peptide **1**, the presence of fragments FVGIGTPIS and FVGIGTPISF showed that the cleavage occurred before and after the C-terminal Phe residue (Phe19). This suggests that the C-terminal cysteine is present outside the ring (N-terminal ring between Gly1 and Glu8) allowing access to the C-terminal residues for cleavage by enzymes such as pepsin. Peptide **6** also gave similar degradation products after incubation with pepsin. However, fragments from cleavage near Phe5 residue, which is present inside the N-terminal ring (between Cys1 and Cys9) of **6**, were not detected. Interestingly, the evaluation of thermostability of **1** and **6** showed that only peptide **1** was active after incubation in boiling water for 3 hours. This may be due to its rigid bicyclic ring structure allowing high heat resistance similar to wild-type MccJ25. The disulfide bond was found to be intact for peptide **1** after boiling treatment. Peptides **1** and **6** with reduced cysteine residues (absence of disulfide bond) were found to display no antimicrobial activity.



Fragment #	Sequence	Mass Found
<i>Peptide 1</i>		
1	FVGIGTPIS and FVGIGTPISF	889.1 and 1036.5
2	GGACHVPEY-C and GGACHVPEY-FG	1034.6 and 1181.2
3	GGACHVPEY-IGTPISFC	1748.8
<i>Peptide 6</i>		
1	FVGRGTPIS	932.2
2	CGAGFHVPCY	1052.1
3	FVGRGTPISF and FVGRGTPISFY	1079.2 and 1242.6
4	CGAGFHVPCYFVGRGTPIS, CGAGFHVPCYFVGRGTPISF, and CGAGFHVPCYFVGRGTPISFY	1966.9, 2112.9 and 2276.0

**Figure 5.4.** RP-HPLC chromatograms of peptides 1 (top), 6 (middle) and MccJ25 (bottom) after incubation with pepsin at time 0 and 30 min. On the right side are shown the cleavage sites for the peptides. A linear gradient was run on a C18 Vydac column (4.6 mm x 250 mm) over 35 min from 15 to 50% isopropyl alcohol/water 0.05% (v/v) TFA with a flow rate of 2 mL/min.

MccJ25 displays antibacterial activity by inhibiting the RNA polymerase (RNAP) and/or the respiratory chain in the target organism, depending on the bacterial species.<sup>31,,19,37,38</sup> For *Salmonella* species MccJ25 targets both the RNAP and the cell respiration, however, for *E. coli* the target is mainly RNAP. Peptides **1** and **6** most likely do not inhibit RNAP as they are inactive against *E. coli* as well as the lasso structure essential for RNAP inhibition is absent in these peptides. Different structure activity relationship studies of MccJ25 showed that lasso conformation (tail locked in ring) is important in RNAP interaction and inhibition.<sup>19,17</sup> Thermolysin-cleaved MccJ25 and MccJ25 lacking amino acids 13 to 17 inhibit RNAP transcription suggesting that the unusual lasso ring-tail part of the MccJ25 molecule interacts with RNAP, and blocks the secondary channel of the enzyme.<sup>17</sup> Whereas, amidation of the C-terminal glycine threaded through the MccJ25 lariat ring specifically blocks the RNAP inhibition. The amidated MccJ25 peptide inhibits cell respiration.<sup>19</sup>

To assess the effect of peptides **1** and **6** on the inhibition of cell respiration, the oxygen consumption of *Salmonella newport* in the presence of MccJ25, **1** or **6** was assayed. Peptide **1** inhibited oxygen consumption, whereas, peptide **6** had no effect on oxygen consumption (**Figure 5.5**). The findings from this experiment suggest that peptide **1** inhibits cell respiration in a manner analogous to MccJ25, and peptide **6** that did not inhibit cell respiration has an alternative mechanism of action. Peptide **1**, which lacks the lasso structure, seems to act primarily by inhibition of cell respiration which may also account for its decreased antimicrobial activity compared to MccJ25.

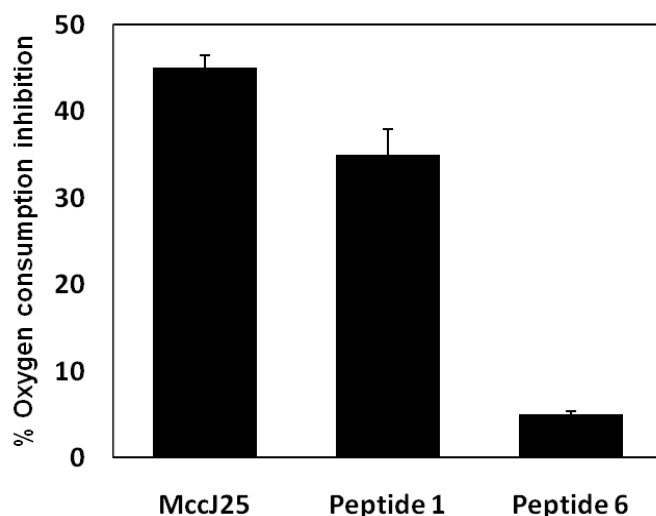


**Figure 5.5.** Effects of treatment with MccJ25, peptide 1 and peptide 6 on the oxygen consumption. Oxygen consumption of bacteria growing in the presence of peptides was expressed as a percentage of the oxygen concentration of the control culture (without peptides). Data correspond to mean values of three independent experiments. Error bars correspond to the standard deviations.

Finally, the cellular toxicity of MccJ25 and peptides **1-6** was investigated as a lead antibiotic must display low toxicity to mammalian cells. The cytotoxicity of the peptides was evaluated using cell viability MTT assay against two cancer cell lines, MDA-MB-435 and MCF-7 cells (**Figure A.12**). MccJ25 and the peptide derivatives displayed very low cytotoxicity (>80% cell viability) up to the highest concentration tested (100  $\mu$ M). Under similar conditions, a known antitumor agent doxorubicin showed only 20% cell viability at low concentration (3  $\mu$ M). Peptides **3-4** with charged residues or involving electrostatic interactions displayed slightly higher cytotoxic effect (75% cell viability) compared to the other peptides (> 90% cell viability). In general, the

toxicity values observed were not significant when compared to the known antitumor agents. In this context, it is of particular interest to note that Lopez *et al.* observed low hemolytic activity for MccJ25 against red blood cells.<sup>32</sup> Although MccJ25 displays antiapoptotic properties with isolated mitochondria,<sup>39</sup> the low cytotoxicity could be due to its inability to permeate human cells.

#### **5.4. Conclusions**

To summarize, two active peptides (**1** and **6**) derived from the sequence of MccJ25 are reported. The design strategy used for obtaining active synthetic sequences from the MccJ25 sequence suggests that (i) the folding of the C-terminal tail (in order to constraint the C-terminal tail near the lactam ring) can be achieved with a covalent disulfide bond formation (peptide **1**) and (ii) the lactam (or lariat) ring can be substituted with a ring formed by a disulfide bond, however, it may require ring expansion (peptide **6**). The CD and resistance to proteases experiments suggest that the active peptides (**1** and **6**) do not fold into a lasso conformation, and peptide **1** displays antimicrobial activity by inhibition of target cell respiration. Finally, the synthetic peptide derivatives of MccJ25 display minimal toxicity to mammalian cells and act specifically on bacterial cells.

## 5.5. References

- (1) Vincent, P. A.; Morero, R. D. The Structure and Biological Aspects of Peptide Antibiotic Microcin J25 *Curr. Med. Chem.* **2009**, *16*, 538-549.
- (2) Pavlova, O. A.; Severinov, K. V. [Posttranslationally modified microcins] *Genetika* **2006**, *42*, 1636-1646.
- (3) Salomon, R. A.; Farias, R. N. Microcin-25, a novel antimicrobial peptide produced by *Escherichia coli* *J. Bacteriol.* **1992**, *174*, 7428-7435.
- (4) Sable, S.; Pons, A. M.; Gendron-Gaillard, S.; Cottenceau, G. Antibacterial activity evaluation of microcin J25 against diarrheagenic *Escherichia coli* *Appl. Environ. Microbiol.* **2000**, *66*, 4595-4597.
- (5) Wilson, K. A.; Kalkum, M.; Ottesen, J.; Yuzenkova, J.; Chait, B. T.; Landick, R.; Muir, T.; Severinov, K.; Darst, S. A. Structure of microcin J25, a peptide inhibitor of bacterial RNA polymerase, is a lassoed tail *J. Am. Chem. Soc.* **2003**, *125*, 12475-12483.
- (6) Rosengren, K. J.; Clark, R. J.; Daly, N. L.; Goransson, U.; Jones, A.; Craik, D. J. Microcin J25 has a threaded sidechain-to-backbone ring structure and not a head-to-tail cyclized backbone *J. Am. Chem. Soc.* **2003**, *125*, 12464-12474.
- (7) Bayro, M. J.; Mukhopadhyay, J.; Swapna, G. V. T.; Huang, J. Y.; Ma, L. C.; Sineva, E.; Dawson, P. E.; Montelione, G. T.; Ebright, R. H. Structure of antibacterial peptide microcin J25: A 21-residue lariat protoknot *J. Am. Chem. Soc.* **2003**, *125*, 12382-12383.
- (8) Delgado, M. A.; Salomón, R. A. Molecular characterization of a DNA fragment carrying the basic replicon of pTUC100, the natural plasmid encoding the peptide antibiotic microcin J25 system *Plasmid* **2005**, *53*, 258-262.
- (9) Clarke, D. J.; Campopiano, D. J. Maturation of McjA precursor peptide into active microcin MccJ25 *J. Org. Biomol. Chem.* **2007**, *5*, 2564-2566.
- (10) Duquesne, S.; Destoumieux-Garzon, D.; Zirah, S.; Goulard, C.; Peduzzi, J.; Rebuffat, S. Two enzymes catalyze the maturation of a lasso peptide in *Escherichia coli* *Chem. Biol.* **2007**, *14*, 793-803.
- (11) Solbiati, J. O.; Ciaccio, M.; Farias, R. N.; Gonzalez-Pastor, J. E.; Moreno, F.; Salomon, R. A. Sequence Analysis of the Four Plasmid Genes Required To Produce the Circular Peptide Antibiotic Microcin J25 *J. Bacteriol.* **1999**, *181*, 2659-2662.

- (12) Blond, A.; Péduzzi, J.; Goulard, C.; Chiuchiolo, M. J.; Barthélémy, M.; Prigent, Y.; Salomón, R. A.; Farías, R. N.; Moreno, F.; Rebuffat, S. The cyclic structure of microcin J25, a 21-residue peptide antibiotic from *Escherichia coli* *Eur. J. Biochem.* **1999**, *259*, 747-756.
- (13) Pomares, M. F.; Salomon, R. A.; Pavlova, O.; Severinov, K.; Farias, R.; Vincent, P. A. Potential Applicability of Chymotrypsin-Susceptible Microcin J25 Derivatives to Food Preservation *Appl. Environ. Microbiol.* **2009**, *75*, 5734-5738.
- (14) Blond, A.; Cheminant, M.; Destoumieux-Garzon, D.; Segalas-Milazzo, I.; Peduzzi, J.; Goulard, C.; Rebuffat, S. Thermolysin-linearized microcin J25 retains the structured core of the native macrocyclic peptide and displays antimicrobial activity *Eur. J. Biochem.* **2002**, *269*, 6212-6222.
- (15) Pan, S. J.; Link, A. J. Sequence Diversity in the Lasso Peptide Framework: Discovery of Functional Microcin J25 Variants with Multiple Amino Acid Substitutions *J. Am. Chem. Soc.* **2011**, *133*, 5016-5023.
- (16) Pavlova, O.; Mukhopadhyay, J.; Sineva, E.; Ebright, R. H.; Severinov, K. Systematic structure-activity analysis of microcin J25 *J. Biol. Chem.* **2008**, *283*, 25589-25595.
- (17) Semenova, E.; Yuzenkova, Y.; Peduzzi, J.; Rebuffat, S.; Severinov, K. Structure-Activity Analysis of Microcin J25: Distinct Parts of the Threaded Lasso Molecule Are Responsible for Interaction with Bacterial RNA Polymerase *J. Bacteriol.* **2005**, *187*, 3859-3863.
- (18) Bellomio A, V. P., de Arcuri BF, Salomón RA, Morero RD, Farías RN. The microcin J25 beta-hairpin region is important for antibiotic uptake but not for RNA polymerase and respiration inhibition. *Biochem. Biophys. Res. Commun.* **2004**, *325(4)*, 1454-1458.
- (19) Vincent, P. A.; Bellomio, A.; de Arcuri, B. F.; Farías, R. N.; Morero, R. D. MccJ25 C-terminal is involved in RNA-polymerase inhibition but not in respiration inhibition *Biochem. Biophys. Res. Commun.* **2005**, *331*, 549-551.
- (20) de Cristóbal, R. E.; Solbiati, J. O.; Zenoff, A. M.; Vincent, P. A.; Salomón, R. A.; Yuzenkova, J.; Severinov, K.; Farías, R. N. Microcin J25 Uptake: His5 of the MccJ25 Lariat Ring Is Involved in Interaction with the Inner Membrane MccJ25 Transporter Protein SbmA *J. Bacteriol.* **2006**, *188*, 3324-3328.
- (21) Ferguson, A. L.; Zhang, S.; Dikiy, I.; Panagiotopoulos, A. Z.; Debenedetti, P. G.; James Link, A. An Experimental and Computational

Investigation of Spontaneous Lasso Formation in Microcin J25 *Biophys. J.* **2010**, *99*, 3056-3065.

(22) Kaur, K.; Andrew, L. C.; Wishart, D. S.; Vederas, J. C. Dynamic Relationships among Type IIa Bacteriocins: Temperature Effects on Antimicrobial Activity and on Structure of the C-Terminal Amphipathic  $\alpha$  Helix as a Receptor-Binding Region‡ *Biochemistry (Mosc)*. **2004**, *43*, 9009-9020.

(23) Kaiser E, C. R., Bossinger CD, Cook PI. Color test for detection of free terminal amino groups in the solid-phase synthesis of peptides *Anal. Biochem.* **1970**, *34* 595-598.

(24) Ellman, G.L., Tissue sulfhydryl groups *Arch. Biochem. Biophys.* **1959** *82(1)*, 70-77.

(25) Lewus; C. B., and Montville; T. J. Detection of bacteriocins produced by lactic acid bacteria *Journal of Microbiological Methods* **1991**, *13*, 145-150

(26) Layne, E. Spectrophotometric and Turbidimetric Methods for Measuring Proteins *Methods Enzymol.* **1957**, *3*, 447-455. .

(27) Sreerama, N.; Venyaminov, S. Y.; Woody, R. W. Estimation of protein secondary structure from circular dichroism spectra: inclusion of denatured proteins with native proteins in the analysis *Anal. Biochem.* **2000**, *287*, 243-251.

(28) Bryant, K. J.; Read, L. C.; Forsberg, G.; Wallace, J. C. Design and Characterisation of Long-R3-Insulin-Like Growth Factor-I Muteins Which Show Resistance to Pepsin Digestion *Growth Factors* **1996**, *13*, 261-272.

(29) Chalon, M. C.; Bellomio, A.; Solbiati, J. O.; Morero, R. D.; Farias, R. N.; Vincent, P. A. Tyrosine 9 is the key amino acid in microcin J25 superoxide overproduction *FEMS Microbiol. Lett.* **2009**, *300*, 90-96.

(30) van de Loosdrecht AA, B. R., Ossenkoppele GJ, Broekhoven MG, Langenhuijsen MM. A tetrazolium-based colorimetric MTT assay to quantitate human monocyte mediated cytotoxicity against leukemic cells from cell lines and patients with acute myeloid leukemia *J. Immunol. Methods* **1994**, *174*, 311-320

(31) Rintoul, M. a. R.; de Arcuri, B. F.; Salomón, R. A.; Farías, R. N.; Morero, R. D. The antibacterial action of microcin J25: evidence for disruption of cytoplasmic membrane energization in *Salmonella newport* *FEMS Microbiol. Lett.* **2001**, *204*, 265-270.

(32) Fabian E. Lopez, P. A. V., Ana M. Zenoff, Rau´l A. Salomó'n and Ricardo N. Fari´as Efficacy of microcin J25 in biomatrices and in a mouse model

of Salmonella infection *J. Antimicrob. Chemother.* **2007**, *59*, 676–680.

(33) Blond, A.; Cheminant, M.; Segalas-Milazzo, I.; Peduzzi, J.; Barthelemy, M.; Goulard, C.; Salomon, R.; Moreno, F.; Farias, R.; Rebuffat, S. Solution structure of microcin J25, the single macrocyclic antimicrobial peptide from *Escherichia coli* *Eur. J. Biochem.* **2001**, *268*, 2124-2133.

(34) Liu, S.; Zhou, L.; Li, J.; Suresh, A.; Verma, C.; Foo, Y. H.; Yap, E. P.; Tan, D. T.; Beuerman, R. W. Linear analogues of human beta-defensin 3: concepts for design of antimicrobial peptides with reduced cytotoxicity to mammalian cells *Chembiochem* **2008**, *9*, 964-973.

(35) Woody, R. W. Aromatic side-chain contributions to the far ultraviolet circular dichroism of peptides and proteins *Biopolymers* **1978**, *17*, 1451-1467.

(36) Sreerama, N.; Woody, R. W. Estimation of protein secondary structure from circular dichroism spectra: comparison of CONTIN, SELCON, and CDSSTR methods with an expanded reference set *Anal. Biochem.* **2000**, *287*, 252-260.

(37) Delgado, M. A.; Rintoul, M. R.; Farias, R. N.; Salomon, R. A. *Escherichia coli* RNA Polymerase Is the Target of the Cyclopeptide Antibiotic Microcin J25 *J. Bacteriol.* **2001**, *183*, 4543-4550.

(38) Yuzenkova, J.; Delgado, M.; Nechaev, S.; Savalia, D.; Epshtein, V.; Artsimovitch, I.; Mooney, R. A.; Landick, R.; Farias, R. N.; Salomon, R.; Severinov, K. Mutations of Bacterial RNA Polymerase Leading to Resistance to Microcin J25 *J. Biol. Chem.* **2002**, *277*, 50867-50875.

(39) Chirou, M. N.; Bellomio, A.; Dupuy, F.; Arcuri, B.; Minahk, C.; Morero, R. Microcin J25 induces the opening of the mitochondrial transition pore and cytochrome c release through superoxide generation *FEBS J.* **2008**, *275*, 4088-4096.

**Chapter 6 : A Conjugate of Antimicrobial Peptide Microcin J25 with a Cancer Targeting Peptide Displays Cancer Cell Specific Cytotoxicity**

## 6.1. Introduction

Cancer treatment by conventional chemotherapy is hindered by its toxic side effects to noncancerous tissues, and the frequent development of multi-drug resistance by cancer cells.<sup>1-3</sup> Multi-drug resistance can result from a number of cellular changes, such as overexpression of drug transporters such as P-glycoprotein and multi-drug resistance protein-1, induction of various drug-detoxifying enzymes, and defects in apoptotic pathways such as abnormal expression of the antiapoptotic protein Bcl-2 and mutation or inactivation of p53.<sup>3</sup> There is clearly an urgent need to develop new forms of cancer therapy that are effective against multi-drug-resistant cells, and more selective and less toxic to the patient. In the last two decades, an increasing interest has developed in the study of some cationic antimicrobial peptides (CAMPs) for their potential therapeutic use in the fight against cancer.<sup>4-9</sup> Antimicrobial peptides may avoid the shortcomings of conventional chemotherapy, as many of them exhibit selective cytotoxicity with high specificity against a broad spectrum of human cancer cells that have acquired a multi-drug-resistant phenotype.<sup>10,11</sup> These AMPs do not affect normal proliferating cells suggesting that they may be administered *in vivo* with minimal nonspecific toxicity.<sup>12</sup> Another advantage of AMPs is that they kill cancer cells via promoting apoptosis through mitochondrial membrane disruption.<sup>13-16</sup> Apoptosis is a preferred cell death mechanism because it eliminates cells without inducing an inflammatory response, compared to necrosis which cause leakage of intracellular contents resulting in severe inflammatory response.<sup>17</sup>

Several reports have shown that antimicrobial pro-apoptotic peptides can cause an impairment of the membrane integrity of the mitochondria either by inserting in the membrane or activating the mitochondrial permeability transition pore complex (PTPC), which in turn dissipates the proton motive force and finally leads to mitochondrial swelling with the consequent activation of the apoptotic cascade.<sup>14,16,18,19</sup> Microcin J25, is a 21-amino acid antimicrobial peptide with an unusual lasso structure.<sup>20-22</sup> It kills Gram negative bacterial strains by inhibiting RNA polymerase,<sup>23</sup> as well as it acts on the cytoplasmic membrane of *Salmonella Newport* cells producing alteration of membrane permeability, and the subsequent gradient dissipation inhibits oxygen consumption.<sup>24</sup> Besides its antibacterial activity, different studies showed that MccJ25 disrupts the isolated rat mitochondrial membrane potential and diminishes the ATP level.<sup>25</sup> Furthermore, MccJ25 induces the overproduction of reactive oxygen species (ROS),<sup>26</sup> which in turn leads to the oxidation of mitochondrial proteins and lipids. The oxidation of cardiolipins, a key mitochondrial phospholipid induced by MccJ25 might trigger the release of cytochrome c.<sup>27</sup>

MccJ25 peptide offers several advantages over conventional chemotherapeutic drugs and cationic antimicrobial peptides as an anticancer agent. Most antimicrobial peptides have the disadvantage of being erythrolytic, and this could limit their potential therapeutic utility, for example, melittin and tachyplesin are known to cause red blood cell lysis at high concentrations.<sup>28,29</sup> On the other hand, MccJ25 shows no hemolytic activity. In addition, MccJ25 is effective in biomatrices such as in artificial media, indicating that its activity was

not affected by any blood component.<sup>30</sup> Along with that, MccJ25 can withstand extreme temperature, it is stable in a wide range of pH and it is resistant to proteolytic digestion against proteolytic enzymes of the stomach (pepsin) and the intestinal contents (trypsin, chymotrypsin, carboxypeptidase). Altogether, MccJ25 seems to be a promising drug candidate of potential use as anticancer agent.<sup>31</sup>

We initially assessed the anticancer activity of MccJ25 by examining the cytotoxicity of MccJ25 against five distinct cancer cell lines, namely, MCF-7 human breast cancer, MDA-MB-435 human breast cancer cells, Hep G2 human hepatic carcinoma, HCT-29 human colorectal cancer, and HT-1080 human fibrosarcoma.<sup>32</sup> Our screening results up to 100  $\mu$ M MccJ25 showed no noticeable cytotoxicity in all cell lines for 48 h incubation. Another study was published, that confirmed our results, where MccJ25 failed to show any cytotoxicity in COS-7 cells after 48 h of incubation with 100  $\mu$ M MccJ25.<sup>33</sup> Niklison-Chirou *et al.* reported that a MccJ25-Ga variant of MccJ25 having C-terminal carboxylic group amidated can induce apoptosis in COS-7. They postulated that MccJ25-Ga peptide variant can inhibit mitochondrial RNA polymerase, while native MccJ25 is not capable of inhibiting the same enzyme.

Based on previous cytotoxicity results, we hypothesized that lack of cell cytotoxicity of MccJ25, despite of its reported apoptotic effects on isolated mitochondria rat originates from its inability to cross the cell membrane to reach its cytoplasmic target (mitochondria). Therefore, conjugation of MccJ25 to

cancer targeting peptide might improve its delivery to cancer cells and consequently enhance its cytotoxicity. We recently identified a 10 amino acid peptide **18-4** (WxEAAAYQrFL) that binds to breast cancer cells with high affinity and selectivity, and has minimal binding to noncancerous cells. Peptide **18-4** most likely internalize into cells by endocytosis. Our objective in the current study was to conjugate MccJ25 to a carrier peptide **18-4** to enhance its cellular uptake and improve its cytotoxicity toward breast cancer cells, including drug-resistant cells.<sup>34</sup>

Here, we report the synthesis, characterization, *in vitro* cytotoxicity, cellular uptake, and intracellular anticancer efficacy of **MccJ25-18-4** peptide conjugate. *In vitro* cytotoxicity results showed that MccJ25 conjugation to peptide **18-4** significantly enhanced its cytotoxicity; it inhibits the proliferation of breast cancer cells, as well as, drug resistant cells in a dose-dependent manner with no toxicity to normal cells. These results highlight the potential use of our peptide **18-4** as a vector for targeted drug delivery.

## **6.2. Materials and methods**

### **6.2.1. Microcin J25 Expression and Purification**

The expression and purification of native MccJ25 were performed as described in Chapter 5 with some modifications.<sup>31</sup> We optimized the overexpression and purification procedure to obtain large amounts of expressed

MccJ25 purified to homogeneity. The microcin is produced in *E. coli MC4100* strain that harbor the high copy number plasmid pTUC202, which carries the MccJ25 biosynthetic gene cluster. The cells were grown in M9 minimal media (12 L) for 24 h at 37 °C. The culture supernatant was obtained by centrifugation at 4000 g for 15 min in Beckman Coulter rotor, and then subjected to two successive purification steps. First, the supernatant was applied to flex column filled with XAD16 resin (Aldrich, CA), followed by elution in two successive steps with 30:70 (v/v) and 80:20 (v/v) methanol/water mixtures. Antibacterial assay was used to follow the peptide. MccJ25 found in 80:20 (v/v) methanol/water fractions was evaporated, lyophilized, and then it was further purified using C18 RP-HPLC (2 mL/min flow rate and absorbance monitored at 220 nm) under linear gradient from 55-80% methanol/water (0.05% TFA) in 45 min. The concentration of the peptide was determined spectrophotometrically at 278 nm (molar absorptivity 3340 M/L),<sup>35</sup> and the yield was 24 mg from 12 L cell culture.

### **6.2.2. MccJ25-18-4 Conjugate Synthesis**

Peptide 18-4 was manually synthesized using Fmoc solid phase peptide synthesis on 2-chlorotrityl chloride resin (0.015 mmol, 1 mmol/g) as described previously.<sup>36</sup> After removal of Fmoc of the last amino acid,  $\beta$ -alanine amino acid was coupled to the peptide as a spacer. The **MccJ25-18-4** peptide conjugate was then constructed using fragment condensation as follows: In a separate vessel

**MccJ25** peptide (24 mg, 12  $\mu$ M) was activated using DIC/HOBT (24  $\mu$ M each) to activate C-terminal carboxylic group in 2 ml DMF for 5 min, and then it was added to the dry resin having peptide **18-4** (0.015 mM) and the mixture was agitated for 24 hours, after which the resin was washed and peptide conjugate was cleaved from the resin with all the protecting groups using acid cleavage mixture (50:50% TFA/DCM, 5% TIPS). The conjugate was then purified by RP-HPLC (55-80% methanol/water (0.05% TFA each) in 45 min. Conjugate mass were confirmed using MALDI-TOF mass spectrometry. The purity of the conjugate was analyzed by analytical RP-HPLC

### 6.2.3. Cytotoxicity Assay

The cytotoxicity of the **MccJ25-18-4** conjugate, free **MccJ25**, and peptide **18-4**, were assessed against MCF-7, MDA-MB-435, MDA-MB-435-MDR and HUVECs using 3-(4,5-dimethylthiazol-2-yl)-2,5-diphenyl tetrazolium bromide (MTT) assay as previously described.<sup>36</sup> Doxorubicin was used as a positive control. Briefly, cells were seeded onto 96-well microtiter plates at a density of  $10^3$  cells per well. Next day, the media was replaced with 160  $\mu$ l of fresh media and 40  $\mu$ l of a solution containing different concentrations of the different treatments (double dilutions from 100  $\mu$ M till 0.4  $\mu$ M), then incubated for 48 h at 37 °C. Cell survival assay was performed by discarding the medium, then adding 20  $\mu$ L MTT solution (5 mg/mL in cell media) and 100  $\mu$ L cell medium to each well and incubate for 4 hr. The media was then discarded and 200

$\mu\text{l}$  of DMSO were added to dissolve formazan crystals. The absorbance of each sample was measured at 570 nm. The results of the cytotoxicity assay were used to calculate the  $\text{IC}_{50}$  relative to a control of non-treated cells.

A competition experiment was performed to prove that the conjugate enter the cells through endocytosis mechanism. We preincubated  $5 \times 10^3$  MDA-MB-435 cells with free peptide **18-4** (200  $\mu\text{M}$ , 20  $\mu\text{l}$ ). After 10 min, the conjugate was added and incubated for 48 h followed by the MTT assay as directed before.

#### **6.2.4. Peptide Cellular Uptake**

Since MccJ25 peptide lacks an amino functional group for fluorescent labelling, cell uptake studies were carried out using RP-HPLC. Exponentially growing MDA-MB-435 cells were centrifuged and resuspended in RPMI 1640 medium at a concentration of  $2 \times 10^6$  cells/mL, 250  $\mu\text{L}$  of the cell suspension was distributed into a 48-well tissue culture plate for 24 h to adhere. Then, **MccJ25-18-4**, or **MccJ25** solutions (100  $\mu\text{M}$ , 250  $\mu\text{L}$ ) were added, and the cells were incubated in a humidified atmosphere with 5%  $\text{CO}_2$ . After specific time periods (0, 2, 8 and 48 h) the cells of three wells at each time point were transferred to 2 mL centrifugation tube, and acetonitrile (500  $\mu\text{L}$ ) was added, samples were vortexed for 2 min followed by sonication at 37  $^\circ\text{C}$  for 30 min. After sonication, the samples were vortexed again for 2 min and centrifuged at 14 000 rpm for 10 min. Aliquots from the cell solutions, as well as supernatant (20  $\mu\text{L}$ ) were mixed with 20  $\mu\text{L}$  of solvent (52: 48 ratio of acetonitrile and water in the presence of

0.05% TFA). Each sample was then injected into the analytical reverse-phase HPLC system with a C18 column and detected at an absorption wavelength of 480 nm. The elution was performed using a gradient program involving 55-80% methanol/water (0.05% TFA each) in 45 min with a flow rate of 1 mL/min.

### **6.2.5. Detection of Apoptosis Using Annexin V and PI Staining**

To detect apoptosis, double staining with FITC-Annexin V (green) and propidium iodide (red) was used. MDA-MB-435 cells ( $1 \times 10^5$ ) were seeded onto a 24-well plate and incubated for 24 h. The next day after medium was removed, cells were treated with two concentrations of **MccJ25-18-4** conjugate  $IC_{50}$ , and 2x  $IC_{50}$  (20, and 40  $\mu$ M) for 24 h at 37° C. After incubation, cells were collected, harvested by trypsinization, washed with PBS and resuspended in a 100  $\mu$ l binding buffer (10 mM HEPES buffer, 140 mM sodium chloride solution, 2.5 mM  $CaCl_2 \cdot H_2O$  pH 7.4). 5  $\mu$ l of Annexin V-FITC (0.15 mg/ml) and 5  $\mu$ l of PI (500  $\mu$ g/ml) were added to 0.5 ml of the cell suspension and incubated at room temperature for 15 min, in the dark. The cell-associated fluorescence was determined immediately using flow cytometry (FACS experiments were performed on a Beckman Coulter QUANTA™ SC Flow Cytometer. The data was analyzed by CellQuest software, excitation at 485 nm, emission at 525 nm using a green channel for detecting Annexin V-FITC staining, and a red channel for detecting PI staining). Cells stained with FITC-Annexin V alone (Annexin V+/PI-) were considered an early apoptosis, whereas those stained with both

FITC-Annexin V and PI (Annexin V+/PI+) were considered in the advanced stages of apoptosis or necrosis. The FITC-Annexin V and PI double-negative (Annexin V-/PI-) cells were considered alive.

## 6.3. Results and Discussion

### 6.3.1. Design and Synthesis of Conjugate

Peptide **18-4** is a promising vector for specific targeting and selective delivery of bioactive compounds such as Doxorubicin to the inside of breast cells.<sup>36</sup> Peptide **18-4** was used to guide MccJ25 to target cancer cells, allowing its internalization and consequently enhancing its cytotoxicity. Our designed conjugate is composed of two functional domains, one is a homing motif (peptide**18-4**), and the other is a proapoptotic peptide sequence (MccJ25). This conjugate was designed to be nontoxic outside cells, but toxic when internalized into targeted cells by the disruption of mitochondrial membrane.

**MccJ25-18-4** conjugate was constructed using fragment condensation as depicted in **Figure 6.1**. This conjugation was performed in DMF using DIC/HOBT as activating agents. The introduction of beta alanine between the peptide and MccJ25 acts as a spacer to give flexibility for both peptides to interact with their putative receptors. It is noteworthy to mention that peptide MccJ25 has no further reactive groups that would interfere in the coupling reaction. The identity of **MccJ25-18-4** conjugate was verified using RP-HPLC and MALDI-

TOF,  $[M+H]^+$  3457.2. RP-HPLC purification furnished **MccJ25-18-4** conjugate with good yield (50% overall yield from native MccJ25).

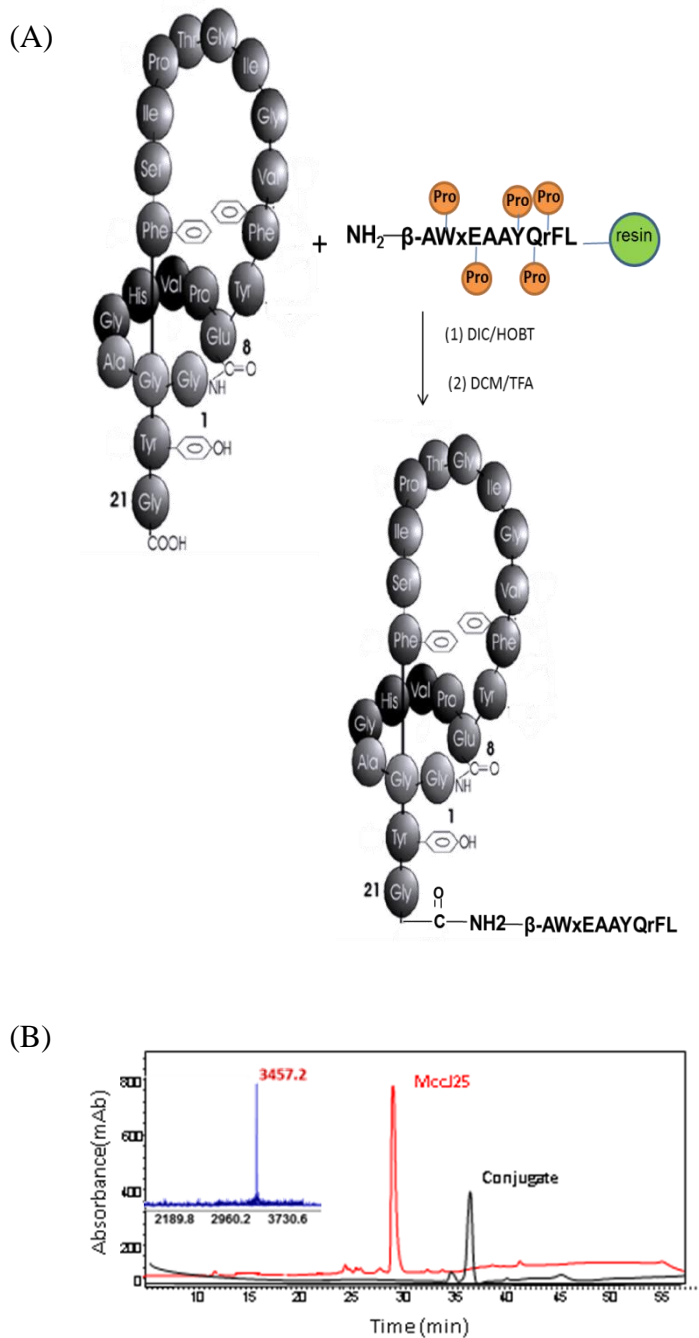
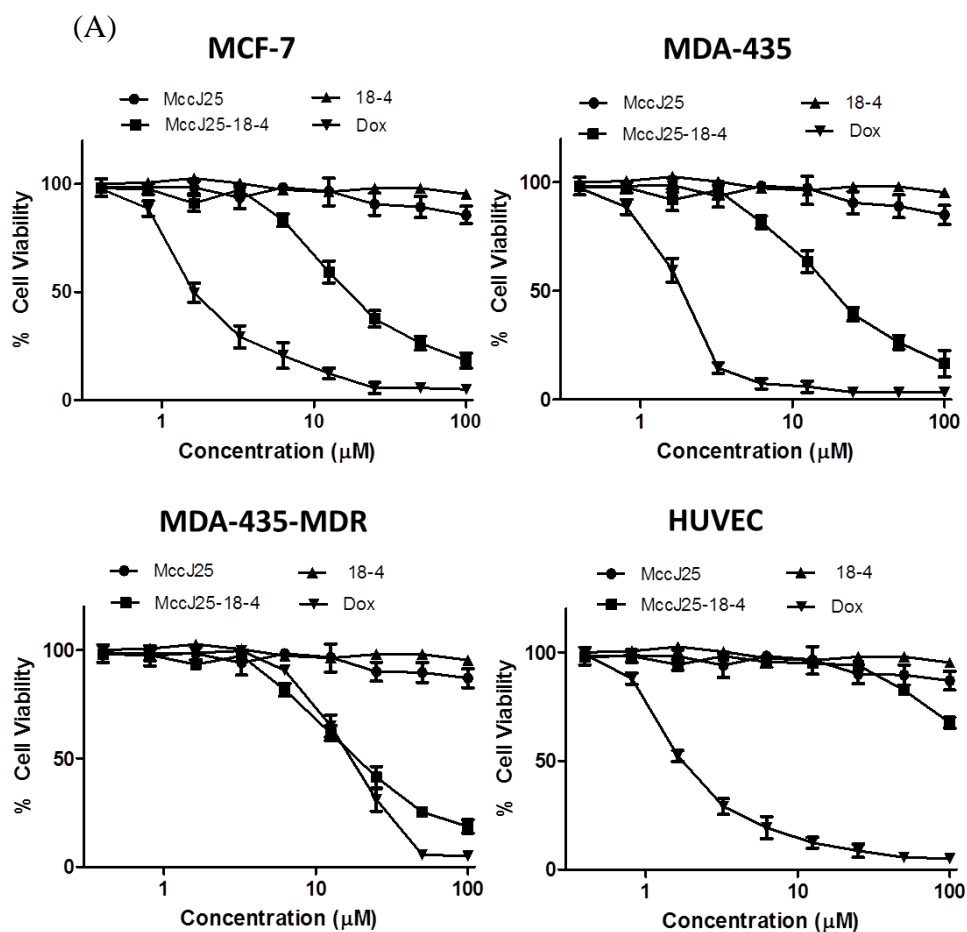


**Figure 6.1.** (A) Synthesis of MccJ25-18-4 conjugate using on resin fragment condensation. Peptide 18-4 synthesized on a chlorotrityl resin was coupled to MccJ25 peptide using DIC/HOBT for 24 h, and then cleavage from resin and deprotection was done using DCM/TFA mixture. (B) RP-HPLC of purified conjugate compared to native MccJ25. Inset of MALDI-TOF of purified conjugate showing  $[M+H]^+$  3457.2.

### 6.3.2. Cytotoxicity assay

Previously, MTT cytotoxicity of MccJ25 peptide with various cell lines did not show any noticeable antiproliferative activity for concentration reaching 100  $\mu\text{M}$ . On the other hand, MTT assay showed that **MccJ25-18-4** conjugate inhibited the growth of breast cancerous cells in a dose-dependent manner, with an  $\text{IC}_{50}$  of  $14.2 \pm 1.5 \mu\text{M}$  for MCF-7 tumor cells, and  $20 \pm 0.5 \mu\text{M}$  for MDA-MB-435 tumor cells. (**Figure 6.2**) More interestingly, the conjugate showed good inhibition for MDA-MB-435MDR resistant cell line with  $\text{IC}_{50}$  of  $23 \pm 2.6 \mu\text{M}$  similar to that of nonresistant cell line, suggesting that the conjugate can escape the p-glycoprotein resistance pathway in the cells. This cytotoxic effect was also reflected in the morphology of the cells. After exposure to **MccJ25-18-4** conjugate for 48 h, a significant fraction of treated cells had become rounded and detached, whereas cells spindle shape was maintained after treatment with the free MccJ25 (data not shown). To determine whether noncancerous cells were also affected by **MccJ25-18-4** conjugate, the cytotoxicity was assessed against normal endothelial HUVEC cells. Results showed that **MccJ25-18-4** conjugate caused very slight cell inhibition of normal cells at 100  $\mu\text{M}$  concentration compared to that of cancer cells, indicating that non-cancerous cells are less sensitive to our conjugate. (**Figure 6.2**)



(B)

Cells	IC <sub>50</sub> (µM)	
	MccJ25 -18-4	Dox
MCF-7	14.2±1.5	1.5±0.5
MDA-MB-435	20±0.5	1.1±0.2
MDA-MB-435-MDR	25±0.5	20±0.5
HUVEC	ND	1.4±0.5

**Figure 6.2.** (A) *In vitro* MTT cell cytotoxicity of MccJ25-18-4 conjugate, compared to native MccJ25, and free peptide 18-4 in MCF-7, MDA-MB-435, MDA-MB-435-MDR cancer cells, and in normal HUVEC cells. Doxorubicin was used as positive control. Treatments were applied at various concentrations for 48 h in serum free media. (B) Mean IC<sub>50</sub> values in comparison with doxorubicin. The results shown are the mean values ±SD of three independent experiments, in triplicates.

To prove that the improved cytotoxicity of **MccJ25-18-4** conjugate was merely due to the targeting peptide, a competition experiment was carried out using MDA-MB-435 cells. The cells were preincubated with free peptide **18-4** for 10 min, followed by incubation with **MccJ25-18-4** conjugate for 48 h, and then cell viability was evaluated using MTT assay. We observed that addition of 10 fold excess of free peptide **18-4** (200  $\mu$ M) caused increase in cell viability to 90% compared to 46% without preincubation. **Figure 6.3**. These results confirm that cell uptake was specifically induced by the peptide.

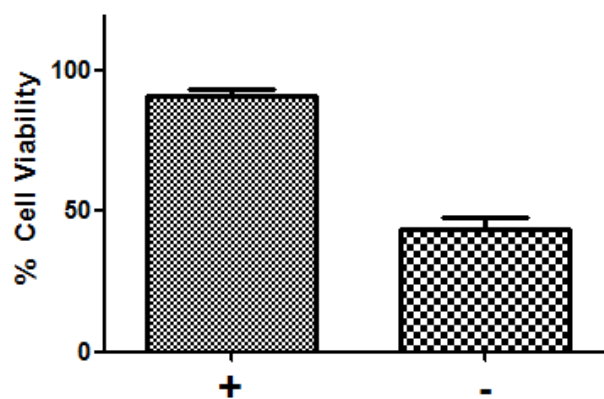


**Figure 6.3.** MDA-MB-435 cells was incubated with 10 fold excess of free peptide 18-4 for 10 min at 37 °C, followed by incubation with MccJ25-18-4 conjugate (20  $\mu$ M) for 48 h, then cell viability was measured using MTT cytotoxicity assay. The results shown are the mean values $\pm$ SD of three independent experiments, in triplicates.

### 6.3.3. Peptide Cellular Uptake

To prove that the **MccJ28-18-4** enhanced antiproliferative activity is due to improved **MccJ25** cellular uptake and internalization, the amount of internalized peptide was assessed using RP-HPLC at specific time points after

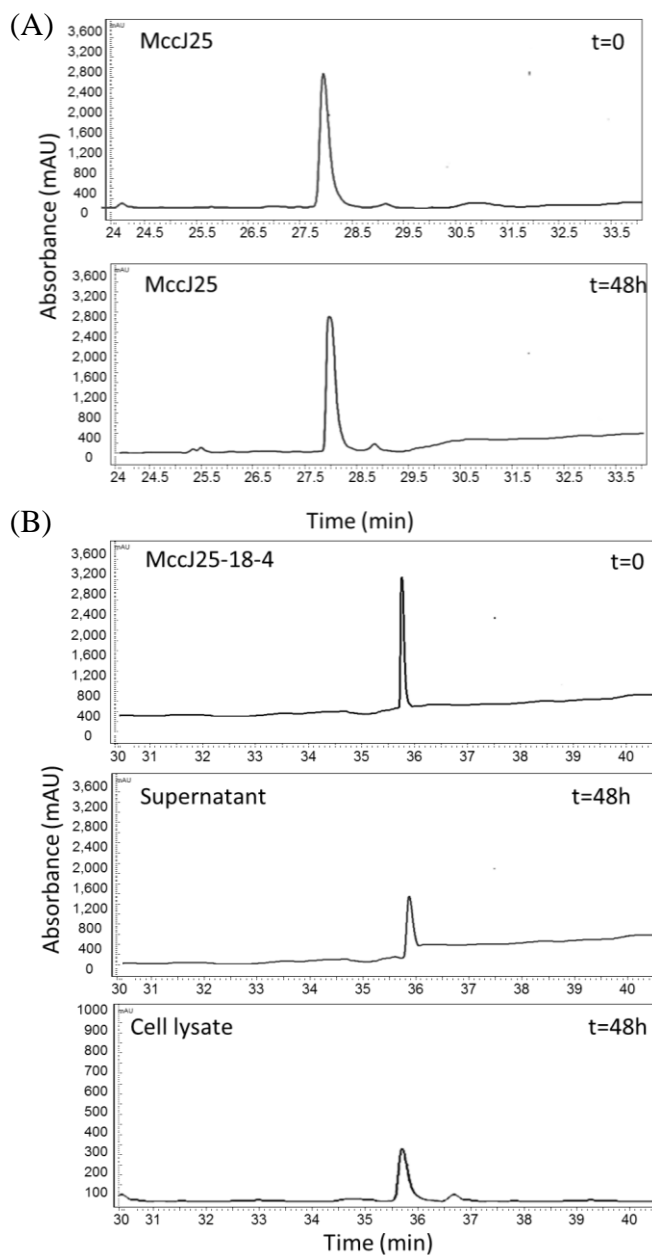


**Figure 6.4.** Cell uptake of MccJ25 (A), and MccJ25-18-4 conjugate (B) in MDA-MB-435 cells analyzed by RP-HPLC. Cells were incubated with 20  $\mu$ M peptide for 48 h and the amount of peptide or peptide conjugate in the cell supernatant and cell lysate was assessed.

incubation with the cells. **Figure 6.4** HPLC results showed that the level of MccJ25 in the supernatant measured by the peak area did not change after

incubation with cells for 48 h, which indicates that no cellular binding or uptake took place with free MccJ25 peptide. On the contrary, the level of **MccJ25-18-4** conjugate showed marked decrease in the supernatant as evidenced by decrease in the peak area corresponding to the peptide conjugate, and the conjugate was also detected in the cell lysate, indicating that the conjugate was internalized into the cells.

#### **6.3.4. Detection of Apoptosis**

Most of the pro-apoptotic antimicrobial peptides preferentially disrupt prokaryotic membrane and eukaryotic mitochondrial membrane rather than eukaryotic plasma membrane.<sup>14</sup> This preferential activity could be due to their similar composition, where, both prokaryotic membranes and eukaryotic mitochondrial membrane maintain large transmembrane potentials, and have a high content of anionic phospholipids.<sup>37,38</sup> In contrast, eukaryotic plasma membrane generally has low membrane potential, and is almost exclusively composed of zwitterionic phospholipids.<sup>38,39</sup> To test whether apoptosis was indeed the mechanism of **MccJ25-18-4** conjugate cell death, cells were treated for 24 h with the conjugate and then they were stained with FITC-annexin and propidium iodide and then analyzed using flow cytometry. FITC-annexin V binds to phosphatidylserine, which is exposed on the outer leaflet of the plasma membrane of cells in the initial stages of apoptosis, whereas propidium iodide preferentially stains the nucleus of dead cells, but not living cells. Annexin V<sup>+</sup>/PI<sup>+</sup> cells were considered necrotic cells or apoptotic cells at an advanced stage

of apoptosis. Annexin V<sup>+</sup>/PI<sup>-</sup> cells were considered apoptotic cells at an early stage of apoptosis.

Results showed that cells treatment with **MccJ25-18-4** following 24 h drug exposure triggers significant apoptosis in MDA-MB-435 cells (annexin V positive, propidium iodide negative). The percentage ratio of apoptotic/necrotic cells resulting from 0, 20, and 40  $\mu$ M conjugate was 2.2/4.0, 21.2/18.1, and 22.1/21.8, respectively (**Figure 6.5**). These data support the conclusion that **MccJ25-18-4** kills cells mainly by apoptosis. The results obtained from the Annexin V assay clearly support the toxicity of the **MccJ25-18-4** as determined by cell-viability MTT assay.

Peptides capable of invading the mitochondria of mammalian cells and triggering apoptosis have been employed in numerous studies directed at the development of new targeted therapeutics for cancer therapy.<sup>40-42</sup> The mitochondria-disrupting peptide D(KLAKLAK)<sub>2</sub>, a 14-amino-acid cationic and  $\alpha$ -helical forming peptide, has been shown to induce apoptosis in cancer cells.<sup>43</sup> This peptide does not disrupt the zwitterionic plasma membranes of eukaryotic cells, but when internalized, D(KLAKLAK)<sub>2</sub> can disrupt the negatively charged mitochondrial membrane,<sup>43</sup> resulting in cell death by mitochondrial-dependent apoptosis.<sup>40</sup> Chemical conjugates of the D(KLAKLAK)<sub>2</sub> with the RGD peptide,<sup>40</sup> the NGR motif,<sup>40</sup> the protein transduction domain (PTD-5),<sup>41</sup> have been previously used for intracellular and extracellular targeting. These targeted D(KLAKLAK)<sub>2</sub>-peptide conjugates effectively induced apoptosis of endothelial

cells following internalization, indicating that the peptide itself can escape intact into the cytosol from endosomal and lysosomal compartments to target mitochondria.

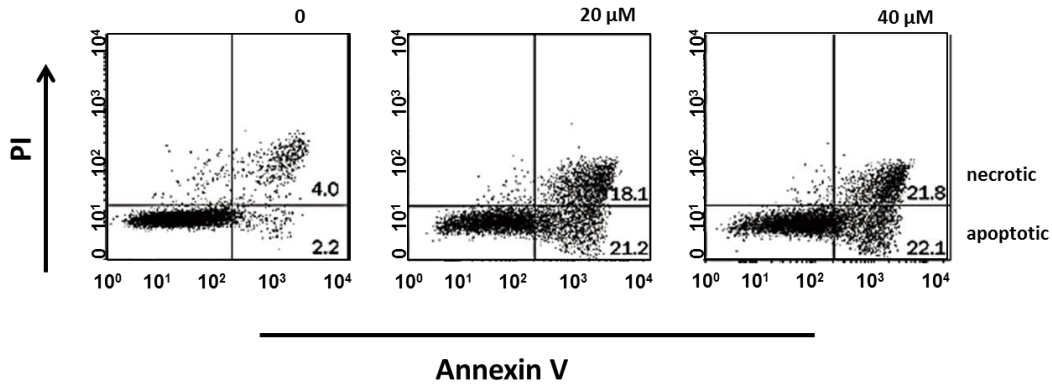


**Figure 6.5.** Flow cytometry analysis of cell death induction in MDA-MB-435. Cells were incubated for 24 h with 20, and 40 μM MccJ25-18-4 conjugate. The left-upper quadrant represents cells stained by PI, while the right bottom quadrant cells stained mainly by Annexin V (early apoptosis). The top right quadrant represents cells stained by both PI and Annexin V (late apoptosis/necrosis).

#### 6.4. Conclusions

In conclusion, this study proved that conjugation of MccJ25 peptide to breast cancer homing peptide 18-4 significantly enhanced the cytotoxicity of MccJ25 in breast cancer cells through improved cell uptake. Moreover, the MccJ25-18-4 conjugate selectively induced cell death in cultured cancer cells, as well as, it can overcome p-glycoprotein multidrug resistant pathways. Apoptosis was the major mechanism for induction of cell death following exposure to the conjugate. The specificity of our conjugate to breast cancer cells makes it a good candidate for further investigation as an antitumoral agent.

## 6.5. References

- (1) Cassidy, J.; Misset, J. L. Oxaliplatin-related side effects: characteristics and management *Semin. Oncol.* **2002**, *29*, 11-20.
- (2) Kalyanaraman, B.; Joseph, J.; Kalivendi, S.; Wang, S.; Konorev, E.; Kotamraju, S. Doxorubicin-induced apoptosis: Implications in cardiotoxicity *Mol. Cell. Biochem.* **2002**, *234-235*, 119-124.
- (3) Gatti L, Z. F. Overview of tumor cell chemoresistance mechanisms *Methods. Mol. Med.* **2005**, *111*, 127–148.
- (4) Hoskin, D. W.; Ramamoorthy, A. Studies on anticancer activities of antimicrobial peptides *Biochimica et Biophysica Acta (BBA) - Biomembranes* **2008**, *1778*, 357-375.
- (5) Shin, S. Y.; Yang, S. T.; Park, E. J.; Eom, S. H.; Song, W. K.; Kim, J. I.; Lee, S. H.; Lee, M. K.; Lee, D. G.; Hahm, K. S.; Kim, Y. Antibacterial, antitumor and hemolytic activities of  $\alpha$ -helical antibiotic peptide, P18 and its analogs *J. Pept. Res.* **2001**, *58*, 504-514.
- (6) Chen, Y.; Xu, X.; Hong, S.; Chen, J.; Liu, N.; Underhill, C. B.; Creswell, K.; Zhang, L. RGD-Tachyplesin Inhibits Tumor Growth *Cancer Res.* **2001**, *61*, 2434-2438.
- (7) Yang, N.; Lejon, T.; Rekdal, Ø. Antitumour activity and specificity as a function of substitutions in the lipophilic sector of helical lactoferrin-derived peptide *J. Pept. Sci.* **2003**, *9*, 300-311.
- (8) Gietema, J. A.; de Vries, E. G. E. Clinical cancer research 2002: new agents and therapies *Drug Resist. Update.* **2002**, *5*, 192-203.
- (9) Ellerby, H. M.; Arap, W.; Ellerby, L. M.; Kain, R.; Andrusiak, R.; Rio, G. D.; Krajewski, S.; Lombardo, C. R.; Rao, R.; Ruoslahti, E.; Bredesen, D. E.; Pasqualini, R. Anti-cancer activity of targeted pro-apoptotic peptides *Nat. Med.* **1999**, *5*, 1032-1038.
- (10) Moore, A. J.; Devine, D. A.; Bibby, M. C. Preliminary experimental anticancer activity of cecropins *Pept. Res.* **1994**, *7*, 265-269.
- (11) Risso, A.; Zanetti, M.; Gennaro, R. Cytotoxicity and Apoptosis Mediated by Two Peptides of Innate Immunity *Cell. Immunol.* **1998**, *189*, 107-115.
- (12) Mader, J. S.; Salsman, J.; Conrad, D. M.; Hoskin, D. W. Bovine lactoferricin selectively induces apoptosis in human leukemia and carcinoma cell lines *Mol. Cancer Ther.* **2005**, *4*, 612-624.

- (13) Kim, R.; Emi, M.; Tanabe, K. Role of mitochondria as the gardens of cell death *Cancer Chemother. Pharmacol.* **2006**, *57*, 545-553.
- (14) Risso, A.; Braidot, E.; Sordano, M. C.; Vianello, A.; Macrì, F.; Skerlavaj, B.; Zanetti, M.; Gennaro, R.; Bernardi, P. BMAP-28, an Antibiotic Peptide of Innate Immunity, Induces Cell Death through Opening of the Mitochondrial Permeability Transition Pore *Mol. Cell. Biol.* **2002**, *22*, 1926-1935.
- (15) Eliassen, L. T.; Berge, G.; Leknessund, A.; Wikman, M.; Lindin, I.; Løkke, C.; Ponthan, F.; Johnsen, J. I.; Sveinbjørnsson, B.; Kogner, P.; Flægstad, T.; Rekdal, Ø. The antimicrobial peptide, lactoferricin B, is cytotoxic to neuroblastoma cells in vitro and inhibits xenograft growth in vivo *Int. J. Cancer* **2006**, *119*, 493-500.
- (16) Hetz, C.; Bono, M. R.; Barros, L. F.; Lagos, R. Microcin E492, a channel-forming bacteriocin from *Klebsiella pneumoniae*, induces apoptosis in some human cell lines *Nat. Acad. Sci. Proc.* **2002**, *99*, 2696-2701.
- (17) Israels, L. G.; Israels, E. D. Apoptosis *Oncologist* **1999**, *4*, 332-339.
- (18) Costantini, P.; Jacotot, E.; Decaudin, D.; Kroemer, G. Mitochondrion as a Novel Target of Anticancer Chemotherapy *J. Natl. Cancer Inst.* **2000**, *92*, 1042-1053.
- (19) Cornut, G.; Fortin, C.; Soulières, D. Antineoplastic Properties of Bacteriocins: Revisiting Potential Active Agents *Am. J. Clin. Oncol.* **2008**, *31*, 399-404
- (20) Rosengren, K. J.; Clark, R. J.; Daly, N. L.; Goransson, U.; Jones, A.; Craik, D. J. Microcin J25 has a threaded sidechain-to-backbone ring structure and not a head-to-tail cyclized backbone *J. Am. Chem. Soc.* **2003**, *125*, 12464-12474.
- (21) Bayro, M. J.; Mukhopadhyay, J.; Swapna, G. V. T.; Huang, J. Y.; Ma, L. C.; Sineva, E.; Dawson, P. E.; Montelione, G. T.; Ebright, R. H. Structure of antibacterial peptide microcin J25: A 21-residue lariat protoknot *J. Am. Chem. Soc.* **2003**, *125*, 12382-12383.
- (22) Wilson, K. A.; Kalkum, M.; Ottesen, J.; Yuzenkova, J.; Chait, B. T.; Landick, R.; Muir, T.; Severinov, K.; Darst, S. A. Structure of microcin J25, a peptide inhibitor of bacterial RNA polymerase, is a lassoed tail *J. Am. Chem. Soc.* **2003**, *125*, 12475-12483.
- (23) Delgado, M. A.; Rintoul, M. a. R.; Farías, R. N.; Salomón, R. A. Escherichia coli RNA Polymerase Is the Target of the Cyclopeptide Antibiotic Microcin J25 *J. Bacteriol.* **2001**, *183*, 4543-4550.

- (24) Bellomio, A.; Vincent, P. A.; de Arcuri, B. F.; Farias, R. N.; Morero, R. D. Microcin J25 Has Dual and Independent Mechanisms of Action in *Escherichia coli*: RNA Polymerase Inhibition and Increased Superoxide Production *J. Bacteriol.* **2007**, *189*, 4180-4186.
- (25) Niklison Chirou, M. a. V.; Minahk, C. J.; Morero, R. D. Antimitochondrial activity displayed by the antimicrobial peptide microcin J25 *Biochem. Biophys. Res. Commun.* **2004**, *317*, 882-886.
- (26) Niklison Chirou, M.; Bellomio, A.; Dupuy, F.; Arcuri, B.; Minahk, C.; Morero, R. Microcin J25 induces the opening of the mitochondrial transition pore and cytochrome c release through superoxide generation *FEBS J.* **2008**, *275*, 4088-4096.
- (27) Niklison-Chiroua, M. V.; Dupuya, F.; Penab, L. B.; Gallegob S. M., Barreiro-Arcosc; M. L., Avilaa, C., Torres-Bugeaua; C., Arcuria; B. E., Bellomioa; A., Minahka, C., Morero, R. D. Microcin J25 triggers cytochrome c release through irreversible damage of mitochondrial proteins and lipids *Int. J. Biochem. Cell Biol.* **2010**, *42*, 273-281
- (28) Raghuraman, H.; Chattopadhyay, A. Cholesterol inhibits the lytic activity of melittin in erythrocytes *Chem. Phys. Lipids* **2005**, *134*, 183-189.
- (29) Katsu, T., Nakao; S., Iwanaga S Mode of action of an antimicrobial peptide, tachyplesin I, on biomembranes *Biol. Pharm. Bull.* **1993**, *16*, 178-181.
- (30) Fabian; E. L., Paula, A. V., Ana, M. Z., Rau' l; A. S., and Ricardo N. F. Efficacy of microcin J25 in biomatrices and in a mouse model of Salmonella infection *J. Antimicrob. Chemother.* **2007**, *59*, 676-680.
- (31) Blond, A.; Peduzzi, J.; Goulard, C.; Chiuchiolo, M. J.; Barthelemy, M.; Prigent, Y.; Salomon, R. A.; Farias, R. N.; Moreno, F.; Rebuffat, S. The cyclic structure of microcin J25, a 21-residue peptide antibiotic from *Escherichia coli* *Eur. J. Biochem.* **1999**, *259*, 747-755.
- (32) Souady, R.; Wang, L.; Kaur, K. Synthetic peptides derived from the sequence of a lasso peptide microcin J25 show antibacterial activity *Bioorg. Med. Chem.* **2012**, *20*, 1794-1800.
- (33) Niklison-Chirou, M. V.; Dupuy, F.; Saavedra, L.; Hebert, E.; Banchio, C.; Minahk, C.; Morero, R. D. Microcin J25-Ga induces apoptosis in mammalian cells by inhibiting mitochondrial RNA-polymerase *Peptides* **2011**, *32*, 832-834.

(34) Rybak, J.-N.; Trachsel, E.; Scheuermann, J.; Neri, D. Ligand-Based Vascular Targeting of Disease *ChemMedChem* **2007**, *2*, 22-40.

(35) Bellomio A, V. P., de Arcuri BF, Salomón RA, Morero RD, Farías RN. The microcin J25 beta-hairpin region is important for antibiotic uptake but not for RNA polymerase and respiration inhibition. *Biochem. Biophys. Res. Commun.* **2004**, *325(4)*, 1454-1458.

(36) Soudy, R.; Gill, A.; Sprules, T.; Lavasanifar, A.; Kaur, K. Proteolytically Stable Cancer Targeting Peptides with High Affinity for Breast Cancer Cells *J. Med. Chem.* **2011**, *54*, 7523-7534.

(37) de Kroon, A. I. P. M.; Dolis, D.; Mayer, A.; Lill, R.; de Kruijff, B. Phospholipid composition of highly purified mitochondrial outer membranes of rat liver and *Neurospora crassa*. Is cardiolipin present in the mitochondrial outer membrane? *BBA - Biomembranes* **1997**, *1325*, 108-116.

(38) Hovius, R.; Thijssen, J.; van der Linden, P.; Nicolay, K.; de Kruijff, B. Phospholipid asymmetry of the outer membrane of rat liver mitochondria: Evidence for the presence of cardiolipin on the outside of the outer membrane *FEBS Lett.* **1993**, *330*, 71-76.

(39) Daum, G. Lipids of mitochondria *BBA-Rev Biomembranes* **1985**, *822*, 1-42.

(40) Ellerby, H. M.; Arap, W.; Ellerby, L. M.; Kain, R.; Andrusiak, R.; Rio, G. D.; Krajewski, S.; Lombardo, C. R.; Rao, R.; Ruoslahti, E.; Bredesen, D. E.; Pasqualini, R. Anti-cancer activity of targeted pro-apoptotic peptides *Nat. Med.* **1999**, *5*, 1032-1038.

(41) Law, B.; Quinti, L.; Choi, Y.; Weissleder, R.; Tung, C.-H. A mitochondrial targeted fusion peptide exhibits remarkable cytotoxicity *Mol. Cancer Ther.* **2006**, *5*, 1944-1949.

(42) Mai, J. C.; Mi, Z.; Kim, S.-H.; Ng, B.; Robbins, P. D. A Proapoptotic Peptide for the Treatment of Solid Tumors *Cancer Res.* **2001**, *61*, 7709-7712.

(43) Javadpour, M. M.; Juban, M. M.; Lo, W.-C. J.; Bishop, S. M.; Alberty, J. B.; Cowell, S. M.; Becker, C. L.; McLaughlin, M. L. De Novo Antimicrobial Peptides with Low Mammalian Cell Toxicity *J. Med. Chem.* **1996**, *39*, 3107-3113.

## **Chapter 7 :Conclusions and Future Directions**

## 7.1. Conclusions

Over the past two decades, peptides have shown encouraging results as therapeutics since they offer remedies to different diseases with unmet medical needs. Moreover, peptide drug candidates offer numerous advantages over small molecules in treating a wide variety of diseases, such as high specificity, potency, and low toxicity. The number of peptides entering clinics is increasing every year, and a rise in the number of marketed ones is expected. In the current dissertation, we were interested in exploring the applicability of two classes of peptides which have been extensively studied in the past two decades; the first class is cancer targeting peptides, and the second class is antimicrobial peptides. These two classes are believed to fill in the gaps in two vital therapeutic areas, which are cancer therapy, and antimicrobial therapy. The use of cancer targeting peptides in chemotherapeutic tumor targeting will assist in the development of more selective, less toxic agents for cancer therapy, which in turn would have a positive impact of the quality of cancer patients lives and on the health system in general. On the other side, antimicrobial peptides are considered as an alternative for currently used antibiotics in the treatment of infectious diseases to overcome the emergence of antibiotic resistance, as well as, their promising proapoptotic anticancer activity open a new research avenue for using them as anticancer agents with novel mechanism of action.

As mentioned in **Chapter 1**, current cancer therapies suffer from low tumor specificity and serious toxic side effects. These side effects are due to the non-specific delivery of the cytotoxic drugs to both normal and cancer cells.

Along with that, the administration of cytotoxic drugs at suboptimal doses to decrease the side effects led to the emergence of tumor resistance, and both problems greatly affect the patient quality of life. Targeting drugs to the cancer cells can help improve the outcome of existing cancer therapies. This can be achieved by using targeting ligands that could bind selectively to an overexpressed receptor on tumor tissue. This would sequentially increase the specific delivery of current therapies to the tumor site with decreased side effects. Antibodies are commonly used targeting ligands, but there are some limitations for their clinical use, such as, their large size, poor stability and their non-specific uptake by reticuloendothelial cells (liver and spleen) and their immunogenicity. Recently, several peptides have been identified by phage display for targeting different tumor types. These peptides displayed favorable results for their application in drug delivery to tumors and tumor diagnosis. Despite the encouraging results, we can still find that the number of cancer targeting peptides entering clinics is very low. This is presumably due to the practical hurdles that limit peptides therapeutic applications such as poor serum stability, low affinity, poor biological membranes penetration. In future studies, it will be important to increase the binding affinity of lead peptide sequences identified using phage display and chemically modify them to increase their proteolytic stability, as well as, screen and identify peptides that would target other tumor overexpressed receptors. Thus, our main goal in the first part of the thesis was the structure optimization of two promising lead peptide sequences identified using phage display, namely, NGR (cCVLNGRMEC),<sup>1</sup> and p160 (VPWMEYPAQRFL)<sup>2</sup> for

identification of analogues with enhanced binding affinity to tumor vasculature and breast cancer cells respectively, besides increasing their proteolytic stability. This will be followed by assessing the targeting competency of our new peptide variants in chemotherapeutic drug delivery to cancerous and multidrug resistant breast cells. The newly identified sequences are believed to have a clinical impact in functional diagnosis and tumor-specific drug delivery.

Towards this goal, a library of forty five NGR peptide sequences based on a 9-mer lead sequence (cCVLNGRMEC) was synthesized on cellulose membrane in an array format, followed by library screening against a panel of CD13<sup>+</sup> and CD13<sup>-</sup> cell lines (**Chapter 2**). Peptide-array cell binding assay was able to screen for cyclic and acyclic NGR peptides that bind to CD13<sup>+</sup> cell lines. Screening allowed identification of at least five new NGR peptides that display higher binding to CD13<sup>+</sup> cells with negligible binding to CD13<sup>-</sup> cell lines compared to the lead sequence. Membrane cell binding results, as well as *in vitro* binding experiments including co-culture fluorescence microscopy suggest that the identified NGR peptides bind selectively to CD13 receptor in CD13<sup>+</sup> cell lines. Interestingly, peptide 21 (CNGRC) identified in our study is a well-known NGR peptide that has been widely used as a CD13 tumor vasculature targeting peptide. Among the newly identified sequences presented in this study, peptide 5 offer additional advantages to the previously reported NGR sequence. Peptide 5 (YNGRT) showed a significant increase (up to 13-fold) in uptake by the CD13<sup>+</sup> cells compared to the lead peptide 1. Peptide 5 is a linear peptide that can be cyclized to further enhance its binding properties toward CD13<sup>+</sup> cells. In

addition, peptide 5 displays better APN enzyme inhibition and selectivity toward CD13<sup>+</sup> cells. We proved in our study that peptide array library screening method is a powerful research tool for analyzing peptide-cell interactions with rapid and efficient screening of potent peptides, and quickly fast-track the structure-activity relationship. Screening peptide libraries using this method on intact cells is more likely to enrich for peptides that bind to cell surface receptors in their native conformation. In addition, the NGR peptides identified herein closely resemble NGR sequences present in human fibronectin most likely will have low immunogenicity, making them ideal candidates for the development of ligands for targeting loaded delivery systems and imaging agents to tumor angiogenic blood vessels with reduced side effects.

Peptide p160 (VPWMEYPAQRFL) is a 12-mer peptide that has been identified using phage display, it binds specifically to breast cancer tumors. We were interested in studying this peptide, because when it was studied *in vivo* it displayed higher tumor accumulation versus normal organs, relative to the well-known RGD-4C integrin targeting peptide. We followed a two-step strategy for optimization of p160 peptide sequence to develop breast cancer specific peptide analogues with high binding affinity plus high proteolytic stability. First, a synthetic library based on peptide p160 was screened for specific binding to breast cancer cells, through which a 10-mer peptide 18 (WXEYAAQRFL) was identified. Peptide 18 displayed 3-fold higher binding affinity for MDA-MB-435 and MCF-7 breast cancer cell lines compared to lead p160 peptide, with a negligible affinity for HUVEC normal cells.<sup>3</sup> Second, analogues of peptide 18

were engineered for improved proteolytic stability while maintaining high specificity for breast cancer cells. Enhancing the *in vivo* proteolytic stability would preserve the targeting efficacy of these peptides in the development of clinically useful products. In **Chapter 3**, we designed and synthesized stable analogues of peptide 18 by chemical modification of their structure. Our design strategy involved the replacement of two or three amino acids in the sequence of 18 with D-residues or  $\beta$ -amino acids. The beta amino acids used in the current study were derived from L-aspartic acid, compared to the commercially available  $\beta$ -amino acid, our  $\beta$ - amino acids are readily synthesized during peptide assembly and they are cheaper in price. Furthermore, the addition of  $\beta$ -amino acid side chain on the  $\alpha$ -carboxylate of L-Asp during peptide assembly allows introduction of a variety of unnatural side chains. This provides flexibility to control physicochemical properties of peptides and modulate binding affinity and selectivity. In the current investigation, three analogues of peptide 18 (18-4, 18-9, and 18-10) with high specific binding to breast cancer cell lines were discovered. These new analogues are capable of cellular internalization through receptor-mediated endocytosis; they exhibit resistance to proteolytic degradation in human serum and in liver homogenate, as well as they impart no cell cytotoxicity. These peptides have a high degree of secondary structure that correlates with their binding affinity and internalization. In conclusion, the stepwise procedure delineated here may be adapted for the optimization of other targeted peptides for targeting other cancer cell types. Hence, the peptides reported here are useful, proteolytically stable peptides that can either be directly coupled to an anticancer

drug, decorate a drug carrier that encapsulates the drug or it can be conjugated to a diagnostic moiety such as a fluorophore for use in cancer drug targeting or diagnosis.

Next, we examined the cancer drug targeting efficacy of one of the stable peptide analogues of p160 (peptide 18-4, WxEYAAQrFL) toward breast cancer cells *in vitro* by generating novel peptide Dox conjugates (**Chapter 4**). In this context, two peptide 18-4 Dox conjugates with variable conjugation chemistry, and variable rates of drug release were synthesized. Our results demonstrated that peptide 18-4 conjugation to Dox through an ester linkage maintained the peptide targeting affinity and selectivity towards breast cancer cells. The peptide drug ester conjugate was able to internalize into the breast cells to deliver the drug selectively with equipotent cytotoxicity to that of free Dox. Besides, the ester conjugate was able to circumvent multidrug resistance mechanism in Dox resistant cell lines. Peptide 18-4 holds a promise as a drug delivery agent, it is a short peptide (10 aa), it can be easily synthesized with low cost, and it can be easily conjugated to different agents without affecting its targeting affinity. Altogether, our results suggest that our breast cancer stable peptide carrier 18-4 is a promising targeting ligand for tumor targeted delivery of not just Dox, but it can be used for the selective delivery of different cargos to breast cancer tumors either for prognostic or therapeutic applications. These data lay the foundations for the development of other peptide-conjugates with antitumor potential.

In **Chapter 1**, we also shed light on the ongoing research for the development of AMPs as human therapeutics for antimicrobial and cancer

treatments. As we know that resistance to conventional antibiotics is a global public health problem, and that the need of new antibiotics has stimulated interest in the use of AMPs. Moreover, some of these peptides showed promising anticancer activity against different tumors and cell lines, which open a new path in research for using them as novel anticancer agents. In **Chapter 5**, and **6** we studied antimicrobial peptide microcin J25. MccJ25 peptide has a characteristic folded lasso structure which confers several properties to it, such as, resistance to proteolytic degradation stability towards chaotropes, organic solvents, and extreme temperatures. Such properties amplify its potential applicability for a number of applications including food preservation and treatment of food-borne diseases. Because the lasso scaffold is a promising architecture for bioactive peptide development, we explored the possibility of chemically synthesizing active analogues of MccJ25 peptide (**Chapter 5**). The characteristic lasso structure of MccJ25 is formed with the help of two processing enzymes McjB and McjC that are expressed from the producing plasmid. All attempts for producing active analogues of MccJ25 were carried out using site directed mutagenesis. Chemical synthesis of lasso peptides has always been a challenge, and no successful attempt has been reported.

Our design strategy was based on designing MccJ25 derived sequences with specific amino acid substitutions. The purpose of these substitutions was that they would enhance peptide folding using a combination of intra-peptide disulfide bond formation and electrostatic or hydrophobic interactions. Two MccJ25 peptide mimetics 1 and 6 displayed good activity (low micromolar range) against

*Salmonella newport* with MIC values of 25 and 30  $\mu\text{M}$ , respectively were synthesized. To our knowledge, peptides 1 and 6 are the first synthetic derivatives of MccJ25 that display antibacterial activity. Peptide 1 also displayed activity against several (five) other *Salmonella* strains including two MccJ25 resistant strains. For all of these strains, MIC of 1 was in the range of 75–90  $\mu\text{M}$ . Our results suggest that both the active peptides (1 and 6) may adopt a constrained and compact folded structure, however, they do not adopt the true lasso structure as observed in MccJ25. The reduced activity of 1 and 6 compared to the native MccJ25 could be due to the loss of characteristic lasso conformation. The CD and resistance to proteases experiments suggest that the active peptides (1 and 6) do not fold into a lasso conformation, and peptide 1 displays antimicrobial activity by inhibition of target cell respiration. Finally, the synthetic peptide derivatives of MccJ25 display minimal toxicity to mammalian cells and act specifically on bacterial cells. This study paves the way for further exploration of chemical synthetic ways to develop potent derivatives of lasso structures peptides.

In addition to MccJ25 antimicrobial activity, studies have shown that MccJ25 can interact with mitochondrial membrane in isolated rat mitochondria causing a cascade of events which ends up causing apoptosis. Peptides capable of invading the mitochondria of mammalian cells, and triggering apoptosis have been employed in numerous studies directed at the development of new targeted therapeutics for cancer therapy.<sup>4-6</sup> So our aim was to explore the possibility of using MccJ25 as a potential anticancer agent. MTT cytotoxicity studies showed that MccJ25 did not cause any cytotoxicity when incubated with different panel of

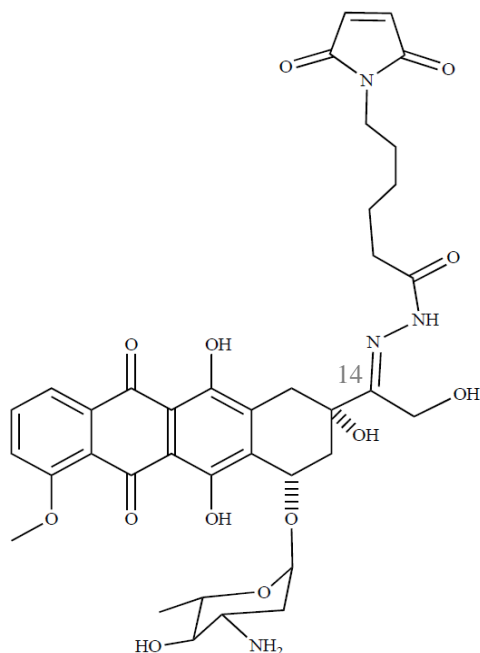
cell lines. So our hypothesis was that the diminished anticancer activity of MccJ25 is due to its inability to enter the cell, and conjugating MccJ25 to one of our cancer targeting peptides 18-4 would enhance its intracellular delivery as well as its cytotoxicity. This was addressed in **Chapter 6**; in this study an efficient synthetic approach was developed to conjugate the MccJ25 peptide to the carrier peptide 18-4. The conjugate showed *in vitro* improved cytotoxicity in different breast cancer cell lines, with very low toxicity to normal cells. RP-HPLC uptake studies showed that peptide 18-4 has dramatically enhanced MccJ25 uptake into human cancer cells. Apoptosis was the major mechanism for induction of cell death following exposure to conjugate. In conclusion, conjugation of MccJ25 to a peptidic carrier is a promising approach to enhance its cellular uptake and *in vitro* selectivity. As developing new anticancer drugs with a new mode of action is a prerequisite to face tumor resistance towards current anticancer therapy.

Overall, the work presented in this dissertation supports the use of synthetic peptides as a mean of developing novel therapeutics in cancer targeted therapy, and as antimicrobial therapy. By using peptide libraries and innovative design strategies to carry out structure–activity studies, we are confident that a wealth of peptide leads can be generated to be used for the development of new promising targeted delivery agents of therapeutics and diagnostics.

## 7.2. Future directions

The encouraging *in vitro* results for the ester peptide 18-4 Dox conjugate would stimulate its further testing *in vivo*. Calculating the tumor volume and mice survival rate are good prognostic indicators for the therapeutic efficacy of the conjugate in mice. In addition, the *in vivo* biodistribution experiments will detect the conjugate preferential tumor targeting compared to other normal tissues. This could be carried out in a mouse breast cancer model, where a fluorescently labeled peptide Dox conjugate is injected in mice followed by assessing the amount of fluorescence in the different isolated organs. Following the therapeutic efficacy testing, further bioavailability studies will be helpful to clarify if the conjugate is ready to be tested in the clinical arena which is our ultimate goal.

Similarly, for further optimization of peptide-Dox conjugates, other Dox peptide constructs can be synthesized and evaluated *in vivo*. For instance, an acid sensitive conjugate having hydrazone linkage between the peptide and the Dox through attachment at the carbonyl group at C14 can be synthesized. This acid sensitive conjugate is believed to be relatively stable in the physiological pH (blood), and capable of liberating the attached drug at low pH such as at tumor site or intracellularly in lysosome (pH 4-5).



Another avenue that needs to be explored is using our newly discovered peptides (peptide **5**, **Chapter 2**, and peptide **18-4**, **Chapter 3**) to construct a dual targeted delivery system (liposome, polymeric micelles) for drug delivery. Compared to using a single peptide decorated drug carriers, carriers bearing multiple tumor targeting peptides (dual targeting) display increased tumor specificity and interaction as well as tumor internalization which would in turn allows improving the total accumulation of drug in the tumor.<sup>7-9</sup> Therefore, our promising refined peptide sequences that were discovered in through the NGR peptide library screening (peptide 5, YNGRT), and the stable analogue of peptide p160 (peptide 18-4, WxEYAAQrFL) can be used to construct a dual targeting drug delivery system (micelle) for breast cancer targeted delivery. **(Figure 7.1)** This delivery system would target the tumor vasculature and tumor cells simultaneously, so enhance the active-targeting ability via targeting two receptors. This limits the ability of the cancer cells to escape cell death mediated by only one

receptor. This work will be done in collaboration with Dr. Afsaneh Lavasanifar, Faculty of Pharmacy, University of Alberta.

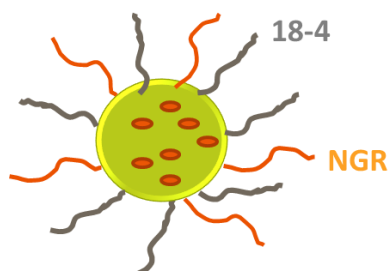


**Figure 7.1.** Dual targeting nanocarrier decorated with NGR peptide as well as p18-4 peptide.

In addition to the previously postulated future experiments, the generation of multivalent peptide ligands of peptide 18-4 to enhance its tumor binding affinity is highly encouraged. Monomeric peptide ligands showed efficient tumor targeting, but still they lack the high binding affinity to their receptors (micromolar range) due to the small size. One approach to compensate for the low binding strength is to attach many of peptide ligands to a single molecule to form a multivalent ligand. Researchers reported that synthesis of peptides in branched multimeric form results in molecules with improved targeting by preferentially binding to cells overexpressing the intended receptor.<sup>10,11</sup> There are two major modes by which multivalent ligands may improve binding: first, they can provide a second ligand moiety in close proximity to the first bound ligand moiety, improving the chances of the multivalent construct as a whole remaining bound to the cell; second, they can bridge multiple receptors, keeping the

multivalent construct tightly bound to the cell. In this context, for synthesizing more efficient targeting moiety based on peptide 18-4, multimeric peptide drug conjugates of peptide 18-4 can be designed to improve the tumor uptake/retention as well as the *in vivo* kinetics compared to monomeric peptide drug conjugates. This would result in improved tumor drug delivery and drug uptake in breast cancer *in vivo* models. This multimeric construct can be synthesized on the maleimido tetrameric core as reported.<sup>12</sup>

Another area that remains to be explored is to uncover the identity of the receptor for p160 peptide. This could be approached in several ways. First, the membrane fraction of the breast cancer cells MCF-7 could be harvested and run on a 2D protein gel. The biotin peptide of interest could be panned across these proteins, and then streptavidin-conjugated horseradish peroxidase (HRP-streptavidin) is added, which binds to the biotin-labeled peptide. The detected zones could be cut out of the gel and their identity determined using mass spectrometry. Identifying the receptor can also be done by using a peptide affinity column, where a peptide is synthesized onto an affinity resin, then an affinity chromatography was run with a breast cancer cell lysate to separate the desired protein of interest, then after its elution with concentrated peptide, the sequence is identified using mass spectrometry.<sup>13</sup> Also it would be interesting to confirm that the receptor for the newly identified sequences peptides 18-4 or 18-9 is the same receptor as p160. Identification of the receptor would be very interesting for further construction of chemically modified structures.

The promising anticancer activity results obtained from the microcin J25 peptide 18-4 conjugate against breast cancer cell lines, will allow for further *in vivo* studies to examine the conjugate antitumor efficacy and tumor selectivity in a mouse model. These studies will broaden the applicability of using proapoptotic peptides as anticancer agents. Therefore, employing these proapoptotic peptides in cancer therapy might be beneficial in chemo-sensitizing tumor cells, as well as overcome apoptosis resistance which is one of the major causes of chemotherapeutic treatment failure. Studies can be further expanded for conjugating MccJ25 to other cancer targeting peptide sequences that would target other tumor types.

Such above mentioned studies will certainly increase the potential use of cancer targeting peptides as well as apoptotic antimicrobial peptides in cancer therapy and diagnosis to establish efficient and reliable delivery of therapeutics into cancer cells.

### 7.3. References

- (1) Pasqualini, R.; Koivunen, E.; Ruoslahti, E. A peptide isolated from phage display libraries is a structural and functional mimic of an RGD-binding site on integrins *J. Cell Biol.* **1995**, *130*, 1189-1196.
- (2) Askoxylakis, V.; Zitzmann, S.; Mier, W.; Graham, K.; Krämer, S.; von Wegner, F.; Fink, R. H. A.; Schwab, M.; Eisenhut, M.; Haberkorn, U. Preclinical Evaluation of the Breast Cancer Cell-Binding Peptide, p160 *Clin. Cancer Res.* **2005**, *11*, 6705-6712.
- (3) Ahmed, S.; Mathews, A. S.; Byeon, N.; Lavasanifar, A.; Kaur, K. Peptide Arrays for Screening Cancer Specific Peptides *Anal. Chem.* **2010**, *82*, 7533-7541.
- (4) Ellerby, H. M.; Arap, W.; Ellerby, L. M.; Kain, R.; Andrusiak, R.; Rio, G. D.; Krajewski, S.; Lombardo, C. R.; Rao, R.; Ruoslahti, E.; Bredesen, D. E.; Pasqualini, R. Anti-cancer activity of targeted pro-apoptotic peptides *Nat. Med.* **1999**, *5*, 1032.
- (5) Law, B.; Quinti, L.; Choi, Y.; Weissleder, R.; Tung, C.-H. A mitochondrial targeted fusion peptide exhibits remarkable cytotoxicity *Mol. Cancer Ther.* **2006**, *5*, 1944-1949.
- (6) Mai, J. C.; Mi, Z.; Kim, S.-H.; Ng, B.; Robbins, P. D. A Proapoptotic Peptide for the Treatment of Solid Tumors *Cancer Res.* **2001**, *61*, 7709-7712.
- (7) Murase, Y.; Asai, T.; Katanasaka, Y.; Sugiyama, T.; Shimizu, K.; Maeda, N.; Oku, N. A novel DDS strategy, “dual-targeting”, and its application for antineovascular therapy *Cancer Lett.* **2010**, *287*, 165-171.
- (8) Kluza, E.; Jacobs, I.; Hectors, S. J. C. G.; Mayo, K. H.; Griffioen, A. W.; Strijkers, G. J.; Nicolay, K. Dual-targeting of  $\alpha\beta 3$  and galectin-1 improves the specificity of paramagnetic/fluorescent liposomes to tumor endothelium in vivo *J. Controlled Release* **2012**, *158*, 207-214.
- (9) Meng S., S. B., Li W., Ding Y., Tang L., Zhou W., Song Y., Li H., Zhou C. Enhanced antitumor effect of novel dual-targeted paclitaxel liposomes *Nanotechnology* **2010**, *21*, 415103.
- (10) Bracci, L.; Falciani, C.; Lelli, B.; Lozzi, L.; Runci, Y.; Pini, A.; De Montis, M. G.; Tagliamonte, A.; Neri, P. Synthetic Peptides in the Form of Dendrimers Become Resistant to Protease Activity *J. Biol. Chem.* **2003**, *278*, 46590-46595.

(11) Kiessling, L. L.; Gestwicki, J. E.; Strong, L. E. Synthetic Multivalent Ligands as Probes of Signal Transduction *Angew. Chem. Int. Ed* **2006**, *45*, 2348-2368.

(12) Li S, M. M., Lin M, Liu YH, Oyama T, Sun X, Brown KC Synthesis and characterization of a high-affinity  $\alpha v\beta 6$ -specific ligand for in vitro and in vivo applications *Mol. Cancer Ther.* **2009**, *8*, 1239-1249.

(13) Daxecker, H.; Raab, M.; Bernard, E.; Devocelle, M.; Treumann, A.; Moran, N. A peptide affinity column for the identification of integrin  $\alpha IIb$ -binding proteins *Anal. Biochem.* **2008**, *374*, 203-212.

## Appendix

- Figure A.1.** MALDI-TOF mass spectra  $[M+H]^+$  of FITC- $\beta$ -Ala-peptides 1, 5, 14, 21, 22, 34, and FITC- $\beta$ -Ala-43..... 284
- Figure A.2.** Analytical RP-HPLC chromatograms of the pure FITC- $\beta$ -ala-peptides 1, 5, 14, 21, 22, 34, and FITC- $\beta$ -Ala-43. Inset shows zoom-in for the peaks. The HPLC method used was 15-55% ACN/water in 35 min with a flow rate of 1 mL/min (Vydac C18 analytical column). ..... 286
- Table A.1.** Peptide degradation in the presence of human serum (A) and liver homogenate (B). ..... 287
- Table A.2.** Chemical shift assignments for peptide p160 in water and TFE, and peptide 18 in TFE/water (4:1). ..... 288
- Table A.3.** Structure calculation statistics for peptides p160 and 18. .... 290
- Figure A.3.** Solid phase peptide synthesis of FITC- $\beta$ A-18 or FITC-18..... 291
- Figure A.4.** Analytical RP-HPLC chromatograms of the pure FITC- $\beta$ -ala-peptides (18-1 - 18-10) and parent peptide 18 (FITC- $\beta$ -ala-18) in two solvent systems, namely, (A) IPA/water or solvent 1 and (B) acetonitrile/water or solvent 2. The HPLC method used for solvent 1 was 15-50% IPA/water in 35 min with a flow rate of 1 mL/min and for solvent 2 was 15-55% acetonitrile/water in 35 min with a flow rate of 1 mL/min (Vydac C18 analytical column). ..... 294
- Figure A.5.** MALDI-TOF of  $\beta$ -ala-peptides showing  $[M+H]^+$  peaks. .... 297
- Figure A.6.** Fluorescence of the cells observed after uptake of the FITC-labeled peptides using flow cytometry. The FITC-labeled peptides ( $10^{-5}$  mol/L) were incubated with breast cancer cell lines MDA-MB-435, MCF-7, and MDA-MB-231, or control cell lines MCF-10A and HUVEC for 30 min prior to FACS analysis. Bars represent the percent number of fluorescent cells bound with the peptide as mean (SD of data obtained from three separate experiments). ..... 298
- Figure A.7.** FACS analysis for the competitive binding of the peptides 18-4 (A) and 18-9 (B) to MDA-MB-435 cells, showing autofluorescence of MDA-MB-435 cells (grey), fluorescence (blue) of the cells after incubation with  $10^{-5}$  mol/L FITC-18-4 (A) or FITC-18-9 (B), and fluorescence (red) of cells after

incubation with the FITC-peptides in the presence of 50-fold excess unlabeled 18-4 (A) or 18-9 (B). Experiments were done using Beckman Coulter QUANTA SC flow cytometer. .... 299

**Table A.4.** Cytotoxicity of conjugates 1 and 2 versus free Dox on different cancer cell lines after 2 h treatment then further 48 hr incubation. Mean IC<sub>50</sub> values from three experiments in comparison with doxorubicin. .... 300

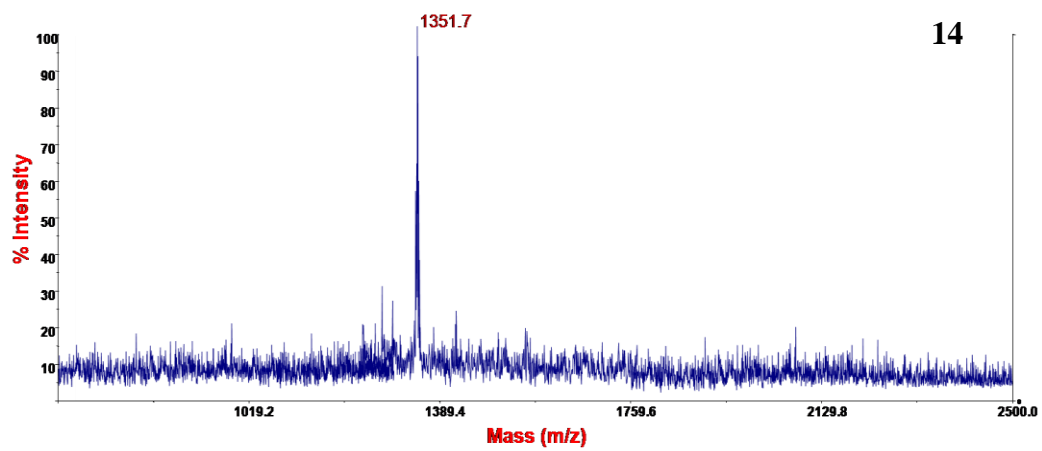
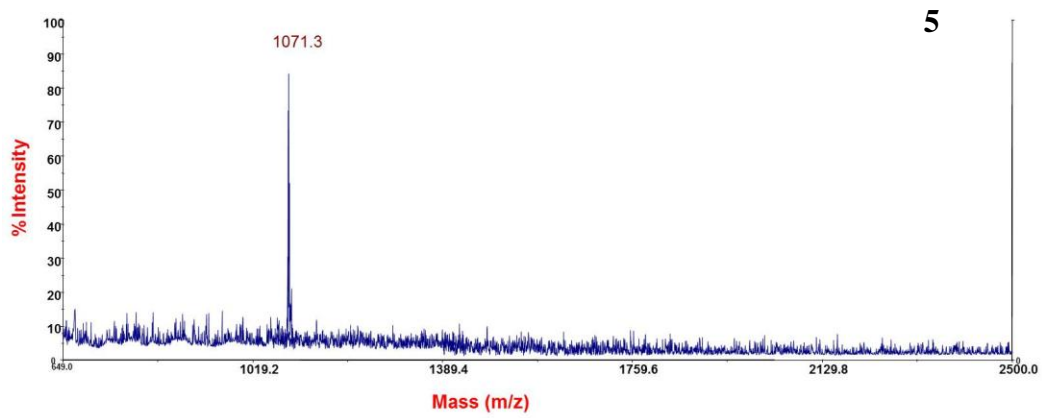
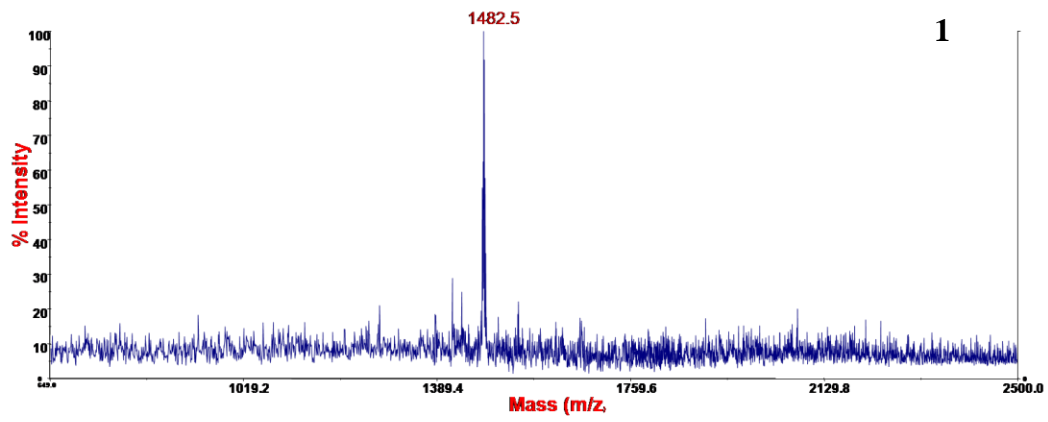
**Figure A.8.** MALDI-TOF mass spectra. .... 302

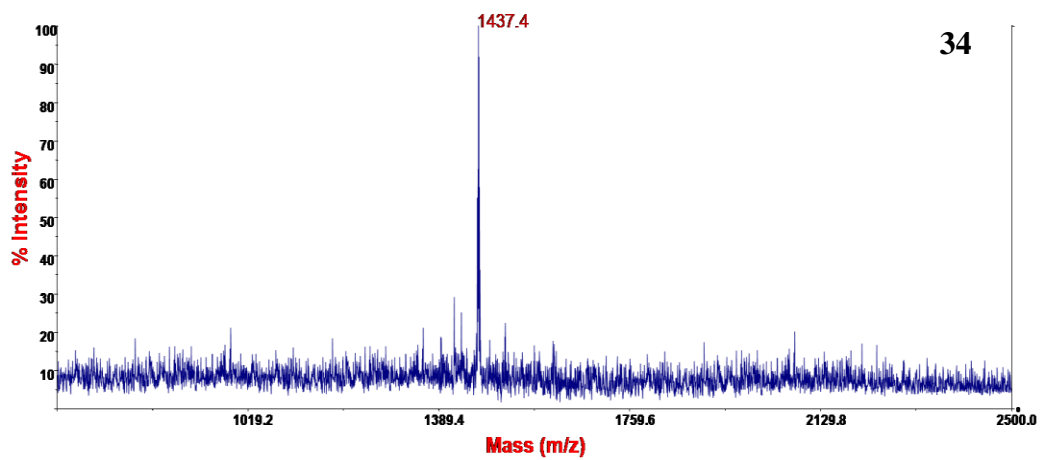
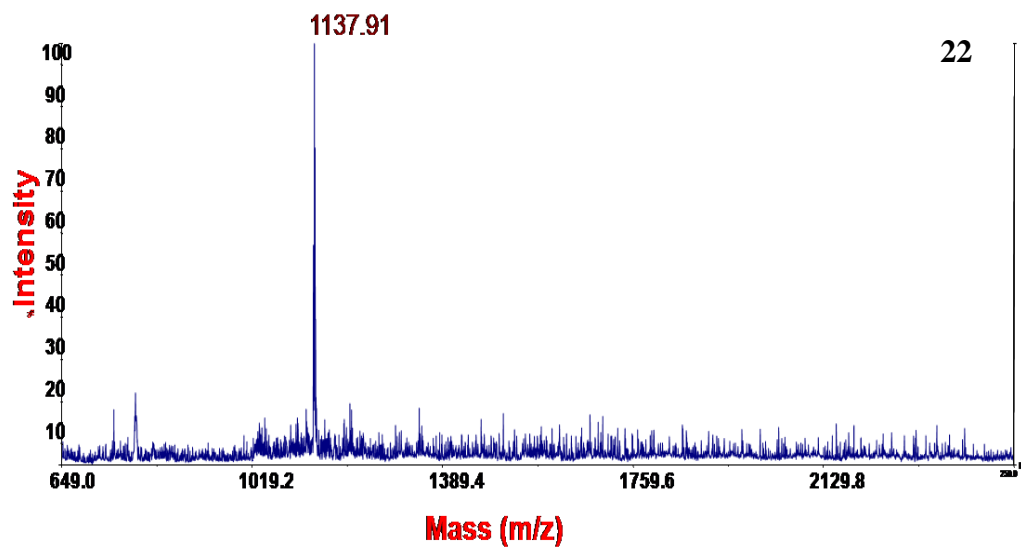
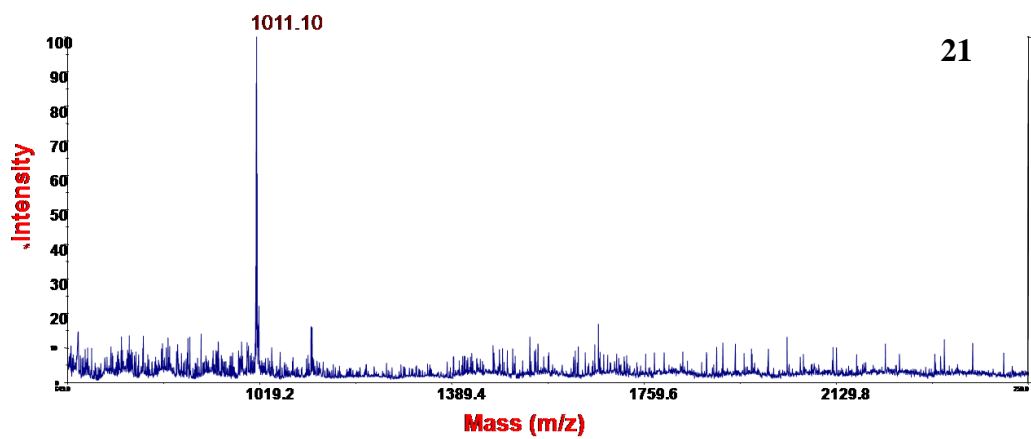
**Figure A.9.** Analytical RP-HPLC chromatograms of pure conjugates 1 and 2. The HPLC method used was 15-55% ACN/water in 35 min then till 100 in 15 min with a flow rate of 1 mL/min (Vydac C18 analytical column). .... 303

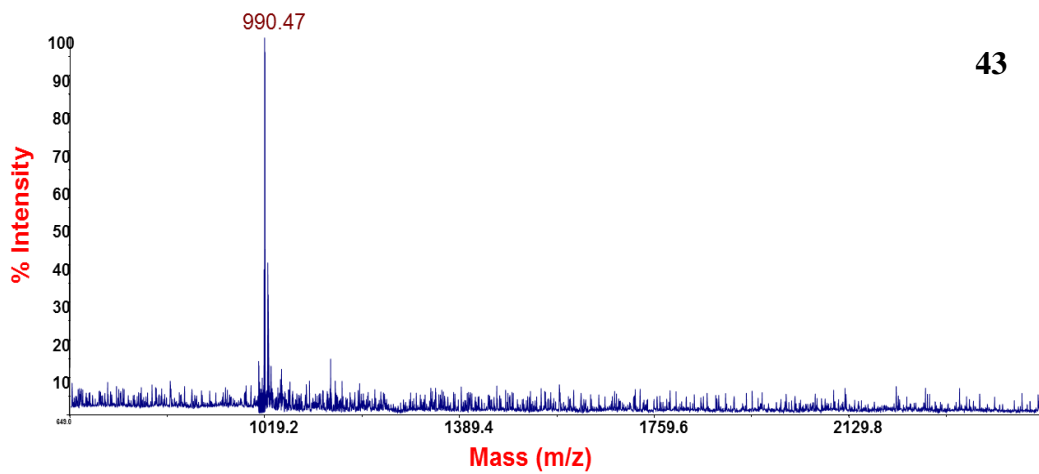
**Figure A.10.** Analytical RP-HPLC chromatograms of the pure peptides 1-6. The HPLC method used was 15-55% IPA/water in 40 min with a flow rate of 1 mL/min (Vydac C18 analytical column). .... 304

**Figure A.11.** MALDI-TOF-MS of pure peptides 1-6 and MccJ25 showing the [M+H]<sup>+</sup> as major peaks. .... 305

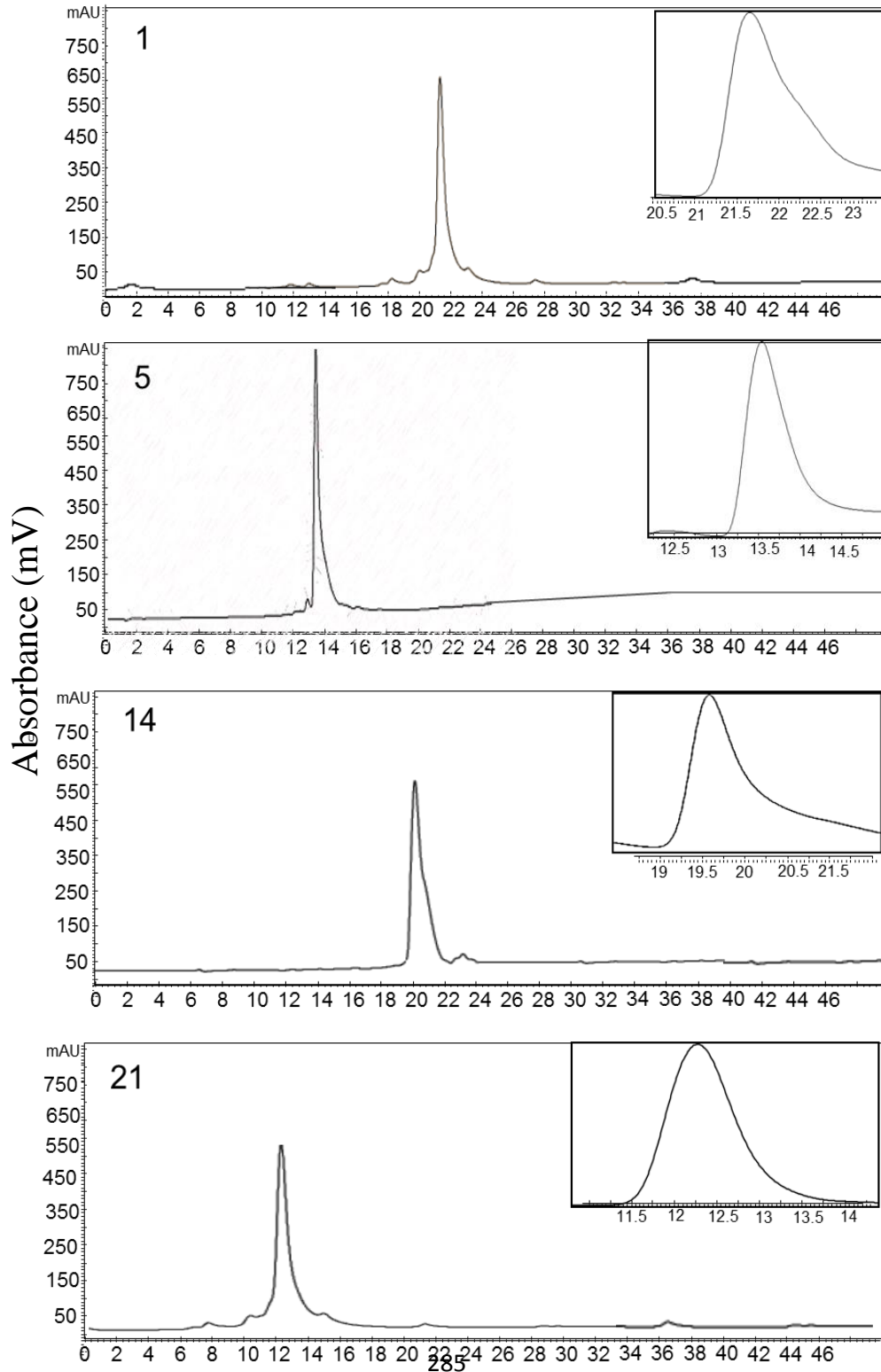
**Figure A.12.** Cell viability as a function of peptide concentration. MccJ25 and peptide analogues 1-6 were incubated with MDA-MB-435 (top) or MCF-7 (bottom) cells for 24 h at 37 °C. .... 306







**Figure A.1.** MALDI-TOF mass spectra  $[M+H]^+$  of FITC- $\beta$ -Ala-peptides 1, 5, 14, 21, 22, 34, and FITC- $\beta$ -Ala-43.



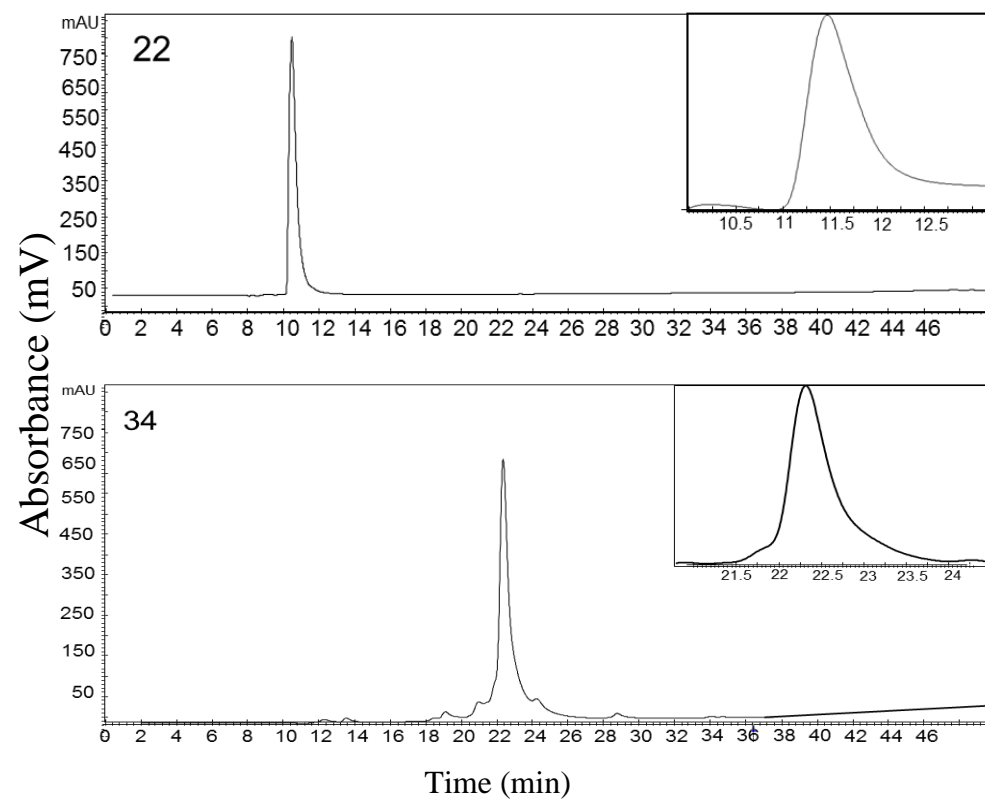


**Figure A.2.** Analytical RP-HPLC chromatograms of the pure FITC- $\beta$ -ala-peptides 1, 5, 14, 21, 22, 34, and FITC- $\beta$ -Ala-43. Inset shows zoom-in for the peaks. The HPLC method used was 15-55% ACN/water in 35 min with a flow rate of 1 mL/min (Vydac C18 analytical column).

**Table A.1.** Peptide degradation in the presence of human serum (A) and liver homogenate (B).

**(A)**

Time (h)	% Intact Peptide <sup>a</sup>			
	<b>18</b>	<b>18-4</b>	<b>18-9</b>	<b>18-10</b>
0	100	100	100	100
0.5	5	99.86	99.52	97.85
1	0	99.71	98.33	98.6
5	0	99.63	98.41	97.91
24	0	99.68	98.22	99.7

<sup>a</sup>Percent intact peptide was calculated based on the area under the HPLC peak for the parent peptide.

**(B)**

Time (min/h)	% Intact Peptide <sup>a</sup>			
	<b>18</b>	<b>18-4</b>	<b>18-9</b>	<b>18-10</b>
0	100	100	100	100
5 min	35	98.35	100.2	98.8
15 min	3	99.6	99.54	99.6
30 min	0	98.36	97.86	99.12
1 h	0	97.91	95.65	100.4
6 h	0	98.25	98.33	97.5
24 h	0	100.3	97.96	98.31
48 h	0	97.5	100.56	99.56

<sup>a</sup>Percent intact peptide was calculated based on the area under the HPLC peak for the parent peptide.

**Table A.2.** Chemical shift assignments for peptide p160 in water and TFE, and peptide 18 in TFE/water (4:1).

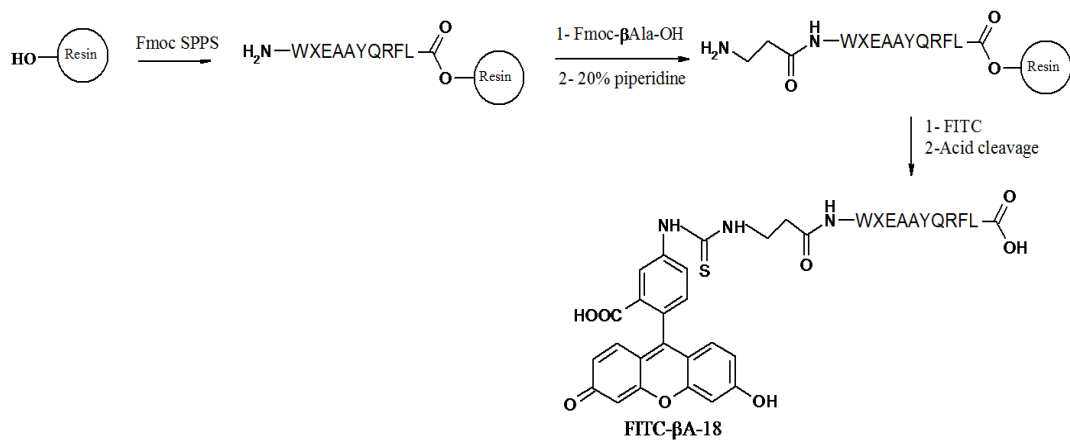
P160 Chemical Shifts, H <sub>2</sub> O, 15°C, referenced to H <sub>2</sub> O at 4.868 ppm				
Residue	NH	H $\alpha$	H $\beta$	Other
Val 1	-	4.13	2.06	$\gamma$ CH <sub>3</sub> 0.87, 1.02
Pro 2	-	4.48	1.90, 2.30	$\gamma$ CH <sub>2</sub> 1.99, 2.00, $\delta$ CH <sub>2</sub> 3.72, 3.54
Trp 3	8.16	4.58	3.30, 3.21	2H 7.22, 4H 7.50, 5H 7.26, 6H 7.16, 7H 7.61, NH 10.25
Nle 4	7.58	4.17	1.44, 1.56	$\gamma$ CH <sub>2</sub> 1.08, $\delta$ CH <sub>2</sub> 1.19, $\epsilon$ CH <sub>3</sub> 0.80
Glu 5	8.12	4.29	1.86, 1.99	$\gamma$ CH <sub>2</sub> 2.29
Pro 6	-	4.28	1.78, 2.23	$\gamma$ CH <sub>2</sub> 2.0, $\delta$ CH <sub>2</sub> 3.71, 3.79
Ala 7	8.49	4.21	1.30	
Tyr 8	7.99	4.51	3.01	2,6H 7.09, 3,5H 6.81
Gln 9	8.10	4.14	1.89, 1.84	$\gamma$ CH <sub>2</sub> 2.15, $\delta$ NH <sub>2</sub> 7.50, 6.89
Arg 10	8.11	4.19	1.63	$\gamma$ CH <sub>2</sub> 1.44, $\delta$ CH <sub>2</sub> 3.11, $\epsilon$ NH 7.17
Phe 11	8.29	4.68	3.24, 2.95	2,6H 7.28, 3,5H 7.33
Leu 12	7.85	4.29	1.58	$\gamma$ CH 1.58, $\delta$ CH <sub>3</sub> 0.90, 0.86
P160 Chemical Shifts, TFE, 15°C, referenced to TFE at 3.88 ppm				
Residue	NH	H $\alpha$	H $\beta$	Other
Val 1	-	3.83	1.23	$\gamma$ CH <sub>3</sub> 0.46, 0.85
Pro 2	-	4.33	2.06, 2.34	$\gamma$ CH <sub>2</sub> 2.06, 2.17, $\delta$ CH <sub>2</sub> 3.38, 3.56
Trp 3	6.71	4.68	3.28, 3.48	2H 7.09, 4H 7.50, 5H 7.32, 6H 7.22, 7H 7.59, NH 9.41
Nle 4	6.94	4.46	1.43	$\gamma$ CH <sub>2</sub> 1.76, $\delta$ CH <sub>2</sub> 1.13, $\epsilon$ CH <sub>3</sub> 0.94
Glu 5	7.43	4.54	2.06, 2.14	$\gamma$ CH <sub>2</sub> 2.52
Pro 6	-	4.31	1.81,2.30	$\gamma$ CH <sub>2</sub> 2.03,2.09, $\delta$ CH <sub>2</sub> 3.65, 3.78
Ala 7	7.41	4.15	1.45	

Tyr 8	7.52	4.49	3.20	2,6H 7.10, 3,5H 6.84
Gln 9	7.98	4.14	2.08, 2.14	$\gamma$ CH <sub>2</sub> 2.42, $\delta$ NH <sub>2</sub> 7.09, 6.14
Arg 10	7.52	4.15	1.70	$\gamma$ CH <sub>2</sub> 1.35, 1.45, $\delta$ CH <sub>2</sub> 3.06, $\epsilon$ NH 6.66
Phe 11	7.66	4.70	3.03, 3.30	2,6H 7.30, 3,5H 7.24
Leu 12	7.56	4.50	1.73	$\gamma$ CH 1.69, $\delta$ CH <sub>3</sub> 0.96

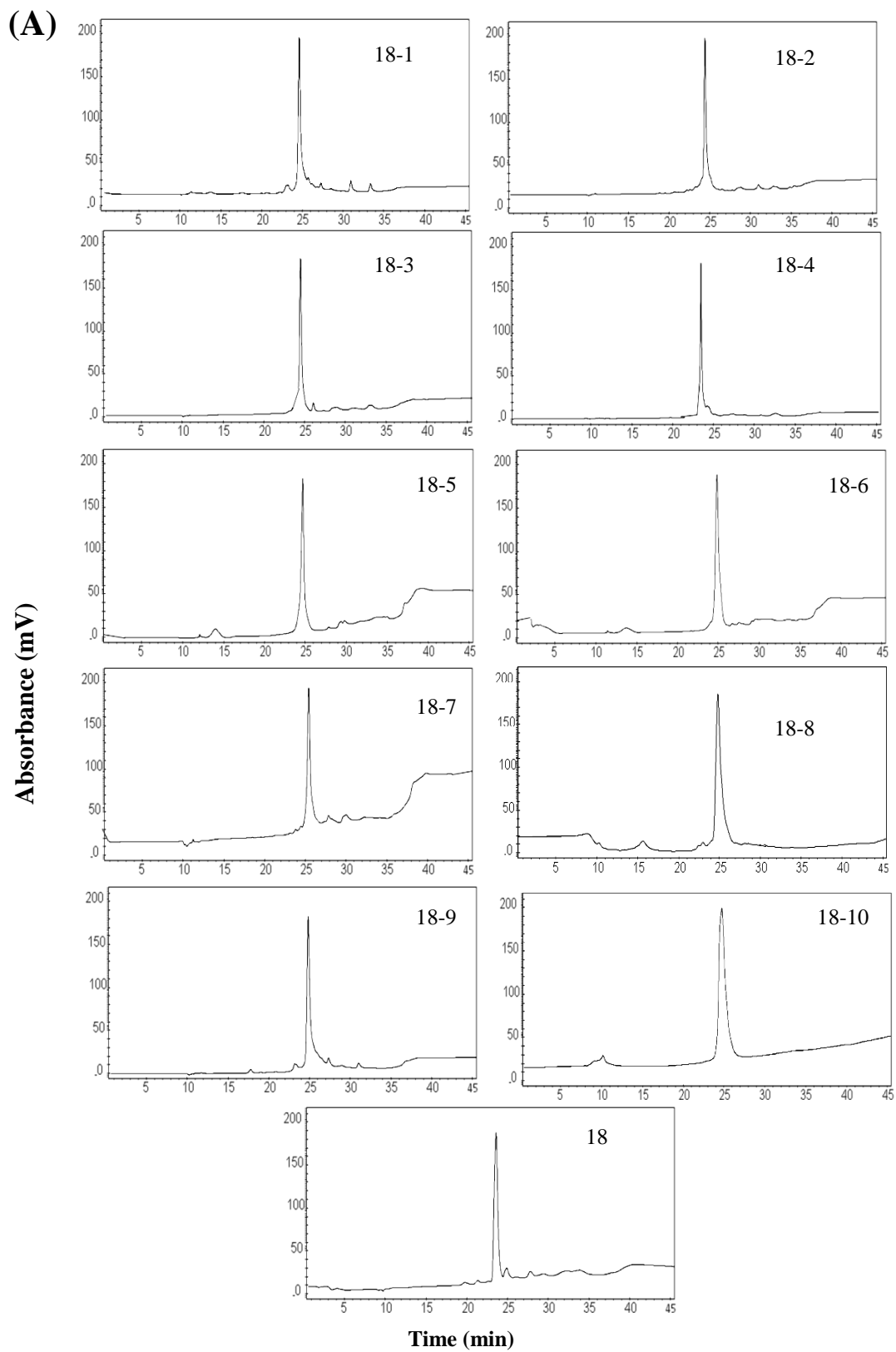
Peptide <b>18</b> Chemical Shifts, 80% TFE, 20% H <sub>2</sub> O 15°C, referenced to TFE at 3.88 ppm				
Residue	NH	H $\alpha$	H $\beta$	Other
Trp 1	-	4.32	3.41, 3.52	2H 7.28, 4H 7.47, 5H 7.24, 6H 7.15, 7H 7.63, NH 9.74
Nle 2	7.89	3.98	1.50, 1.71	$\gamma$ CH <sub>2</sub> 0.96, $\delta$ CH <sub>2</sub> 1.22, $\epsilon$ CH <sub>3</sub> 0.82
Glu 3	8.97	4.22	2.03, 1.96	$\gamma$ CH <sub>2</sub> 2.41
Ala 4	7.82	4.10	1.39	
Ala 5	7.76	4.22	1.38	
Tyr 6	7.55	4.44	3.07, 3.12	2,6H 7.09, 3,5H 6.81
Gln 7	7.77	4.10	2.04	$\gamma$ CH <sub>2</sub> 2.23, 2.30, $\delta$ NH <sub>2</sub> 7.14, 6.38
Arg 8	7.66	4.18	1.666	$\gamma$ CH <sub>2</sub> 1.35, 1.43, $\delta$ CH <sub>2</sub> 3.05, $\epsilon$ NH 7.01
Phe 9	7.77	4.69	2.98, 3.28	2,6H 7.28, 3,5H 7.21
Leu 10	7.50	4.14	1.66	$\gamma$ CH 1.72, $\delta$ CH <sub>3</sub> 0.89, 0.91

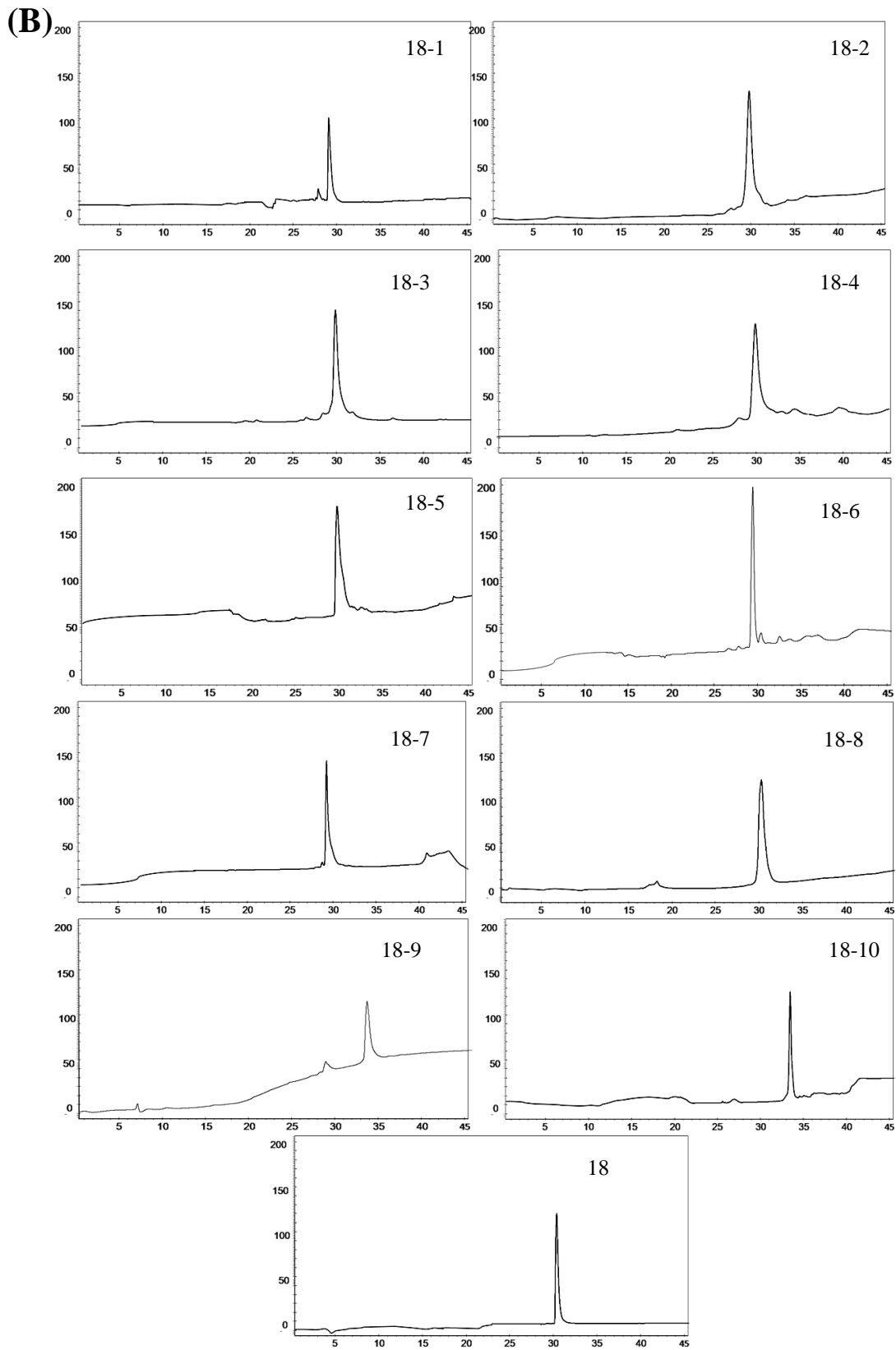
**Table A.3.** Structure calculation statistics for peptides p160 and 18.

	<b>P160 in H<sub>2</sub>O</b>	<b>P160 in TFE</b>	<b>P18 in TFE/H<sub>2</sub>O (8:2)</b>
No. of NOE upper distance limits	109	175	176
Intra-residue	41	53	55
Sequential	57	71	72
Medium range (i to i-2 or i+3)	11	51	49
Long range (i to i+4)	0	7	13
Final CYANA structures			
CYANA target function	$6.0 \times 10^{-2} \pm 1.74 \times 10^{-3} \text{ \AA}^2$	$0.13 \pm 0 \text{ \AA}^2$	$0.21 \pm 2.9 \times 10^{-2} \text{ \AA}^2$
Average backbone RMSD to mean	$1.81 \pm 0.47 \text{ \AA}$ (1-12)	$0.41 \pm 0.10 \text{ \AA}$ (1-12)	$0.61 \pm 0.36 \text{ \AA}$ (1-10)
Average heavy atom RMSD to mean	$3.10 \pm 0.53 \text{ \AA}$ (1-12)	$0.82 \pm 0.10 \text{ \AA}$ (1-12)	$1.32 \pm 0.64 \text{ \AA}$ (1-10)
Distance restraint violations	1	0	0

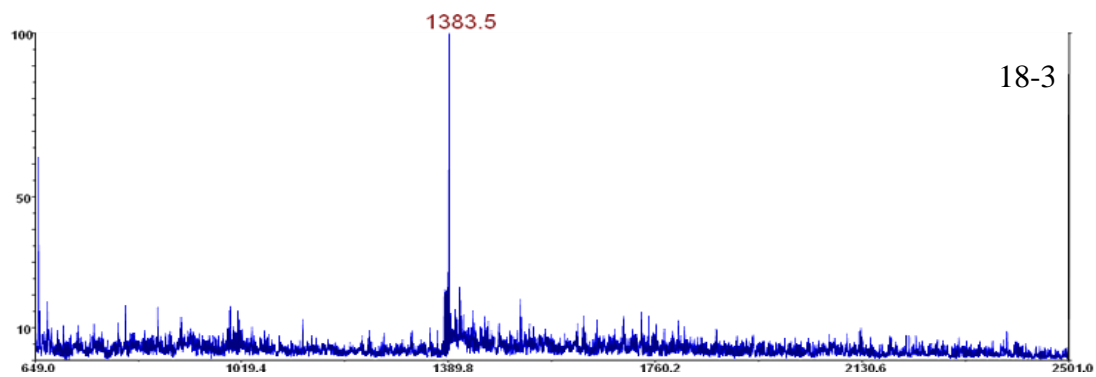
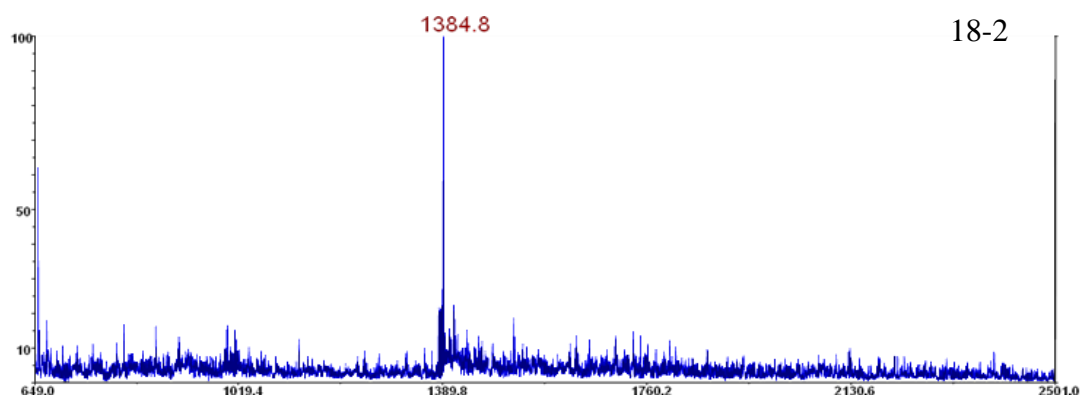
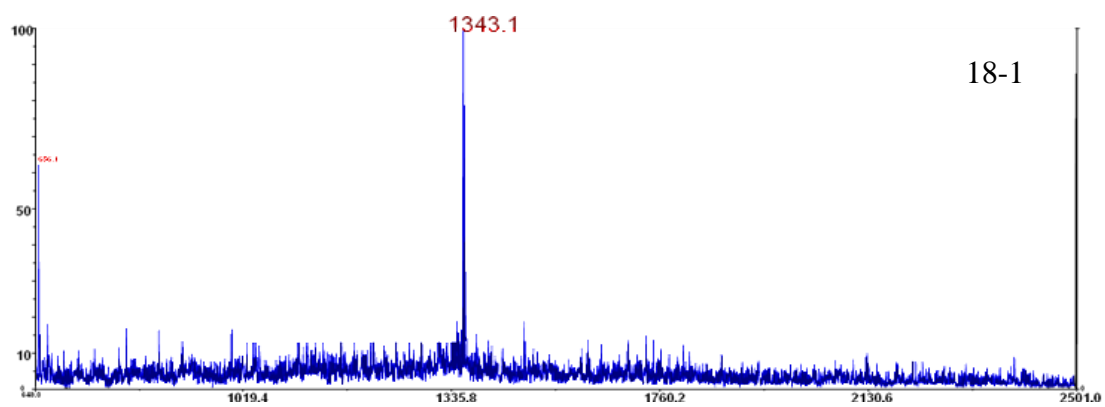


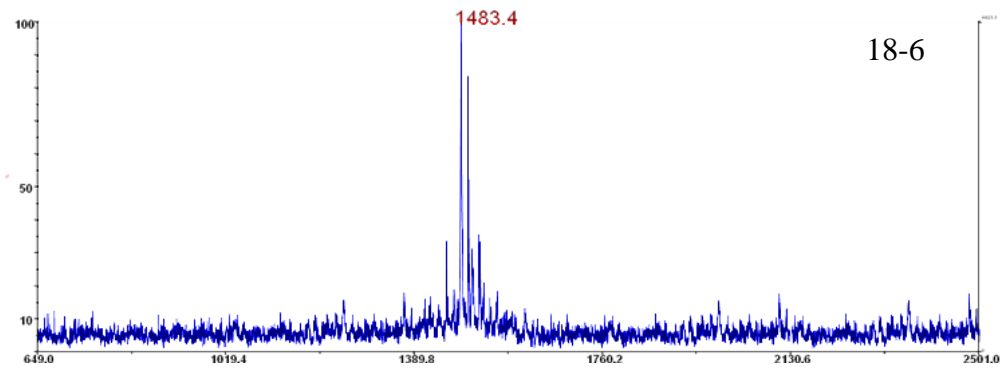
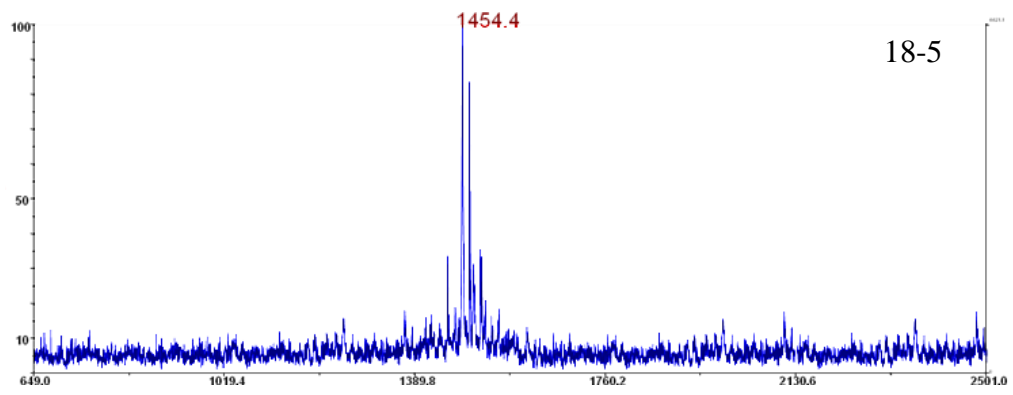
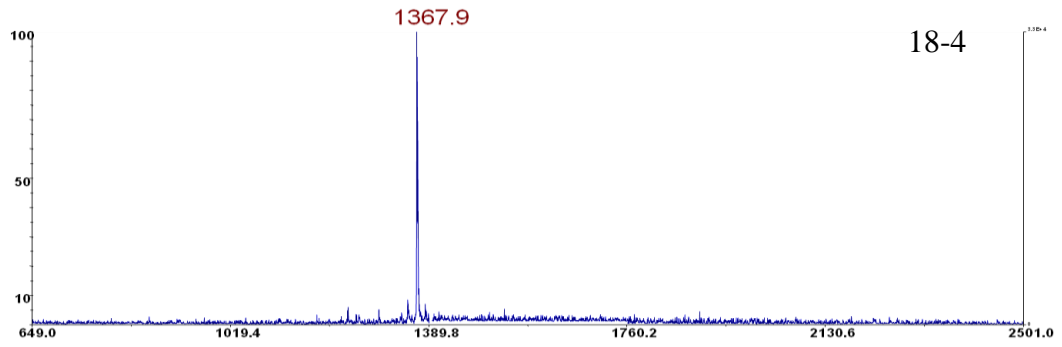
**FigureA.3.** Solid phase peptide synthesis of FITC-βA-18 or FITC-18.

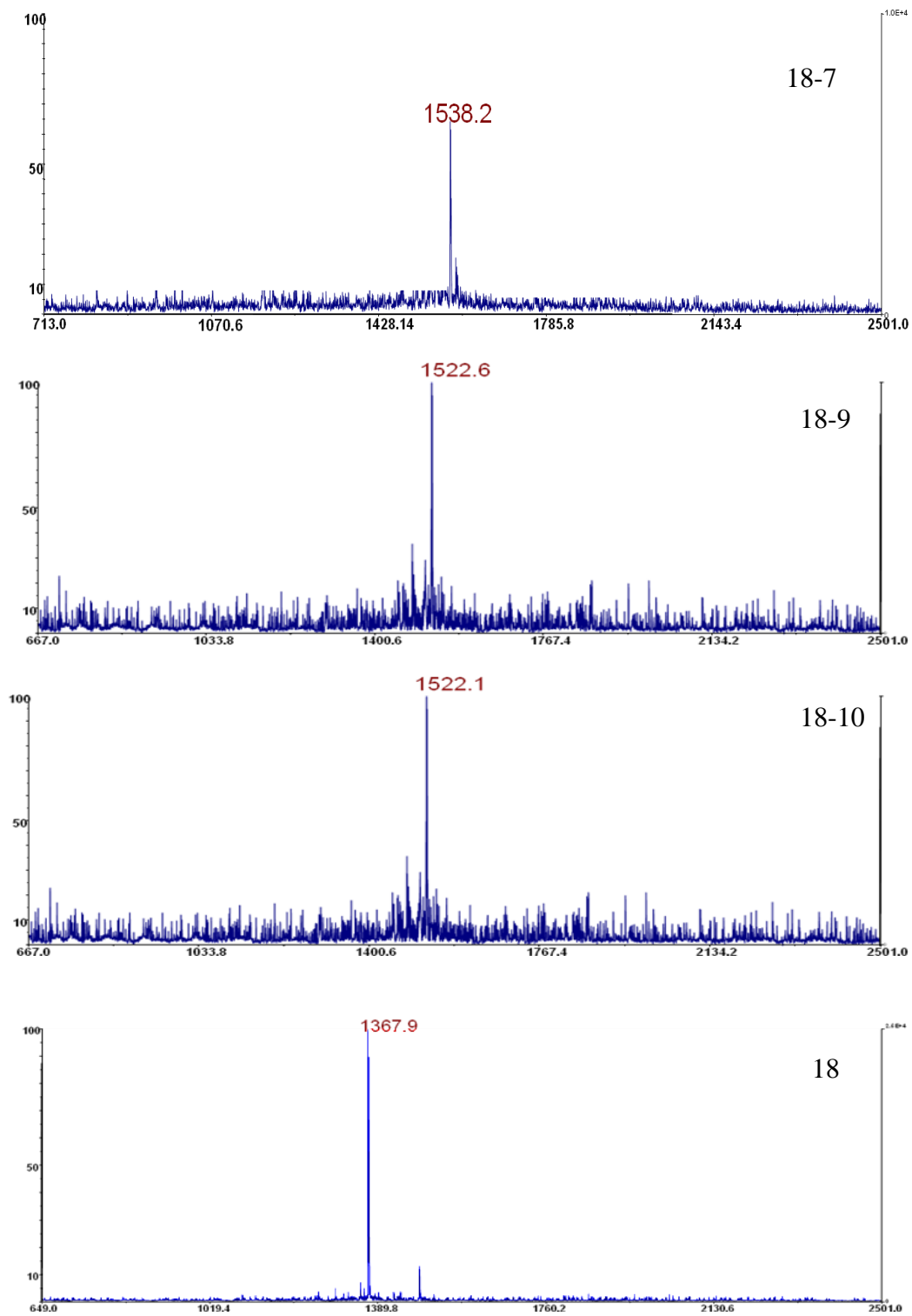




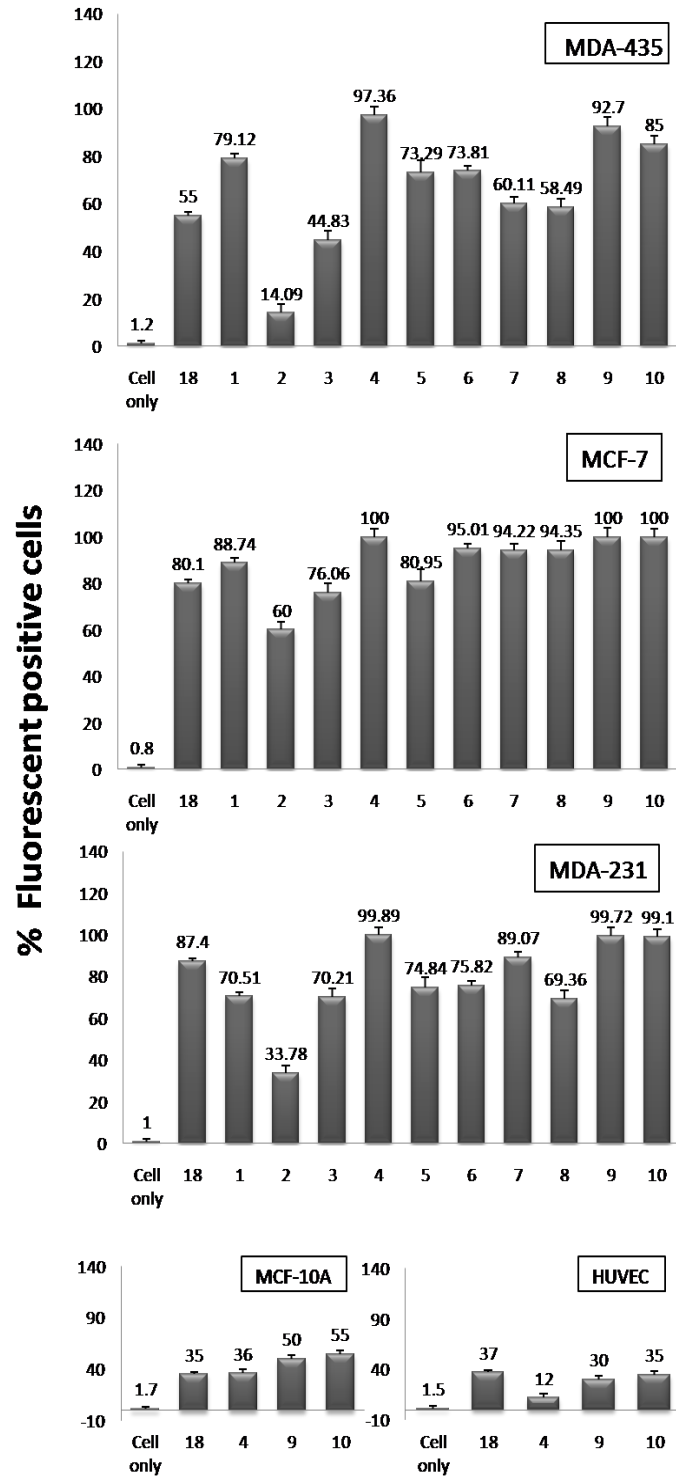
**Figure A.4.** Analytical RP-HPLC chromatograms of the pure FITC- $\beta$ -ala-peptides (18-1 - 18-10) and parent peptide 18 (FITC- $\beta$ -ala-18) in two solvent systems, namely, (A) IPA/water or solvent 1 and (B) acetonitrile/water or solvent 2. The HPLC method used for solvent 1 was 15-50% IPA/water in 35 min with a flow rate of 1 mL/min and for solvent 2 was 15-55% acetonitrile/water in 35 min with a flow rate of 1 mL/min (Vydac C18 analytical column).





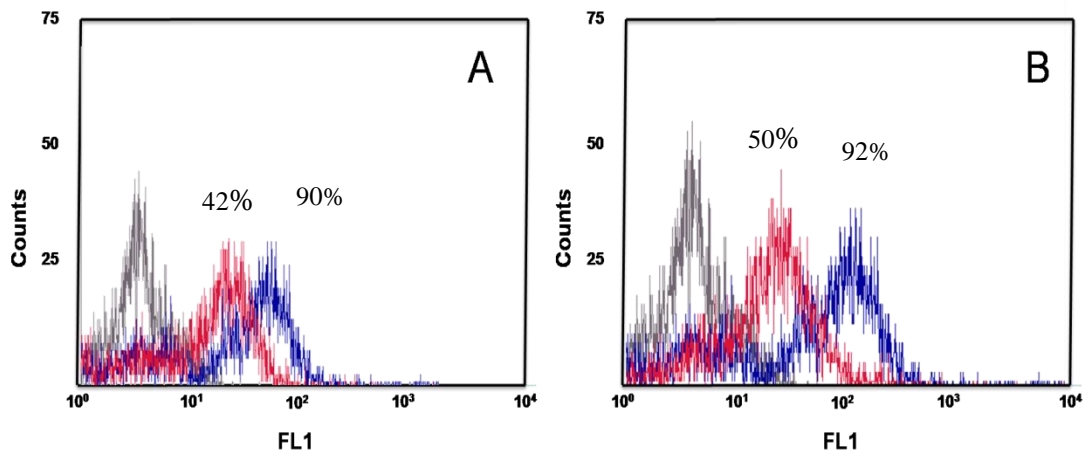


**Figure A.5.** MALDI-TOF of  $\beta$ -ala-peptides showing  $[M+H]^+$  peaks.



**Figure A.6.** Fluorescence of the cells observed after uptake of the FITC-labeled peptides using flow cytometry. The FITC-labeled peptides ( $10^{-5}$  mol/L) were incubated with breast cancer cell lines MDA-MB-435, MCF-7, and MDA-MB-

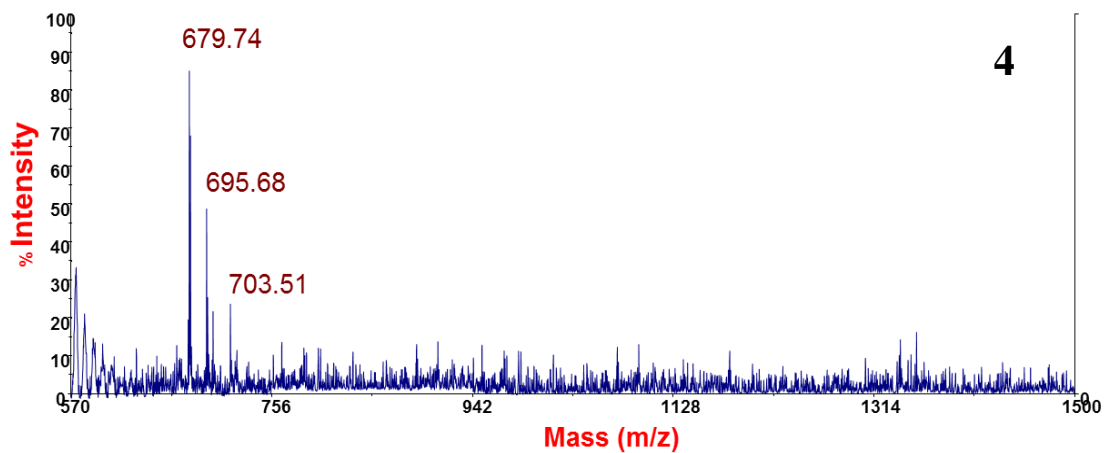
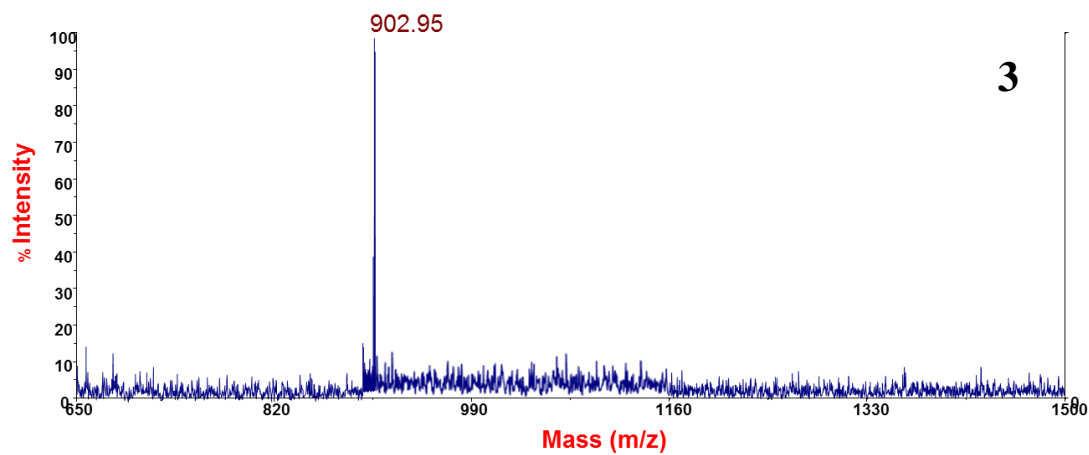
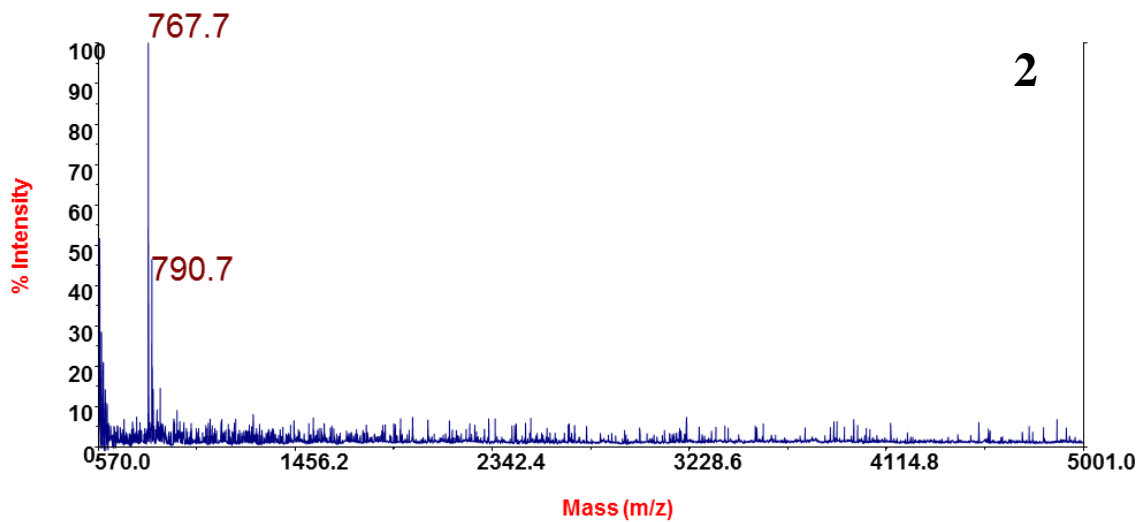
231, or control cell lines MCF-10A and HUVEC for 30 min prior to FACS analysis. Bars represent the percent number of fluorescent cells bound with the peptide as mean (SD of data obtained from three separate experiments).



**Figure A.7.** FACS analysis for the competitive binding of the peptides 18-4 (A) and 18-9 (B) to MDA-MB-435 cells, showing autofluorescence of MDA-MB-435 cells (grey), fluorescence (blue) of the cells after incubation with 10<sup>-5</sup> mol/L FITC-18-4 (A) or FITC-18-9 (B), and fluorescence (red) of cells after incubation with the FITC-peptides in the presence of 50-fold excess unlabeled 18-4 (A) or 18-9 (B). Experiments were done using Beckman Coulter QUANTA SC flow cytometer.

**Table A.4.** Cytotoxicity of conjugates 1 and 2 versus free Dox on different cancer cell lines after 2 h treatment then further 48 hr incubation. Mean IC<sub>50</sub> values from three experiments in comparison with doxorubicin.

Treatments	Cell lines IC <sub>50</sub> ± SD (μM)				
	MCF-7	MDA-MB-435	MDA-MB-435-MDR	MCF-10A	HUVEC
<b>Free Dox</b>	5.5±0.6	3.6±0.4	45±3.5	12±1.8	15.5±0.7
<b>Conjugate 1</b>	9.6±1.2	8.7±1.3	12.5± 1.6	80±7.2	>100
<b>Conjugate 2</b>	48.3±5.1	55.4±2.5	69.7±8.1	>100	>100



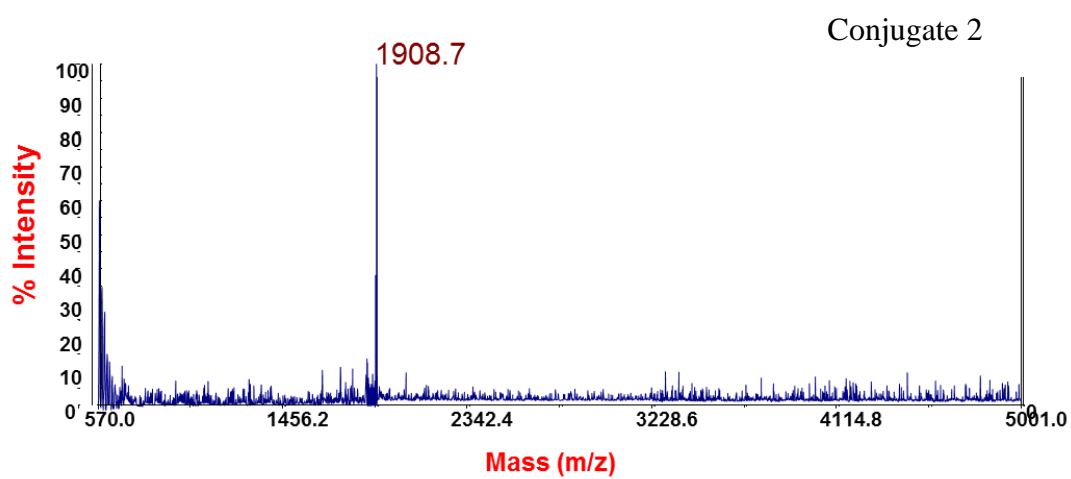
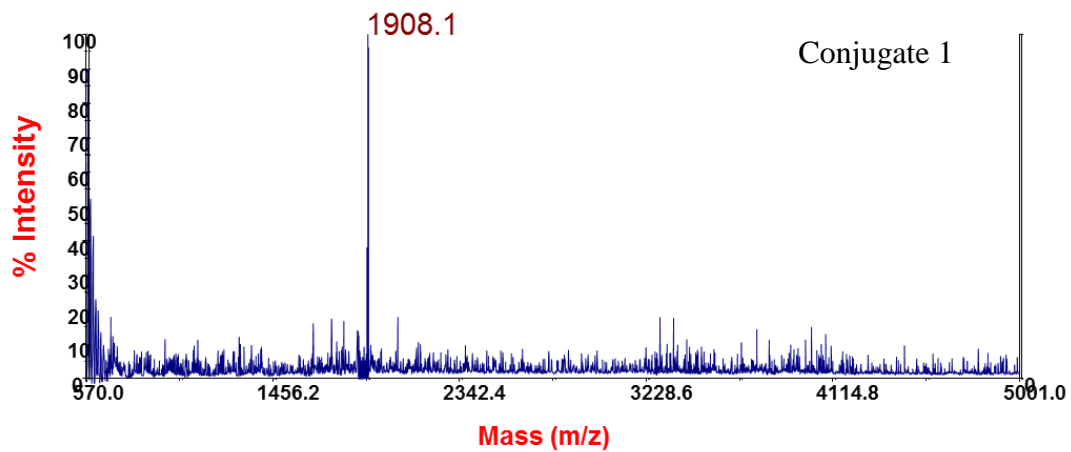
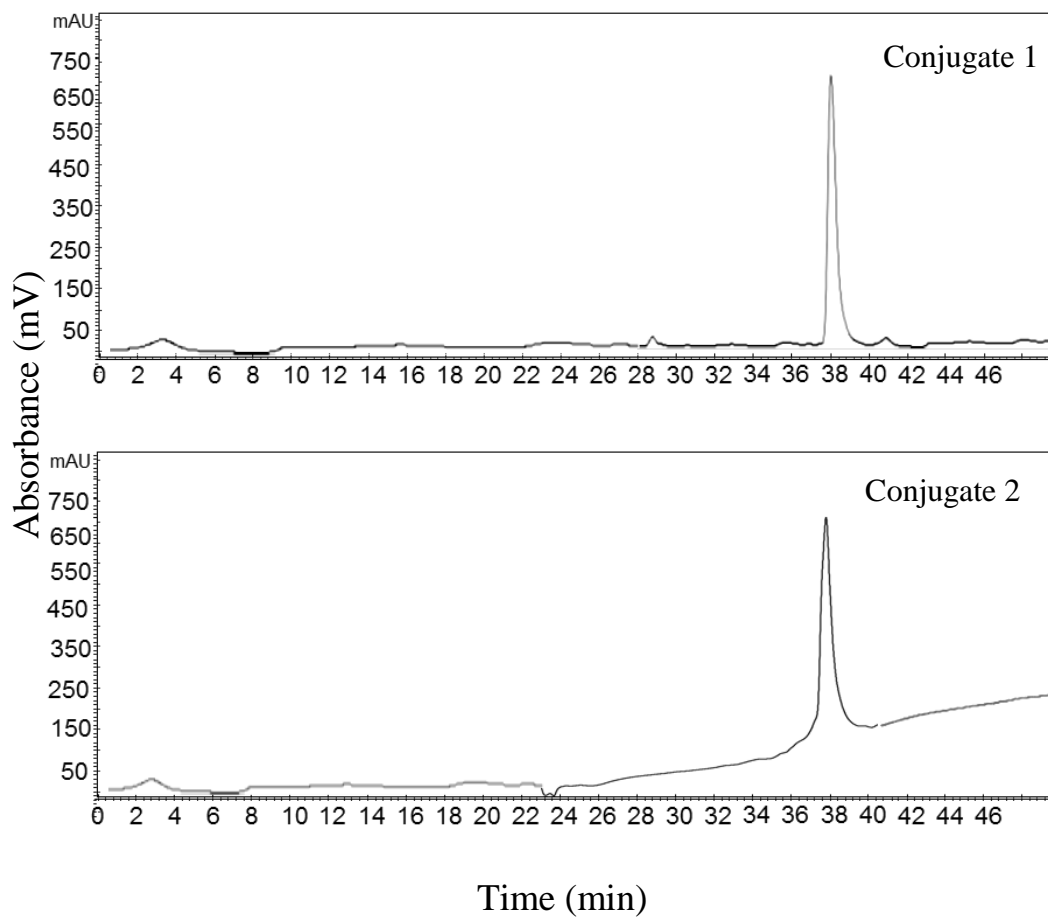
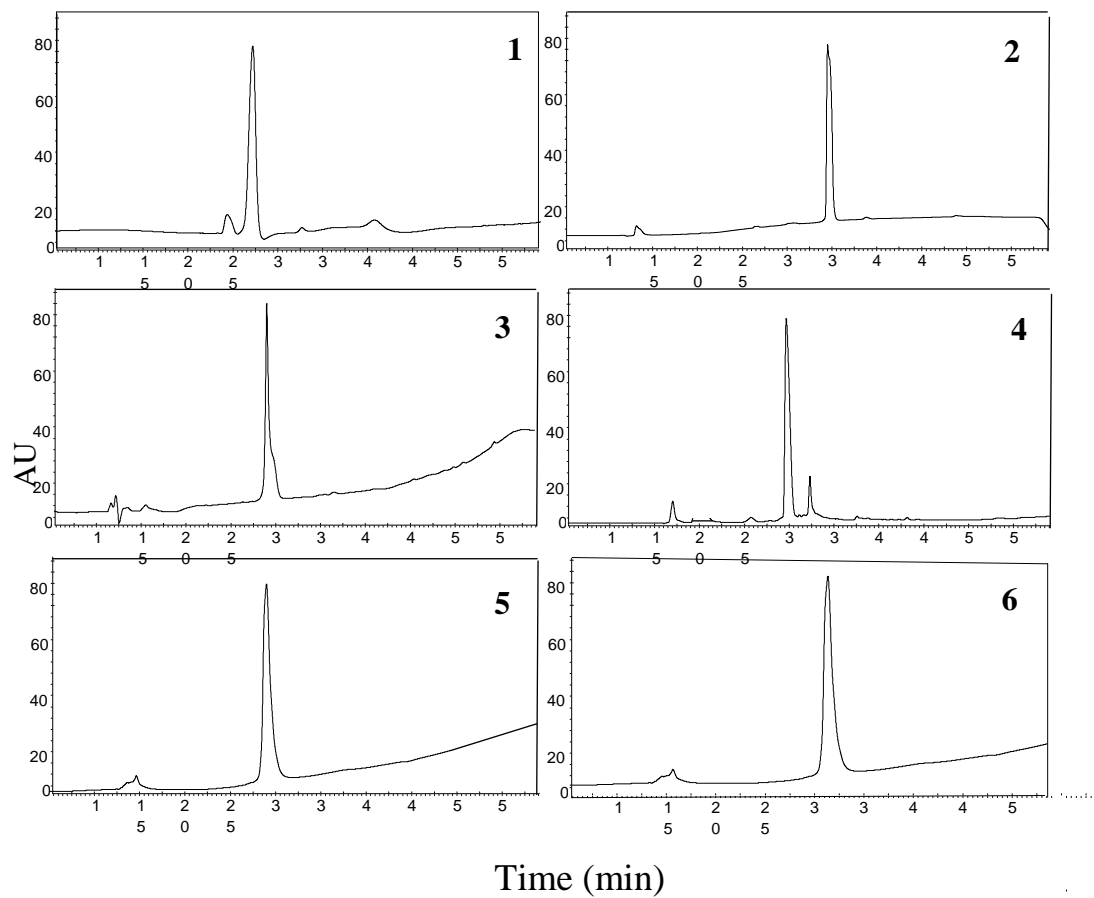


Figure A.8. MALDI-TOF mass spectra.



**Figure A.9.** Analytical RP-HPLC chromatograms of pure conjugates 1 and 2. The HPLC method used was 15-55% ACN/water in 35 min then till 100 in 15 min with a flow rate of 1 mL/min (Vydac C18 analytical column).



**Figure A.10.** Analytical RP-HPLC chromatograms of the pure peptides 1-6. The HPLC method used was 15-55% IPA/water in 40 min with a flow rate of 1 mL/min (Vydac C18 analytical column).

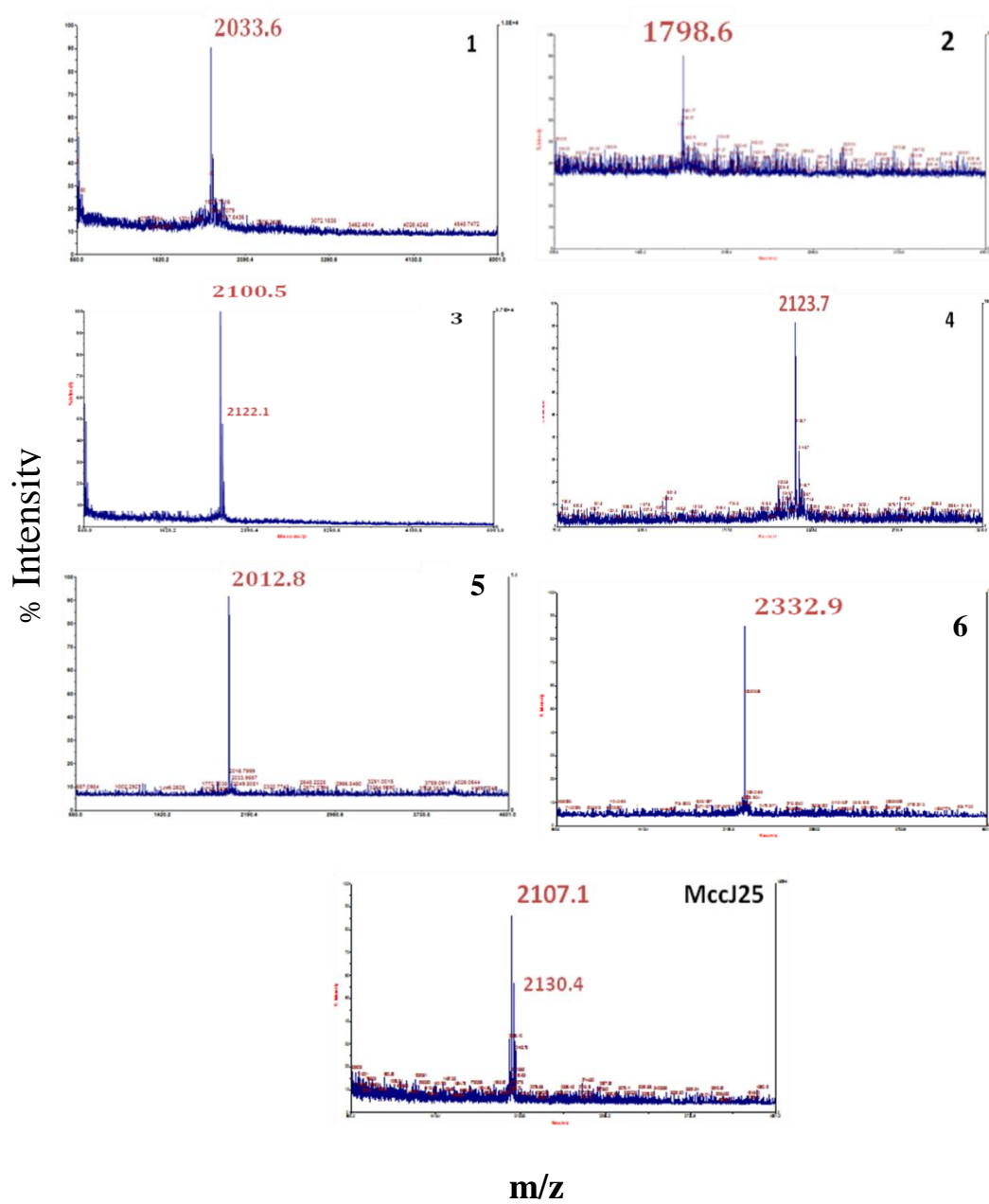


**Figure A.11.** MALDI-TOF-MS of pure peptides 1-6 and MccJ25 showing the  $[M+H]^+$  as major peaks.

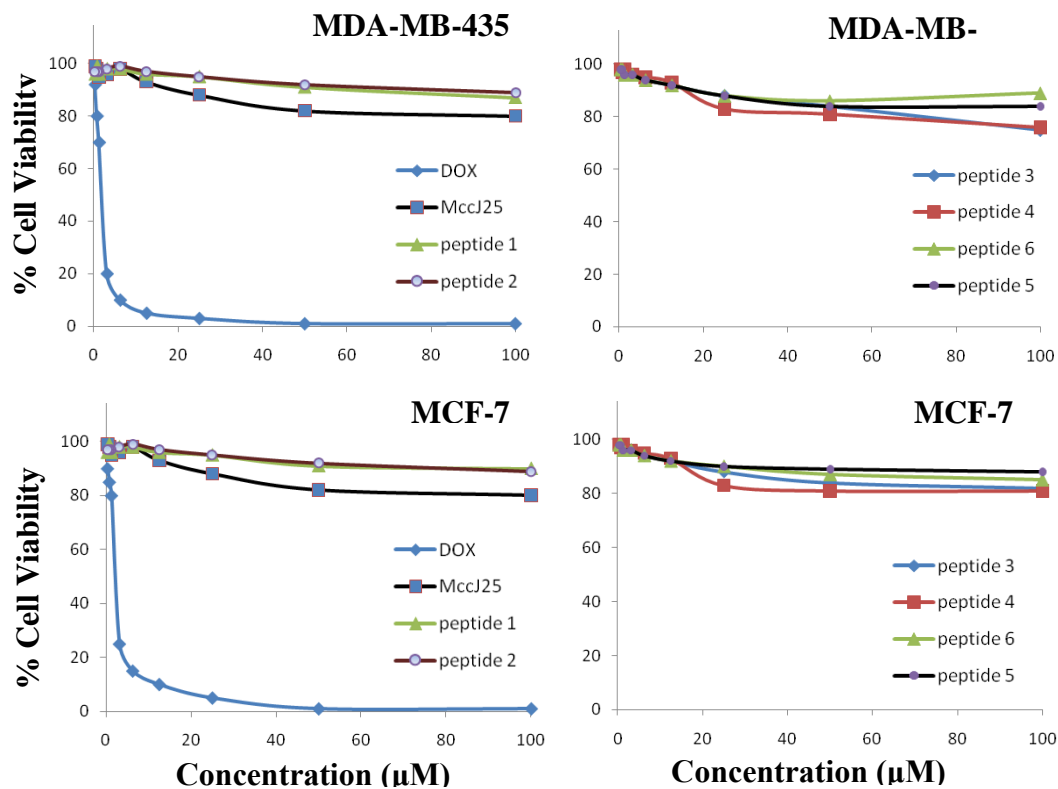


**Figure A.12.** Cell viability as a function of peptide concentration. MccJ25 and peptide analogues 1-6 were incubated with MDA-MB-435 (top) or MCF-7 (bottom) cells for 24 h at 37 °C.